

Département de Chimie
Université de Fribourg (Suisse)

**Novel iron tweezers complexes for
hydrogenation and polymerization of olefins**

THESE

Présentée à la Faculté des Sciences de l'Université de Fribourg
(Suisse) pour l'obtention du grade de *Doctor rerum
naturalium*

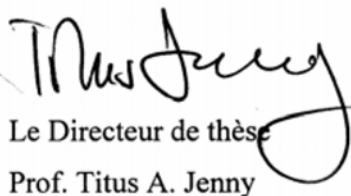
par

Roger Mafua
d' Angola

Thèse n° 1503
Edition Privée, Fribourg
2006

Acceptée par la Faculté des Sciences de l'Université de Fribourg (Suisse) sur la proposition du Prof. Titus A. Jenny, Prof. Alan Williams (Université de Genève) et du Prof. Thomas Bally, président du jury.

Fribourg, le 08 février 2006



Le Directeur de thèse
Prof. Titus A. Jenny



Le Doyen
Prof. Marco R. Celio

Remerciements

Ce travail a été réalisé de décembre 2001 à novembre 2005 sous la direction du Professeur Titus Jenny au département de Chimie de l'Université de Fribourg. Qu'il soit ici remercié de la confiance qu'il m'a accordée, de l'intérêt qu'il a porté à mon travail et du soutien qu'il m'a octroyé en maintes circonstances. Les nombreux échanges que nous avons eu concernant ce travail mais aussi en rapport à d'autres activités ont été très enrichissants et ont rendu mon travail agréable dans ce département.

Je remercie également le Professeur Alan Williams du Département de Chimie minérale, Analytique et Appliquée (Université de Genève) pour avoir accepté de juger et corriger ce travail.

Mes remerciements s'adressent aussi au Priv. Doc. Dr. Norbert Engel pour m'avoir permis d'exercer la tâche d'assistant durant la durée de ce travail.

Je tiens également à exprimer ma reconnaissance à Félix Fehr pour les mesures RMN, en particulière pour les nombreuses heures passées à fouiller la région sensible à la résonance de carbone carbénique. Un grand merci à Fredy Nydegger pour tout ce que touche la spectrométrie de masse et la chromatographie en phase gazeuse. J'exprime ma gratitude à Raoul Buffat de l'Ecole d'Ingénieurs et d'Architectes de Fribourg pour les mesures en spectroscopie Raman et aussi pour les analyses CHN. Dr Gaël Labat, Dr. Antonia Neels et Professeur Helen Stoeckli-Evans à l'Université de Neuchâtel ont toute ma reconnaissance pour les structures et les conseils dans le domaine cristallographique.

Pour la lecture, la correction de ce document et les bons moments partagés, j'adresse mes remerciements aux membres du groupe Jenny : Christophe Eggerstwyler, Olivier Aebischer, Ludwig Muster, Martine Poffet, Patrick Tondo et Daniela Bossi.

Que soient remerciés également tous ceux qui de près ou de loin ont contribué à la réalisation de ce travail : Manuel Raemy, Christophe Allemann, Guoliang Chen, Sandra Laübli, Jean-Luc Débieux, Viviane Fluxa, Mihailo Miletic, Mauro Schindler, Yvan Schindelholz, Michael Derada, Angélique Mugny, Géraldine Thalmann, Corinne Savary, Michel Piccand, Lucienne Rouillet, Noëlle Chassot, Xavier Hanselmann, Emerith Brügger, Verena Schwalm, Tibor

Kiss, Géraldine Martin, Fabrice Levrat, Jaime Lage Robles, Huber Favre, Alphonse Crottet, Sebastien Mercier, Emmanuel Riguet, Aspasia Theodossiou, Frédéric Birbaum, Marion Heckenroth, Laszlo Mercs, Anne Schuwey, Pasi-Kato et Josefina Sanda, Victoria Binz, Dona Luisa Assis, Clyde Fohouo, Denis Nguie, David Munoz, Claudia et Alyssa Sigrist, Yoël Chriqui, Claire-Lise Ciana, Olivier Graber, les étudiants en chimie, biochimie, pharmacie et biologie.

Une mention spéciale à Bassam Alameddine, Christophe Eggerstwyler et Simona Ruccareanu pour le soutien moral et aussi pour toute la philosophie autour de la Chimie, de l'être humain et de la société en générale.

Ce travail a reçu le soutien du Fonds National Suisse pour la Recherche Scientifique.

A mon oncle

A ma famille

Le seul, l'unique voyage, c'est changer de regard

Marcel Proust

Résumé

L'utilisation des complexes organométalliques comme catalyseurs est devenu un domaine très important de la chimie des matériaux. Cependant et malgré ce développement, les catalyseurs à base de fer(II) sont peu employés dans la polymérisation d'oléfines. Un de rares catalyseur utilisé dans ce contexte est le complexe tridenté diimine pyridine développé par Gibson et Brookhart. Cependant ce modèle souffre par son manque de tolérance envers le moindre changement effectué dans son enveloppe, résultant par une diminution drastique de son activité catalytique.

Le but de ce travail est de synthétiser des catalyseurs de fer(II) contenant des ligands chelates et d'étudier leur utilisation dans la polymérisation d'oléfines. Il est important de signaler que des travaux précédents dans notre groupe ont montré une très bonne corrélation entre la polymérisation et l'hydrogénation d'oléfines. Ainsi nous avons aussi exploité l'habileté de nos complexes dans l'hydrogénation.

Deux projets ont été menés en parallèle : il s'agit de la synthèse de complexes de fer(II) contenant d'un côté le ligand benzylétherfurane et de l'autre côté les ligands carbenes bisimidazol-2-ylidene.

Le complexe de fer(II) benzylétherfurane a été employé avec succès dans l'hydrogénation d'oléfines sous des conditions très douces (1-3 bar d'hydrogène et à température ambiante), cependant son emploi comme catalyseur de polymérisation d'oléfines n'a pas donné les résultats escomptés. Compte tenu de ceci, ce projet a été mis à côté au profit des complexes de fer(II) bisimidazol-2-ylidene qui eux ont montré une bonne activité dans les deux réactions, polymérisation et hydrogénation des oléfines sous des conditions douces.

Durant la préparation de ces précatalyseurs, plusieurs autres complexes de fer(II) et fer(III) ont été isolés comme étant des produits secondaires de la réaction. Dans le but de caractériser les produits obtenus, nous avons aussi préparé plusieurs dérivés en introduisant des ligands supplémentaires dans la sphère de coordination; c'est ainsi que des dérivés formiate, carboxylate, triflate et cyclopentadiényle ont été synthétisés.

Plusieurs voies ont été exploitées pour synthétiser les complexes fer(II) bisimidazol-2-ylidene, une d'elles, la transmetallation, nous a conduit à préparer des nouveaux complexes d'argent; ces complexes ont été caractérisés entre autre par diffraction de rayons – X.

Enfin dans une démarche purement comparative, deux complexes nickel bisimidazol-2-ylidene ont été préparés et leur activité catalytique dans la polymérisation d'éthylène a été sommairement étudiée, donnant de très bons résultats.

Abstract

The use of organometallic complexes as catalysts became a very significant topic in the field of material chemistry. However, despite of this development, only few of them contain iron(II), except the tridentate complex diimine pyridine developed by Gibson and Brookhart and employed in the olefin polymerization. Unfortunately, this model suffers by its lack of tolerance towards the minor changes carried out in its envelope, resulting by a drastic reduction from its catalytic activity.

The goal of this work is to synthesize iron(II) complexes containing pincer ligands and to study their use as catalyst for polymerization of olefins. It has to be noted that previous work in our group showed a very good correlation between the polymerization and the hydrogenation of olefin. Thus, we have also exploited the ability of our news complexes in hydrogenation.

Two projects were carried out in parallel: one was the synthesis of iron(II) complexes containing benzyletherfuran ligand and the second one was the preparation of iron(II) bisimidazol-2-ylidene complexes.

First project :

The prepared iron(II) benzyletherfuran complex was successfully tested in the hydrogenation of olefin under very mild conditions (1-3 bar of hydrogen at room temperature); however, its employment as catalyst for olefin polymerization did not give the expected results. Thus, this project was left aside with the profit of the second one.

Second project :

The prepared iron(II) bisimidazol-2-ylidene complexes showed a good activity in both reactions, polymerization and hydrogenation of olefins under mild conditions. During the preparation of these complexes, several other complexes of iron(II) and iron(III) were isolated as secondary products from the reaction.

With the purpose of characterizing the obtained products, we also prepared several derivatives by introducing additional ligands into the coordination sphere of iron(II) bisimidazol-2-

ylidene complexes. Thus, formiate, carboxylate, triflate and cyclopentadienyl derivatives were synthesized.

Several ways were exploited to synthesize the iron(II) bisimidazol-2-ylidenes complexes, one of them was the transmetallation which led us to prepare new silver complexes. These complexes were characterized amongst other analytical tools by X-ray diffraction.

Finally, in a purely comparative approach, two nickel bisimidazol-2-ylidene complexes were prepared and their catalytic activity in the ethylene polymerization was studied, giving very good results.

Table of contents

I. Theoretical Part	14
1. General introduction	15
2. Polymers as giant molecules	15
3. Application of surface-modified polyolefins	17
4. Techniques of surface modification and characterization of polyolefins	19
5. Analytical tools for surface-modified polyolefins	28
6. Functionalized polyolefins	30
7. The scope of this work	48
II. Results and discussion	49
8. General strategy	51
9. Benzyloxyfuran complexes of iron(II)	61
10. Synthesis of bisimidazolium salts	70
11. Direct metallation by reaction of bisimidazolium salts with adequate iron(II) precursors (Fe[N(SiMe ₃) ₂], Fe(OSO ₂ CF ₃) and Fe(O ₂ CH) ₂ ·2H ₂ O))	88
12. Complexation of iron(II) precursors with free carbene ligands: 1,3-bis(aryl)-3,3'-methyleneimidazol-2-ylidene	102
13. Synthesis of Iron (II) precursors soluble in THF (FeX ₂ (THF) ₂) and FeX ₂ (PPh ₃) ₂	126
14. Silver biscarbene imidazole-2-ylidene as intermediates for a synthesis of iron(II) complexes	133
15. Silver bisaryl N-heterocyclic biscarbene complexes as transfer agents for the synthesis of iron(II) and Ni(II) complexes	148
16. Analytical tools	178
III. Catalytic Reactions	194
17. Catalytic reactions	195
IV. Conclusions	219
18. Conclusions	220
V. Experimental part	223
19. General considerations	224
20. Synthesis of organic substrates	227
21. Synthesis of silver complexes: Typical procedure	245
22. Synthesis of iron precursors	251
23. Iron (II) bischloro-2-(4-isopropyl-benzyloxymethyl)-tetrahydrofurfuran (50)	255
24. Synthesis of iron(II) complexes by direct metallation of bisimidazolium salts	258
25. Reaction of free biscarbene with FeX ₂ and modified FeX ₂ (THF) ₂ (X = Br, Cl)	266
26. Synthesis of iron(II) containing bisimidazol-2-ylidene and carboxylate ligands	270

27.	Synthesis of iron(II) containing cyclopentadienyl ligands	273
28.	Reaction of free biscarbene imidazole-2-ylidenes 63 and 64 with $\text{FeCl}_2(\text{PPh}_3)_2$	275
29.	Transmetallation reaction of silver complexes 65-67 with iron(II) in different solvents	277
30.	Deprotonation of bisimidazolium iron tetrahalides complexes	281
31.	Reaction of silver complexes with $\text{FeCl}_2(\text{PPh}_3)_2$	283
32.	Transmetallation reaction of silver complexes 66d and 67b with $\text{NiCl}_2(\text{PPh}_3)_2$	284
33.	Catalytic reactions	286
VI. Annexes		287
VII. References		294
VIII. Curriculum Vitae		305

Abbreviations

Ac	acetyl
AFM	atomic force microscopy
AES	auger electron spectroscopy
Bn	benzyl
BP	benzophenone
BPO	benzoyl peroxide
Bpy	2,2'-bipyridine
Bz	benzoyl
COD	cyclooctadiene
COE	cyclooctene
COSY	correlated spectroscopy
DAD	1,4-diazadiene
Dat	2,5-diazatriene
DFT	density functional theory
DIBAH	diisobutylaluminiumhydride
EI	electron impact
ENB	5-ethylidene-2-norbornene
ESI	electrospray ionisation
Et	ethyl
FAB	fast atom bombardement
FTIR	fourrier transform infrared
GC	gas chromatography
HDPE	high density polypropylene
HETCOR	heteronuclear correlation
HREELS	high resolution electron energy loss spectroscopy
iPr	isopropyl
LiAlH	lithium aluminiumhydride
LPE	linear polyethylene
LLDPE	linear low density polyethylene
LDPE	low density polyethylene
M	molar

Me	methyl
MAO	methylaluminumoxan
MMAO	modified methylaluminumoxan
MS	mass spectrometry
NBD	norbornadiene
n-BuLi	n-butyllithium
NEXAFS	near edge X-ray absorption fine structure
NMR	nuclear magnetic resonance
PE	polyethylene
Ph	phenyl
PMMA	polymethyl methacrylate
PP	polypropylene
RT	room temperature
SEM	scanning electron microscope
SFA	surface force apparatus
SFM	scanning force microscopy
SIMS	secondary ion mass spectrometry
SSIMS	static secondary ion mass spectroscopy
STM	scanning tunnelling microscope
TEM	tunnelling electron microscopy
THF	tetrahydrofuran
ToF	time-of-flight
TOF	turn-over frequency
TON	turn-over number
UHMWPE	ultra high molecular weight polyethylene
ULDPE	ultra low density polyethylene
UV/Vis	ultraviolet/visible
XLPE	cross linked polyethylene
XPS	X-ray photoelectron spectroscopy

I. Theoretical Part

1. General introduction

Organometallic compounds are defined as materials which possess one or more bonds between metal and carbon atoms. Since Zeise synthesized in 1827 the complex $K[PtCl_3(CH_2=CH_2)]$, generally accepted as the first organometallic compound, organometallic chemistry has never stopped to grow. Nowadays the transition metal catalyzed assembly of carbon-element (element = H, C, N, etc) bonds is an indispensable element of synthesis due to the unique ability to control and enhance chemical reactivity, furthermore it is rare to find complex total syntheses that don't involve at least a few transition metal mediated key steps. In addition, industry has lost much of its aversion to use homogeneous catalysis. Finally the use of transition metals in the synthesis of polymers and materials has also increased dramatically^{1,2}. Typically many catalysts employed in these transformations are derived from heavy or rare metals (Cr, Os, Co, Ru, Pd, Pt, Rh, Ir...) and require tedious, energy-intensive separation procedures to remove trace metal impurities from the products and call for environmentally responsible waste disposal. Toxicity and prohibitive prices of these metals constitute severe drawbacks for large scale applications.

In contrast to toxic metals, iron is an inexpensive, physiologically and environmentally friendly metal. Its very low cost offers the possibility to engage iron either in catalytic or stoichiometric amounts. However wonderful this sounds, it is surprising that, until recently the use of iron in the field of catalysis was relatively underrepresented, compared to other transition metals. Many famous applications are limited to the use of carbonyl complexes or ferrocene derivatives. More recently, researchers have developed a series of well-defined diiminopyridine iron compounds that are active for catalytic polymerization of olefins.

2. Polymers as giant molecules

The importance of polymerisation reactions for almost all of the aspects of nowadays life is obvious. Polymers exist as essential materials for sophisticated objects such as the computers used to write this thesis and the space shuttle and as simple materials such as rubber bands and plastic spoons. They may be solids capable of stopping a bullet, or they may be inert liquids such as silicone oils offering a wide variety of flow characteristics. Many polymers are important commercial materials and constitute one of the fast moving frontiers of daily life.



Figure 1. Polymers are everywhere

Another way to measure the importance of polymers is to take account the associated work force. The USA polymer industry employs more than 1 million people directly or indirectly. This corresponds favorably to the employment of the entire metal-based industry. Furthermore, about one-half of all professional chemists and chemical engineers are engaged in polymers science technology, including monomer/polymer synthesis and characterization. This demand will increase as this industry sector is predicted to continue to increase³.

Polyolefins are amongst the oldest and well accepted synthetic polymers due to their excellent physical and chemical properties. Although polyolefins such as polyethylene (PE), polypropylene (PP), polybutadiene (PB) and their copolymers have excellent bulk physical/chemical properties, they are inexpensive and easy to prepare. Polyethylene in particular holds a unique status due to its excellent manufacturer and user-friendly properties, but it has not gained considerable importance as a specialty material due to its inert surface. Thus, special surface properties, which saturated polyolefins do not possess, like printability, roughness, hydrophilicity, selective permeability, and adhesion of microorganisms, are required for their success for specific applications⁴.

During the last two decades, different physical and chemical means of surface modifications have been thoroughly explored. Generation of technologically useful surfaces with desired interfaces using surface-modifications techniques have become an important tool to convert these inexpensive polymers in the valuable commercial products. Advances have been made to alter the chemical and morphological properties of the surface in the desired way with negligible change in the polymer bulk properties^{5,6}. Many recent studies emphasized the

necessity for product compatibility in the multiphase systems to provide new materials with improved properties. The following changes at the polymer interface have been used to enhance the surface properties; of course, each surface modification of polymers is carried out taking into consideration the potential applications and the desired surface properties⁷.

3. Application of surface-modified polyolefins

Since surface-modified polyolefins bear a wide range of applications, it is only possible to mention a few of them and many more are included as referred literature in the following section.

3.1 Automotive application

High density polyethylene (HDPE) is used to make automotive fuel tanks as alternative material to replace steel. HDPE has many advantages over steel, specially the design freedom to utilise unused space and its low weight. However, the shortcoming of HDPE is its permeability to gasoline and methanol. Therefore, it cannot fulfil the right emission standards³. Since the permeability of the liquid in the polymer depends both on the nature of the bulk as well as the surface of the polymer, the surface modification of this polymer was almost inevitable. This shortcoming is successfully overcome by fluorination of the HDPE surface using a plasma/corona treatment⁵.

3.2 Conductivity

Polymer metal interfaces are encountered in many applications of polymers such as electronics devices, packaging applications, electrical appliances etc... Many desirable surface properties, such as electrical conductivity and optical characteristics, can be achieved with metal coating on polymer surfaces by sputtering or electroless plating^{5,7,8}. The third and most recent approach for metallization of PE surfaces is the surface grafting of conducting polymers such as polythiophene⁹.

3.3 Selective permeability

Polymeric membranes are used in many fields to control selective flow of mixtures of gases and liquids. The transport of material through a membrane depends on the chemical and physical characteristics of both the bulk and the surface. For instance, polytrimethylsilyl propylene (PTMSP) is reported to exhibit the highest gas (oxygen) permeability among all existing polymers. Cations exchange polymers modified with carboxylic acid groups for a battery separator were prepared by radiation-induced grafting of acrylic acid (AA) and methacrylic acid (MA) onto a PE film^{10,11}.

3.4 Biomedical application

Due to the freedom of design and their inert and non-corrosive nature, polyolefins have proved to be the most favourable alternative for biomedical applications¹². Biocompatibility and anti-thrombogenicity of several plastic materials have been improved by radiation-induced grafting^{5,13}. A true biocompatible material should certainly possess surface merits like blood compatibility, antibacterial activity, cell/immuno-adhesivity, tissue binding etc. Among the first artificial human implants were artificial heart valves, pacemakers, vascular grafts and kidney dialysis tubes. In the past years, advances in materials engineering made possible the use of orthopaedic devices such as knee and hip joint replacements using HDPE and PP. Temperature-responsive controlled drug delivery¹⁴ using biodegradable polymers are presently under extensive study worldwide. Biocompatible materials have been prepared by various methods since their discovery. PEG chains were grafted onto the surface of PE to obtain protein-resistant surfaces.

3.5 Adhesion

Due to their inert surface, polyolefins suffer from a large number of adhesion problems, which can be overcome by physical surface modification techniques. For example, the auto-adhesion of PE films can be improved considerably by plasma treatment, corona discharge and oxidation by inorganic oxidants^{5, 12, 15}. Ishihara and co-workers have recently reported photo-induced graft polymerisation of phospholipids on PE membrane surface. This treatment of PE improved its resistance towards blood cell adhesion. This shows that resistance to

adhesion is equally important for some specialty applications. Laser induced surface modifications of ultra-high-strength PE fibres enhanced their adhesion to epoxy resins³⁴⁻³⁶. The PE-wood interfacial bonding strength was improved by using a surface-modified PE in this composite material⁵.

4. Techniques of surface modification and characterization of polyolefins

Since understanding these surfaces modifications techniques is very important, we will review some of existing techniques of surface modification and characterization of polyolefins.

4.1 Flame treatment

Flame treatment is one of the oldest methods used by industries for the modification of polymeric surfaces. For this technique a very simple set up is required (comprising of a burner and a fuel tank) and very high degree of craftsmanship is needed to produce consistent results. Oxidation of the polymer surface can be attributed to the high flame temperature range (1000–1500 °C) and its interaction with many excited species in the flame. Garbassi and co-workers¹⁸ studies this technique on polyethylene using X-ray photoelectron spectroscopy. Functional groups like hydroxyl (-OH), carbonyl (C=O) and carboxyl (COOH and COOR) were generated and detected on the surface of polymer. Studies also reveal that for the best results of flame treatment, an oxidizing flame should be used, which requires a slightly higher concentration of oxygen than that needed for complete combustion. One of the surfaces of adhesive tapes (consist of a co-extruded support having one layer of PP and another of HDPE) was treated by flame to increase its surface energy. Thus, the tape had improved the printability and fixing of the adhesive on the support^{5,18,19}.

4.2 Corona discharge

Corona discharge is a well-accepted, relatively simple and most widely used continuous process for the surface treatment of polyolefins films^{5,20}. This technique is mainly used in the plastic industry to improve the printability of polyolefin films and goods. The corona discharge consist of a high voltage/high frequency generator, an electrode and a grounded metal roll covered with an insulating material as shown in figure 2.

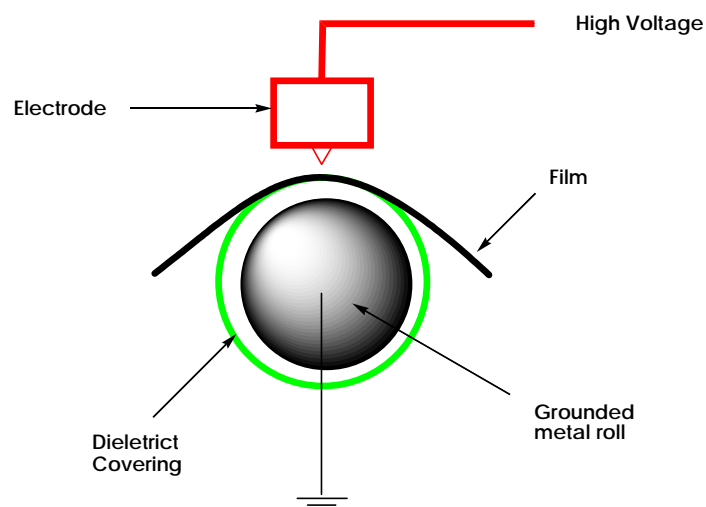
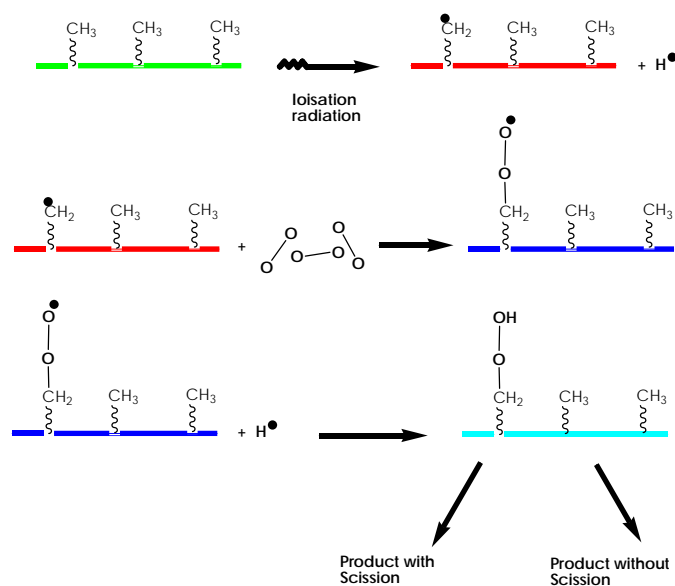


Figure 2. Schematic diagram of corona treatment assembly⁵.

The entire system works as a large capacitor, with the electrode and the grounded roll as the plates of the capacitor and the roll covering and air as the dielectric. In this system, a high voltage, when applied across the electrode, ionizes the air producing plasma (often identified by the formation of a blue flame in the air gap). This atmospheric pressure plasma popularly known as the corona discharge brings about physical and chemical changes on the polymer surface for improved bonding and dyeing ability. A number of chemical reactions are bound to take place at the polymer surface because of corona treatment. Electrons, ions and photons that are present in a discharge, react with the polymer surface to form radical. These macro radicals react with atmospheric oxygen to give oxidation products scheme 1.



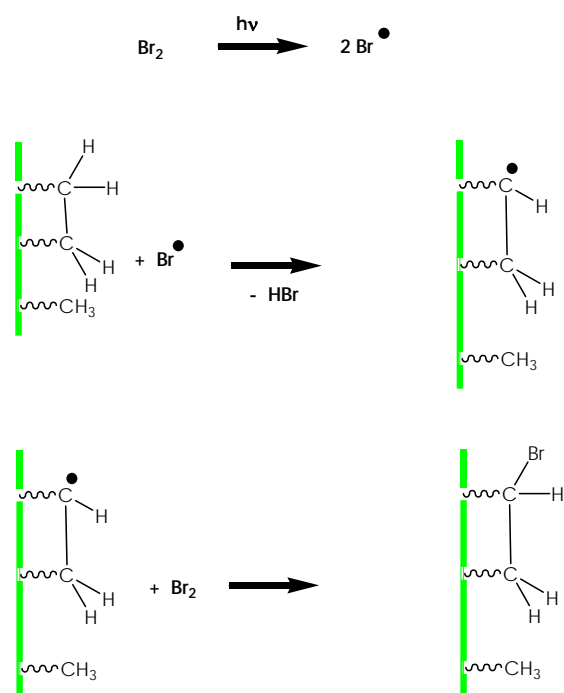
Scheme 1. Electrons, ions and photons that are present in a discharge react with the polymer to form radicals. The macro-radicals formed on the polymer react at their turn with atmospheric oxygen to give oxidation products.

Decomposition of these hydroperoxydes produces alcohols, carbonyls and carboxylic groups on the treated polymer surface. Though this technique has its advantages, it is also associated with some shortcomings such as non-consistent treatment due to the variation in ambient conditions (such as temperature and humidity), a high possibility of contamination due to the treatment carried out in air and, at times, lack of homogeneity/uniformity of surface modifications and low molecular weight oxidized products^{5, 20a}.

4.3 Irradiation

High energy radiation (X-rays, γ -rays, electron beam from cobalt (^{60}Co) and magnesium (^{58}Mg) sources), mid-energy radiations (usually obtained from UV rays, pulsed/excimer laser and plasma sources) and low energy radiation yielded by infrared, ultrasonic, microwave and visible light source can bring about desired changes in the polymer backbone depending upon the irradiation time and energy of radiation²¹. The role of any of these radiations is to activate the molecules on the surface of the polymer, which react with the functional species present in its vicinity to render it a functional surface. For example, polyethylene samples were irradiated with UV light in an atmosphere containing SO_2 and air to achieve the photosulfonation of the surface²². Photobromination of low density polyethylene (LDPE) was

achieved by exposing the LDPE films to the bromine vapour and irradiating them with mercury vapour lamp for stipulated irradiation cycles (each cycle lasting 30 seconds)^{9,13}.



Scheme 2. Simplified mechanism of photochemical polyolefins bromination.

The IR of a brominated LDPE film revealed three bands at 550, 568 and 620 cm^{-1} , assigned to C-Br stretching bands. Photo-bromination of PE surface followed by derivatisation has also been reported recently.

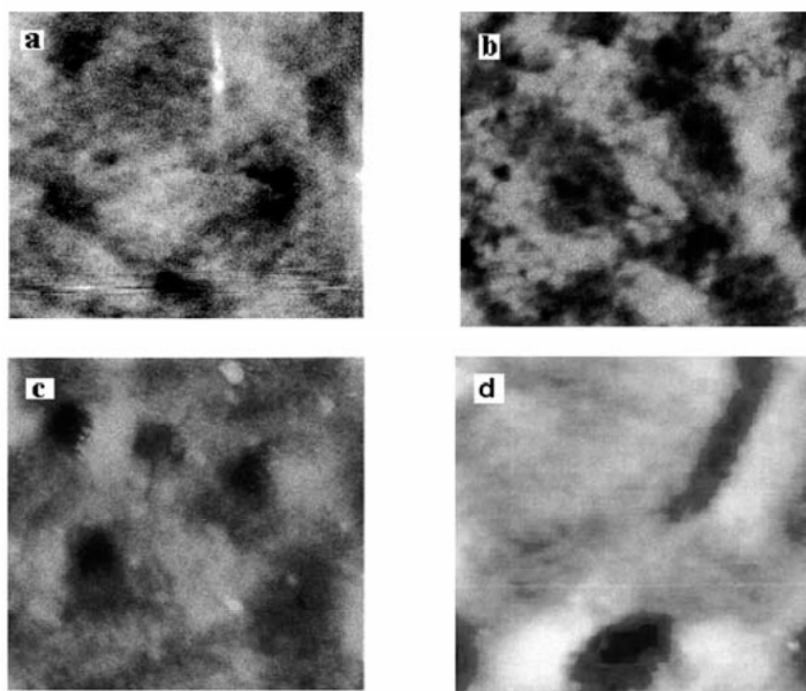


Figure 3. AFM topography of PE films: **a)** untreated, **b)** after one irradiation cycle, **c)** after three irradiation cycles, **d)** after two brominations cycle⁹.

4.4 Graft copolymerization

This is the most well-know and fundamental method of surface modification. A graft copolymer is a polymer consisting of molecules with one or more type of blocks connected as pendant chain to the backbone, having configurationally features different from those in the main chain. Graft copolymerization can be represented by:

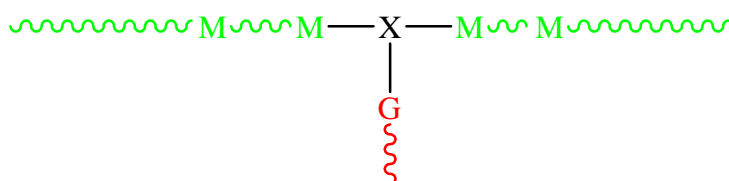


Figure 4. Representation of a graft copolymer.

Where M is the monomer unit in the backbone polymer G represents the pendant chain (graft) and X the unit in the backbone to which G is attached. Graft copolymerization can be brought about mainly through free radical and ionic mechanisms^{12,23}. The former mechanism includes ionization-, photo- and plasma-induced grafting. There is a variety of techniques to obtain

graft copolymers; one of them involves the diffusion across a phase boundary between a monomer and the polymeric material.

Photo grafting

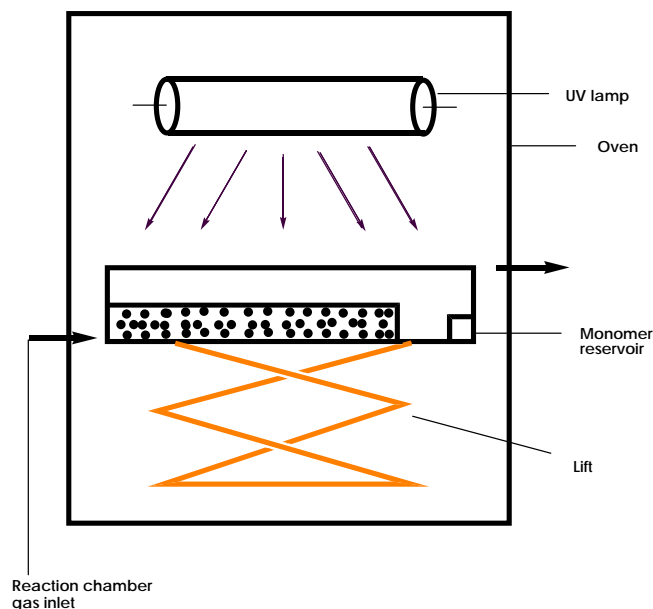
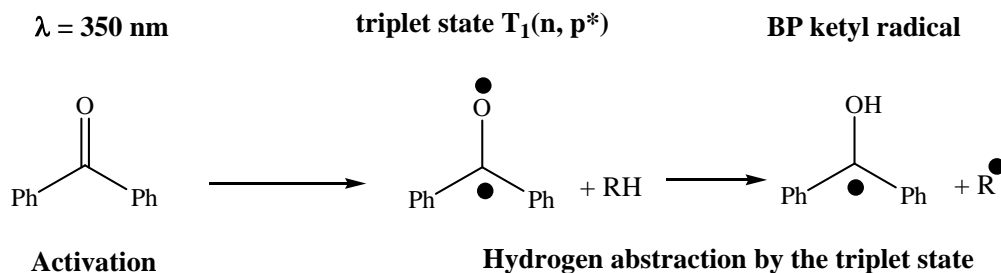
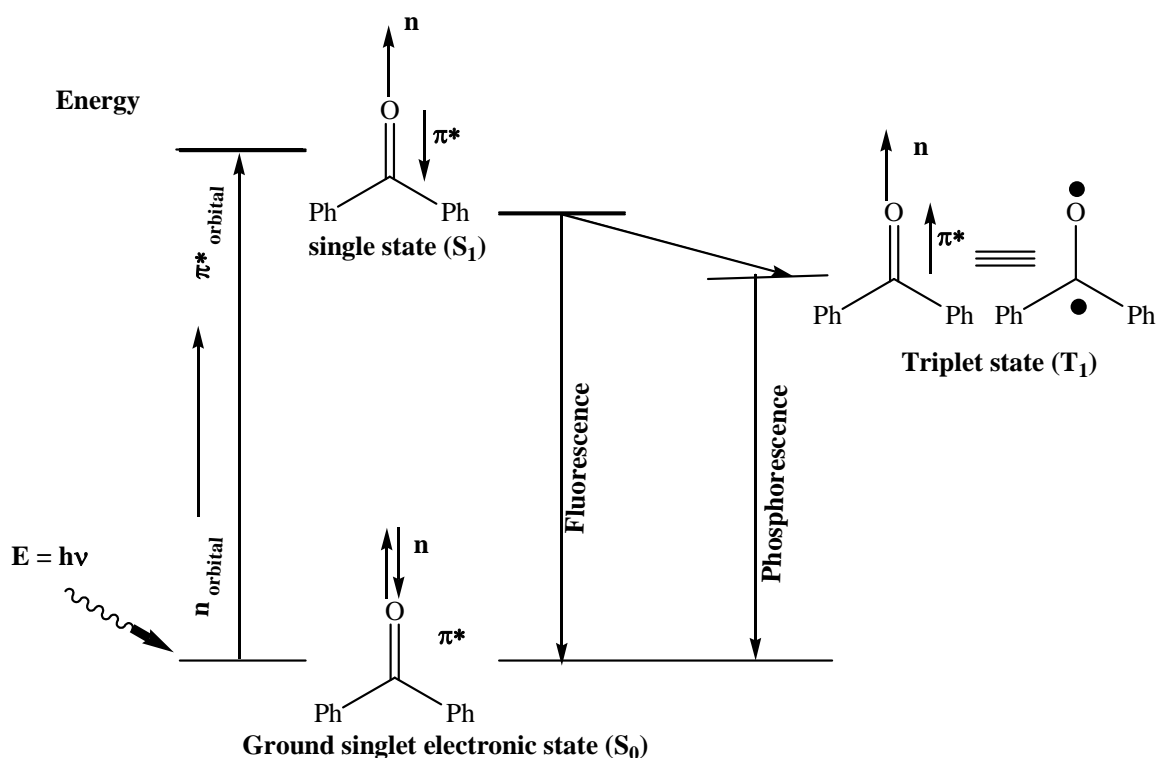


Figure 5. Reactor used for vapor phase photo-grafting of acrylic acid onto HDPE powders.

The basic difference between ionization radiation and photo radiation is that the energy as compared of ionization irradiation is much higher than that delivered by the light source employed in the photo-irradiation. Capital photo graft is usually brought about by the UV radiation obtained from various sources including the most commonly used mercury vapor lamp⁵.

It is know that in a photochemical process, absorption of a photon by an organic molecule (commonly called *chromophore*) results in excitation of the molecule from its ground state, giving rise to $n-\pi$ and $\pi-\pi^*$ transitions. The extra energy associated with the excited molecule is then dissipated by various processes, amongst which energy transfer is the most desirable process for grafting reactions. Absorption of UV light produces an excited (S_1) transition, which then release a part of its absorbed energy to form an excited triplet (T_1). Before the excited triplet undergoes decay, the absorbed energy is used for photochemical induced reactions¹².



Scheme 3. Simplified diagram of energy states in benzophenone.

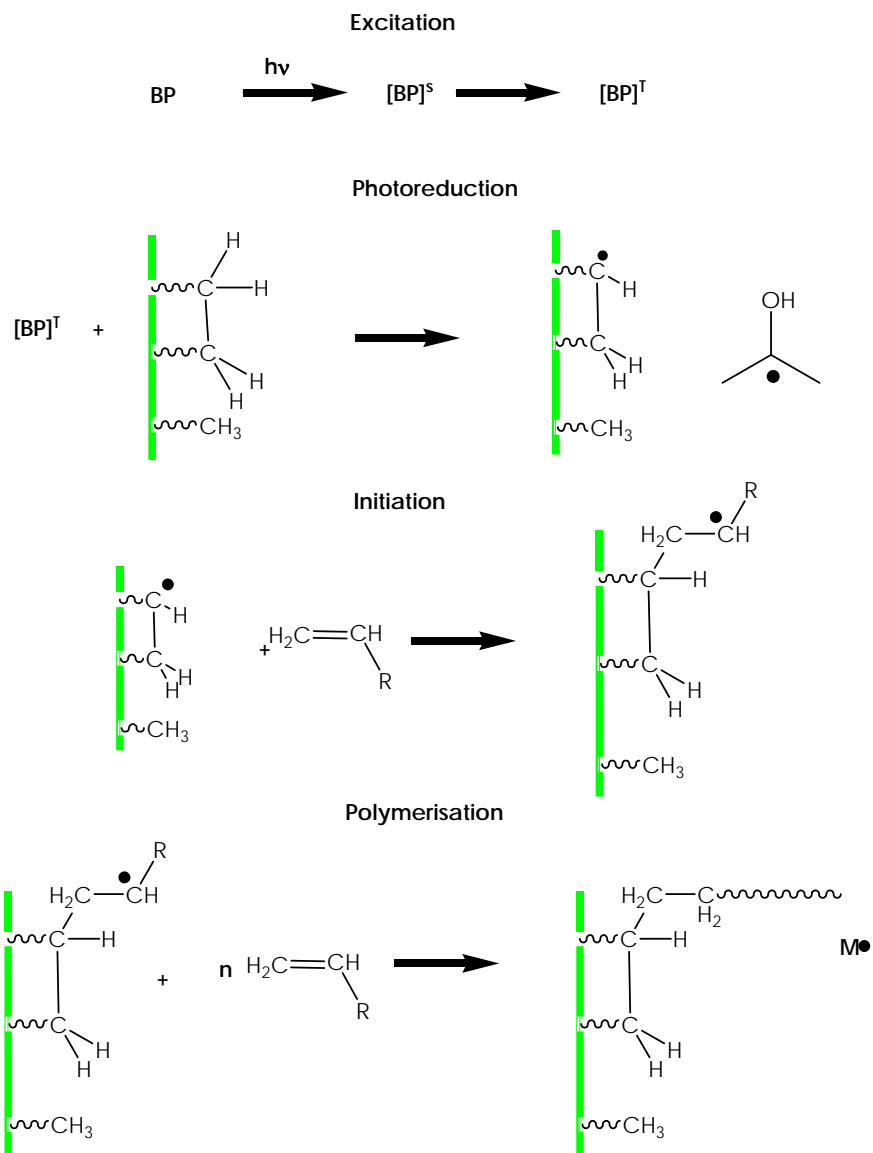
Two main advantages of photo-grafting over ionization radiation grafting are:

1. The modification produced by this technique is virtually restricted to the surface and is then helpful in generating properties like adhesion, antifogging, wear resistance, antistatic, printability, dye ability and biocompatibility at the polymer surfaces.
2. The energy associated with UV light is in the range of the chemical bond energies associated with atoms¹². Hence, UV radiation often has the potential for retention of the properties of polymers and monomers while the other surface grafting techniques,

which use ionization radiation, cause damage to the substrate polymers due to excessive degradation.

Photo-grafting can be performed in two different manners: the first technique is the simultaneous grafting, in which the substrate, monomer, photosensitizer, and solvent are taken in a photoreactor under inert conditions and irradiated with UV. In the second approach, post irradiation grafting, the substrate is irradiated in air to generate hydroperoxydes on the surface followed by the decomposition of these peroxides in the presence of monomer to yield grafted surfaces^{5,15,24}.

Organic ketones, peroxides and their derivatives are well-known photo-initiators for surface photo grafting. Benzophenone and its derivatives are the most commonly used photo-initiators. Benzophenone is excited to the short-lived singlet state that relaxes to a more stable triplet state, which then abstracts a hydrogen atom from the polymer backbone generating a polymer macro radical (P°). This macro radical acts as an active site for the graft copolymerization (so called *from grafting*). Under favorable conditions, when the initiator abstracts a proton from the monomer, the later undergoes homopolymerisation. This homopolymer bearing a radical at the chain end attacks the polymer backbone leading to a graft copolymer (so called *onto grafting*). The accepted mechanism of surface photo grafting is represented in scheme 4.



Scheme 4. Graft surface-copolymerisation polymerisation of alkene using benzophenone as photoinitiator²⁵.

5. Analytical tools for surface-modified polyolefins

The following section describes some of techniques used for the analysis of modified polyolefins surfaces. The modification of surfaces usually varies from a few angstroms to a couple of microns. Depending upon the type of information desired, there are a variety of analytical techniques such as angle goniometer X-ray photoelectron spectroscopy, attenuated total reflectance-infrared spectroscopy, surface plasmon resonance, static secondary ion mass spectroscopy, neutron refractometer etc.

Therefore, the choice of the surface analysis technique must be made very judiciously, keeping in mind sample suitability, sample depth, analysis environment and the surface information desired. Different surface investigation methods have different detection limits and lateral resolutions; in general, the information supplied by each technique is often different but complementary. The techniques like scanning electron microscopy (SEM), atomic force microscopy (AFM) and tunnelling electron microscopy (TEM) are employed when high resolution, three-dimensional images of the surface are desired, whereas, X-ray photoelectron microscopy (XPS) and static/dynamic secondary ion mass spectroscopy (SSIMS) are employed to understand the chemical changes on the substrate backbone^{25,26}.

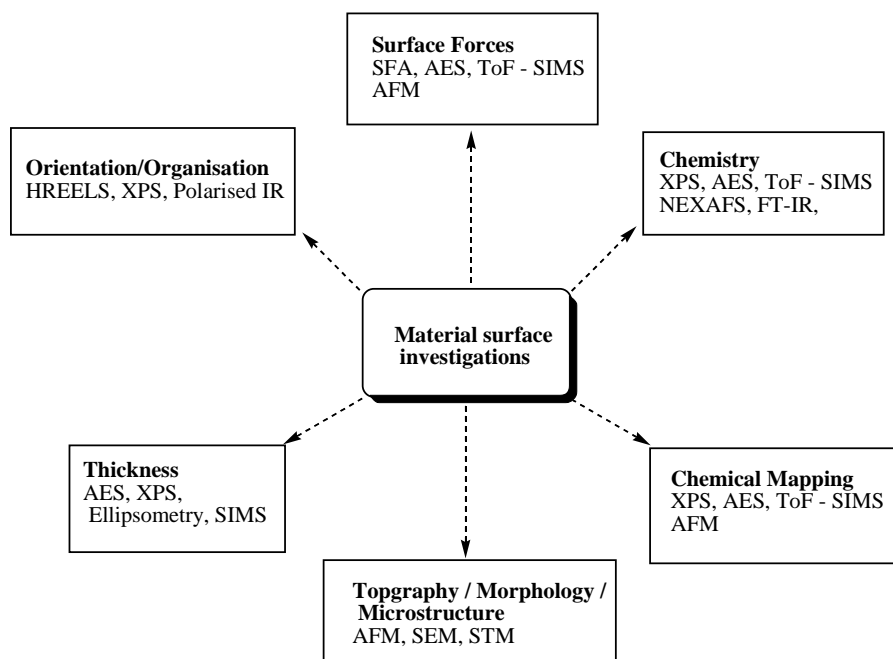
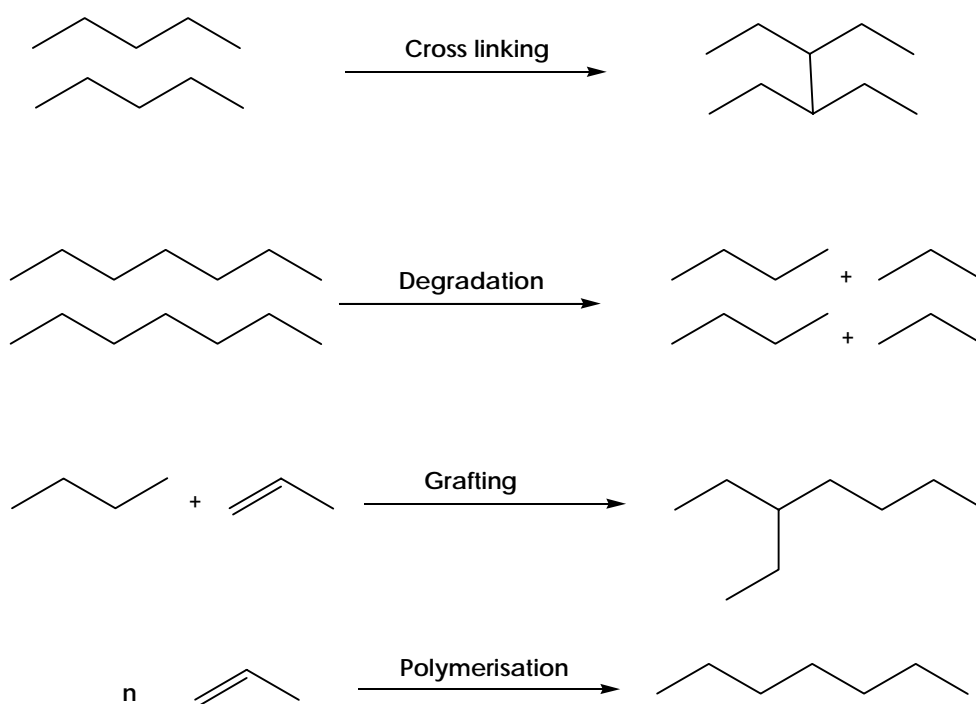


Figure 6. Map of different techniques used to characterize the surfaces of material.

Despite the fast development of polymer science, there are only few polymers with great film properties available. The production of functionalized polyolefins on a commercial scale is currently based on high pressure, free radical processes in which comonomers such as vinyl acetate and methyl or butyl acrylates are used. Another extensively utilised route for adding polar groups to polyolefins is postpolymerisation modification, which is usually performed by free radical grafting in reactive extraction^{2b,15}. However, these commercial processes are far from ideal since it is very difficult to control the composition and the structure of the copolymers obtained. Disadvantages such as non-homogeneity/uniformity of surfaces modified, side reactions during the grafting and severe polymerisation conditions of a high pressure radical can be noted during these processes^{5,15,28,29}.



Scheme 5. Modifications produced at the polymer surface as a result of irradiation products obtained from photografting.

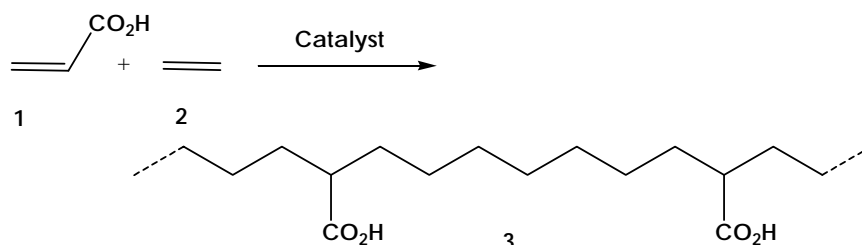
Today, the most straightforward way to produce functionalized polyolefins would be the direct copolymerisation of ethylene or propylene with functional monomers by an appropriate organometallic catalyst. More recently, with the introduction of single-site transition metal

coordination catalysts (metallocene and non-metallocene), many research activities have been conducted on the preparation of functional polyolefin polymers^{28,29}.

6. Functionalized polyolefins

Functionalized polyolefins is a term used for saturated polymers that, in addition to the hydrocarbon backbone, contain reactive functional groups.

Thus, the new emerging frontier in olefin polymerisation is the controlled copolymerisation of α -olefins with a monomer bearing a polar functional group²⁸. Of particular interest are the copolymers of monomers with oxygen and nitrogen-containing polar groups, such as vinyl alcohols, acids, esters, amides and nitriles.



Scheme 6. Functionalized polymers.

One of the most interesting features of organometallic compounds is that they can be used as homogeneous catalysts in processes where all the reacting partners are present in one phase, usually the liquid one³⁰. Transition metal complexes react in different ways within the catalytic reaction: they bring the substrates together, activate the substrates by coordinating them to the metal and lower the activation energy of the reaction between substrate and reagent. Organometallic catalysts success lies in the ease of modification of their environment, e.g. by ligand exchange which allows to dramatically change in its reactivity³.

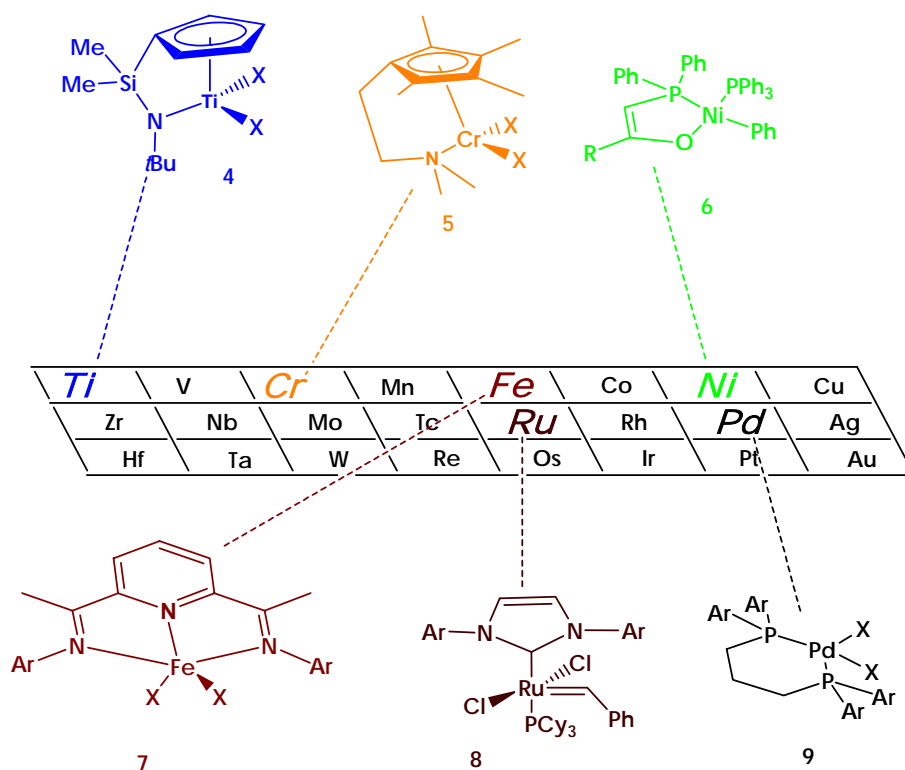
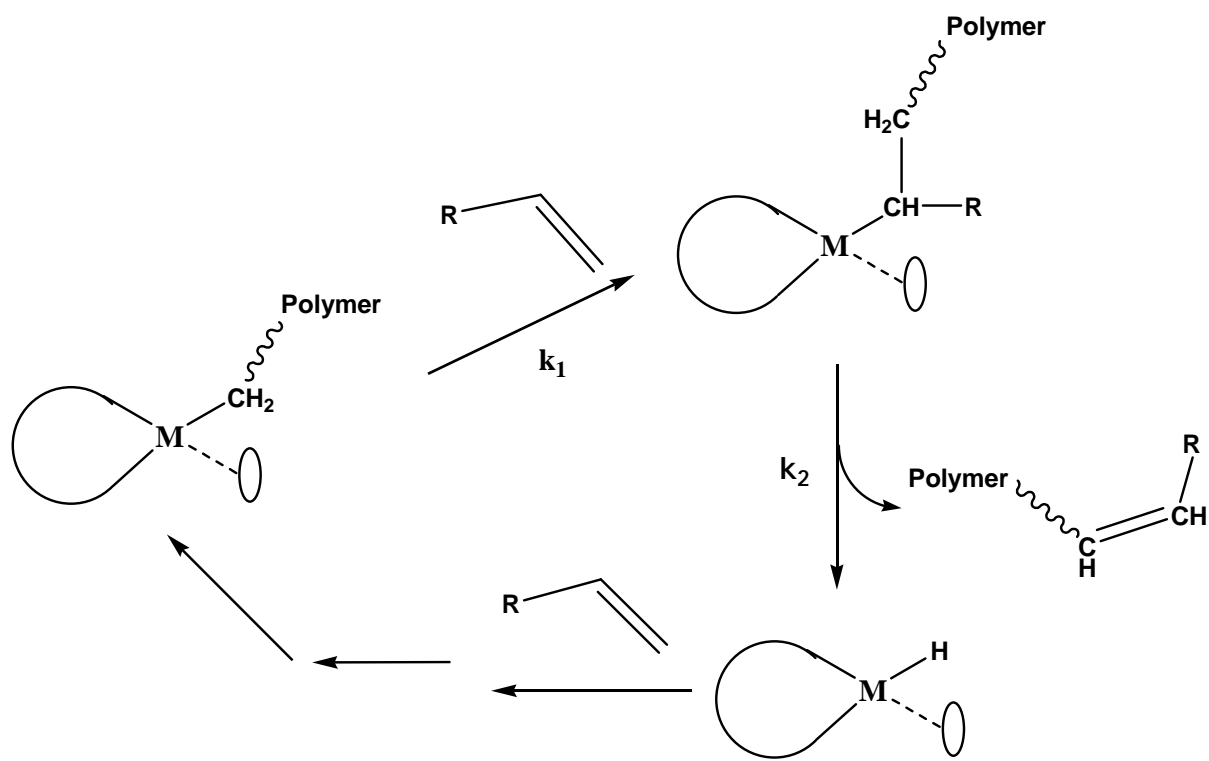


Figure 7. Example of high active non-metallocene olefin polymerisation catalyst across the transition series.

Because of their low oxophilicity and greater tolerance towards functionalised monomers, the late transition metals are often preferred over the early transition metals in the synthesis of polymers bearing functional groups³¹. However, the disadvantages of using late-metal polymerisation catalysts is their lower activity for alkene insertion (k_1) and the more favoured β -elimination (k_2), which competes with chain growth³². As long as $k_1 \gg k_2$ high molecular weight polymers would be obtained. However, often with late transition metal catalysts, k_1 equals k_2 , and then hydrogen abstraction becomes a competing reaction.



Scheme 7. Simplified catalytic cycle of olefin polymerisation. O represents the active site.

To give a feeling for how active a particular catalyst is compared to other systems, Gibson and co workers²⁹ have proposed a scale of merit ranging of the catalysts. This scale goes from very low to very high activity; all activities reported in the literature were converted to units of grams of polyolefin product per mol catalyst per hours at given monomer feed pressure ($\text{g}\cdot\text{mmol}^{-1}\cdot\text{h}^{-1}\cdot\text{bar}^{-1}$). Since experimentally determined values are highly dependent upon the precise reaction conditions, including stirring rate and the configuration of the reactor, it is very important to be careful when comparing catalyst activities reported by different groups of researchers. Furthermore, often little or no information is given about the kinetic profile of the catalyst lifetime, with the consequence that a short polymerization runs with a catalyst that is active only for few seconds before dying, may gives an inflated figure of merit compared to an activity reported for a many hours run.

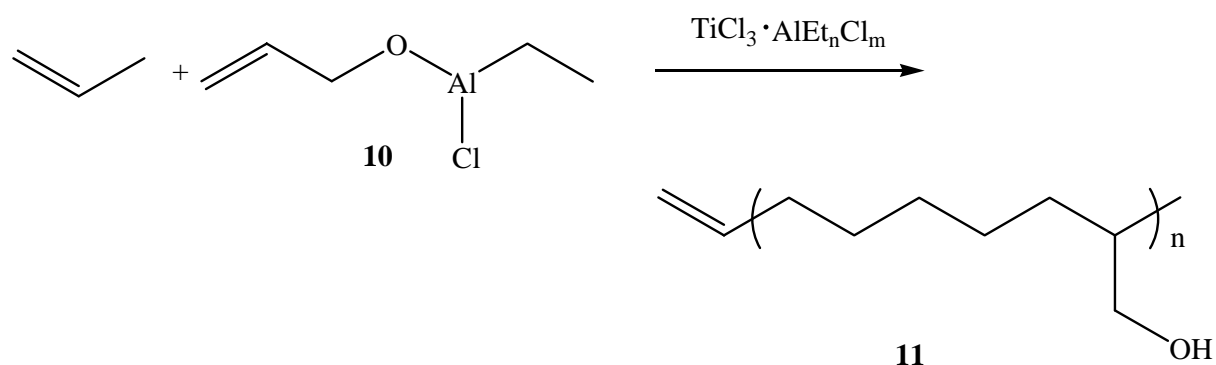
Table 1. Rating of the effectiveness of a catalyst based on its activity.

Rating	Activity
Very low	<1
Low	1-10
Moderate	10-100
High	100-1000
Very high	>1000

6.1 Ziegler-Natta metal catalyst

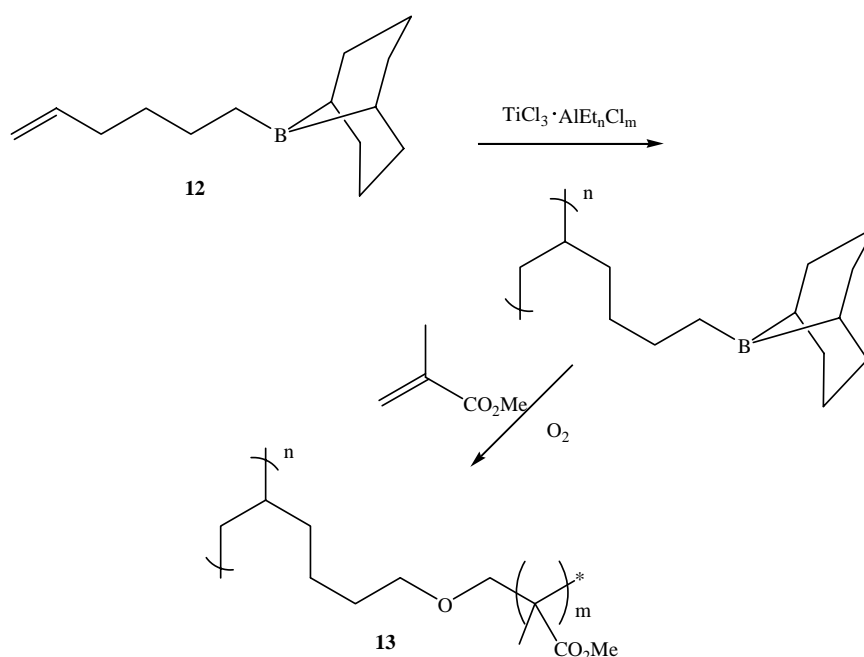
Ziegler and Natta (1955) discovered new catalyst for the polymerisation of α -olefins to produce many of the polyolefin products commonly called “plastics”^{2,35}. The Ziegler-Natta catalyst consists of a mixture of transition metal halides, especially titanium with organic derivatives of nontransition metals, particularly alkylaluminium compounds. This ill-defined mixture of the original discovery constitutes today the most dominant technology used in industry. However, due to their highly oxophilic nature, these catalysts are known for their intolerance to monomers containing functional groups, giving rise to problems such as depression of the catalytic activity, side reactions, mixtures of homo- and copolymers, low crystallinity products difficult for characterisation and low degree of comonomer incorporation, specially in the copolymerisation with ethylene³¹⁻³³.

Nevertheless, polymerisations and copolymerisations of functional groups containing vinyl monomers are reported to be possible with Ziegler-Natta catalysts. This succeeds when the Lewis basicity of the monomer is reduced by masking with aluminium alkyls or by adding silyl or other types of protecting groups on the heteroatom^{28,34-36}. Hagihara and coworkers³⁴ reported the use of α -olefins containing polar group as functional monomers in the copolymerisation with olefins (ethylene, propylene, etc.) in the presence of Ziegler-Natta catalyst system (scheme 8).



Scheme 8. Some of long-chain comonomers employed in the synthesis of functionalized polymer using a Ziegler-Natta catalyst.

The second alternative is the use of unconjugated dienes, *p*-methyl styrene or boranes **12** as comonomers in the preparation of reactive intermediate products that can be converted into functionalised product under mild reaction conditions⁹³⁻⁹⁵. For example, Chung and coworkers³⁸⁻⁴⁰ prepared functionalized polyolefins by using borane-modified monomers, which did not deactivate the conventional Ziegler -Natta catalysts.

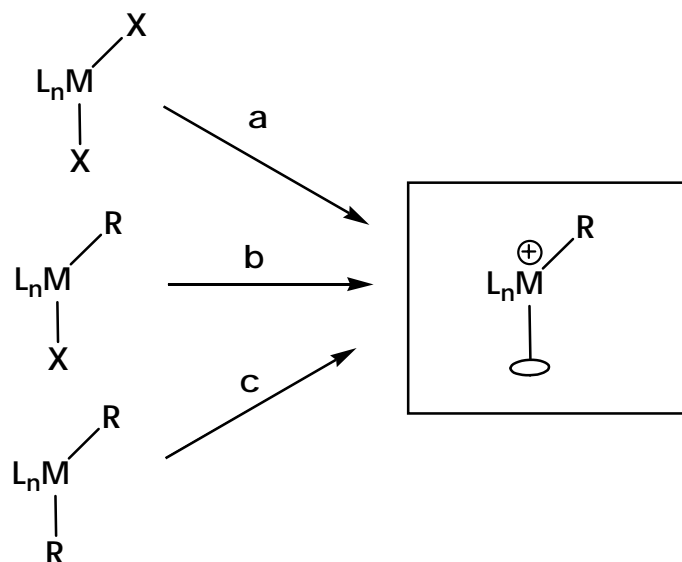


Scheme 9. The use of boron-functionalized monomers in polymerization.

6.2. Group 4 metal catalysts

The development of single-site transition metal coordination catalysts (metallocene and non-metallocene), offers significant advantages over the classical Ziegler–Natta complexes, such as the potential for steric protection of the active site through careful ligand design and the possibility of tailoring chain-process mechanisms to allow functionalities to be incorporated into the polymer^{28,41}.

These well-defined organometallic species activated with alkylaluminium cocatalysts have been used as homogeneous olefin polymerisation catalysts. Industrial interest was not sparked, however, until work by Sinn, Kaminski, Brintzinger, Ewen, Turner and others demonstrated that metallocenes combined with aluminoxanes led to long-lived catalyst systems with a very high activity⁴²⁻⁴⁶. Most important homogeneous catalysts have been based on early metal catalyst (the so called group 4 metals: Ti, Zr and Hf). Important to the success of these systems is the formation of a cationic metal center (L_nMR^+ , where L is a ligand, M is the transition metal center, R is an alkyl, hydrido or aryl group and X is a halide), which is both coordinately unsaturated and highly electrophilic (scheme 10)²⁹.



Scheme 10. Three different ways to the catalytically active species. \bigcirc represents the active site; **a)** Combination of alkylation and abstraction process; **b)** abstraction of an alkyl anion; **c)** abstraction of a halide ligand.

Simple σ -alkylphenyl complexes of group 4 transition metals, like $[Ti(CH_2C_6H_5)_4]$ or $[Zr(CH_2C_6H_5)_4]$, have produced active ethylene polymerisation catalyst when activated with

suitable Lewis acids cocatalyst such as methylaluminiumoxane (MAO) or $B(C_6F_5)_3$, but only moderate activities were obtained with these systems⁴⁸. Lower activities were also observed when monocyclopentadienyl trialkyl and aryl (aryl = C_6F_5) complexes **16** were used as catalyst ($60\text{-}80\text{ g}\cdot\text{mmol}^{-1}\cdot\text{h}^{-1}\cdot\text{bar}^{-1}$)⁴⁹⁻⁵¹. Monocyclopentadienyl titanium trichloride in combination with alkylaluminium cocatalysts is virtually inactive in olefin polymerisation because of a fast reduction of the titanium center⁴. One modification of a Cp ligand, formally obtained by the insertion of a B—Z unity into the Cp ring, was reported, resulting in a boratabenzene. Combination of zirconium complexes bearing boratabenzene ligands **17** with MAO have been reported by Bazan *et al.*⁵² Higher polymerisation activities are observed ($105\text{ g}\cdot\text{mmol}^{-1}\cdot\text{h}^{-1}\cdot\text{bar}^{-1}$). Interestingly, changing the Z substituent on boron from diisopropylamine to phenyl or ethoxide increases the rate of β -elimination, which results in the formation of lower molecular weight oligomers instead of polymers.

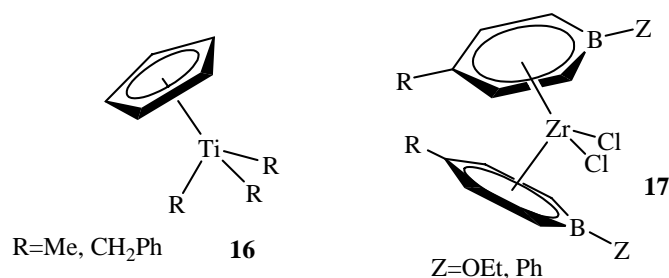


Figure 8. Group 4 precatalyst with alkyl and modified Cp ligands.

It also has emerged that group 4 metal complexes containing monodentate or bisamido ligands are promising systems for applications in olefin polymerisation catalyst. Based on the formal electron count, it is expected that the 10-electron complex $[(R_3N)_2ZrR]^+$ should be more electrophilic than the 14-electron $[Cp_2ZrR]^+$ complex, and consequently a more active catalyst fragment. Olefin polymerisation activities obtained with these complexes vary significantly from very low to moderate, and decrease in the order from **16** to **18a-c**²⁹.

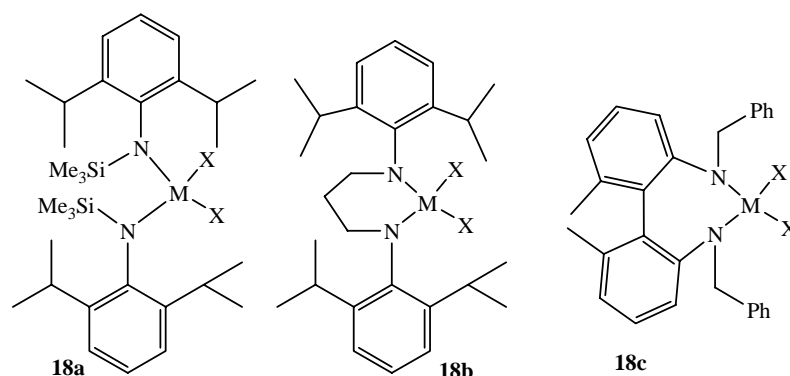


Figure 9. Group 4 pre-catalysts containing diimide [N,N] ligands.

Three different systems have been reported to date of a group 4 bis(amido) complex with an additional donor group, that is an amine pyridyl-, or ether donor- incorporated in the ligand system²⁹. The ligand systems planar-[N-,O,N-] complex **19** developed by Bochmann and co-workers have given moderate activities in the polymerisation of ethylene ($40\text{g}\cdot\text{mmol}^{-1}\cdot\text{h}^{-1}\cdot\text{bar}^{-1}$ respectively)⁷¹. However, an additional pyridyl donor between the amides groups (**20**) afford, both for Zr and Ti, very high activities ($1500\text{g}\cdot\text{mmol}^{-1}\cdot\text{h}^{-1}\cdot\text{bar}^{-1}$)^{53,54}.

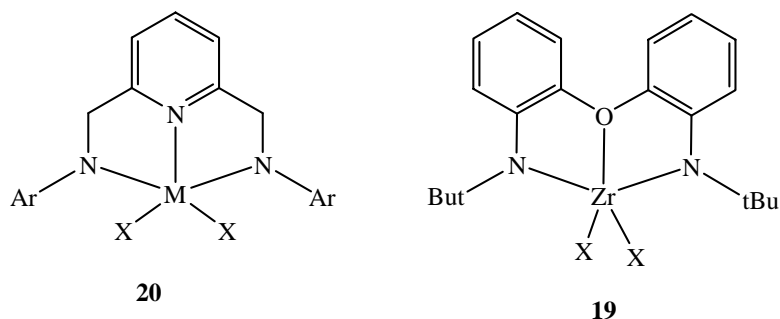


Figure 10. Group 4 complexes with diamide ligands that contain an additional donor.

An important class of olefin polymerisation catalyst has been developed at Dow and Exxon, by combining Cp ligands with an amide functionality [N-,C5-] to form a hybrid half-metallocene, the constrained-geometry catalysts (CGC: **21**, **22**, figure 11). Very high catalytically activities in the polymerisation and copolymerisations were reported when these catalyst are activated with MAO ($1500\text{g}\cdot\text{mmol}^{-1}\cdot\text{h}^{-1}\cdot\text{bar}^{-1}$)⁵⁵. Like metallocenes, these constrained-geometry catalysts have been subject of several theoretical studies and their development for commercial exploitation is under investigation^{4,56,57}.

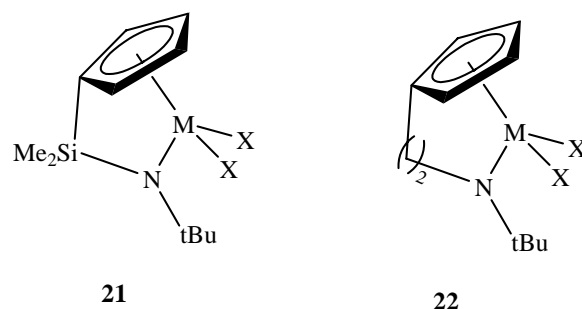


Figure 11. Group 4 catalysts with half-sandwich amide ligands.

6.3 The Phillips and Union Carbide heterogeneous metal catalysts

Group 6 heterogeneous catalysts play a central role in the commercial production of polyethylene. The Phillips catalyst, discovered as early as 1958 by Hogan and Banks, uses a silica support treated with CrO_3 , subsequently reduced to a low valent species that is the active catalyst. By contrast, the Union Carbide catalyst uses silica treated with divalent chromocene; both systems are very highly active. The precise structure of the active site of these systems is still to be elucidated. Maybe the closest model is compound **23** (figure 12) reported by Feher and co-workers^{134,135}, which contains a chromyl fragment supported by two vicinal silyloxy groups of a polyhedral oligosilylsesquioxane^{29,58,59}.

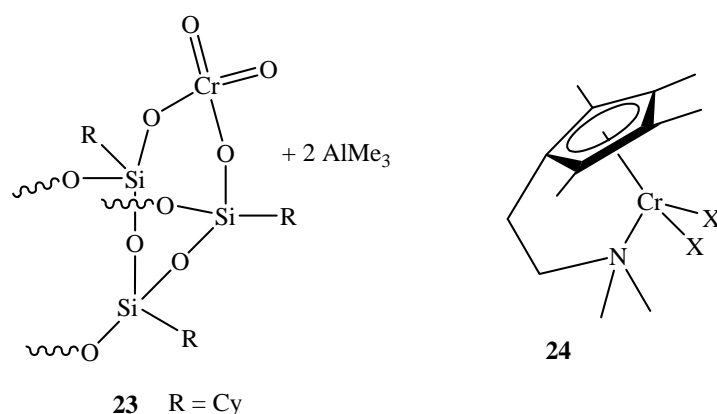


Figure 12. Chromium catalyst for olefins polymerization.

This precatalyst contains a chromium (VI) site and the reduction of Cr(VI) with Me_3Al used as cocatalyst allows the formation of the active catalyst which is believed to be a Cr(III) species. In academic research, Theopold et al. have reported a very highly active catalyst

obtained when a constrained-geometry catalyst complex **24** was treated with as few as 100 equivalents of MAO. Activities as high as about $8300 \text{ g}\cdot\text{mmol}^{-1}\cdot\text{h}^{-1}\cdot\text{bar}^{-1}$ are reported⁶⁰.

6.4 The Brookhart-Gibson and the group 8 metal catalyst

The first application of an iron species as catalyst for olefins polymerisation reaction was reported almost at the same time by Gibson and Brookhart in 1998^{61,62}. In both cases, the active species were generated from iron complexes bearing 2,6-bis(imino)pyrididyl ligands **25**, in which the imino nitrogens had bulky ortho-substituted aryl groups.

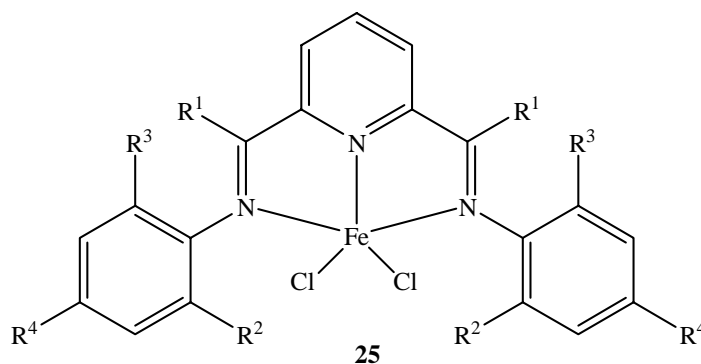


Figure 13. The Brookhart and Gibson iron diimide(pyridine) complex.

Treatment of **25** with MAO or modified methylaluminoxane (MMAO) afforded the active catalyst, which showed a very high activity coupled with a remarkable selectivity, considering that, in contrast with catalysts of the same ligand with other metals, only linear polyethylene were obtained. It should also be noted that the results obtained with iron proved to be superior to those obtained with a similar cobalt species under the same conditions^{61,62}. In the polymerisation of ethylene, the molecular weight of the polyethylene material generated shows a remarkable dependency upon the aryl substituent pattern. High selectivity for the production of α -oligoolefins was observed when the aryl substituent on the nitrogen groups contains only one small ortho substituent⁶¹⁻⁶⁴. Supplementary striking aspect of the catalytic system was found when two bulky ortho substituents (tert-butyl or aryl groups) are present on the aryl substituent; in this case very high molecular weight polyethylene was formed. ¹³C-NMR analysis of these materials reveals saturated end groups in addition to low levels of vinyl unsaturations⁶⁴. This is consistent with a termination mechanism involving alkyl-group chain transfer to the aluminium cocatalyst, in addition to β -H transfer (to monomer or metal);

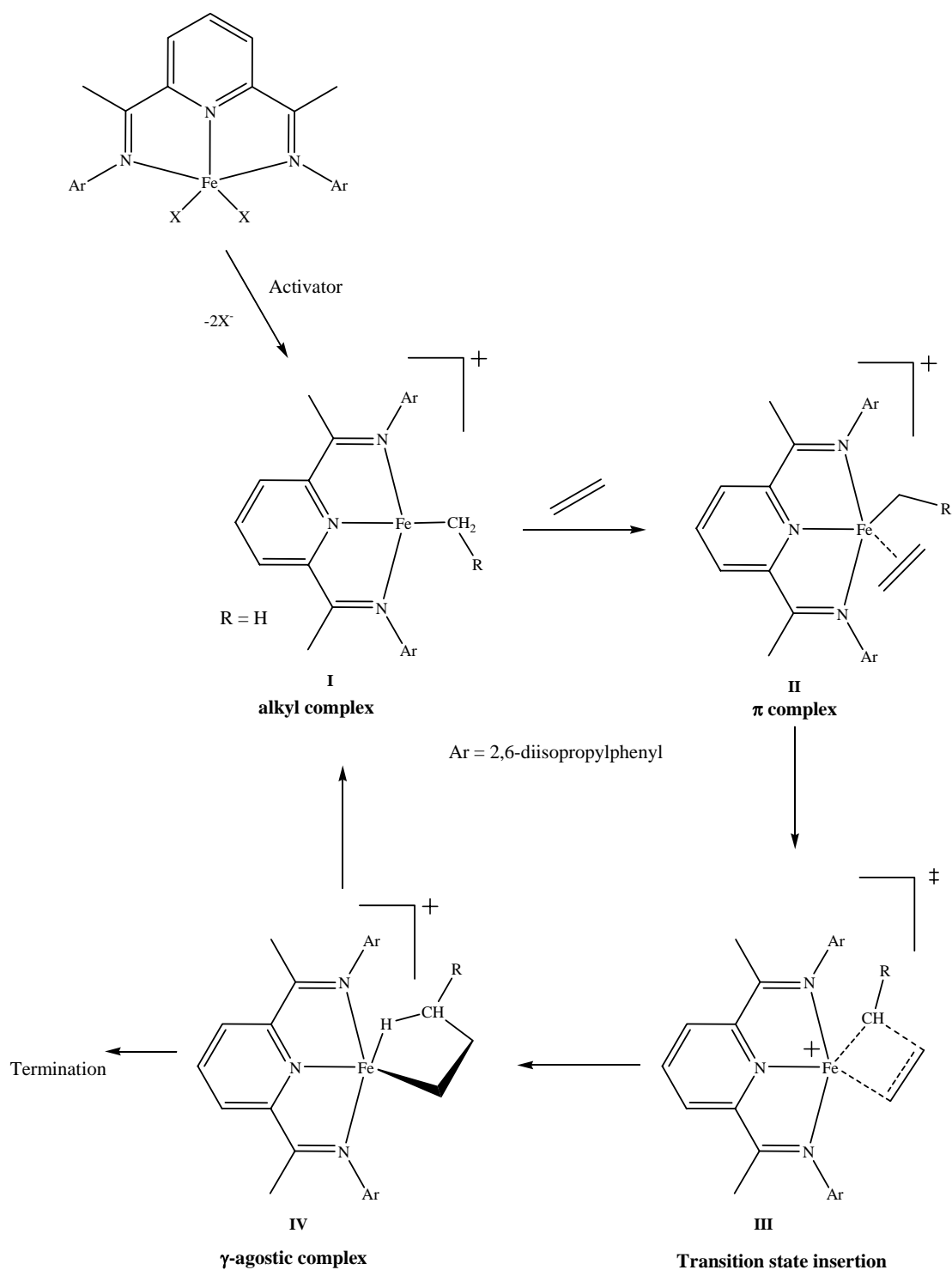
the ratio between the rates of them is influenced by both the structure of the catalyst and the reactions conditions (scheme 11). Interestingly, if the corresponding ortho positions bear only small alkyl groups (like methyl or ethyl) or no substituent at all, the system can be used to perform head-to-head dimerization of α -olefins, the linear product being the preferred¹⁵³.

The molecular weight of the obtained polymer is also dependent of the precatalyst/cocatalyst ratio and the ethylene pressure. Oligomers were formed when the later is increased¹⁵⁴.

As consequence of its unique feature, this system has been subjected to many detailed theoretical studies, directed both to establish the structure of the actual catalyst and to clarify some mechanistical aspects of this process^{3,29,65}.

Unfortunately, despite these investigations, the mechanism of the reaction remains in part still unclear. By analogy to group 4 and 10 metal systems, the formation of 14-electron cationic iron(II) alkyl species was initially presumed upon activation with MAO^{64,67}. A number of theoretical studies were proposed based on this assumption^{65,66,68,69,70}.

Gibson and co-workers have suggested the first theoretical studies on this catalyst system, the key features of the reaction pathway (**I-IV**) are depicted in the scheme 11. It can be pointed out that the level of agreement between the gas phase calculated bond parameters and the experimental data is generally good⁶⁶.



Scheme 11. Proposed intermediates and transition states (TS) of the ethylene polymerisation with the Brookhart-Gibson catalyst via a π complex of the monomer, TS for insertion, and γ -agostic complex with an extended polymer chain.

Various modifications to the original bis(imino)pyridine ligand framework have been reported in the literature⁷¹⁻⁷³. Changing the aryl group on the nitrogen to amino **26** and heterocyclic moieties was recently reported by Gibson and co workers and the resulting catalyst from the activation of the corresponding iron(II) complexes with MAO shows good activities in the polymerisation of ethylene, even if the results were not comparable with those obtained with the catalyst **25**. Electrowithdrawing and electrodonating effects on the aryl substituents at the nitrogen was reported to produce moderate to low ethylene polymerisation activity^{73,74}.

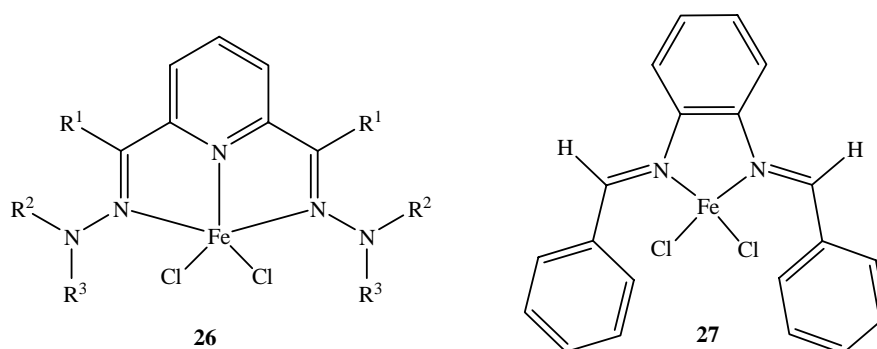
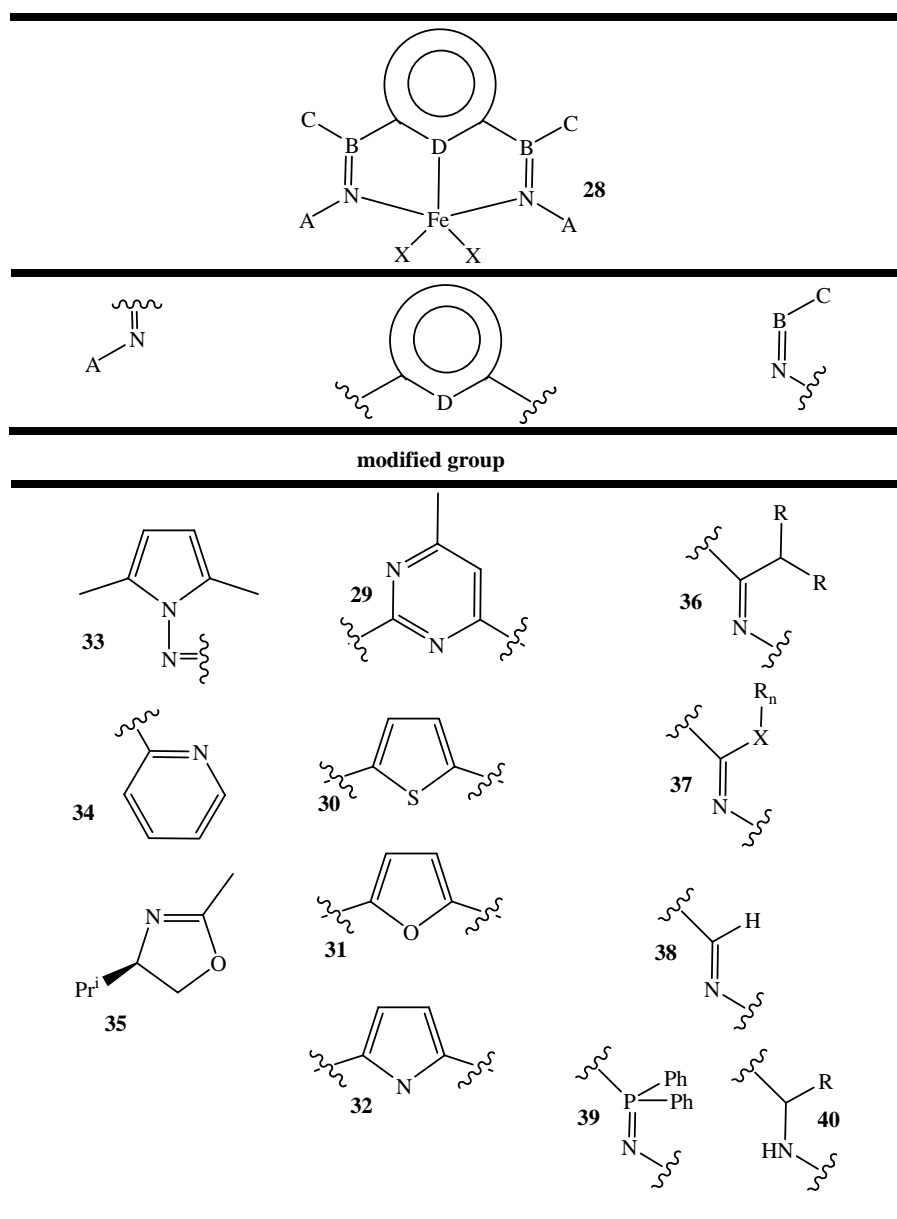


Figure 14. Ligand modification on the originally Brookhart-Gibson catalyst.

Further variations (table 2) such as introduction of donor groups on the bridged pyridyl, replacement of the bridging pyridyl moiety with non functionalised aryl groups, or with five membered rings with donor atoms like thiophene, pyrrolide and furans^{71,74} have been reported, here again the obtained result remain lower as compared to the original precatalyst, in the case of the thiophene (**30**) no activity was observed. For example the substitution of the central pyridine donor for a pyrimidine ring (**29**) resulted in a slight reduction of activity and the formation of a polymer with narrower polydispersity and an increased proportion of unsaturated end groups.

Table 2. Some of structural modifications on the Bis(imino)pyridine iron precatalysts **25**.



The use of ammonium [tetrakis(pentafluorophenoxy)borate] as cocatalyst instead of usual aluminium species and employment of diimine iron(II) complexes such as **26** together with ethylaluminumoxane (EAO), dibutylaluminumhydride (DIBALH) have been described, but once again the originally reported remain unmatched⁷⁵. An isolated example of a tandem catalytic system based on iron and zirconium is present in the literature. By combining the action of an iron complex of type **41** (with $R^1 = \text{Me}$, $R^2 = \text{Et}$, $R^3 = R^4 = \text{H}$) with one Britzinger-type zirconium complex **42** (figure 15), only the branched polyethylene is obtained in the presence of

ethylene as the only monomer. Polar olefins such as methyl methacrylate, vinyl acetate, acrolein and acrylonitrile led to the deactivation of the bis(imino)pyridine iron catalysts⁷⁶.

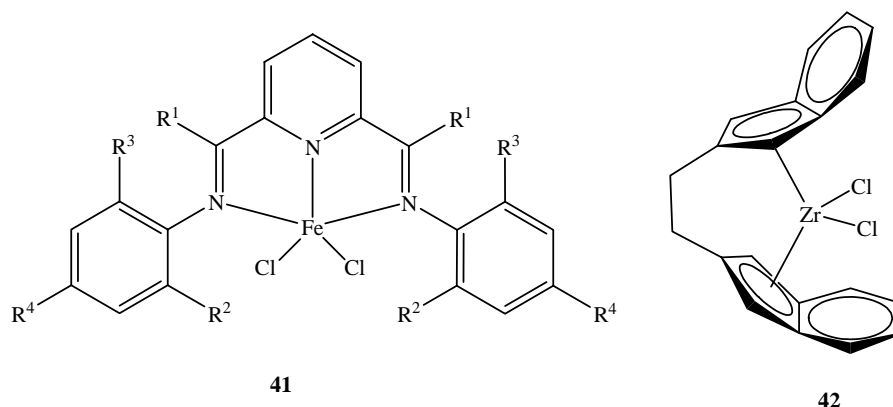


Figure 15. Britzinger-type zirconium complex **42**.

Yamamoto et al. reported the polymerisation of functionalized vinyl monomers by iron complexes, e.g. complex **43**, which does not show any ethylene polymerisation activity. This complex was used as catalyst for acrylonitrile polymerisation, affording 57% conversion in five minutes. Complex **44** is known to polymerise a range of monomers including methyl methacrylate, acrolein, methyl vinyl ketones and acrylonitrile^{29,78}. The mechanism is proposed to be by coordinative pathway involving the partial dissociation of one 2,2'-bipyridyl ligand. Conversion rates are low and ethylene is not polymerised⁷⁷.

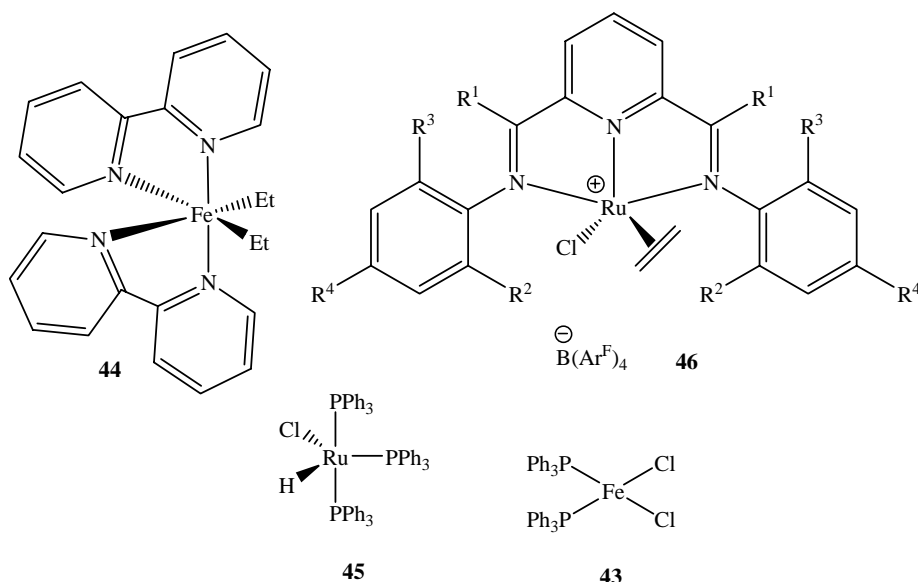


Figure 16. Iron and ruthenium complexes used in olefins polymerisation and copolymerisation.

The complexes of higher homologue bis(imino)pyridine ruthenium (II), such as **46** ($\text{Ar}^{\text{F}} = 3,5\text{-}(\text{CF}_3)_2\text{C}_6\text{H}_3$) are unreactive toward olefins⁷⁴.

6.5 Palladium phosphine catalysts (Group 10)

For various reasons the discussion about the successful use of organometallic complexes as catalysts in polymerisation reactions, would not be complete without referring the copolymerisation of ethylene with carbon monoxide, which yields perfectly alternating polyketones.

One of these reasons is that carbon monoxide is an accessible and cheap monomer and the final products are low cost polymers. Moreover, polyketones have interesting properties: they are thermal plastics, photo and biodegradable and, they can be starting material for a variety of functionalised polymers due to the chemical transformation of the carbonyl groups⁷⁹⁻⁸². The demand of thermoplasts with high performance properties has increased due to their strength, toughness, wear resistance, chemical resistance, UV stability, etc. Application of these materials includes the automotive components such as gears, fittings, fibres, packaging containers, etc.⁷⁹. The permeability of HDPE used as fuel tank to gasoline can be avoided by using these alternating polyketones materials. Shell and more recent BP have commercialised polyketones as aliphatic termpolymers (CO/alkene1/alkene2; Carilon® and Ketonex respectively).



Scheme 12. Alternating CO/alkene copolymerisation.

The first catalyst that was active in the alternating copolymerisation of carbon monoxide and ethylene, was a nickel complex of formula $\text{K}_2[\text{Ni}(\text{CN})_4]$ ^{80a}. This homogeneous copolymerisation catalyst system provided greater control of the polymer than polymerisation initiated via free radicals or γ -rays. However, the essential improvement to the efficient synthesis of polyketones at industrial level came with the discovery of the combined importance of using bidentate ligands and weakly coordinating anions in catalytic systems of

the type $\text{PdX}_2(\text{L-L})$ where (L-L) is a bidentate phosphine and X a weakly or non coordinating anion^{80a,83,84}.

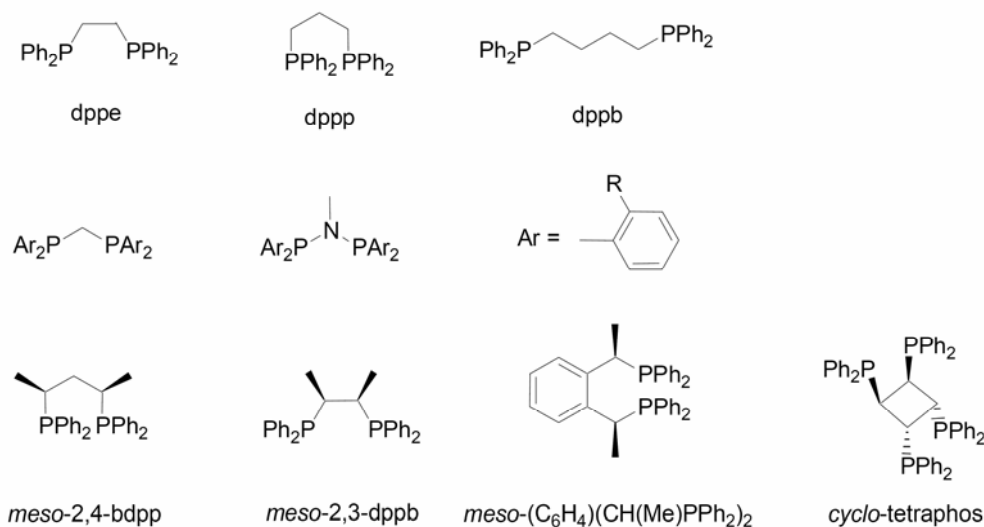
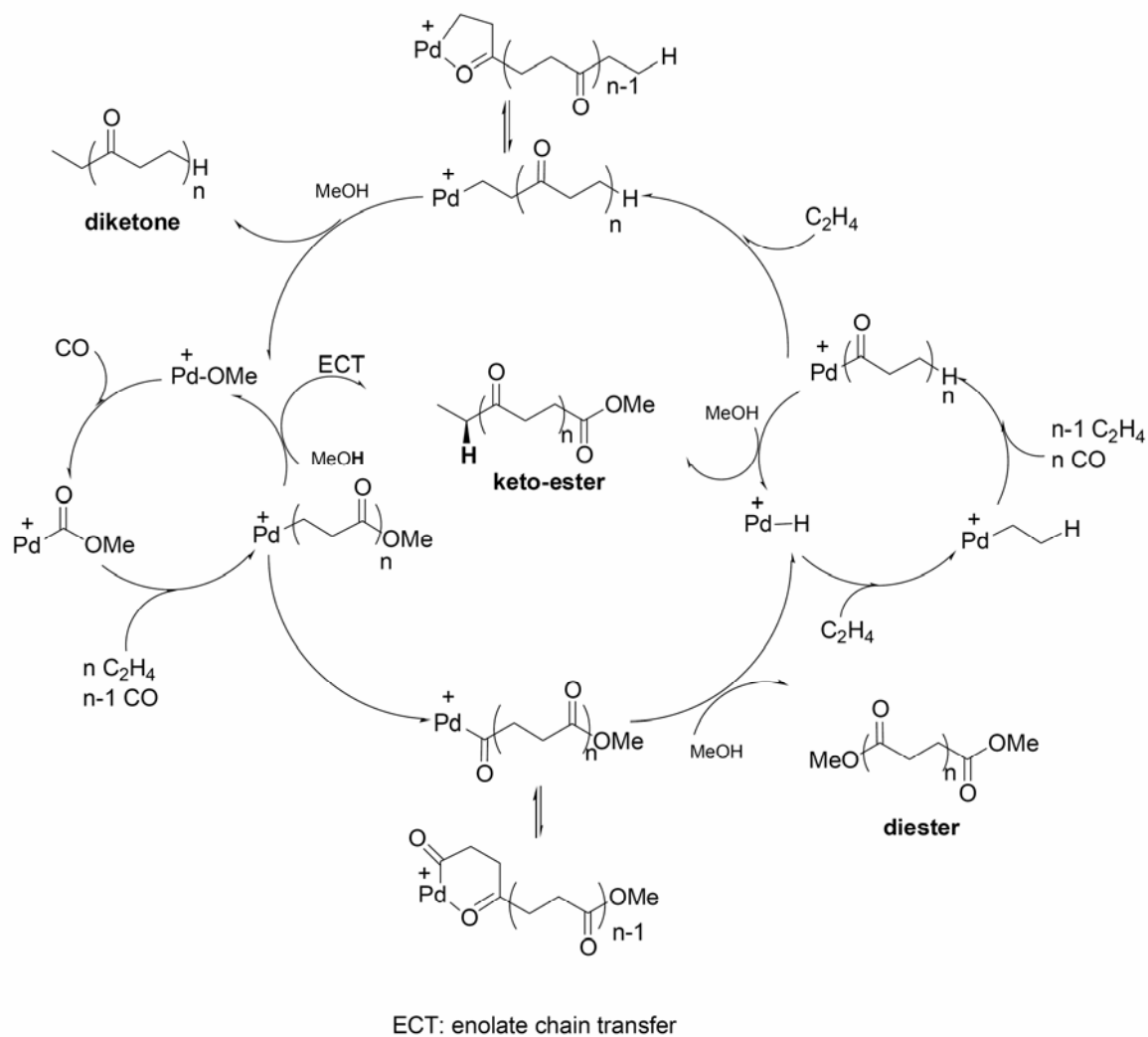


Figure 17. Commonly diphosphine ligands used in CO/ethylene copolymerisation.

The propagation steps in the copolymerisation of carbon monoxide with alkenes by cationic palladium diphosphine complexes are now well understood^{79,80,84}. The mechanism for copolymer chain growth involves two sequential propagation steps: migratory CO insertion into the palladium-alkyl bond of the growing polymerchain followed by migratory ethene insertion into the resulting palladium acyl-bond. Notable recent studies were done by Van Leeuwen and Zuideveld⁸⁴, Bianchini and Iggo⁸⁵ that have consisted in identifying some or all of the intermediates involved in chain transfer by hydrolysis of the acyl and alkyl intermediates.



Scheme 13. Proposed mechanism for the copolymerisation of CO/ethylene in methanol⁸⁴.

7 The scope of this work

The potential of iron complexes as polymerization catalysts has been established by Brookhart and Gibson^{61,62}. Modifications of the original tridentate diimine pyridine ligand have been reported, but are limited to minor changes if the catalytic activity is to be preserved. For this reason, we set out to prepare new iron complexes containing more electron-donating and bulky bis-N-heterocyclic carbene ligands (**47-49**). We will focus our attention on the synthesis, the structural features, and the use of these carbene complexes in hydrogenation and polymerization of olefins.

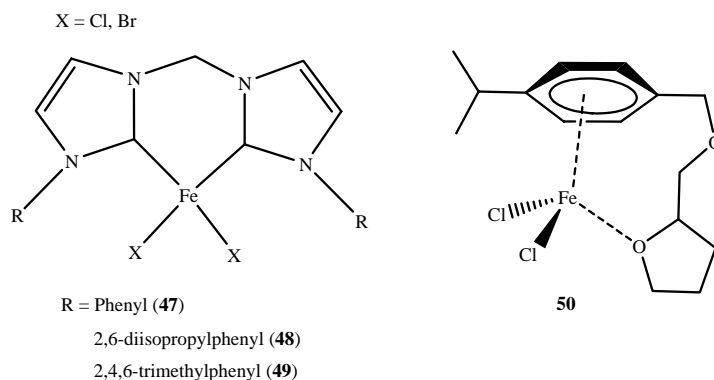


Figure 18. The expected iron(II) complexes

The chemistry of electrophilic metal carbene complexes attracts considerable attention since they offer the possibility of the development of new types of organometallic intermediates that may have unusual reactivity. Thus, a number of metal complexes containing N-heterocyclic carbene ligands have been prepared. However, only two examples of them contain iron(II) as metal were reported and their potential in catalysis have never been examined.

The aim of this work was also to study the synthesis and the reactivity of complexes of proposed structure **50**. Indeed, more recently Raemy⁸⁶, studying the reactivity of arene iron (II) chloride complexes found that these compounds were excellent precatalysts for hydrogenation of olefins, oligo- and polymerization of acetylenes after activation with LiAlH_4 , BuLi or DIBAH. However, the presence of an additional labile ligand such as ethylene or THF is required. In an attempt to link this auxiliary ligand to the arene, we synthesized and tested a series of compounds including the benzyletherfurane ligand shown in the structure **50**.

II. Results and discussion

II-1.Strategy

8. General strategy

8.1 Olefins polymerization strategy

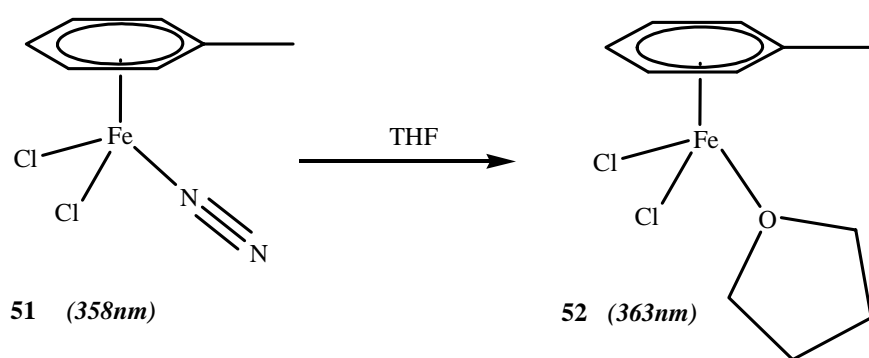
Our original approach for the development of new types of iron polymerization catalysts build on the screening of iron complexes for homogeneous hydrogenation activity, since both reaction types involve similar elementary steps. This relation between hydrogenation and polymerization results from observations of Raemy⁸⁶ and Sieber⁸⁷ during their thesis work with diimine iron(II) complexes used as catalysts for olefin hydrogenation, polymerization and carbon – carbon coupling reactions.

Another important point of our strategy concerns the reactions conditions for both reactions, which appear in general as very mild (2-3 bars, RT) compared to some of present commercial processes based on high-pressure technology^{2b}. There exists thus, a undeniable technological requirement for new meal based catalyst capable of polymerization and copolymerization under low temperature / pressure conditions.

The last point concerns the choice of an *in situ* activator. Instead of large quantities of methylaluminoxane (MAO), the commonly used compound for the activation of precatalysts in polymerization reactions, we prefer to use other reagents such as BuLi or DIBAH. The potential of these compounds for alkyne polymerization and hydrogenation was already studied by Raemy⁸⁶, giving high activity in both reactions.

8.2 Iron Benzyletherfuran complexes

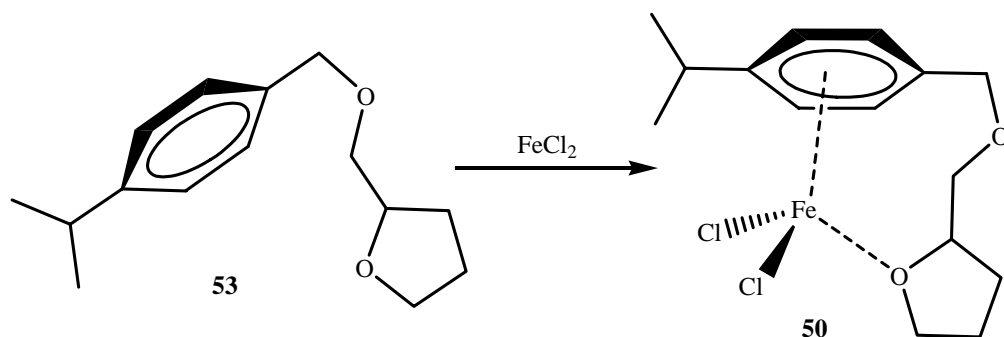
During his thesis, Manuel Raemy⁸⁶ has described a possible existence of the (toluene)iron complex **51** resulting from the treatment of FeCl₂ in toluene under permanent nitrogen bubbling through the reaction mixture. This discovery is important since Fe-N₂ complexes play an important role in biological and industrial nitrogen derivatisation⁸⁶. The UV-Vis spectrum of this material in toluene shows two maxima at 358 nm and 315 nm. This double band was taken as confirmation for the formation of the proposed compound. Additionally, when the UV-Vis spectrum was taken in THF the absorption at 358 nm was slightly shifted to a higher value, 363 nm. This bathochromic shift was assumed due to an exchange of the labile nitrogen ligand with a THF molecule **52** (scheme 14).



Scheme 14. Nitrogen ligand exchange occurred in THF solvent

All attempts to isolate these compounds failed and the use of NMR and MS experiments were unsuccessful; indeed the product decomposes during the measurements. It is important to note that when the reaction was done under argon conditions, the UV-Vis spectra of obtained material show only singular weak absorption.

Since the isolation and characterization of the presumed $\text{FeCl}_2(\text{THF})\text{toluene}$ compound was not possible, it was of interest for us to develop a new type of ligand containing both strong and weak donor groups. The choice was directed to a bidentate ligand in which the tetrahydrofuran moiety was attached to the aryl group via an ether link resulting in the chelate- or tweezers-like benzyletherfuran ligand **53**, thus the linkage would prevent the dissociation of the weakly coordinated furan from the metal in complex **50** by the chelation effect.



Scheme 15. Chelate benzyletherfuran ligand and their complex with FeCl_2 .

Furthermore, the hemilabile arm of such ligands provides the capability to do reversible dissociation from the metal center⁸⁶. Such a dynamic behaviour will produce vacant coordination sites that allow complexation of substrates during the catalytic cycle. At the same time, the strong donor moiety remains attached to the metal center. To our knowledge there is no report in literature concerning complexes of iron(II) with both chelating aryl and dangling donor tetrahydrofuran groups.

8.3. N-heterocyclic carbene ligands (NHC)

It is in generally agreed, that the catalytically active species in olefin polymerisation is a coordinatively unsaturated electrophilic alkyl complex. According to that we have based our strategy on the synthesis of formal 14 electrons tweezers N-heterocyclic carbene iron(II) complexes which, activated under certain conditions, will provide the cationic catalyst. Furthermore, we hypothesize that combining the stronger ligand binding arising from the chelating effect with increase steric bulkiness could improve the catalytic activity by preventing decomposition of highly reactive intermediates.

On the other hand, it is already known that N-heterocyclic carbenes (NHC) form highly active and stable catalysts for various reactions such as C-C coupling (Heck, Sonogashira, Suzuki, etc.), hydrosilylation, olefin metathesis, C-H activation, hydroformylation and cyclopropanation, among many others⁸⁸.

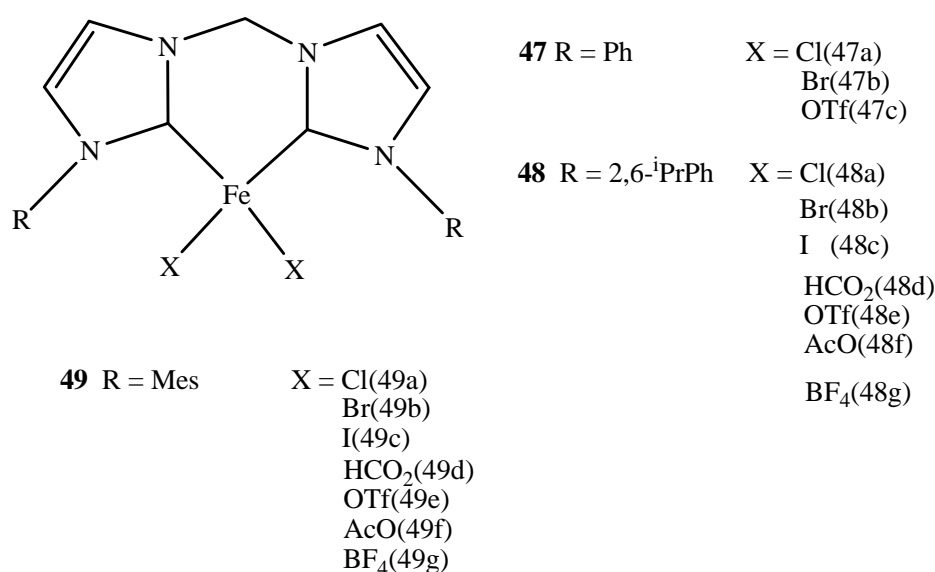


Figure 19. Complex design of expected iron(II) bis-carbene NHC complexes.

- The choice of NHC's is due to their strong donor properties, which are enhanced by the diversity of substituents on the nitrogen atom. It is thus possible to combine strongly functionalized substituents on the nitrogen atom, which can modulate the electronic properties of the metal center or impose a particular stereochemical environment in the ligand sphere of the central metallic atom.
 - Tweezers type imidazolydine-derivatives have been taken because of the stability that they confer to the complex as a consequence of combining a high chelate entropic effect with the strength of Metal-Carbene bonds for low-valent late transition metals^{89,90}. In fact, carbenes are no dissociative ligands as compared to phosphine ligands. Herrmann and co-workers⁹¹ reported theoretical dissociation investigations of various non-chelate and chelating bis-N-heterocyclic carbenes ligands. Concerning the opening of a biscarbene palladacycle, they conclude that a six-membered chelating opening is energetically slightly more disfavoured than the dissociation of the corresponding monodentate carbene ligand and requires +50.2 kcal/mol. In all cases the NHC's complexes suggest very high binding energies which mainly originate from a largely electrostatic ligand-to-metal σ -donor interaction with only little π back-bonding. In contrast, phosphines are in general considered to have non-negligible π -acceptor and σ -donor ability.
 - The necessity to employ sterically demanding substituents when using heteroatom donor was illustrated by the work of Brintzinger and Brookhart^{62,63}; they ensure the protection of the active site and reduce or avoid, in the case of polymerisation, the probability of β -elimination which is responsibly for lower molecular weight polymers.
 - The introduction of a methylene bridged between two carbene unities is not only to assure the *cis*-geometry of the complex, but there is also the possibility to modify that position by introduction of strongly functionalized substituents in order to facilitate electronic tuning on the metal center. For example, substitution of methylene protons by an electrodrawing groups such as trifluorocarbon ($-\text{CF}_3$) or electrodonating moieties for example methoxy ($-\text{OMe}$), could result in dramatic changes of the reactivity of the corresponding complex.
- Figure 20 depicts different positions of a Tweezers NHC ligand, which could be modified; some of those modifications are already reported in the literature⁹¹⁻⁹⁷. In this study, we have restricted our research to the substitution at position *I* because we are convinced that the presence of bulk aryl groups on this position not only plays an important role in the stability of the complex, but as well as previously evoked, they ensure the protection of the active site

during the catalytic reaction. In addition, modification on this position could be easily accomplished by the well-established synthetics routes.

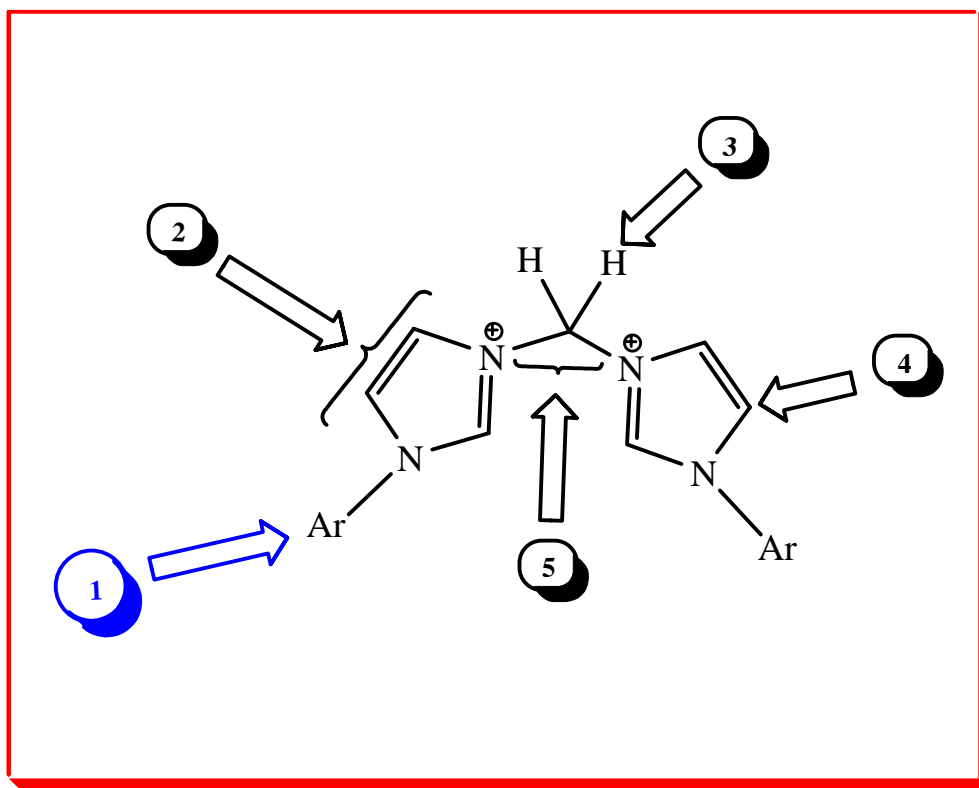
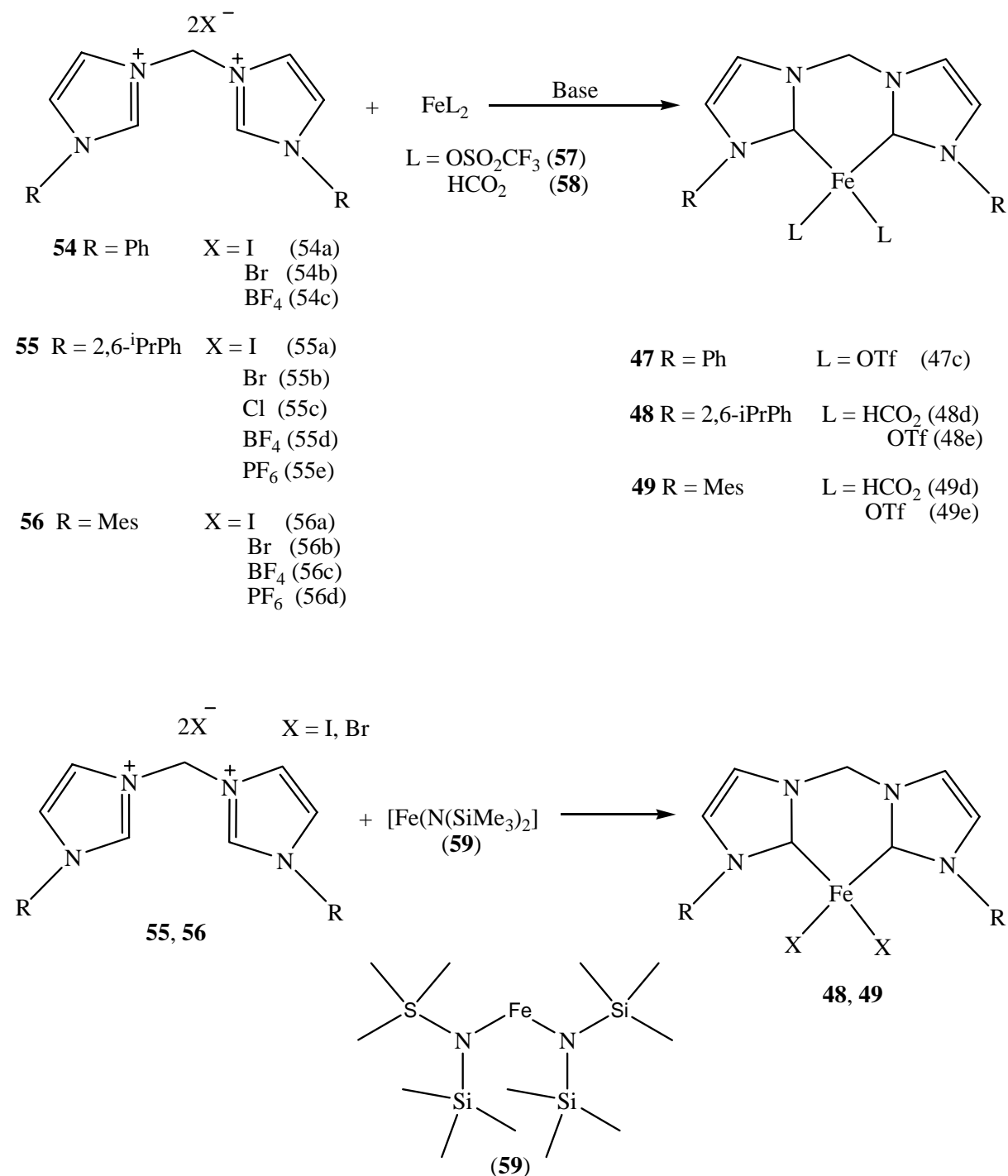


Figure 20. Possible substitutions on bis N-heterocyclic imidazolium patterns.

8.4. Strategy for the synthesis of iron(II) biscarbene NHC's complexes

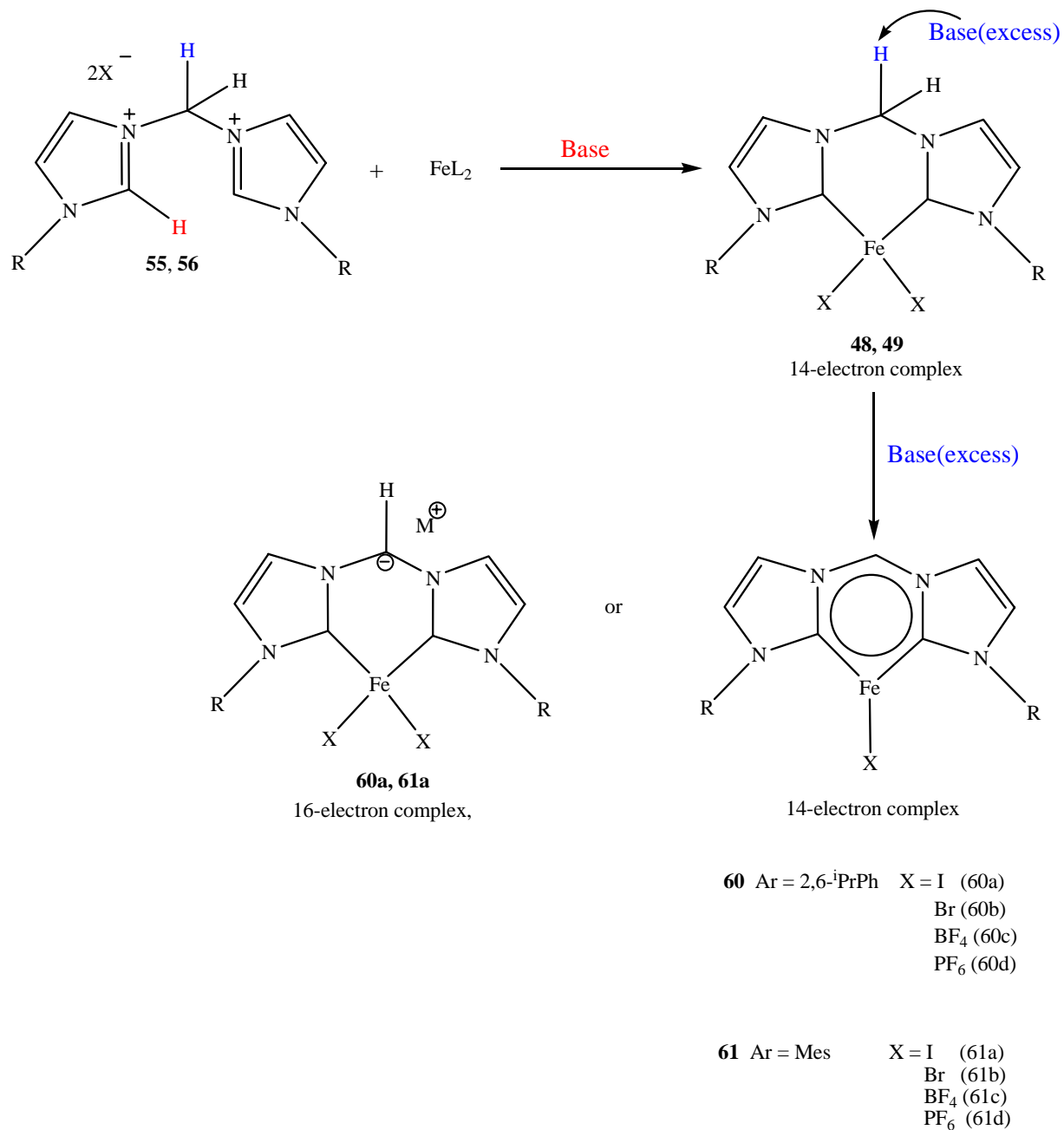
We propose three different approaches for the synthesis of complexes **47** – **49**: I) Interaction of an iron precursor complex with the N-heterocyclic carbene generated in situ from the reaction of the corresponding imidazolium salt and sodium hydride, potassium *tert*butoxide or amide bases in an inert solvent, the reafter referred to as *direct metallation*. II) Interaction of an iron precursor complex with the free carbene N-heterocycle in an inert solvent, the so called *standard synthetic routes*. III) Reaction of iron precursors with *silver carbene* reagents, resulting in a mild and quantitative transmetallation.

I) Direct complexation is the reaction of a bisimidazolium salt with an adequate iron(II) precursor, for example $\text{Fe}[\text{N}(\text{SiMe}_3)_2]_2$ or with iron(II) salts source such as $\text{Fe}(\text{OSO}_2\text{CF}_3)_2$, $\text{Fe}(\text{OOCH})_2 \cdot 2\text{H}_2\text{O}$ in the presence of a supplementary base (NaH, n-BuLi, ^tBuOK, ...).



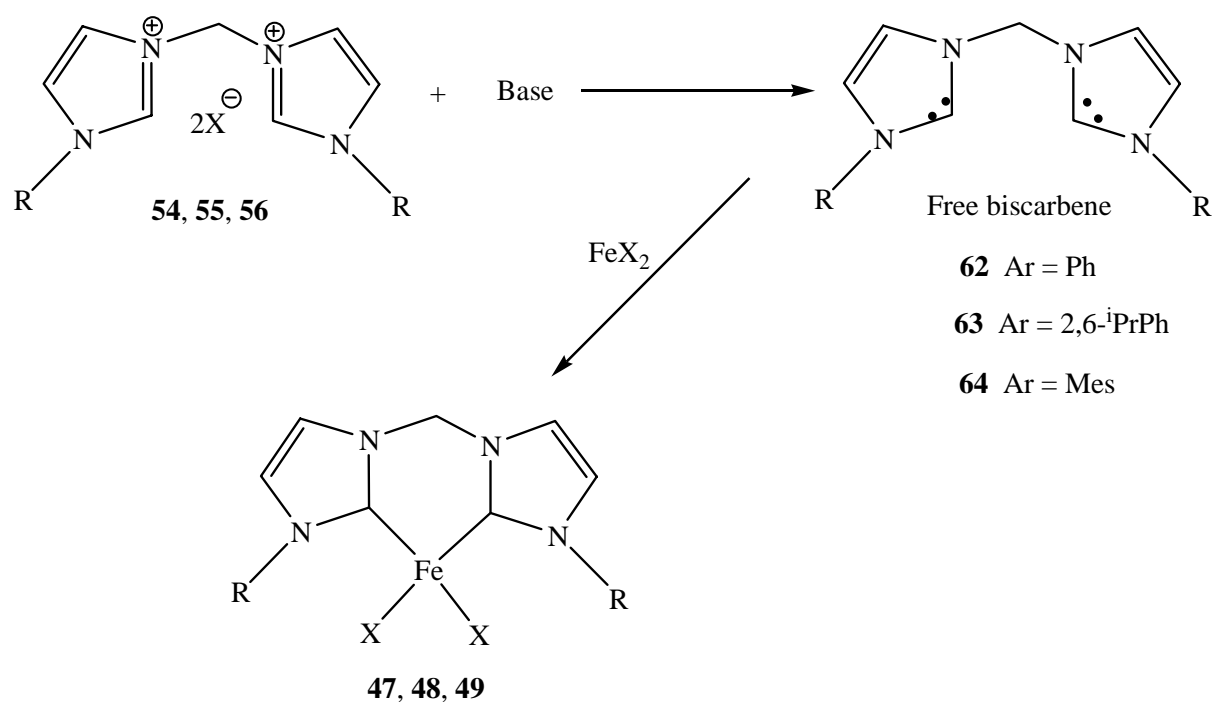
Scheme 16. Direct metallation.

Due to the probably high acidity of the linking methylene protons, this position could be deprotonated during the treatment, allowing the formation of a so far unknown 16 electron complex of iron(II), which remain still a potentially active precatalyst for olefin polymerisation.



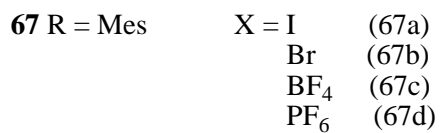
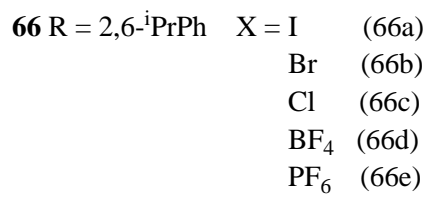
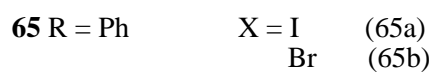
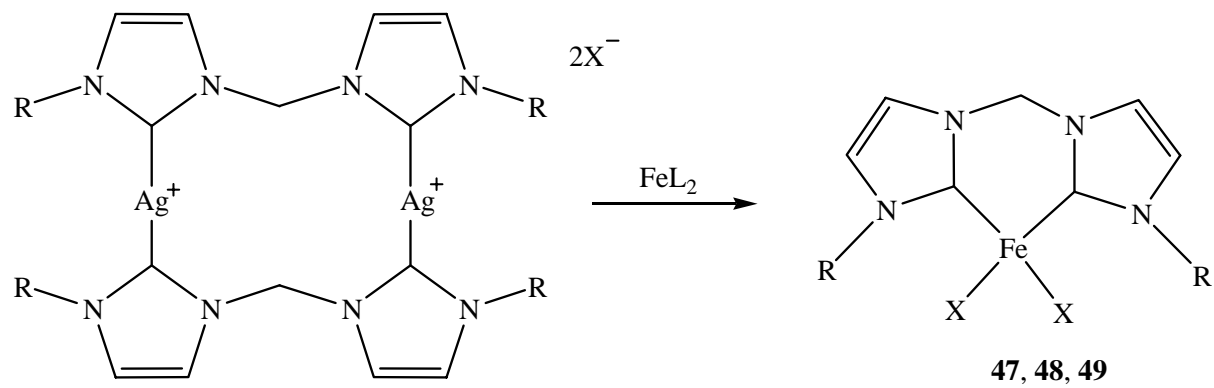
Scheme 17. Deprotonation of the acidic proton on the methylene bridge.

II) Free carbene: the second approach is based on the preparation of the free carbene ligand from the imidazolium salt followed by its reaction with an appropriate iron (II) halide source.



Scheme 18. Synthesis of the Fe(II) NHC complex via free carbene ligand.

III) Silver complexes: The last approach is based on the use of air stable silver N-heterocyclic carbene complexes as ligand transfer reagents for the synthesis of the desired iron (II) compounds. This approach, if commonly applicable, provides a very convenient method for the formation of carbene complexes and overcomes many difficulties arising from the use of strong bases to generate free carbene ligands.

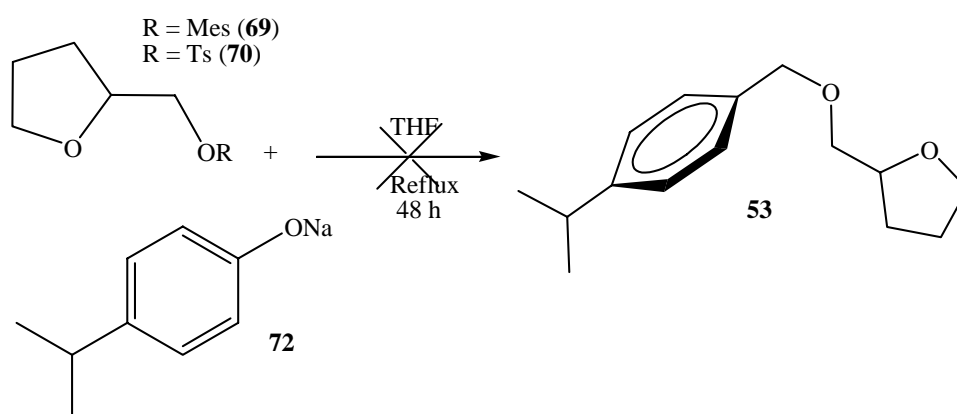


Scheme 19. The transmetalation approach involving silver complexes.

II-2. Benzyletherfuran complex of iron(II)

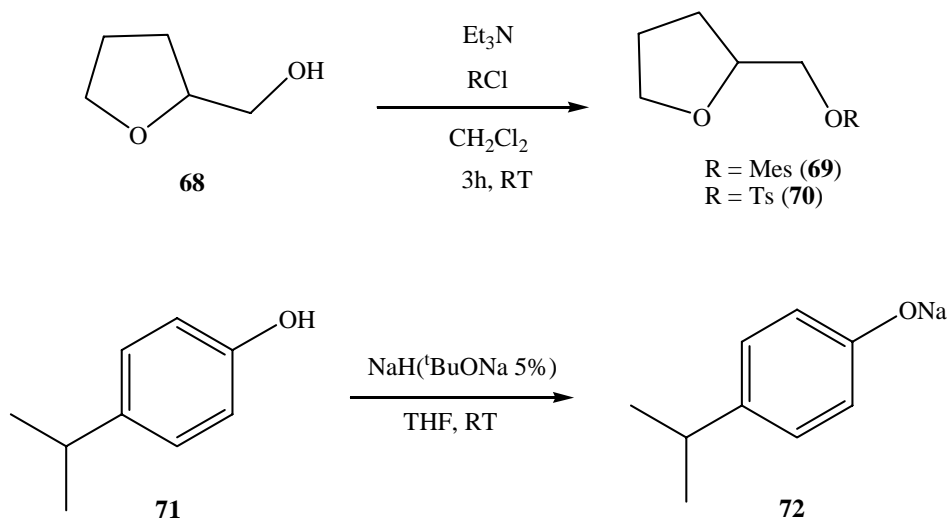
9. Benzyletherfuran complexes of iron(II)

9.1. Synthesis of 2-(4-isopropyl(benzyloxymethyl) tetrahydrofuran **53**



Scheme 20. Synthesis of **53**.

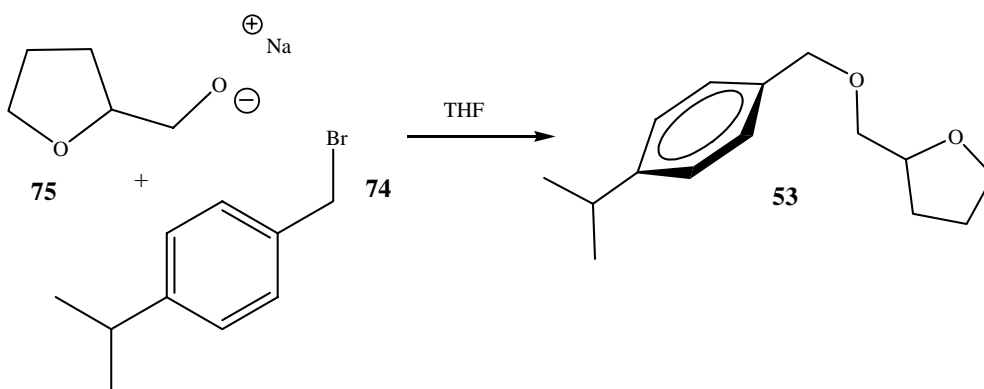
Our first strategy for the preparation of ligand **53** consists in reacting a furfurylmesylate **69** or furfuryltosylate **70** with an *in situ* deprotonated phenol **72** (scheme 20). The furfuryl alcohol **68** was converted to a good leaving group by reaction with mesylchloride in ether affording the desired product as colourless oil **69** in 85% yields after purification by column chromatography with silicagel. We did also the corresponding tosylate **70**, which was formed as a white solid in a quantitative yield. Phenolate **72** was prepared without isolation, by reaction of phenol **71** with NaH in THF; the reaction was monitored following the hydrogen gas evolution.



Scheme 21. Synthesis of compounds **69**, **70** and **72**.

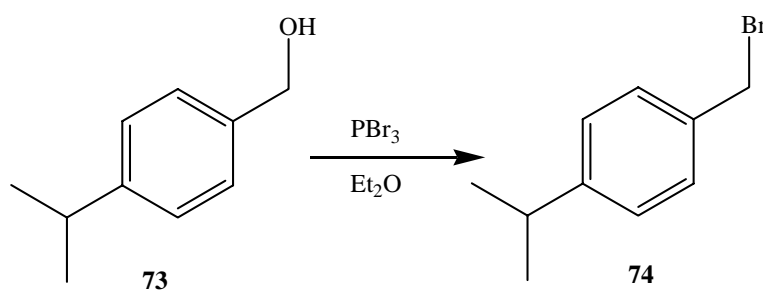
However, the reaction of mesylate **69** or tosylate **99** with alcoholate **72** in THF at RT or at reflux temperature did not yield the desired compound **53**, only the starting materials were recovered (scheme 20).

An alternative was therefore chosen for the synthesis of ligand **53**, which consists in the reaction of *para*-isopropylbenzylbromide **74** with “*in situ*” deprotonated furfuryl alcohol (**75**) in the presence of NaI (scheme 22). Compound **53** was isolated as colourless oil in 92% yield. This approach was already used by Raemy⁸⁶ in his thesis for the synthesis of various ether ligands. The structure of **74** was confirmed by ¹H and ¹³C-NMR, and by GC-MS. We denote two UV-Vis absorption maxima in tetrahydrofuran at 220 nm and 263 nm. The infrared spectrum shows, compared to the starting material **68** and **74** a new absorption band at 1088 cm⁻¹ which was attributed to the ether C-O-C stretching.



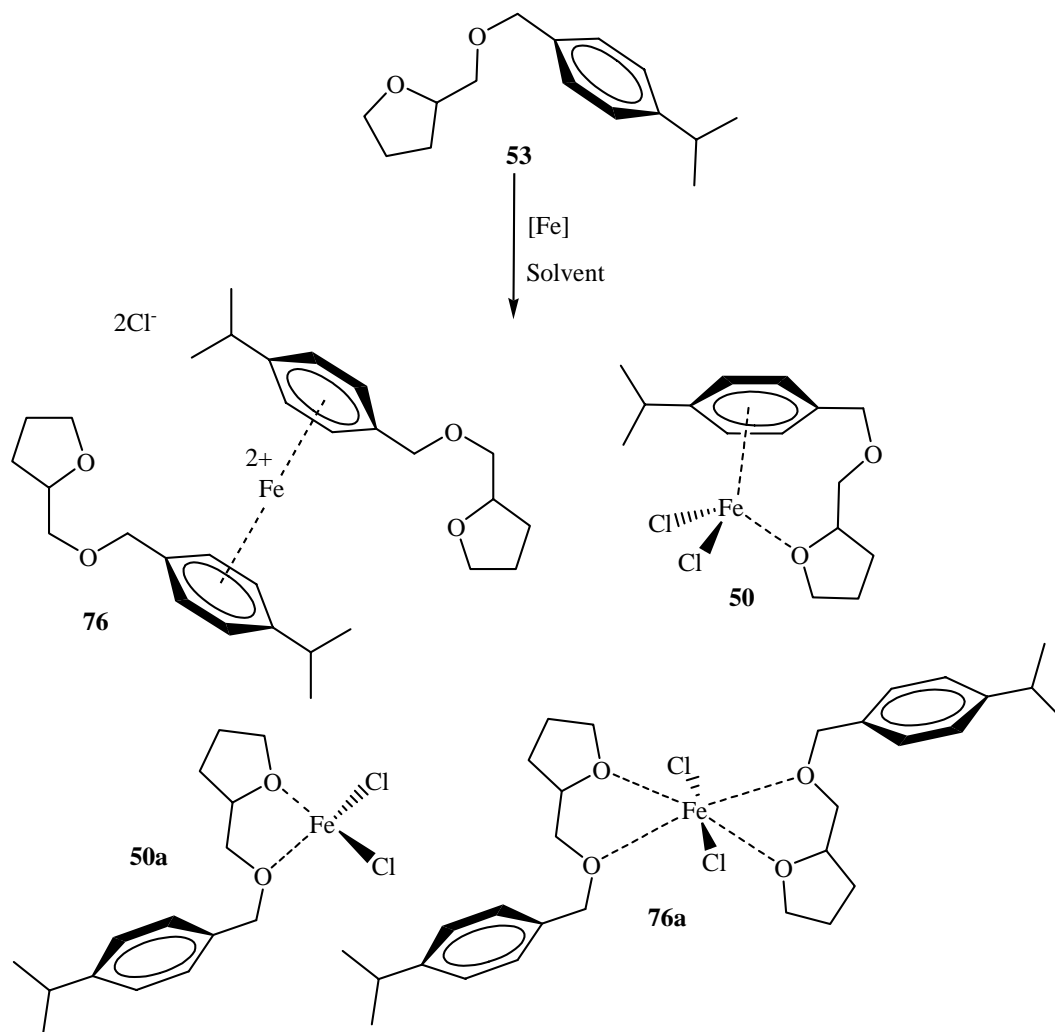
Scheme 22. Synthesis of **53** from the reaction of **74** and **75**.

The *para*-isopropylbenzylbromide **74** was easily prepared by treating *para*-isopropylbenzylalcohol **73** with PBr_3 in diethylether at RT, yielding 57% of colourless oil after purification on silica by column chromatography (scheme 23). The product was identified by ^1H - and ^{13}C -NMR, infrared and GC-MS techniques.



Scheme 23. Preparation of **104**.

9.2. Reaction of 2-(4-isopropyl-phenoxy)methyl)-tetrahydrofurfuryl alcohol **53** with iron chloride



Scheme 24. Synthesis of complex **50** in THF.

Reaction of **53** with $FeCl_2$ or $FeCl_2(THF)_2$ under argon in toluene or in THF at $70^\circ C$ overnight give a yellow solution (scheme 24). Filtration over Celite and evaporation of the solvent affords yellow-green oil. The 1H - and ^{13}C -NMR spectra recorded in THF are in agreement with the expected complex. In the MS(ESI+) spectrum the peak at m/z 594(100%) was attributed to complex **76** or **76a** in which the $FeCl_2$ is complexed with two ligands **53** via the aryl functions or the ether functions respectively. The peak at m/z 360 (40%) corresponds to the expected complex **50** or the ether complex **50a**. we assumed that both complexes exist

in solution as iron(II) species. The cationic Fe(III) species observed in the mass spectrum are most probably form under the spraying conditions of the electrospray ionisation, known to be oxidizing in the positive mode. The UV-Vis spectrum in THF shows three maxima at 364 nm, 308 nm and 256 nm. These absorbance are in the same range as those observed by Raemy in his nitrogen-aryl or allybenzylether iron(II)chloride complexes. For the purpose of comparison, the UV-Vis of FeCl₂ in THF was done, but only a large single maximum was obtained at 302 nm. Compared to the free ligand, the absorptions in the infrared show slight shifts to the low frequencies for the C-O-C ether stretching at 1042 cm⁻¹ instead of 1088cm⁻¹; three new others absorptions appear at 1601 cm⁻¹ (very strong), 920 cm⁻¹ and 820 cm⁻¹. Crystallization attempts in a mixture of toluene and dichloromethane give green crystals. The X-ray analysis yields the unexpected oxo-polymetallic complex **77**, resulting from the decomposition of complex **50** or **76** via ether cleavage induced by Fe(III) impurities (figure 21). The reaction carried out at room temperature does not afford the desired compound; we recover only the starting ligand **50**.

X-ray analysis of complex **77**

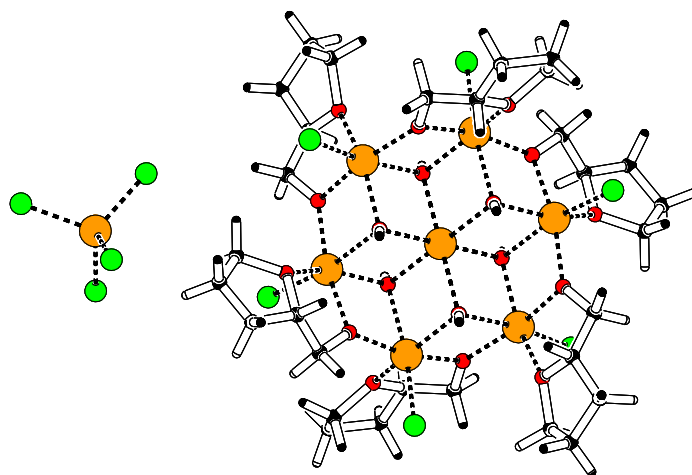


Figure 21. Crystal representation of complex **77**.

Table 3. Selected bondlengths [Å] and angles [°] for complex **77**.

Fe(1)-O(1)	2.105(2)	Fe(2)-Cl(1)	2.235(12)
Fe(1)-O(2)	2.103(2)	Fe(5)-Cl(4)	2.183(2)
Fe(1)-O(3)	2.095(2)	Fe(5)-Cl(5)	2.167(18)
Fe(2)-O(1)	2.008(3)	Fe(5)-Cl(6)	2.175(13)
Fe(2)-O(3)	2.176(3)	Fe(5)-Cl(7)	2.175(15)
Fe(2)-O(5)	2.009(3)	O-H—Cl	2.388
<hr/>			
O(1)-Fe(1)-O(1a)	180	O(3)-Fe(2)-O(4)	84.9(11)
O(1a)-Fe(1)-O(2)	100.7(10)	O(1)-Fe(2)-Cl(1)	101.9(8)
O(1a)-Fe(1)-O(3)	80.2(10)	O(3)-Fe(2)-Cl(1)	169.9(8)
O(1)-Fe(2)-O(4)	150.7(11)	O(4)-Fe(2)-Cl(1)	97
O(1)-Fe(2)-O(5)	76.7(11)	O(5)-Fe(2)-Cl(1)	99.6(8)
O(1)-Fe(2)-O(9)	100.7(11)	O(9)-Fe(2)-Cl(1)	96.2(8)
O(3)-Fe(2)-O(4)	84.9(11)	Fe(2)-O(1)-Fe(1)	102.1(11)
O(3)-Fe(2)-O(5)	90.5(10)	Fe(2)-O(1)-Fe(1)	102.1(11)
O(3)-Fe(2)-O(9)	73.7(10)	Fe(3)-O(1)-Fe(1)	97
O(1)-Fe(2)-O(3)	80.5(10)	Fe(4)-O(9)-Fe(2)	109.1(12)

The starting ligand *para*-isopropylbenzylfurfurylether **53** has lost the benzyl moiety, only the furfuryl part remains attached to the iron centers in **77**. The furfuryl ligand has two possible coordination sites, namely the alkoxy and the cyclic oxygen. The core can be regarded as a wheel with crystallographically imposed S_6 symmetry, in which the central iron atom Fe1 is attached to six other iron atoms Fe2 through six hydroxyl ligands in a μ_3 -oxo mode. Furthermore, each external iron is hexacoordinated with one chloride atom, two other positions are occupied by hydroxyl groups and the two remaining sites are engaged with oxygen atoms of furfuryl molecules. Each of the six exocyclic oxygen atoms of the furfuryl moiety is shared by two-external iron atoms in a μ_2 -oxo mode, while each cyclic oxygen atom complexes one Fe2 center. Selected bond distances and angles are given in the annexe.

The coordination around core Fe1 atom is best described as distorted octahedral, with Fe1—O1 bond lengths in the range of 2.095(2) to 2.176(1) Å, these values are comparable with those reported by Labat⁹⁸ for similar compounds (figure 22). The O—Fe—O cis-angles are 80.23(10)° and 100.69(10)°, but the O—Fe—O trans arrangement is 180°.

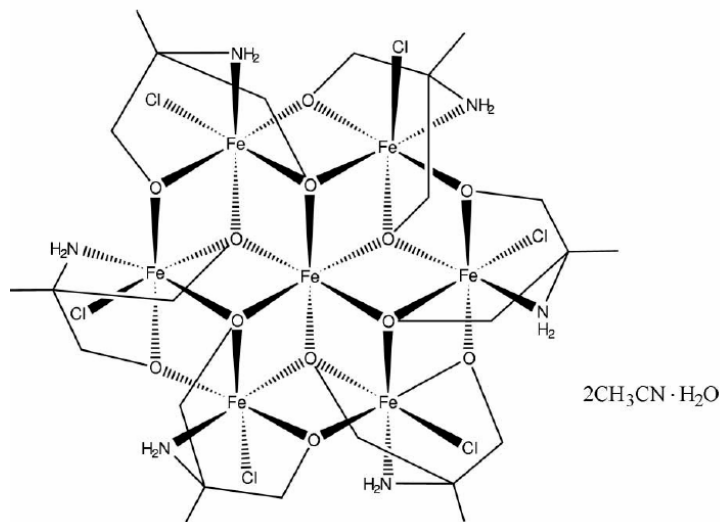


Figure 22. The heptairon(II, III) complex reported by Labat⁹⁸.

The counter ion is clearly Fe(III), Fe—Cl distances in the range of 2.167 to 2.183 Å allows no other interpretation, which imposes for the oxo-polymetallic structure a double positive charge (+2). On the assumption that all μ_3 -oxo ligands are hydroxyl groups and all furfuryl alcohols deprotonated alkoxy ligands, the seven iron centers most possess a Fe(II)₁Fe(III)₆ configuration.

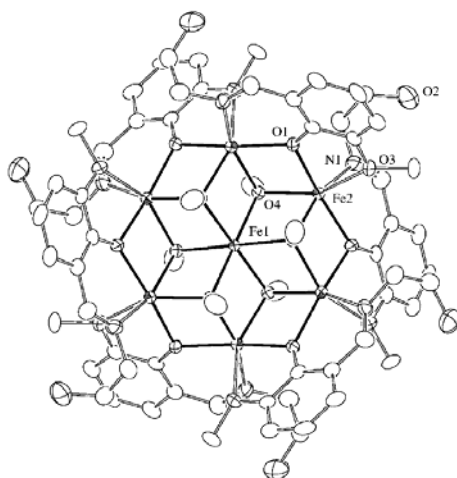


Figure 23. The high-spin heptanuclear mixed-valence Fe(II, III) complex reported by Oshio⁹⁹.

In our case, we were not able to obtain sufficient material for measurement such as Mössbauer spectroscopy. We did MS (ESI+, FAB and MALDI) experiments in order to find if there are hydrogens atoms on all the bridging μ -oxo ligands. Unfortunately, the obtained spectra do not afford peaks in favour of an expected structure.

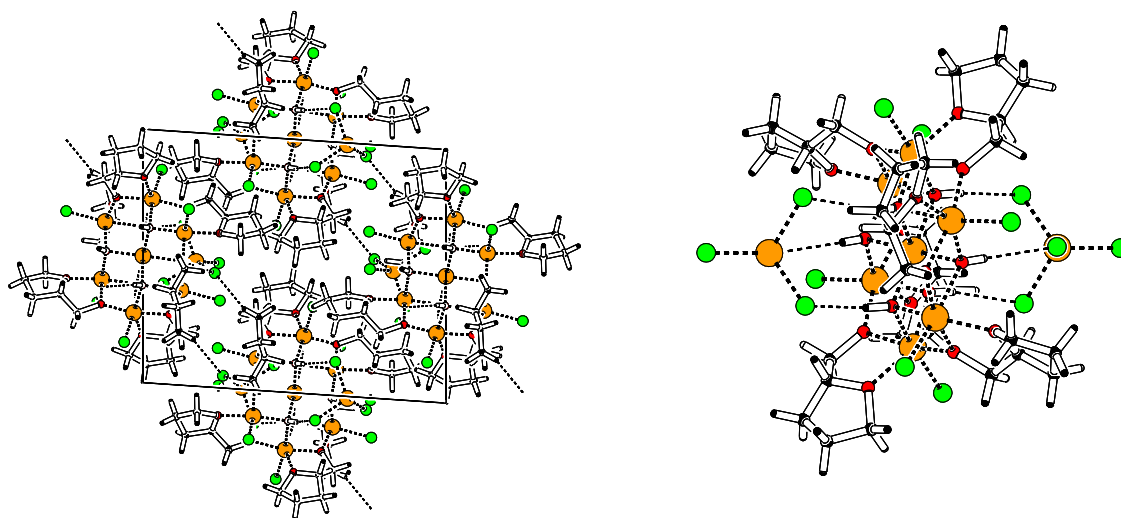


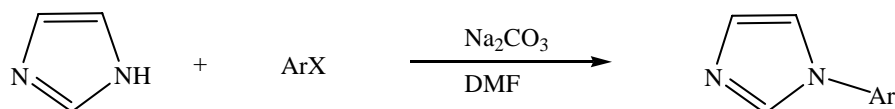
Figure 24. Crystal Packing of complex **77** viewed along the *a*-axis (left) and Cl...H(OH) interactions (right).

II-3. Bisimidazolium salts

10. Synthesis of bisimidazolium salts

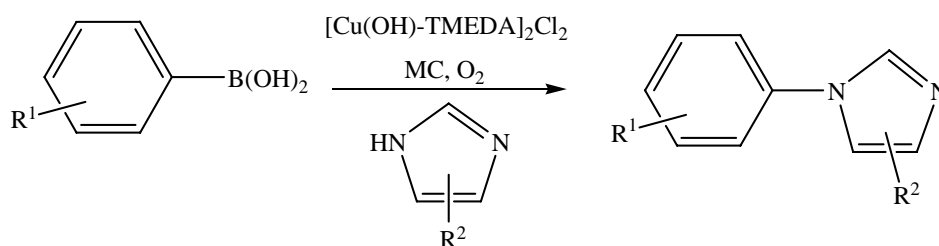
10.1. N-Alkyl and arylimidazoles

Different procedures were reported in the literature for the synthesis of alkyl and aryl imidazoles. One is the nucleophilic displacement of labile alkyl or aromatic halogen by imidazole (scheme 25) in a polar solvent using an adequate base. The simplicity of this one-step procedure is offset by low yields, tedious isolation procedure and failure when there are no electron-withdrawing substituents on the aromatic ring¹⁰⁰. The most successful reaction occur when the aromatic halide ArX has X = F and one or more NO₂, CN, or CO₂H functions *ortho* or *para* to X. The yield can often be improved by addition of catalytic amounts of Cu powder and KI and intractable by-products can usually be removed on fluoresil.



Scheme 25. Nucleophilic displacement of alkyl – or aryl-halide by imidazole.

Synthesis of imidazoles via metal promoted cross coupling reactions has also been reported. This approach consists of the reaction of arylboronic acids with imidazole in the presence of a diamine copper complex allowing for a variety of N-arylimidazole compounds (scheme 26)¹⁰¹.



Scheme 26. Metal promoted cross coupling reaction

The nature of the catalyst is not yet clear. For example, the catalytically active copper is generally formulated as Cu(I) while in some publications it is mentioned as Cu(II). Commonly this catalyst is formulated as a dimeric structure, depicted in figure 25.

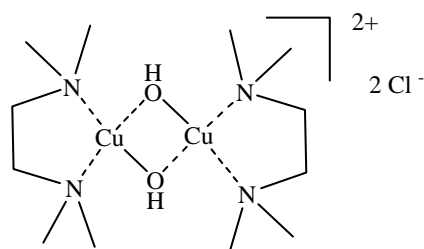
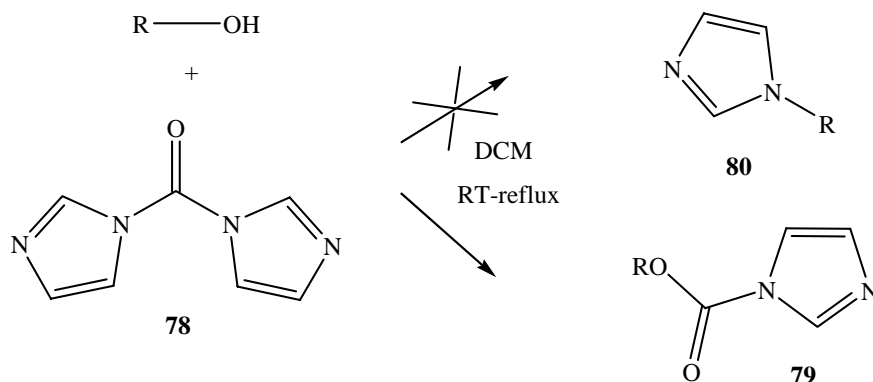


Figure 25. Dimeric structure of Cu catalyst.

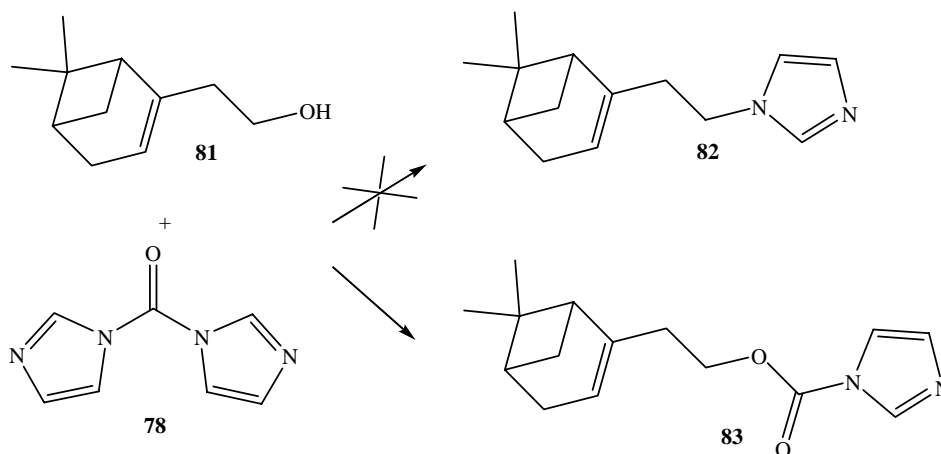
In 2000, Njar¹⁰² has reported a high yielding synthesis of imidazoles and triazoles from alcohols and phenols. According to the procedures described, N-alkyl and N-aryl-imidazoles were prepared from direct reaction of alcohols or phenols with N,N-carbonyldiimidazole **78** (CDI) under very mild conditions (scheme 27).



Scheme 27. Alkyl- and aryl-imidazoles from alcohols and CDI.

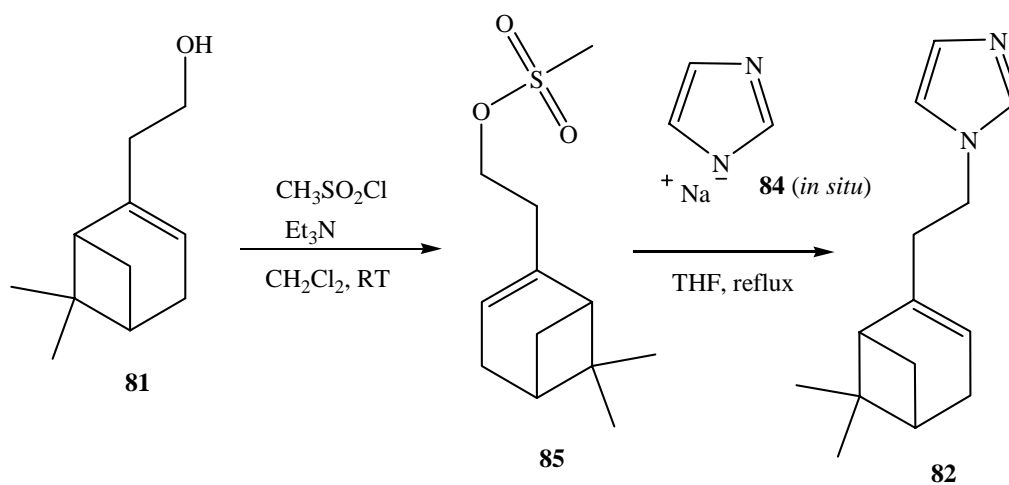
However, Fischer¹⁰³ has exactly repeated this procedure without success; he isolated only the corresponding carbamate **79** as single product. The structure of this carbamate has been confirmed by its infrared absorption at 1769 cm^{-1} (C=O stretch vibration). We also tried to synthesize an 1-nopol imidazole derivative **81** using the Njar procedure, but our results

confirm the observation of Fischer, as only the carbamate product **83** was isolated after purification by column chromatography in 90 % yield. Analysis by ^1H - and ^{13}C -NMR, IR and mass spectrum (ESI+) confirm the carbamate nature of the product (scheme 28).



Scheme 28. Synthesis of nopylimidazole from reaction of nopol with CDI.

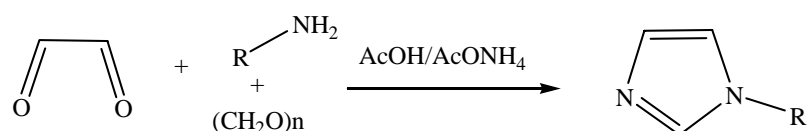
Very high yields (85%) of desired product **82** have been obtained using the alkylation method, which consists of reacting the deprotonated 1H-imidazole **84** with nopylmethylate **85** prepared from the reaction of nopol **81** with mesylchloride and triethylamine in dichloromethane at room temperature (scheme 29).



Scheme 29. Synthesis of **82** by alkylation methods.

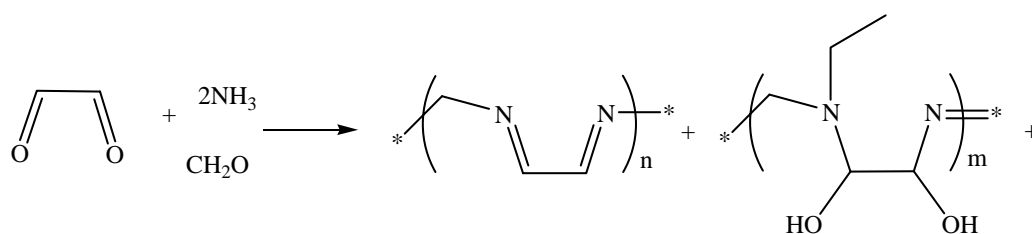
The number of steps and the limited availability of aryl alcohols and aryl halogens discourage us to pursue this way for the synthesis of 1-arylimidazoles.

In our quest to synthesize 1-aryl or alkylimidazoles, we were particularly attracted by an alternative method described by Arduengo in 2001¹⁰⁴. Indeed, he showed that N-1-aryl or alkylimidazoles could be easily obtained in high yield by in situ reaction of an aldehyde, glyoxal, and a primary amine, in the presence of a Brønsted acid whose pK_a is approximately equal to the pK_a of the ammonium (⁺NH₄) cation (scheme 30).

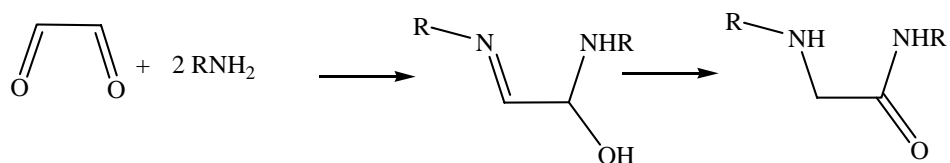


Scheme 30. General equation for a synthesis of N-substituted imidazoles

The acid dependence of this reaction was studied by Alexei Gridnev and co-workers¹⁰⁵. Analyzing the historical synthesis of imidazole (scheme 31), they have concluded that the low yield of this reaction is due to formation of side products from the intermolecular Cannizzaro rearrangement of the Schiff-base in basic conditions. Another side reaction in the imidazole synthesis is the formation of linear and branched Schiff-bases according to the equation in scheme 32.



Scheme 31. The Cannizzaro rearrangement in the synthesis of imidazoles.

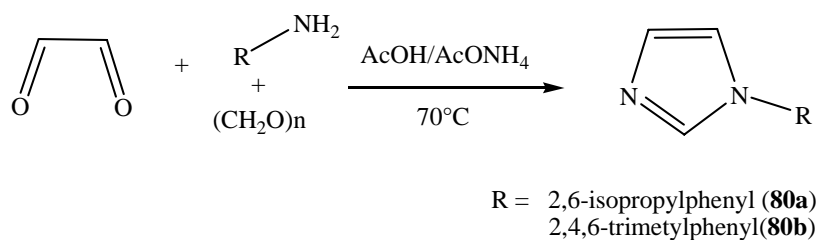


Scheme 32. Formation of linear and branched Schiff – bases.

Previously, it was shown that the yield of imidazole could be increased by 10-20% upon heating the product of the reaction in the presence of palladium and molecular hydrogen under pressure¹⁰⁵. Using these conditions, methylene and azomethylene groups are hydrogenated and imidazolynes are dehydrogenated giving imidazoles.

Davison and Schulse¹⁰⁶ proposed an initially acidification of the reaction mixture in order to minimize formation of by-product and increase the yield of imidazole. Since the side reactions of the imidazole synthesis are suppressed in acidic medium, they observe the pH to decrease from ~5 to ~1 during the reaction. It follows that the side-products are formed mainly during the first stage when the medium is not yet acidic enough.

Taking Gridnev arguments as base, Arduengo¹⁰⁴ introduced the notion of an acidic buffer solution in order to keep the pH of reaction medium constant. Under these conditions, he synthesized a series of N-substituted imidazole compounds. Amongst them 1-mesitylimidazole as a brown solid in 82% yield, from the reaction of mesityl amine with aqueous formaldehyde and aqueous glyoxal at 70°C under acidic buffer conditions (glacial acetic acid, ammonium acetate). Preliminary distillation of the starting mesityl amine permitted us to increase the yield of the crude brown-yellow product to 97%. The ¹H-NMR spectrum of this product corresponds to Arduengo¹⁰⁴ and others author reports^{106,107,123}.



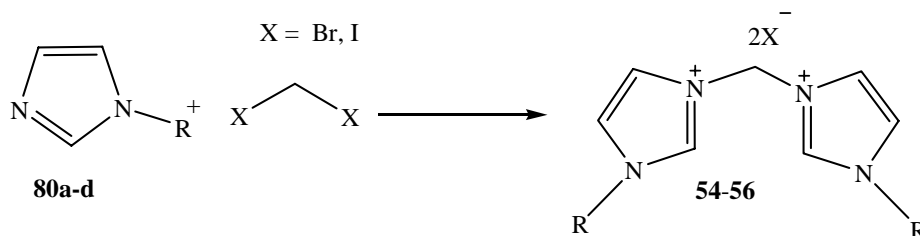
Scheme 33. Synthesis of arylimidazoles **80**.

However, since the GC-MS spectra show the presence of traces of a non-identified product, we were obliged to make further purification. Column chromatography on silica gel or aluminoxid (basic, neutral or acid) was not possible because the product remains on the top of the column. Several washings with organic solvents such as toluene, hexane or pentane do not permit to remove this impurity, as the solid remained brown colored; finally, purification was achieved by sublimation furnishing the desired product in 87% yield as white crystals.

The same approach was performed for the synthesis of 1-(2,6-bisopropylphenyl)imidazole **80a**. The reaction yielded the desired product in 90% as white crystalline needles. The GC-MS spectrum confirms the purity of the obtained compound. The chemical shifts of the protons in arylimidazoles **80**, follow in CDCl₃ solution the predicted order: imidazole-2-proton, benzenoid protons and imidazole-4,5-protons. The ¹³C-NMR spectrum shows all expected signals. The infrared spectra of imidazoles compounds normally show absorption bands at 1550 cm⁻¹, 1492 cm⁻¹, 1451 cm⁻¹, in our case these absorptions could not be clearly distinguished because of the aromatic substituents¹⁰⁰. In general, for both N-1-arylimidazoles we observe several bands in the 1650-1300 cm⁻¹ region that are caused by diverse ring-stretching modes of both the benzenoid and imidazole rings. There is only a single absorption band at 246 nm in the UV-Vis spectra of **80a** and **80b** in dichloromethane.

The 1-phenyl (**80c**) and 1-methyl (**80d**), used in this work were purchased from commercial sources and were analyzed with ¹H-, ¹³C-NMR and GC-MS prior to their use.

10.2. Methylenebis (N-aryl) imidazolium salts



Scheme 34. Synthesis of bisimidazolium salts.

A series of methylene bisimidazolium salts **54–56** was prepared as ligand precursor by quaternisation of the 1-substituted alkyl- and arylimidazole precursors **80a-d** with bis-halidemethylene in refluxing toluene or xylene (scheme 34). High yield of products (98%) were observed in xylene at reflux after only four hours, while the reaction in toluene needs more time. Thus performing the reaction in a mixture of xylene isomers reduces the reaction time drastically as compared to the toluene reaction medium.

Alternatively, methylenebis(N-methyl)imidazolium dibromide **86** has been prepared in 93% yield by simple exposure of the neat reactants in a Schlenk tube to irradiation using a sonification bath for 48 hours. We also tried to use this approach for the synthesis of arylbisimidazolium salts **54–56**, but the observed yields were very low (around 16%). The isolated solids were completely characterized by analytical and spectroscopic tools (¹H- and ¹³C-NMR, IR, UV-Vis, MS(ESI+)).

X-ray structure analysis

Suitable material for X-ray analysis was grown in methanol at low temperature (**54a** and, **55a-b,d** and **56b**); the solid-state structure are given in figure 26-32, supplementary crystallographic data are given in the tables 4-7.

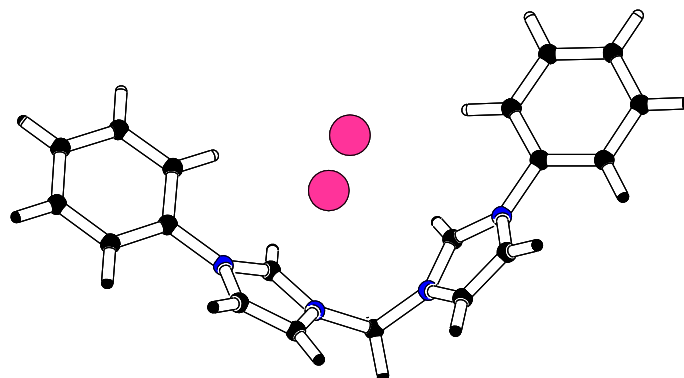


Figure 26. Crystal representation of **54a**.

Table 4. Selected bond lengths [\AA] and angles [$^\circ$] for **54a**.

N(1)- C(2)	1.339(9)	N(3)- C(12)	1.460(12)
N(2)- C(2)	1.327(8)	N(4)- C(13)	1.393(9)
N(1)- C(3)	1.398(8)	C(12)- C(13)	1.343(9)
N(2)- C(4)	1.400(9)	N(1)- C(1)	1.462(8)
C(3)- C(4)	1.324(10)	N(3)- C(1)	1.460(7)
N(3)- C(11)	1.330(8)	N(2)- C(5)	1.446(8)
N(4)- C(11)	1.327(7)	N(4)- C(14)	1.437(8)
<hr/>			
N(1)- C(2)- N(2)	108.8(5)	C(10)- C(5)- N(2)	118.0(6)
N(3)- C(11)- N(4)	108.4(5)	C(15)- C(14)- N(4)	119.3(6)
N(1)- C(1)- N(3)	110.7(5)	C(19)- C(14)- N(4)	119.2(7)
C(6)- C(5)- N(2)	119.5(6)		

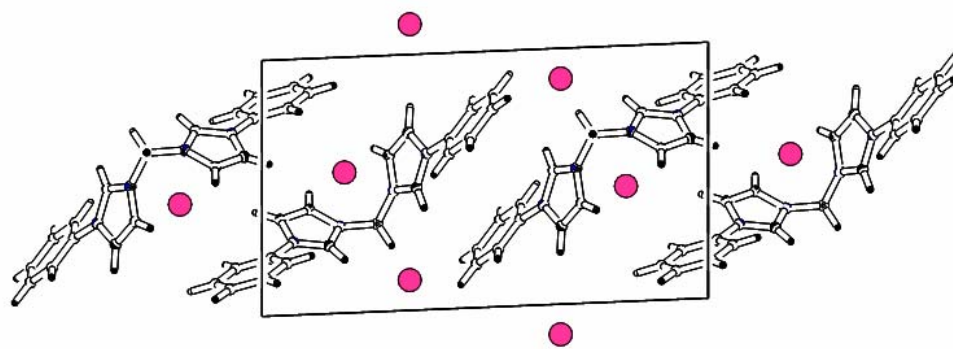


Figure 27. Crystal packing of **54a**, viewed along the *b* axis.

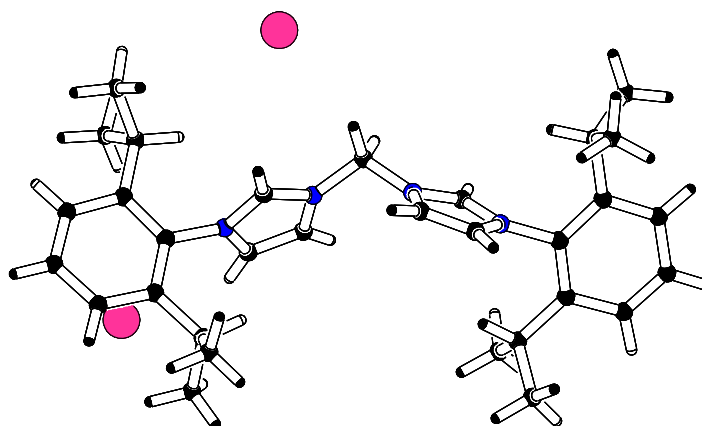


Figure 28. Crystal representation of **55a**.

Table 5. Selected bond lengths [\AA] and angles [$^\circ$] for **55a**.

N(1)-C(2)	1.354(8)	N(3)-C(18)	1.344(10)
N(2)-C(2)	1.322(9)	N(4)-C(19)	1.379(9)
N(1)-C(3)	1.375(9)	C(18)-C(19)	1.343(10)
N(2)-C(4)	1.379(8)	N(1)-C(1)	1.435(9)
C(3)-C(4)	1.347(10)	N(3)-C(1)	1.467(9)
N(3)-C(17)	1.333(8)	N(2)-C(5)	1.447(8)
N(4)-C(17)	1.322(9)	N(4)-C(20)	1.458(8)
N(1)-C(2)-N(2)	108.3(6)	C(10)-C(5)-N(2)	117.7(6)
N(3)-C(17)-N(4)	107.1(7)	C(21)-C(20)-N(4)	115.9(7)
N(1)-C(1)-N(3)	111.0(7)	C(25)-C(20)-N(4)	118.5(7)
C(6)-C(5)-N(2)	118.3(7)		

Remarkably, a counter ion exchange of iodide to chloride occurs in compound **55b** with the recrystallization solvent (MeOH / CH₂Cl₂) already at RT.

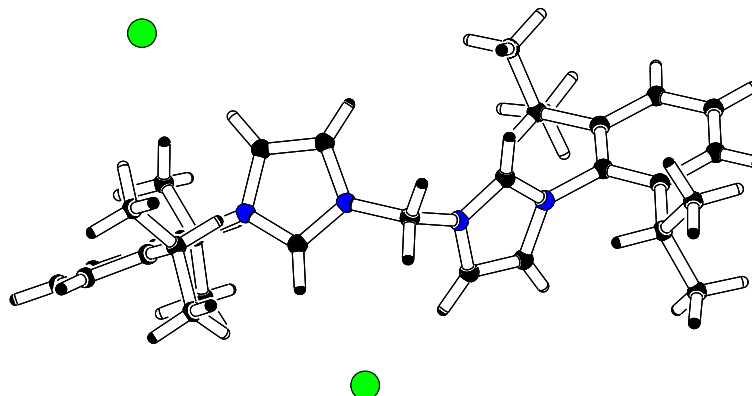


Figure 29. Crystal representation of **55b**.

Table 6. Selected bond lengths [Å] and angles [°] for **55b**.

N(1)- C(2)	1.339(9)	N(3)- C(18)	1.460(12)
N(2)- C(2)	1.327(8)	N(4)- C(19)	1.393(9)
N(1)- C(3)	1.398(8)	C(18)- C(19)	1.343(9)
N(2)- C(4)	1.400(9)	N(1)- C(1)	1.462(8)
C(3)- C(4)	1.324(10)	N(3)- C(1)	1.460(7)
N(3)- C(17)	1.330(8)	N(2)- C(5)	1.446(8)
N(4)- C(17)	1.327(7)	N(4)- C(20)	1.437(8)
N(1)- C(2)- N(2)	108.8(5)	C(10)- C(5)- N(2)	118.0(6)
N(3)- C(17)- N(4)	108.4(5)	C(21)- C(20)- N(4)	119.3(6)
N(1)- C(1)- N(3)	110.7(5)	C(19)- C(20)- N(4)	119.2(7)
C(6)- C(5)- N(2)	119.5(6)		

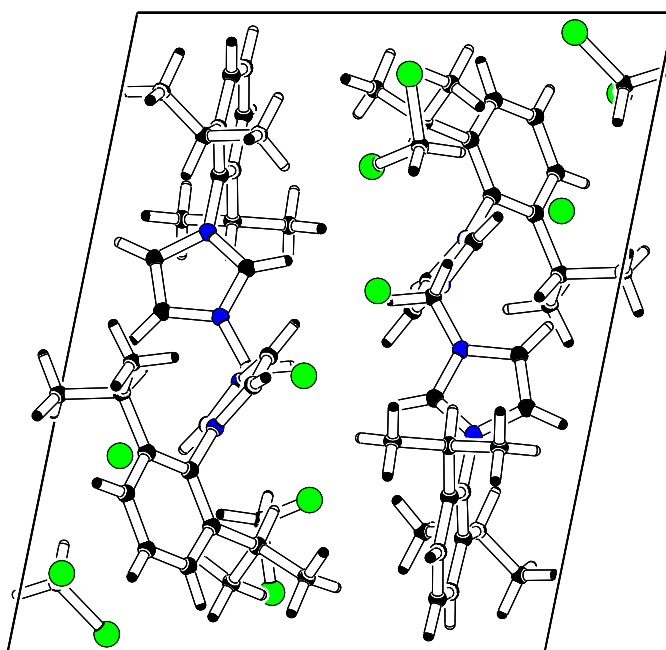


Figure 30. Crystal packing of **55b** with molecules of solvent (CH_2Cl_2), viewed along the *b* axis.

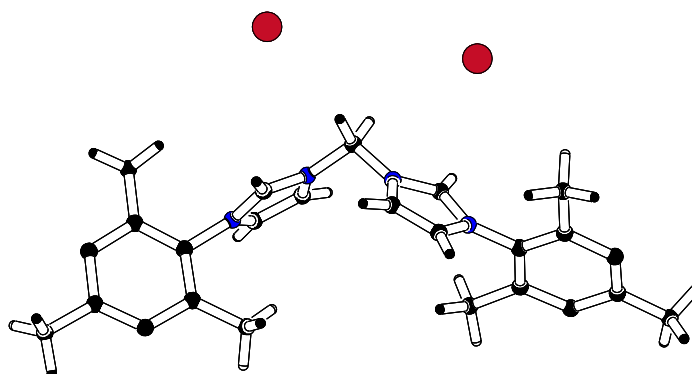


Figure 31. Crystal representation of **56b**.

Table 7. Selected bond lengths [Å] and angles [°] for **56b**.

N(1)-C(2)	1.349(10)	N(3)-C(14)	1.366(12)
N(2)-C(2)	1.330(9)	N(4)-C(15)	1.337(12)
N(1)-C(1)	1.362(11)	C(14)-C(15)	1.335(14)
N(2)-C(4)	1.368(10)	N(1)-C(13)	1.421(10)
C(1)-C(2)	1.342(11)	N(3)-C(13)	1.471(10)
N(3)-C(26)	1.341(10)	N(2)-C(3)	1.428(10)
N(4)-C(26)	1.06(10)	N(4)-C(16)	1.460(10)
N(1)- C(1)- N(2)	108.0(7)	C(8)- C(3)- N(2)	117.7(7)
N(3)- C(17)- N(4)	108.1(8)	C(17)- C(16)- N(4)	117.1(8)
N(1)- C(13)- N(3)	109.7(7)	C(21)- C(16)- N(4)	117.4(7)
C(4)- C(3)- N(2)	119.7(7)		

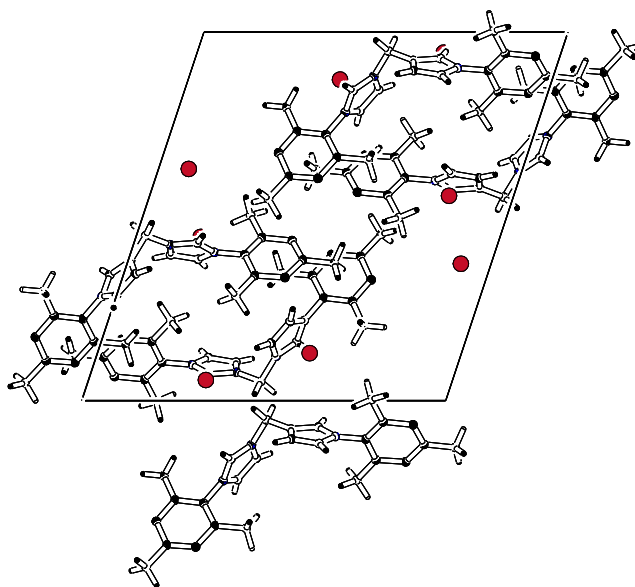
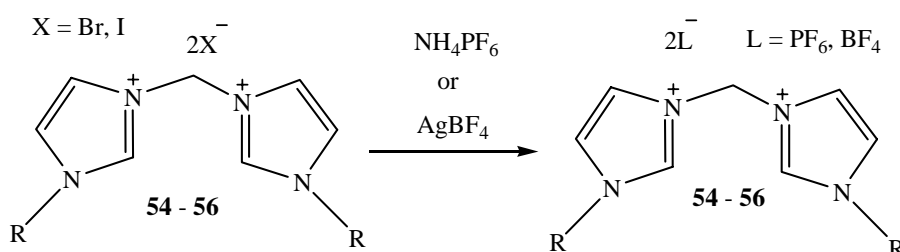


Figure 32. Crystal packing **56b**, viewed along the *a* axis.

The structures of these bisimidazolium compounds are twisted and both imidazole rings (N-C-N) are oriented in the same direction in the compound **54a**, whereas in the compound **55a**,

55b and **56b**, the imidazoles rings are oriented in opposite directions. The bonding within the imidazolium ring in **55b**, indicates a pattern of non delocalization that extends from N(1) to N(2) through C(2), with N(1)—C(2) 1.354(8)Å and C(2)—N(2) 1.322(9)Å being significantly shorter than those between N(1)—C(3) 1.375(9)Å and N(2)—C(4) 1.379(8)Å. The C-N distance at the C-2 center show small differences for N(1) and N(2), the length bond value for N(2) bearing aromatic group is 1.330(9)Å. This value slightly short than 1.362(11)Å for the N(1) attached to the bridged methylene group. Similar difference is observed with **54a**. The N(1)-C(2)-N(2) angle is 108.0(7)° for 1,3-bisarylimidazolium **55b** and 108.8(5)° for **54a**, which is in the same range as this reported by Arduengo¹⁰⁸. The mean plan of the aryl rings are twisted 73° and 80° with respect to the central imidazole rings. Contrary to the previous reported 2-protio-azolium halides¹⁰⁸, there is no X-H-C hydrogen bond in the solid-state structure of **54a**. A projection diagram viewed down the *a*-axis illustrates the arrangement of the bisimidazolium cations and respective anions in the unit cell. The absence of this X-H-C interaction in solid-state structure of these compounds is evident in the package drawing in figures 27 and 30. In **55b** solvent molecules fill the cavities formed in the crystal. The crystal structure of bisimidazolium salts **55a** and **56b** shows similar characteristics as observed in **54a** and **55a**.

10.3. Halide substitution reactions



Scheme 35. Halides counter ion exchange.

The counter ion exchanges are easily realized with silver or ammonium salt in polar solvents. Treatment of methylenebisimidazolium salts (**54 – 56**) with AgBF₄ in acetonitrile leads to the isolation of the corresponding tetrafluoroborate species, as white solids in good yield after filtration and evaporation of solvent (scheme 35).

The hexafluorophosphate salts **55e** and **56e** were obtained by reaction of the corresponding halide species with NH_4PF_6 in methanol or in water at 80°C . No reaction took place at RT because of the poor solubility of the reagents in both solvents. After cooling to room temperature, water-soluble ammonium salts were filtered off and the remaining precipitate was washed with water and diethylether, resulting in a good yield of the desired product as off-white powder in both cases. All products were characterized by analytical and spectroscopic methods (^1H - and ^{13}C -NMR, IR, MS(ESI+)) and in the case of **55e** by X-ray since crystallization was successful. The structure depicted in the figure 33, supplementary crystallographic data are resumed in the table 8.

X- ray analysis of **55e**

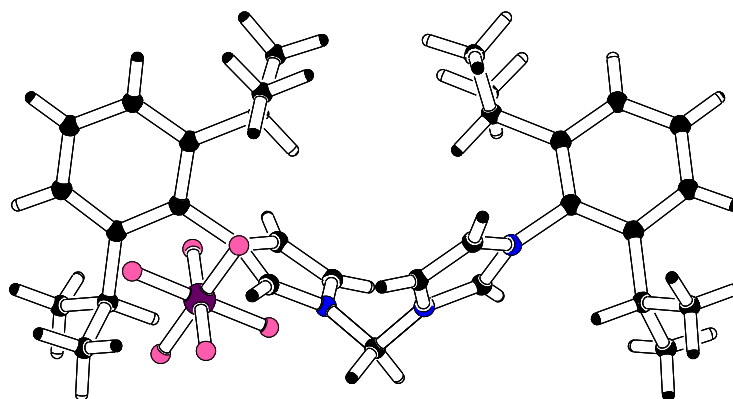


Figure 33. Crystal representation of bisimidazolium salt **55e**.

Table 8. Selected bond lengths [\AA] and angles [$^\circ$] for **55e**.

N(1)-C(2)	1.331(3)	N(2a)- C(4a)	1.373(9)
N(2)- C(2)	1.316(3)	C(3a)- C(4a)	1.335(10)
N(1)- C(3)	1.371(3)	N(1)- C(1)	1.455(2)
N(2)- C(4)	1.373(3)	N(1a)- C(1)	1.455(2)
C(3)- C(4)	1.335(3)	N(2)- C(5)	1.448(3)
N(1a)- C(2a)	1.331(8)	N(2a)- C(5a)	1.448(8)
N(1a)-C(3a)	1.371(10)		
<hr/>			
P(1)-F(1)	1.583(19)	P(1)-F(4)	1.611(17)
P(1)-F(2)	1.574(19)	P(1)-F(5)	1.579(18)
P(1)-F(3)	1.571(2)	P(1)-F(6)	1.563(2)
<hr/>			
F(1)-P(1)-F(4)	179.28(12)	F(3)-P(1)-F(1)	88.01(12)
F(2)-P(1)-F(1)	90.28(11)		
<hr/>			
N(1)- C(2)- N(2)	108.0(2)	C(10)- C(5)- N(2)	116.8(2)
N(1a)- C(2a)- N(2a)	108.0(7)	C(6a)- C(5a)- N(2a)	118.8(4)
N(1)- C(1)- N(1a)	110.2(2)	C(10a)- C(5a)- N(2a)	116.8(4)
C(6)- C(5)- N(2)	118.8(2)		

As previously, the geometry of this imidazolium compound follows a pattern of bond distances and angle similar to the mean values observed for compound **54a**, **55a-c** and **56b**. The C-N distance at the C-2 center show small differences for N(1) and N(2); the value for N(2) bearing aromatic group is 1.316(3) \AA , this value is slightly shorter than 1.331(3) \AA for atom N(1) attached to the bridged methylene group. The N(1)-C(2)-N(2) imidazole ring angle is 108.0(2) $^\circ$ for **55e**. The planes of aryl rings are perpendicular with respect to the central imidazole rings. These data suggest that the imidazole rings are not stressed by the large 2,6-diisopropylphenyl substituents. Contrary to the previously described structures **54a** and **55b**, there is a F – H – C hydrogen bond in the crystal solid-state structure of **55c**, clearly visible in the crystal packing drawing in figure 34. The H—F and H—C(2) distances are 2.427A

and 0.99Å respectively, and the angle C(1)—H—(F) is 148.08°, a value which is slightly higher as compared to the reported hexafluorophosphate 1,3-bisarylimidazolium¹⁰⁸.

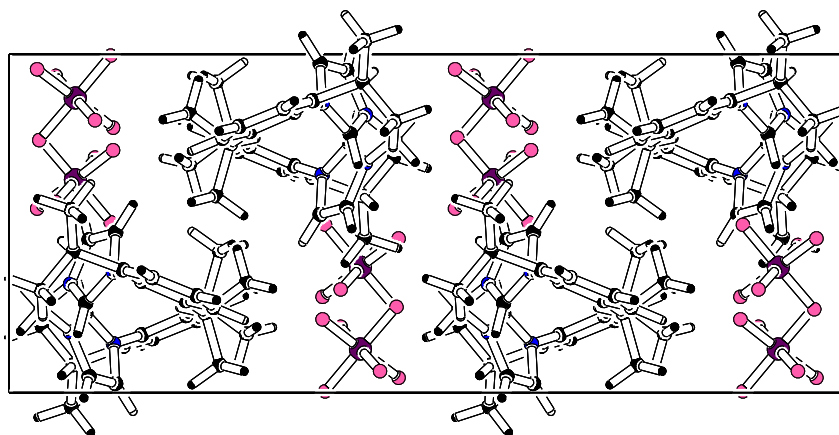
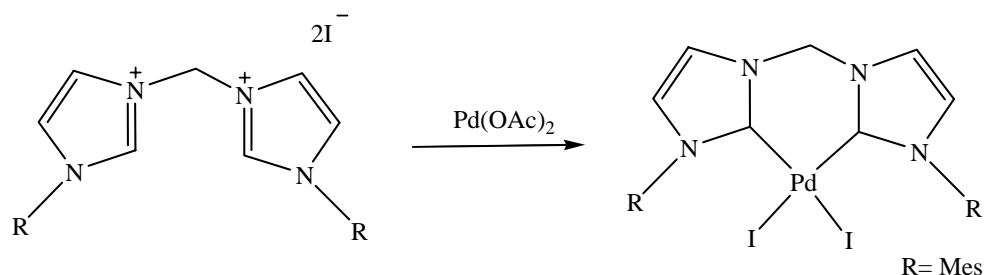


Figure 34. Crystal packing of **55e** viewed along the *a*-axis.

II-4. Direct metallation reactions

11. Direct metallation by reaction of bisimidazolium salts with adequate iron(II) precursors ($\text{Fe}[\text{N}(\text{SiMe}_3)_2]$, $\text{Fe}(\text{OSO}_2\text{CF}_3)_2$ and $\text{Fe}(\text{O}_2\text{CH})_2 \cdot 2\text{H}_2\text{O}$)

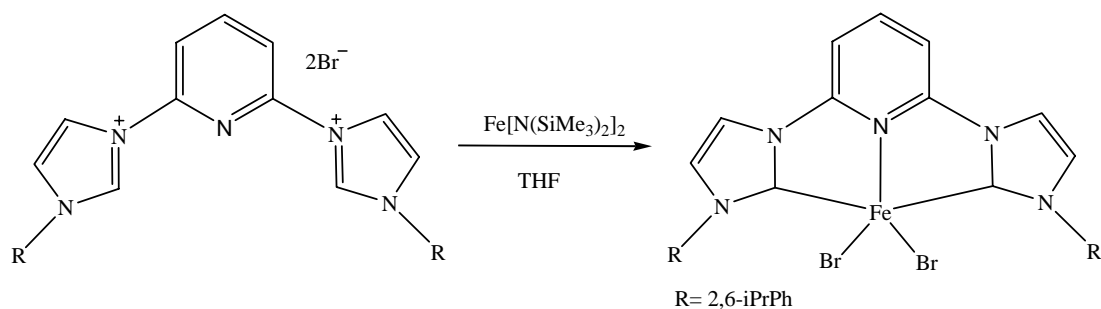
Direct metallation protocols for the reaction of bisimidazolium salts with metal precursors bearing weakly basic ligands such as acetate has been reported in the literature to give chelating complexes with good yield. However, this is limited to Pd, Ru and Ir (scheme 36)^{107,109-111,123}.



Scheme 36. Palladium bismesitylimidazol-2-ylene (Hermann)^{111,123}.

11.1 Reaction of bisimidazolium salts with $\text{Fe}[\text{N}(\text{SiMe}_3)_2]_2$

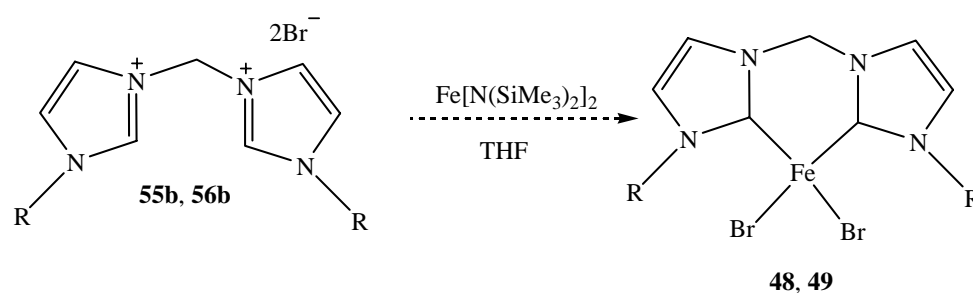
Recently, Danopoulos¹¹² has prepared a new iron bromide 2,6-bis(imidazolylidene)pyridine (C-N-C), based on the aminolysis reaction of the imidazolium salt with bis[bis(trimethylsilyl)amide]iron(II), ($\text{Fe}[\text{N}(\text{SiMe}_3)_2]_2$) **59** (scheme 37).



Scheme 37. Synthesis of iron bromide 2,6-bis(imidazolylidene)pyridine by Danopoulos²⁷.

Our interest in employing new iron(II) sources prompted us to study this reaction. We have first prepared the precursor ($\text{Fe}[\text{N}(\text{SiMe}_3)_2]_2$) according the procedure described by

Andersen¹¹³ which consist of reacting $\text{FeBr}_2(\text{THF})_2^\dagger$ with $\text{KN}(\text{SiMe}_3)_2$ in diethylether at low temperature during 12 hours. The obtained green yellow air sensitive solid was then reacted with methylenebis(N-aryl)imidazolium salts **55b** and **56b**.



Scheme 38. Attempted synthesis of **48** and **49** by direct complexation.

In the reaction of $\text{Fe}[\text{N}(\text{SiMe}_3)_2]_2$ with bisimidazolium dibromide salt **56b** in THF at -78°C , the colour of the reaction mixture turned from purple to red after 12 hours. The solution was then allowed to warm to room temperature for 48 hours.

The red solution was recovered by filtration followed by several washings with pentane. The first addition of pentane on the red filtrate provoked a precipitation of a beige solid, which was isolated by filtration. A new portion of pentane was added to this filtrate allowing the isolation of a new fraction of beige solid. These fractions were submitted to the MS(ESI+) and elemental analysis without success. The characterization with ^{13}C -NMR was not possible because of the paramagnetism of the product. Crystallisation attempts by slow diffusion from THF / diethylether at room temperature and at low temperature didn't furnish any suitable crystals. However, the UV-Vis spectra of the homogeneous orange-yellow solution in THF revealed two absorption bands at 360 nm and 320 nm for both samples (figure 35). The spectra of the starting iron precursor $\text{Fe}[\text{N}(\text{SiMe}_3)_2]_2$, possess one absorption bands at 363 nm, for comparison (figure 36).

[†] For the preparation of $\text{FeBr}_2(\text{THF})_2$ see chapter II-6

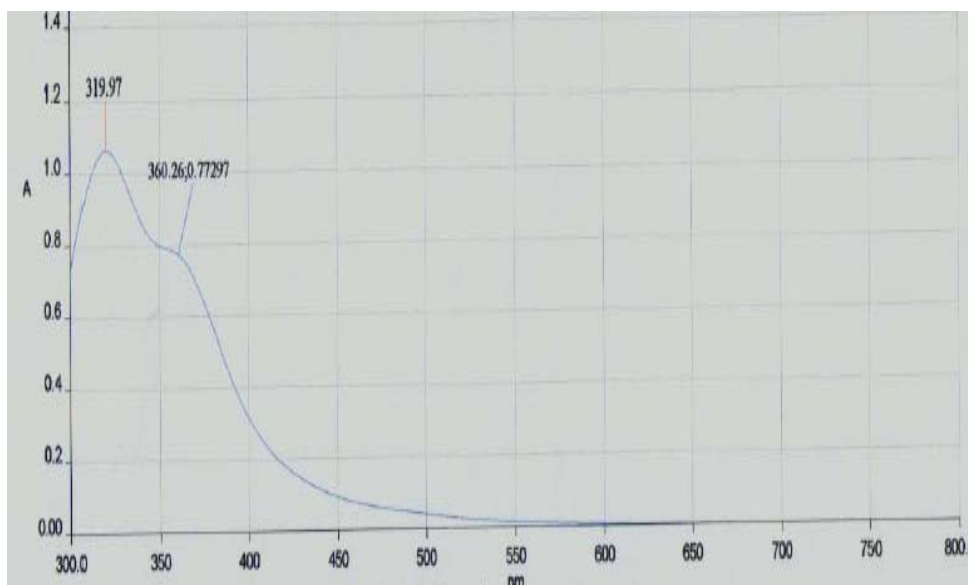


Figure 35. The UV-Vis spectrum of **49** in THF.

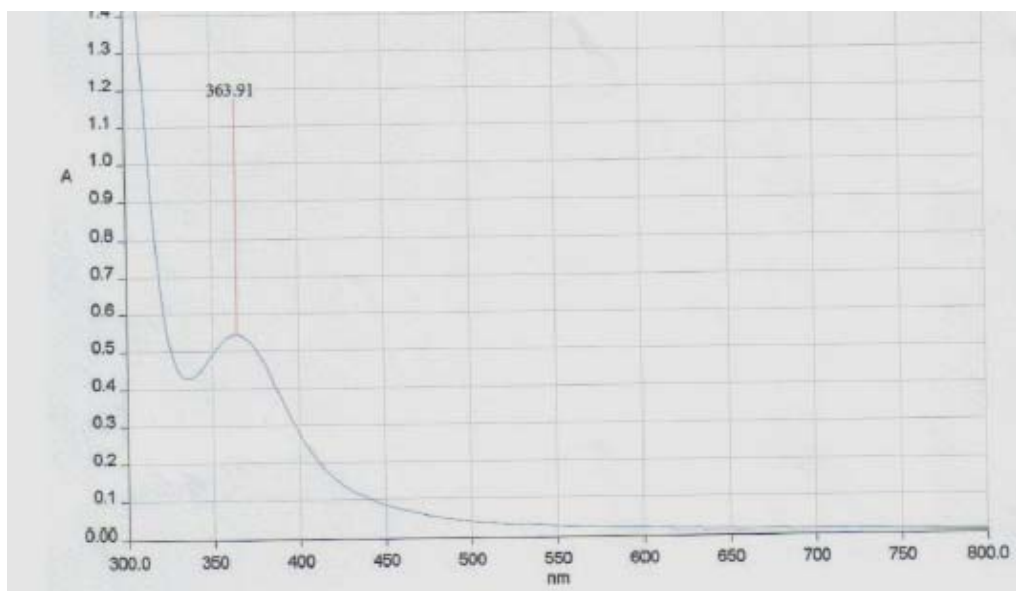


Figure 36. The UV-Vis spectrum of starting iron precursor Fe[N(SiMe₃)₂]₂ in THF.

The white residue left from the previous reaction, has been washed with THF and pentane. Addition of CH₂Cl₂ dissolved the residue and the colour of the solution changes from green at the beginning to red after 24 hours. Filtration and evaporation of the solvent furnish orange yellowish oil. The characterization with ¹³C-NMR was not possible because of the paramagnetism of the product. The UV-Vis spectrum shows two absorptions at 300 nm and 222 nm. Crystallisation attempts by slow diffusion in THF / diethylether at room temperature didn't give any result, we observe degradation of the material after some hours.

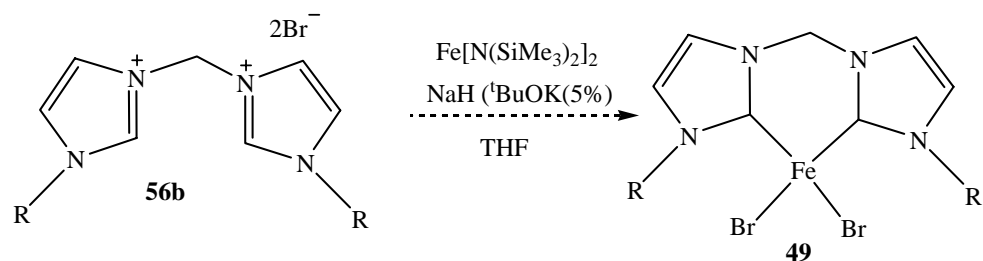
The temperature influence on the reaction was also investigated, we reacted the Fe[N(SiMe₃)₂]₂ with [N-1,1'-(2,6-diisopropylphenyl)-3,3'-methylene]bisimidazolium dibromide salt **55b** in THF at -78°C for 6 hours. The red float solution was recovered by filtration before the solvent was evaporated to yield an orange solid, which was analysed by UV-Vis, as previously the spectra shows two maxima at 358 nm and 322 nm. Again, the NMR and MS technique does not give the expected signals.

In another attempt of the reaction was performed at 0°C for 48 hours. The red filtrate was recovered giving an orange solid after evaporation of solvent. Spectroscopic analysis did not give any result, except for UV-Vis spectrum, which as previously shows two maxima at 362 nm and 320 nm. Slow crystallisation in THF a room temperature affords a microcrystalline orange solid, not suitable for X-ray analysis. Recrystallization was attempted by slow diffusion of non polar solvents (toluene, pentane, diethylether) into THF. Unfortunately, only decomposition of the product into rust is observed. According to the UV-Vis spectra, we conclude that the reaction occurs already at low temperature, but higher temperatures don't harm.

11.1.1. Reaction in presence of NaH

Since it was not clear whether, the previous reaction was a success or a failure, we repeated the reaction by adding an additional strong base, NaH, containing 5% of ^tBuOK as a reaction mediator between the fairly insoluble NaH and the imidazolium salt (scheme 39). During this reaction, the colour of the solution turned rapidly from yellow to red purple. After completion, the upper solution was filtrate and the remained white solid residue was washed with THF and pentane. This product is insoluble in organics solvents, but soluble in water,

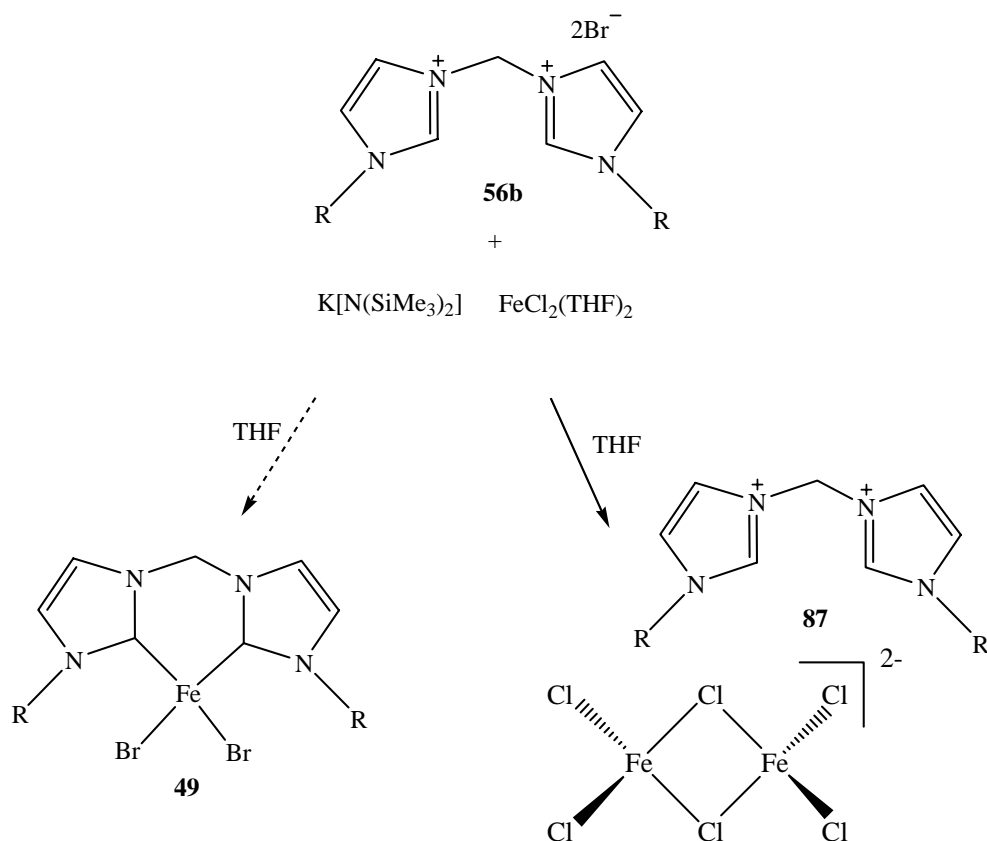
most probably an inorganic salt. This fact was confirmed by elemental analyses, which shows the absence of any carbon atom in the sample.



Scheme 39. Attempted synthesis of **49** by direct complexation of imidazolium **56b** with $(\text{Fe}[\text{N}(\text{SiMe}_3)_2]_2)$ and NaH ($t\text{BuOK}$).

The recovered upper red purple solution was treated as previously by addition of pentane. A yellow precipitate was isolated after filtration; this procedure was repeated two times. The UV-Vis spectrum of each fraction gives two identical absorptions at 350 nm and 268 nm. All fractions were submitted to mass (ESI+) and to elemental analysis, but the results does not correspond our expectation. The ^{13}C -NMR measurement of all fractions was not possible due to the paramagnetism of this compound. A crystallization attempt by slow diffusion of diethylether into the THF of product did not give crystals.

11.1.2. One pot reaction



Scheme 40. The one pot reaction.

The one pot reaction of $\text{FeCl}_2(\text{THF})_2$ with imidazolium dibromide salt **56b** in the presence of $\text{KN}(\text{SiMe}_3)_2$ in THF was tried (scheme 40). After removal of the precipitate by filtration, the orange filtrate was evaporated giving an orange solid. As previously (figure 11), the UV–Vis spectrum of the product in THF shows absorptions at 360 nm and 320 nm. Due to the paramagnetic nature of the isolated product, ^{13}C -NMR was not possible. Crystallization by slow diffusion hexane/THF leads to degradation of the product. However, we were able to isolate colourless crystal plates in THF. The structure determined by X-ray diffraction show a salt of bisimidazolium with a $[\text{Fe}_2\text{Cl}_6]^{2-}$ as counteranion **87** (figure 37). Clearly, this structure does represent the bulk of the product, but rather a minor by product.

X-ray analysis of 87

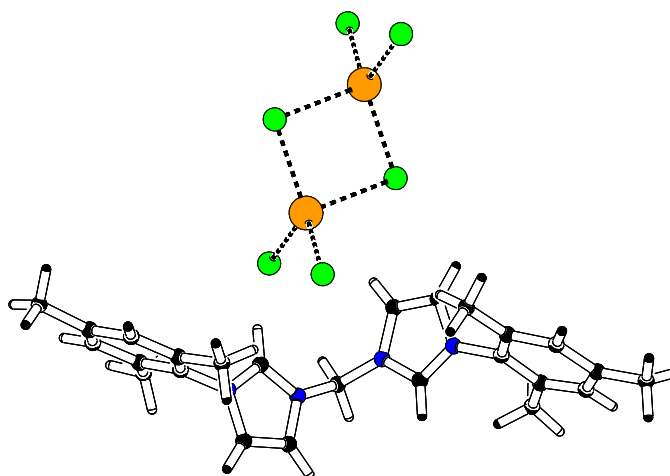


Figure 37. Crystal representation of complex **87**.

Table 9. Selected bond lengths [\AA] and angles [$^\circ$] for **87**.

Fe-Cl(1)	2.575(2)		
Fe-Cl(2)	2.576(3)		
Fe-Cl(3)	2.566(3)		
N(1)-C(2)	1.329(16)	N(4)- C(16)	1.390(16)
N(2)- C(2)	1.283(16)	C(15)- C(16)	1.373(19)
N(1)- C(3)	1.368(17)	N(1)- C(1)	1.452(16)
N(2)- C(4)	1.397(16)	N(3)- C(1)	1.462(16)
C(3)- C(4)	1.324(19)	N(2)- C(5)	1.424(16)
N(3)- C(14)	1.323(16)	N(4)- C(17)	1.420(16)
N(3)-C(15)	1.365(17)	N(4)- C(14)	1.316(16)
N(1)- C(2)- N(2)	110.4(11)	C(10)- C(5)- N(2)	117.9(12)
N(3)- C(14)- N(4)	110.1(11)	C(18)- C(17)- N(4)	117.7(11)
N(1)- C(1)- N(3)	111.8(11)	C(22)- C(17)- N(4)	118.5(11)
C(6)- C(5)- N(2)	119.5(13)		
Fe(1)- Cl(3a)- Fe(1a)	90.7(2)	Fe(1)- Cl(3)- Fe(1a)	88.9(5)
Cl(3)- Fe(1)- Cl(1)	123.3(10)	Cl(1)- Fe(1)- Cl(2)	110.5(10)
Cl(3)- Fe(1)- Cl(2)	116.4(11)		

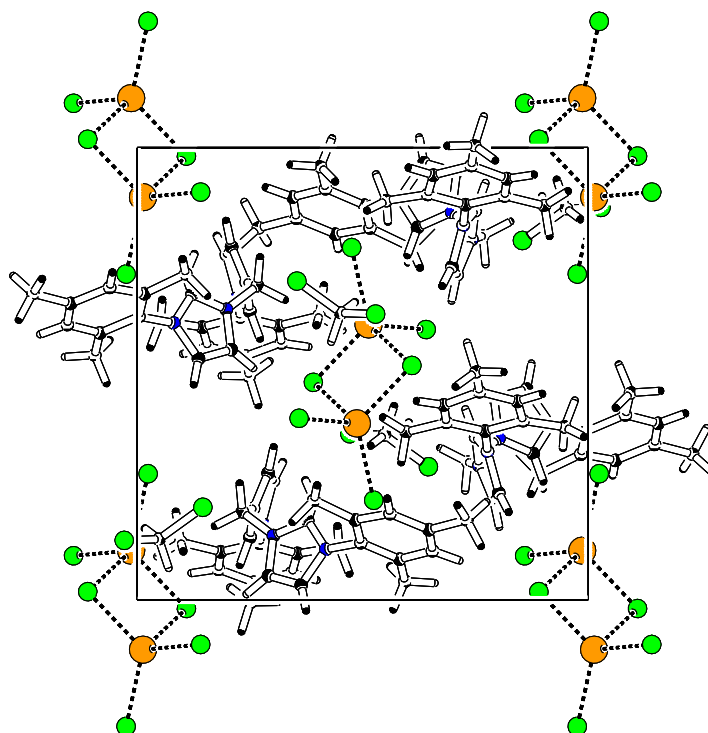


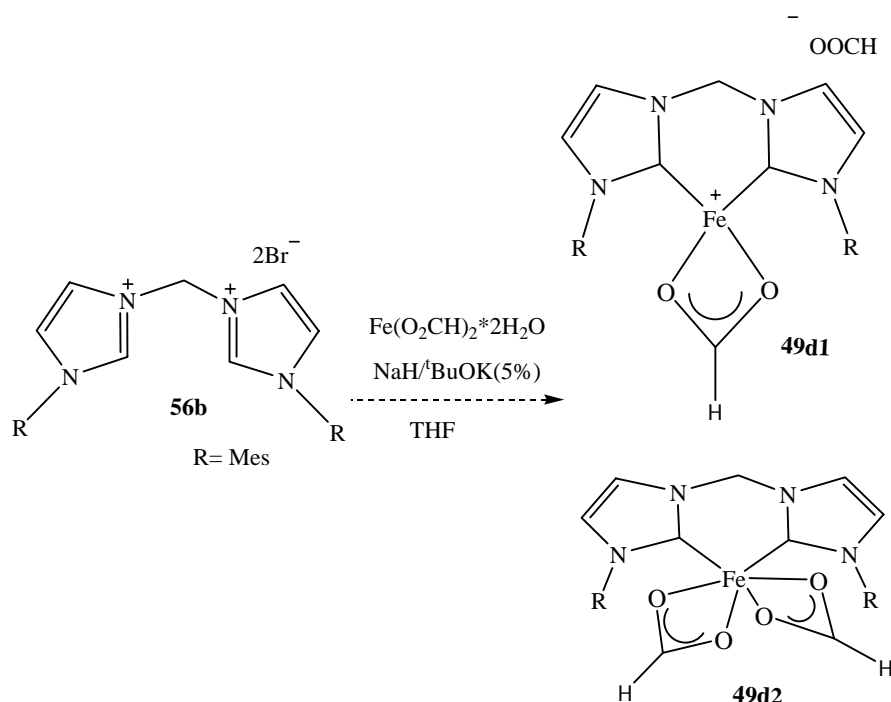
Figure 38. Crystal packing of complex **87** viewed along the *b*-axis.

Important bond lengths and angle are listed in the table 9. The counter ion $[\text{Fe}_2\text{Cl}_6]$ in the complex **87** is probably an Fe(II) chloride-bridged dimer. The coordination sphere of iron is completed with two terminal chlorides. The bridged Fe—Cl (2.566(3)Å) and the terminal Fe—Cl (2.576(2)Å) bond lengths, are much longer than the ones observed in the mononuclear salts $[\text{Fe}^{\text{II}}\text{Cl}_4]^{2-}$ (2.25–2.35Å) or $[\text{Fe}^{\text{III}}\text{Cl}_4]^-$ (2.15–2.20Å)¹¹⁴ and than to those expected for a tetrahedral iron-chlorines bonds (2.195Å for Fe(III) and 2.301Å for Fe(II))¹¹⁵. The bridging angles Fe – Cl(3) – Fe range from 88.9(5)° to 90.73(2)° and are in the range of those reported in literature¹¹⁴. The angles at iron, Cl(3) – Fe – Cl(1) (123.3(10)°), Cl(3)—Fe—Cl(2) (116.4(11)°) and Cl(1)—Fe—Cl(2) (110.5(10)°) are slightly higher to those reported in $[\text{Et}_4\text{N}]_2 [\text{Fe}_2\text{Cl}_6]$ ¹¹⁴, but far away from the ones for idealised tetrahedral geometry (109.5°)¹¹⁵.

11.2. Reaction of bisimidazolium salts with $\text{Fe}(\text{O}_2\text{CH})_2 \cdot 2\text{H}_2\text{O}$

Frequently, the washing of obtained crude products with weakly coordinating solvents like toluene, diethylether, hexane or pentane, leads to unidentifiable, eventually degraded products. This observation prompted us to take the role of the THF in consideration: perhaps the observed product decomposition is due to the replacement of THF with these less or non-coordinating solvents on the coordination sphere. To overcome this problem we planned to introduce supplementary ligands on the metal center by the use of iron(II) sources containing formiate or triflate ligands. The reaction was done with or without the presence of strong bases such as NaH and $t\text{BuOK}$.

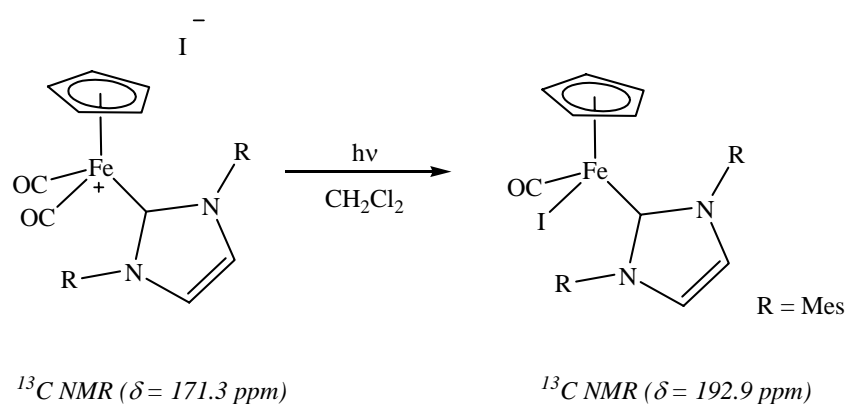
$\text{Fe}(\text{O}_2\text{CH})_2 \cdot 2\text{H}_2\text{O}$ was used as iron(II) source in the reaction with imidazolium salts **56b** in the presence of NaH ($t\text{BuOK}$). We expected that NaH ($t\text{BuOK}$) could promote *in situ* deprotonation of the bisimidazolium salt, which will then react with the iron center to afford an possibly iron formyl bisimidazol-2-ylidene complex such as **49d1** or **49d2** (scheme 41).



Scheme 41. Reaction of imidazolium salts with iron formiate.

The starting iron formiate was dried overnight at 100°C under vacuum ($\sim 10^{-3}$ bar) prior to reaction. We then reacted it in a one pot reaction with the bisimidazolium salt **56b** and 2.2

equivalents of NaH as base in THF at -78°C . The solution turned red - purple after few minutes. Warming up to RT, filtration and evaporation of the solvent give a red-brown solid, which was extracted with pentane yielding a yellowish solid after evaporation of pentane **49d1** or/and **49d2**. The most notable feature is that, this compound gives a well-resolved ^{13}C -NMR spectrum (figure 39). It shows among others signals, a downfield shifted carbene resonance at 172.1 ppm and 171.1 ppm, which is consistent with the values reported by Guerchais¹¹⁶ for $[\text{Cp}^*\text{Fe}(\text{CO})_2\text{Im}]^+$ at 171.3 ppm (scheme 42). For comparison, the resonance of the free carbene is 213.9 ppm. In the spectrum, two signals at 163.6 ppm and 163.3 ppm were attributed to formiate groups since these resonances belong clearly to CH carbons.



Scheme 42. The reported iron carbonyl imidazol-2-ylidene complexes¹¹⁶.

In the infrared spectrum, the signal at 1682 cm^{-1} could be due to the vibration of a carboxylate group. The MS spectra (ESI+, FAB) and the elemental analysis do not give the expected results probably due to the presence of impurities in the samples. Attempts to purify the yellow solid by extraction with different solvents or by chromatography with silica gel or aluminoxid (neutral, basic) failed to work, as the product remained immovable on the TLC. The UV – Vis spectrum of the product in THF shows two absorptions maxima at 453 nm and 358 nm (figure 40). This is different from the 341 nm recorded for the iron formiate starting precursor. No of all the attempts to get crystals in THF at low temperature, or by slow diffusion of pentane or toluene into a THF solution of the product worked.

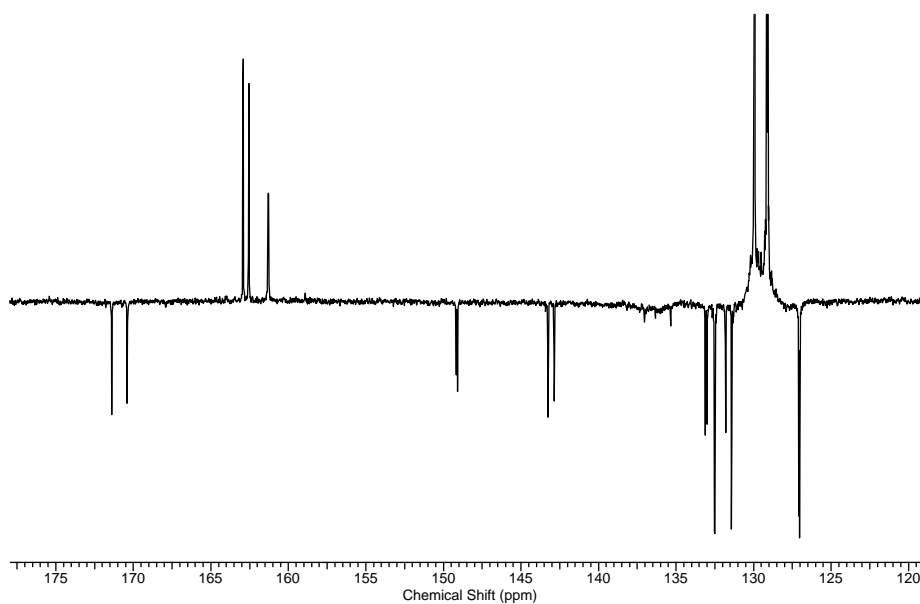


Figure 39. The down field view of APT ¹³C-NMR (125 MHz) spectrum of isolated material **49d**.

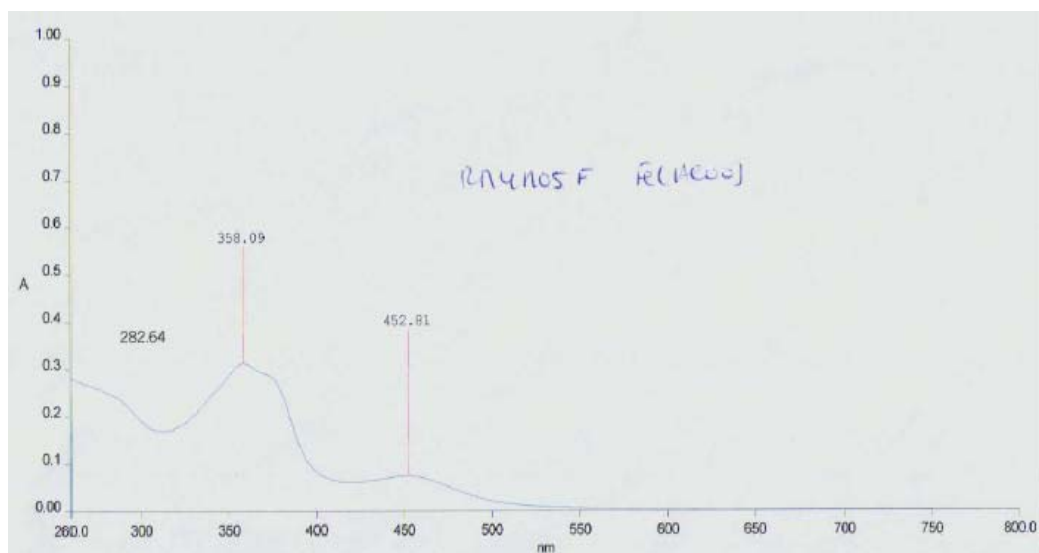
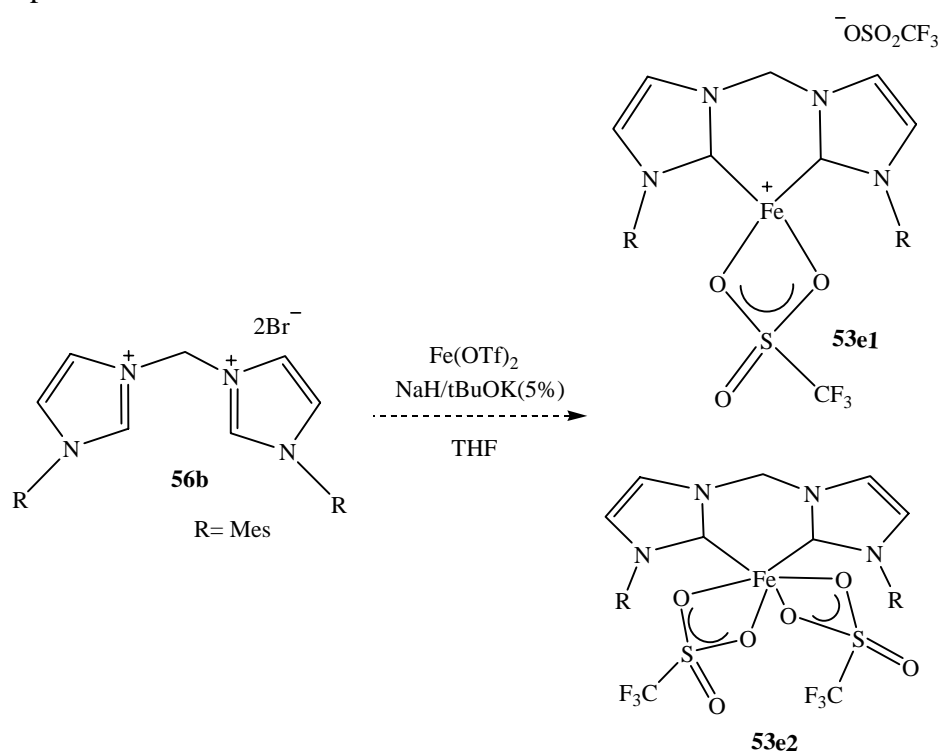


Figure 40. The UV-Vis spectrum of isolated material **49d**.

Since the extracted yellow solid product seems to contain the desired product, we have repeated this reaction in a mixture of solvents (pentane / THF 18:2). Unfortunately, only a small amount of yellow solid was isolated. This time, the resulting ^1H - and ^{13}C -NMR spectra are identical to the previous ones and show as before still some impurities in the sample. Moreover, the MS (ESI+, FAB) and the elemental analysis failed as before.

11.3. Reaction of bisimidazolium salts with iron triflate $\text{Fe}(\text{OSO}_2\text{CF}_3)_2$

For the same purpose as above, $\text{Fe}(\text{OTf})_2$ was reacted with bisimidazolium salt **56b** and NaH (scheme 43). The white iron triflate powder was prepared by modification of a reported procedure^{117,118}, namely reaction of FeCl_2 with silver triflate in acetone or THF at room temperature. The product was identified by comparison of the infrared spectrum with literature^{117,118}. The UV-Vis spectra recorded in THF shows only one maximum at 320 nm for this iron precursor.



Scheme 43. Reaction of imidazolium salt with iron triflate.

The reaction of iron triflate with imidazolium salt **57b** was done in the presence of NaH- t BuOK at low temperature (-78°C). On warming up, the reaction mixture turned orange at -10°C ; filtration and evaporation of the solvent gave an orange–yellow solid **53e** or/and **153e2**, which was washed with pentane and diethyl ether without changing colour. The ^{13}C -NMR

shows, amongst others, two carbenes signals at 177 ppm and 176.8 ppm (figure 41). The UV-Vis spectra in THF shows singular absorption at 374 nm (figure 42). In the infrared spectrum, the stronger signals at 1283 cm^{-1} and 1256 cm^{-1} could be attributed to the vibration of sulfonate groups ($\nu(\text{SO}_3)$ sym, asym), the signal at 639 cm^{-1} corresponds to a S-O asymmetric deformation. However, MS (ESI+) and elemental analysis do not show signals or give results, which would confirm the proposed structure. Purifications attempts by several washings with different solvent and slow diffusion crystallisation from THF / CH_2Cl_2 failed.

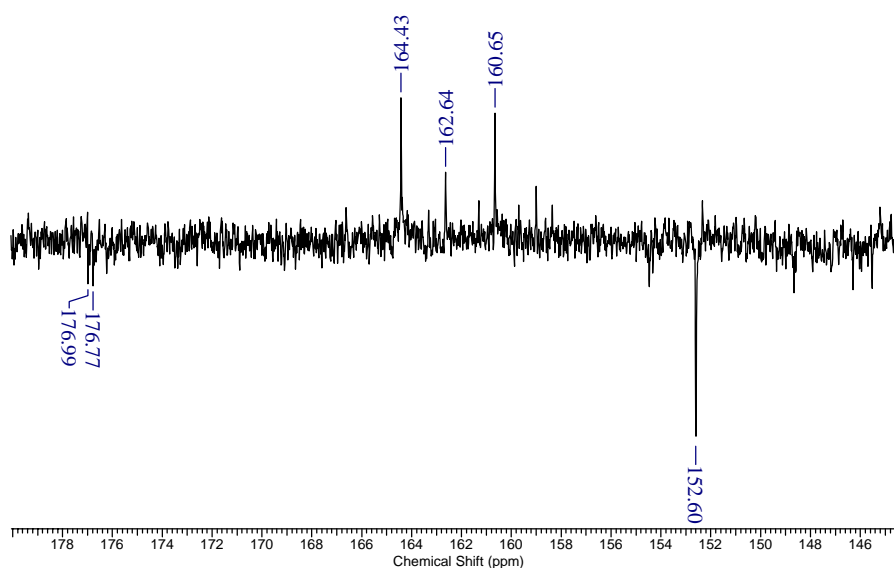


Figure 41. The down field APT ^{13}C -NMR (125 MHz) spectrum of isolated material **49e**.

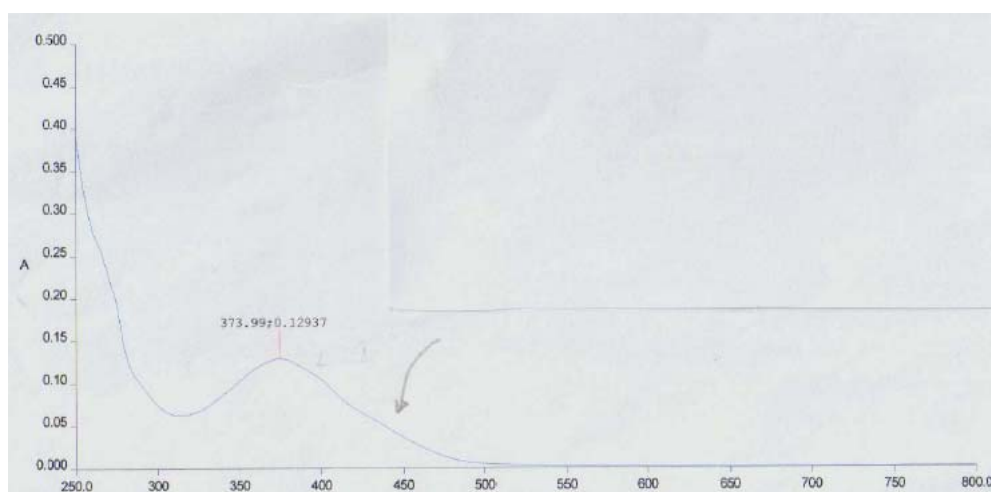


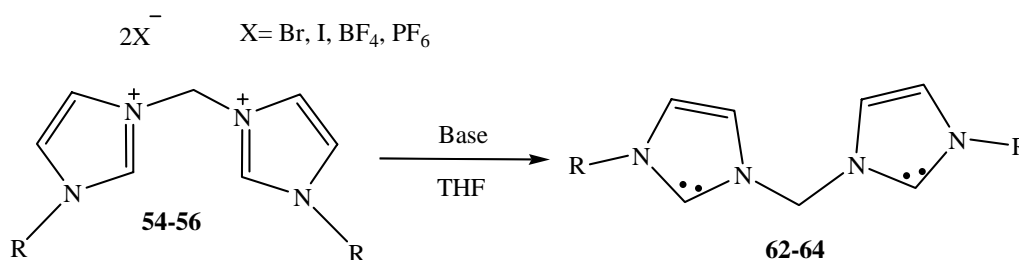
Figure 42. The UV-Vis spectrum of isolated material **49e**.

II-5. Reaction of iron(II) with Free biscalbene ligands

12. Complexation of iron(II) precursors with free carbene ligands: 1,3-bis(aryl)-3,3'-methyleneimidazol-2-ylidene

12.1. Synthesis of free biscarbene

Bisimidazolium salts **54**, **55** and **56** were converted to their corresponding carbene by treatment with strong bases, such as sodium hydride and/or potassium *tert*-butoxide in THF at low temperature. After removing THF under vacuum, the residue was extracted in hot toluene (70°C) to give the corresponding carbenes in 80% yield. Their structure was confirmed by the absence of the N-C(H)-N proton resonance in the ¹H-NMR spectrum and by the appearance of carbene carbon resonance N-C(2)-N in ¹³C-NMR, which was observed in the narrow range of 214 ppm to 210 ppm as reported in the literature¹¹⁹. The UV-Vis spectra of the free carbenes in THF showed absorptions bands in the range of 242 nm to 246 nm.

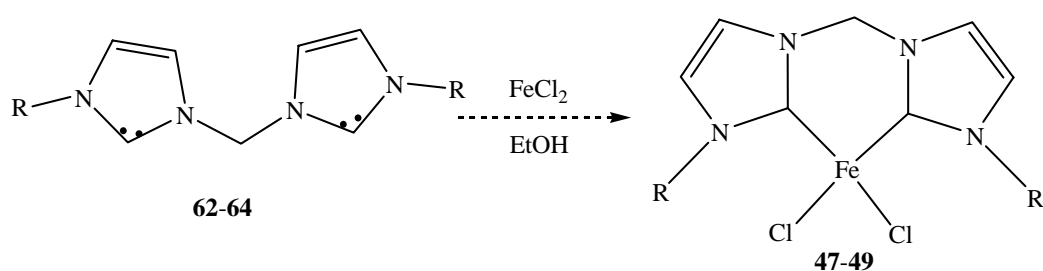


Scheme 44. Synthesis of free carbene bisimidazol-2-ylidenes **62-64**.

12.2. Reaction of free biscarbene with FeX_2 and modified $\text{FeX}_2(\text{THF})_2$ ($\text{X} = \text{Br}, \text{Cl}$)

Preliminary direct metallation with FeCl_2 has been attempted in a polar solvent (ethanol) and non polar solvents (tetrahydrofurane, toluene), in which the iron(II) halides sources are more or less to well soluble.

11.2.1. Reaction in ethanol



Scheme 45. Attempted reaction of free carbene ligands with FeCl_2 in ethanol.

Reaction of carbene bisimidazole-2-ylidene **62-64** with FeCl_2 in ethanol forms brown solids after the work-up. In all cases, the ^{13}C - and ^1H -NMR spectra in THF show only very broad peaks, which confirm the paramagnetic nature of these products. Another reason for these broad peaks could perhaps be the presence of some iron impurities in the sample or some iron(II) survived the reaction conditions. Indeed, we were able to isolate some crystals of two unexpected complexes $[\text{Fe}_2\text{Cl}_6(\mu\text{-O})]^{2-} [\text{Fe}(\text{DMSO})_6]^{2+}$ **88** and $[\text{Fe}_2\text{Cl}_6(\mu\text{-O})]^{2-} [\text{Fe}(\text{DMF})_6]^{2+}$ **89** during the crystallisation attempt of **47** in DMSO and DMF respectively (figure 43 and 44). Crystallisation attempts of **48** in tetrahydrofurane at RT gave orange crystals. The molecular structure determined by the X-ray diffraction consists of cationic bismidazolium μ -oxo-bistrichloroferrate complex **90** (figure 45). We suggest that the protonation of free carbene imidazole-2-ylidene, which is known to be a very strong base (average of $\text{pK}_a \sim 23$)¹²⁰, occurs because of the use of polar protic solvent.

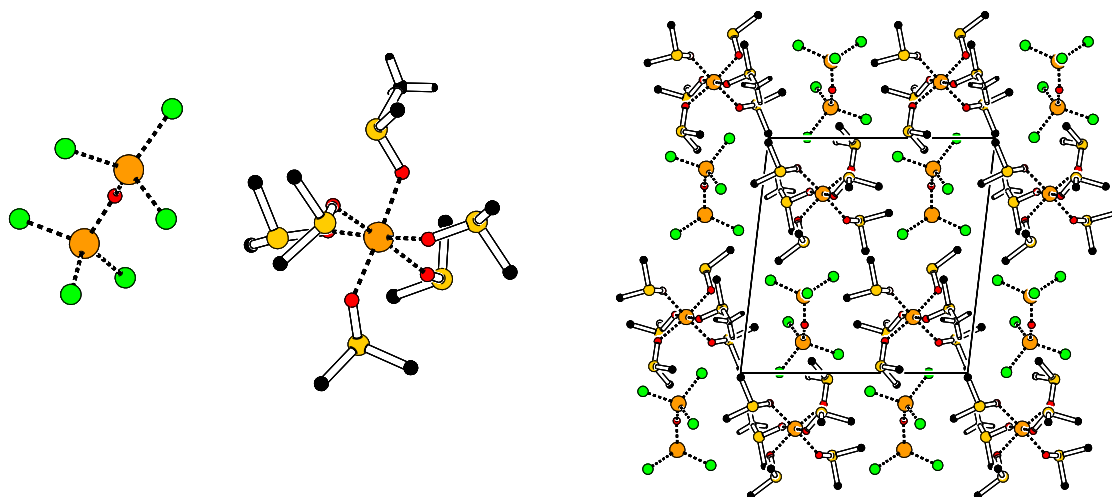


Figure 43. X-ray representation and crystal packing arrangement of the DMSO complex **88**, viewed along the *a*-axis.

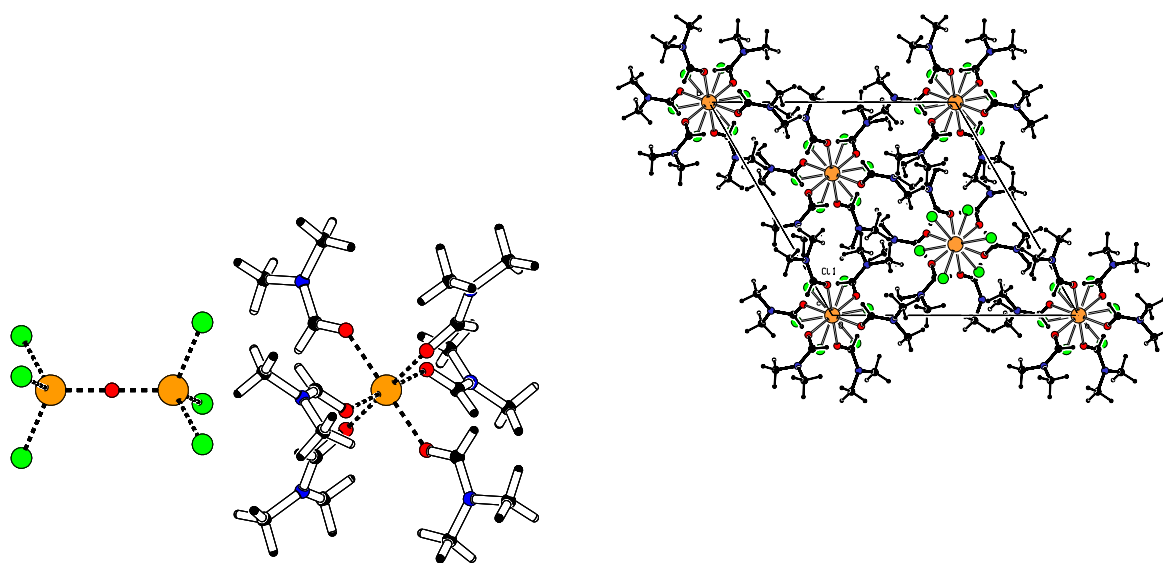


Figure 44. X-ray representation of the DMF complex **89** and crystal packing viewed along the *b* axis.

X-ray analysis of 90

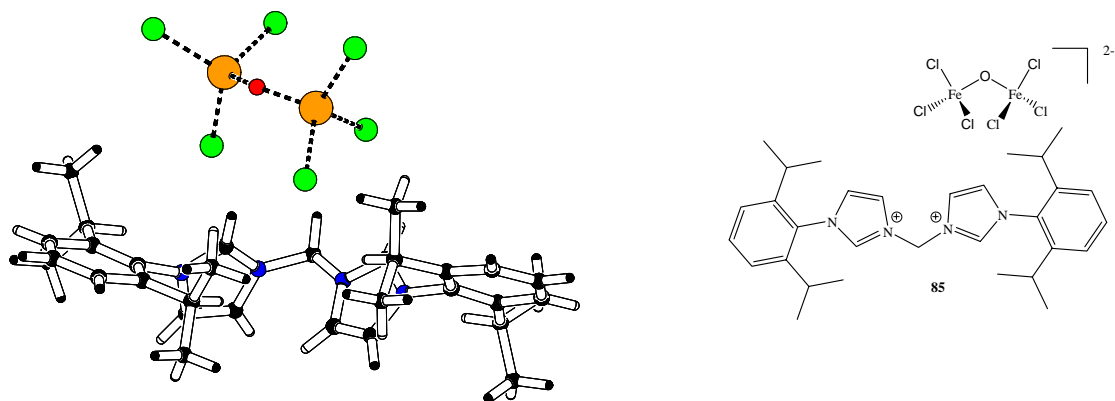


Figure 45. Crystal representation of complex **90**.

Table 10. Selected bond lengths [\AA] and angles [$^\circ$] for **90**.

Fe(1)-Cl(1)	2.229(3)	Fe(2)-Cl(4)	2.241 (3)
Fe(1)-Cl(2)	2.198(3)	Fe(2)-Cl(5)	2.217 (3)
Fe(1)-Cl(3)	2.232(2)	Fe(2)-Cl(6)	2.202 (2)
Fe(1)-O(1)	1.727 (6)	Fe(2)-O(1)	1.772 (6)
N(1)-C(2)	1.360(3)	N(4)- C(19)	1.402(9)
N(2)- C(2)	1.333(9)	C(18)- C(19)	1.362(9)
N(1)- C(3)	1.362(10)	N(1)- C(1)	1.467(9)
N(2)- C(4)	1.396(10)	N(3)- C(1)	1.475(8)
C(3)- C(4)	1.334(10)	N(2)- C(5)	1.472(8)
N(3)- C(17)	1.334(9)	N(4)- C(20)	1.452(9)
N(3)-C(18)	1.377(9)	N(4)- C(17)	1.325(9)
N(1)- C(2)- N(2)	107.0(7)	C(10)- C(5)- N(2)	118.2(6)
N(3)- C(17)- N(4)	107.7(7)	C(21)- C(20)- N(4)	118.3(6)
N(1)- C(1)- N(3)	108.4(6)	C(25)- C(20)- N(4)	118.1(7)
C(6)- C(5)- N(2)	108.6(7)		

The solid-state structure of complex **90**, which crystallizes with one molecule of THF shows that both imidazole rings are orientated in the same directions as in the case of bisimidazolium salts **54a** and **55b** (see figure 26 and 29 respectively). In the counter anion, the metal is tetrahedral with a slight deviation from the idealized geometry. The metal oxo bond lengths are equivalent with $\text{Fe}(1)\text{---O}(1) = 1.727(6)\text{\AA}$ and $\text{Fe}(2)\text{---O}(1) = 1.772\text{\AA}$ and are in agreement with those reported in the literature¹²¹. In contrast to the structures **88** and **89**, the distortion from linearity expressed by a $\text{Fe}(1)\text{---O---Fe}(2)$ angle of $141.4(4)^\circ$ is higher as compared to $161.23(15)^\circ$ for **90**. The formal charge balance consideration requires an iron(III) configuration for the oxo species in complex **90**, which is confirmed by the bond valence sum calculation observed for $\text{Fe}\text{---Cl}$ ($2.198(3)\text{\AA}$ – $2.241(3)\text{\AA}$). Indeed, the typically bond lengths for tetrahedral iron chlorides is 2.301\AA for iron(II) and 2.195\AA for iron(III)¹¹⁵. The packing diagram of **90** presented in figure 46 emphasizes the orientation of the cations around the $[\text{Fe}_2\text{Cl}_6\text{O}]^{2-}$ anions. There are shortest contacts between the hydrogen at carbon C(2) of the imidazolium rings with the chlorides of the counter anion $[\text{Fe}_2\text{Cl}_6\text{O}]^{2-}$, $\text{Cl}\cdots\text{H}$ (average mean of 2.67\AA).

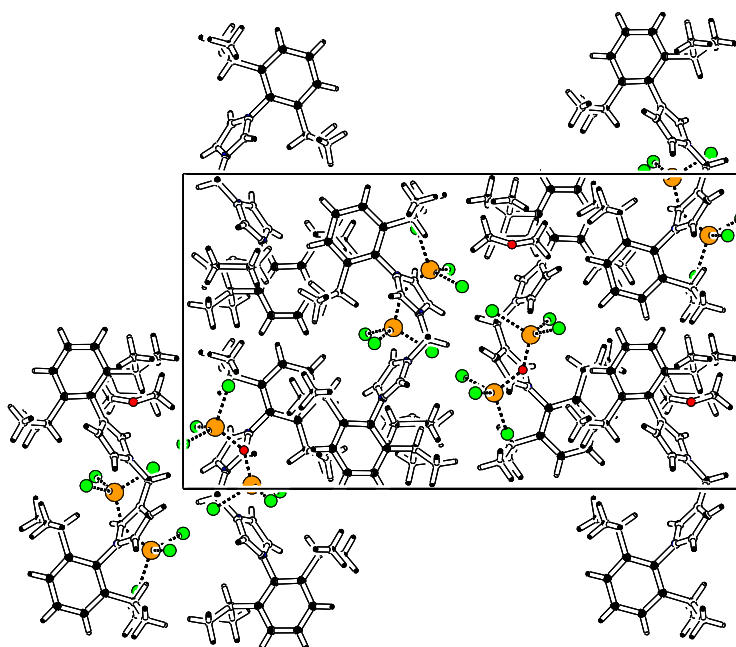


Figure 46. Crystal packing diagram and view along the *b* axis of complex **90**.

The UV–Vis spectra in THF show two absorptions maxima at 359 nm and 318 nm for **47**, 363 nm and 294 nm for **48** and 362 nm and 312 nm for compound **49** (figure 47). For comparison, the spectrum of the corresponding ligand salts exhibits only singular absorption band at 240 nm and that of free carbene show one band at 246 nm.

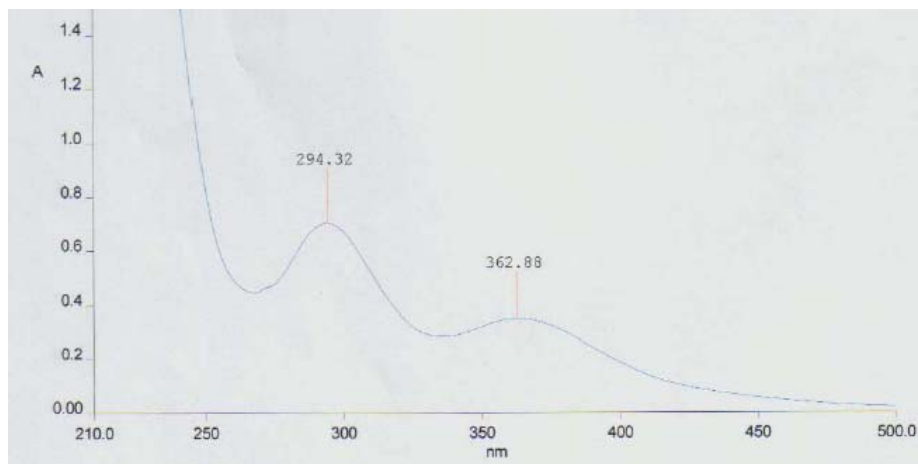
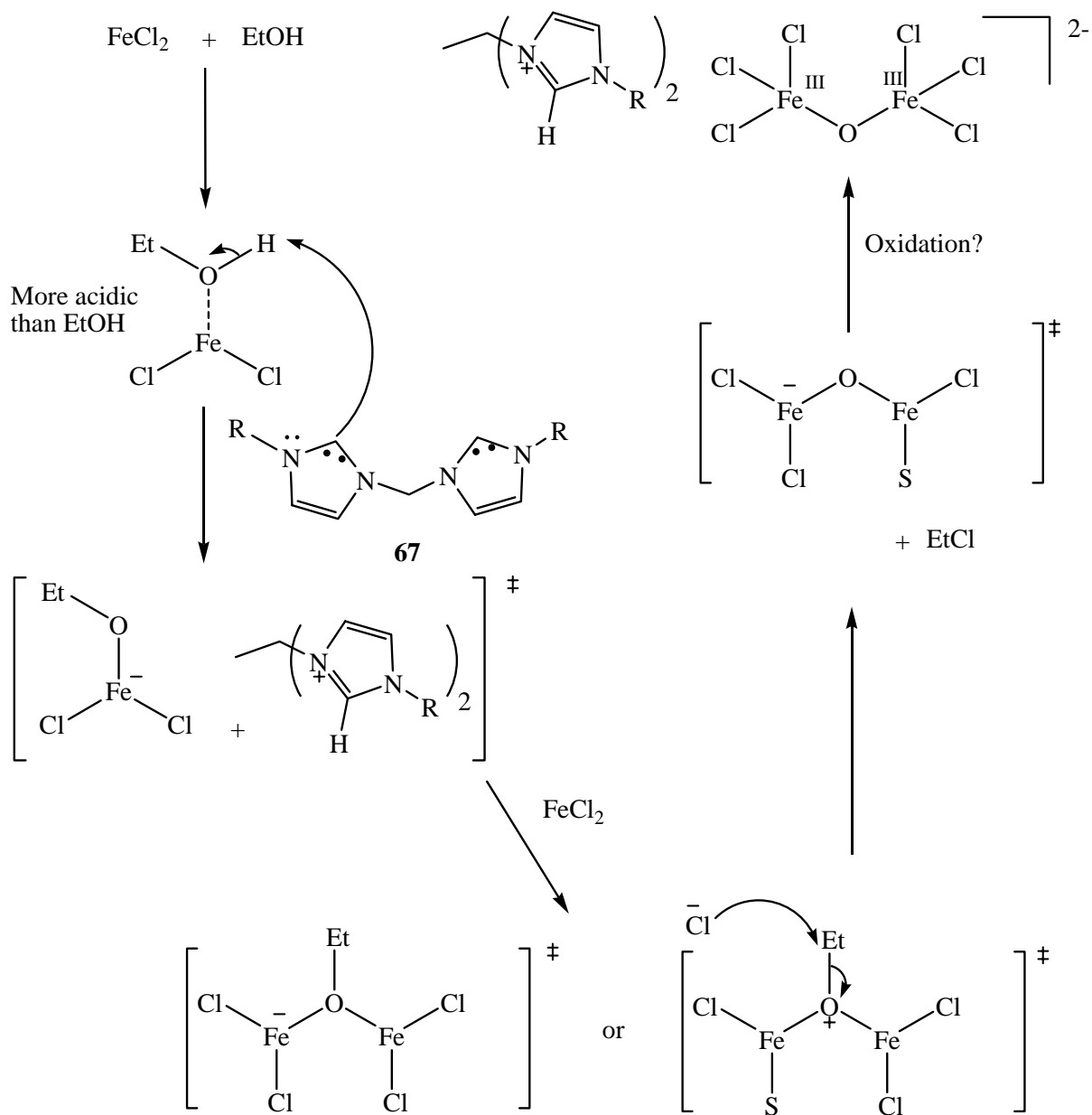


Figure 47. The UV–Vis spectra of complex **90** in THF.

12.2.2 Tentative mechanism for formation of complex **90**

The presence of oxygen could be come from the ethanol, in fact the counter anion $[\text{Cl}_3\text{FeOFeCl}_3]^{2-}$, could simply formed by reacting ethanol or ethanolate and FeCl_2 , since ethanolate is expected to form by proton exchange with the carbenes (scheme 46).



Scheme 46. Tentative mechanism leading to complex **90** ($S = \text{solvent}$).

Further crystallisation attempts in other solvents or in a mixture of solvents such as, toluene, dichloromethane did not work.

For purpose of comparison, the reaction of the salts **54a** and **55b**, respectively, with FeCl_2 in ethanol was done as well, but did not lead to the same products. In fact, the comparison of the

UV-Vis spectra in THF of isolated materials do not show the same absorbance, meaning that preliminary carbene formation is necessary to obtain the iron(III) complexes **90**.

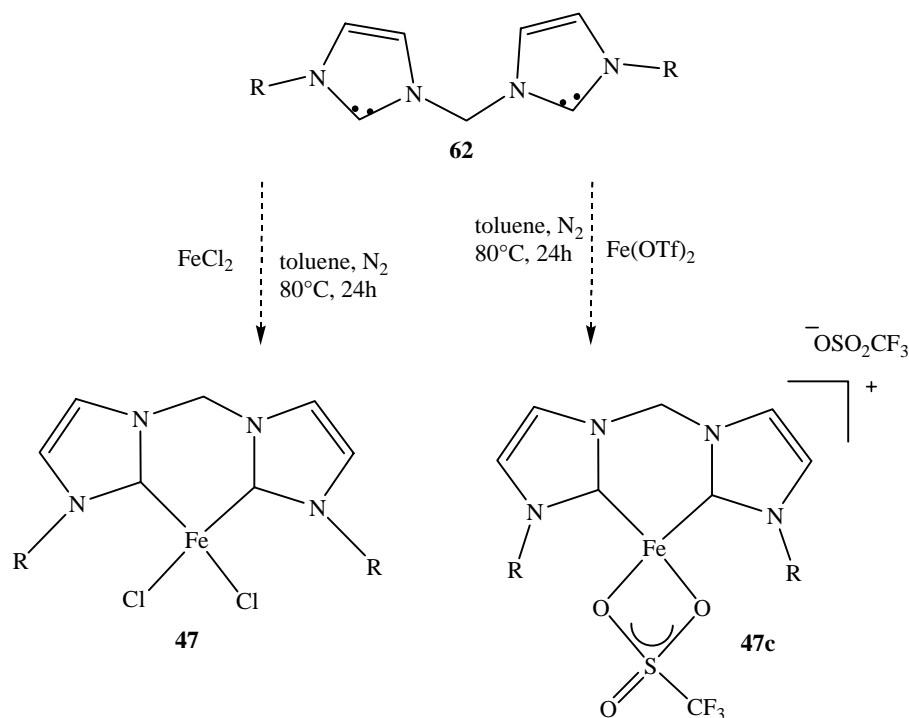
The temperature dependence for the formation of complex **47** has been examined by Aebischer¹²² during his advanced work in organometallic synthesis. Thus, addition of carbene **62** to the iron(II) was starting at -30°C. The progress of the reaction was monitored by UV-Vis spectroscopy. Spectra were recorded on heating every 10°C as shown in table 11. These data shows that the formation of complex already starts at -30°C.

Table 11. Temperature dependence in the preparation of **47**.

Temperature [°C]	Time [min]	UV - Vis [nm]
-30	20	319, 359 (weak)
-20	40	324, 354
-10	60	321, 354
0	80	321, 355
10	100	318, 355
RT	2 days	318, 355

12.2.3. Reaction in toluene

Grubbs and co-workers¹²³ reported the successfully metallation of the carbene 1,3-bisisopropyl-4,5-dimethylimidazol-2-ylidene with FeCl_2 in toluene at 80°C . We applied this procedure for our experiments (scheme 47).



Scheme 47. Reaction of free carbene with iron(II) in toluene.

When the carbene 1,3-bisphenylimidazol-2-ylidene **62** was reacted with FeCl_2 or $\text{Fe}(\text{OTf})_2$ in toluene at 80°C , a red – brownish oil was recovered (**47c**). The UV-Vis of these oily products shows two bands at 298 nm and 242 nm down shifted as compared to the brown solid obtained when the reaction was done in ethanol (359 nm, 318 nm). Probably we have formed the arylbisimidazol-2-ylidene complexes (**91**, **92**; figure 47), since both products have the same aspect and their UV-Vis spectrum shows identical absorption bands. As before, the ^1H - and ^{13}C -NMR spectrum was recorded but resulted in very broad signals. All crystallization attempts using different techniques failed (storage at rt or at low temperature in the freezer, slow diffusion between different solvents).

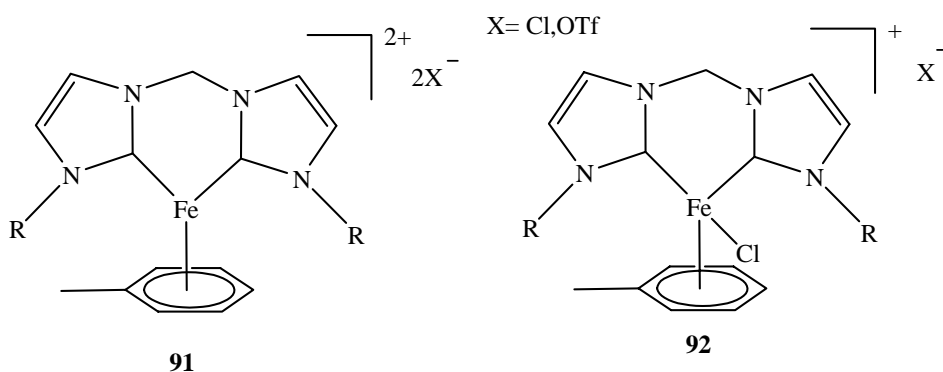
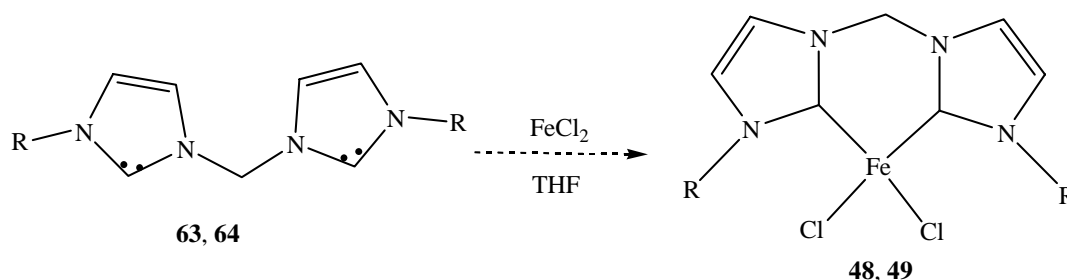


Figure 47. Probably formed arylobiscarbene complexes.

12.2.4. Reaction in tetrahydrofuran

The reaction of free carbene **63** and **64** with FeCl_2 was done at different temperatures (-10°C , RT, 67°C) in THF.



Scheme 48. Complexation reaction of **63** and **64** with FeCl_2 in THF.

The synthesis of the iron(II) complexes **48** and **49** was tried in THF at room temperature. After 48 hours of reaction, the brown–yellow solutions were filtered over celite and the solvent eliminated under vacuum, giving brown solid **48I** and **49I** which were analyzed by UV-VIS. The spectrum shows two bands at 363 nm, 316 nm for compound **48I** and 364 nm, 295 nm for **49I**. These absorptions are different from those observed for the free carbene compound (average values of 246 nm); these changes in the UV–Vis absorption suggest the occurrence of a reaction. However, both samples seem to be highly paramagnetic, thus ^1H - and ^{13}C -NMR spectra were recorded but results only in a broad signals. Attempts to obtain crystals by storage at low temperature and by slow diffusion involving toluene/THF and diethylether/THF failed. The MS did not show any recognizable peak.

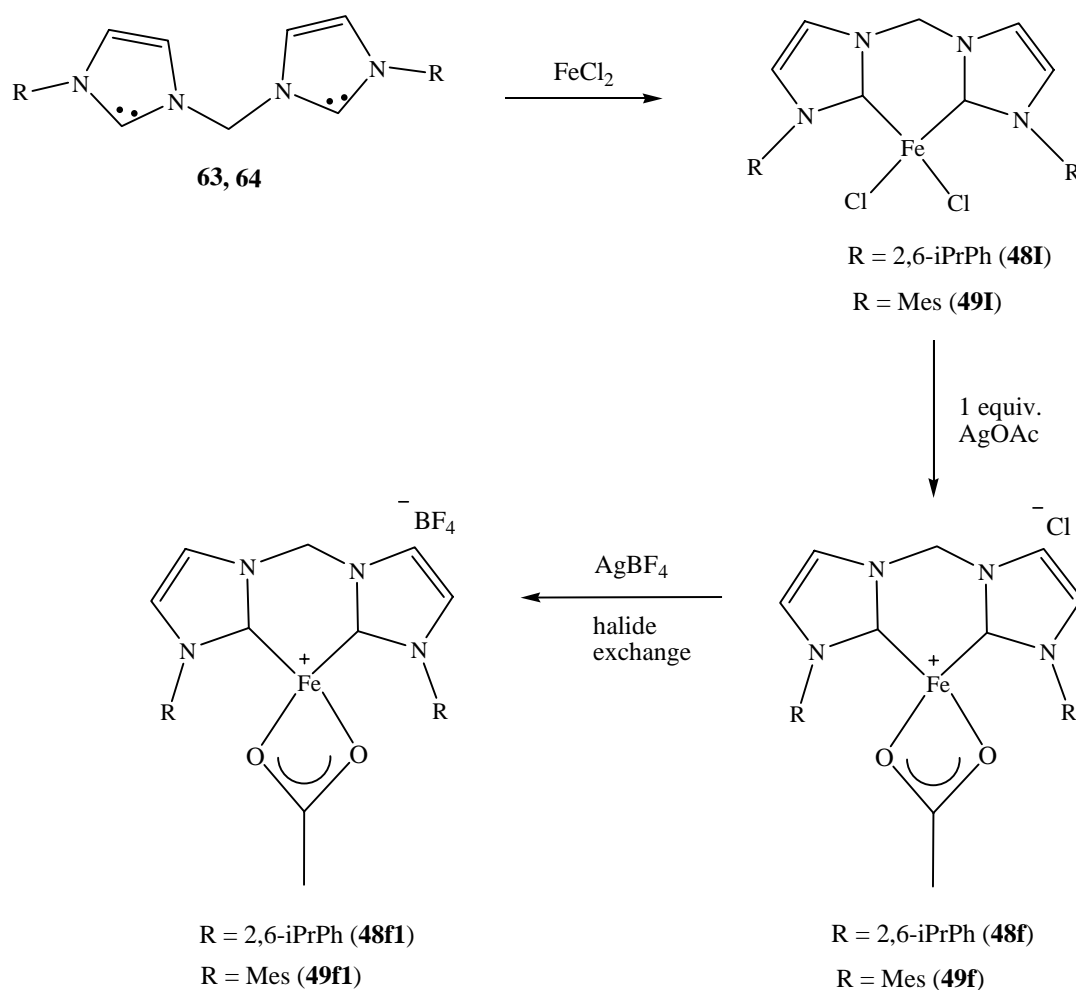
Lower temperature reaction was attempted too: A yellow-orange solution of free carbene ligand in THF was filtrate in a Schlenk at -10°C containing FeCl₂ in THF, and then the mixture was kept at this temperature for 4 hours. The obtained red solution was filtrated and the solvent evaporated. The resulting yellow brownish solid (**48II**) was submitted to MS(ESI(+), MALDI) and ¹³C NMR analyses without success. Attempts to crystallise these materials does not work. The UV–Vis spectrum is in the same range as obtained previously for **48I**.

When the reaction was done at 67°C, we isolated a red solid (**47III**) after the work up. The ¹³C-NMR spectrum shows broad signals. In the UV–Vis spectrum, two absorptions are observed at 362 nm and 298 nm. No desired peak was detected in the mass spectrum (ESI+). Crystallization of this red solid by slow diffusion in Et₂O/THF failed to give suitable crystals.

12.3. Preparation of iron(II) containing bisimidazolydine and carboxylate ligands

The chelate and anionic co-ligands are known to play an important role in the stability of complexes and in catalytic reactions involving transitions metals¹²⁴. Well documented is the change of reactivity and enantioselectivity in the Heck reaction by replacing halides with weakly coordinating triflates, trifluoroacetates, etc. (neutral vs cationic pathway, respectively) or leading to increased polymerization activity.

In order to increase the stability of the obtained complexes and to get eventually crystals, we synthesized halide substitution derivatives. Thus, the previous reaction of FeCl₂ with **63** and **64** was repeated at RT, and then the isolated product **48I** and **49I** were reacted with silver acetate and silver tetrafluoroborate as chlorine scavenger (scheme 49).



Scheme 49. Synthesis of carboxylate iron complexes.

Upon reaction of one equivalent of silver acetate with complex **48I** in THF, an orange solid (**48f**) is obtained after filtration and evaporation of the solvent. The presence of carboxylate ligand on the complex was confirmed by IR (1632 cm^{-1}). The ^1H -, ^{13}C -NMR spectra were recorded, but showed very broad peaks difficult to be assigned. The mass (ESI+) spectrum does not show any expected peaks. The reaction of **48f** with one additional equivalent of silver tetrafluoroborate in THF provokes the immediate precipitation of AgCl, the upper yellow solution was treated by filtration and gave an orange-pale solid **48f1** after evaporation of the THF. The analysis by MS(ESI+/-) and crystallisation attempts by slow diffusion of ether in THF solution of complex did not permit the identification of product. However, infrared and UV-Vis spectra were recorded and the results are summarised in table 12. The absorption in the infrared at 1637 cm^{-1} could be attributed again to the carboxylate group. For

comparison, the carboxylate infrared band of the starting silver acetate salt appears at 1559 cm^{-1} .

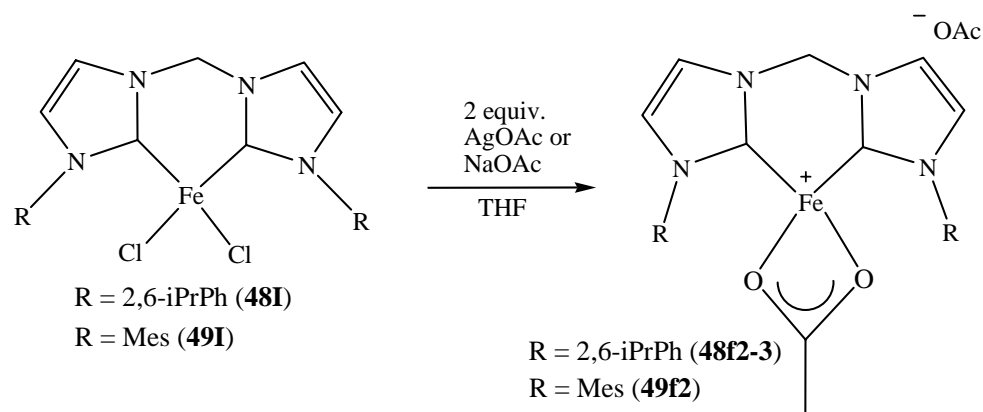
The iron(II) complex **49i** was also reacted with one equivalent of silver acetate under the same conditions as described before for the synthesis of **48f**. An orange–yellow sticky solid **49f** was isolated after treatment of the solution. Again, only the IR and UV–Vis spectra were measured. The UV–Vis spectrum shows only a singular absorption band at 359 nm; the infrared absorptions at 1640 cm^{-1} and 1632 cm^{-1} could be assigned to the carboxylate stretching (table 12). MS(ESI+) was done but the obtained spectra do not show expected peaks.

As previously, we did a counter anion exchange between chloride and tetrafluoroborate by addition of AgBF_4 to the THF solution of **49f**. Filtration of the upper solution and evaporation of solvent permits to isolate an orange solid **49f1** which was analysed by infrared where the presence of a carboxylate was identified at 1636 cm^{-1} , that is in the same range as observed for compound **49f1**. The MS(ESI+) spectra of isolate solid did not show any expected peaks. All crystallisation attempts also failed.

Table 12. Reactions conditions and obtained results.

Exp	Complex (mmol)	[Ag] (mmol)	Solvent (ml)	Temp. [°C]	Time [hours]	Yield [%]	UV-VIS [nm]	IR [cm ⁻¹]
1	48I (0.5)	AcO (0.5)	THF(20)	rt – reflux	4	48f	358; 300	1632m; 1597m; 1439m
2	48f (0.5)	BF ₄ (0.5)		rt	1	48f1	360	1637m; 1523m; 1464m; 1074vs
3	49I (0.5)	OAc (0.5)		rt – reflux	4	49f	359	1640m; 1632s; 1453m
4	49f (0.5)	BF ₄ (0.5)		rt	1	49f1	360	1636m; 1516m; 1464m; 1071vs

We repeated the previous reaction of **48I** and **49I** with silver acetate or sodium acetate, but contrary to the previous run, we used two equivalents of two different acetate sources. The reaction was done in THF first at RT, then at reflux affording **48f2-3** and **49f2**.



Scheme 50. Synthesis of complexes **48f2-3** and **49f2**.

Table 13. Reactions conditions used for a synthesis of complexes **48f2-3** and **49f2**.

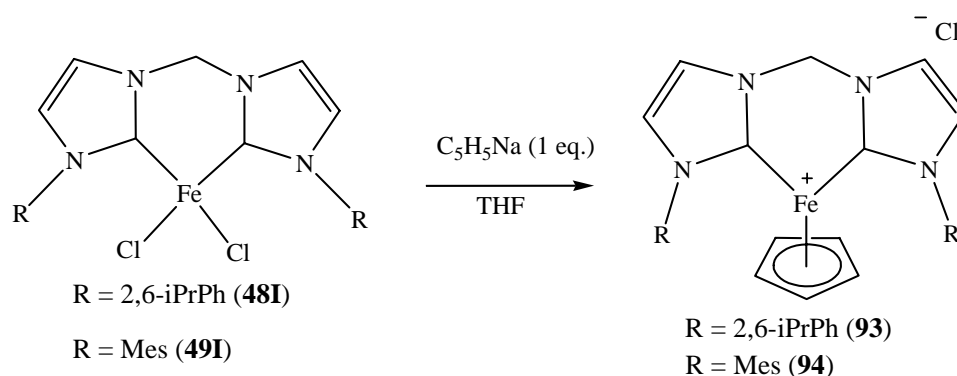
Exp	[Fe] (mmol)	[OAc] (mmol)	Solvent (ml)	Temp. [°C]	Time [hours]	Product	UV-VIS [nm]	IR [cm ⁻¹]
1	48I (0.3)	Ag (0.6)	THF(20)	reflux	4	48f2	340;272; 267	1626s; 1601m
2		Na (0.6)				48f3	362;286; 268	1627m; 1602m
3	49I (0.3)	Ag(0.6)				49f2	358, 235	1680m; 1632m

Analysis of the MS (ESI+) spectra of complex **48f2** shows a peak at m/z 728 $[\text{M}+2\text{THF}]^+$, attributed to the desired product coordinated with two molecules of THF. The vibration at 1626 cm^{-1} in the IR spectra confirms the presence of a carboxylate ligand. The UV-Vis spectra in THF of the starting chloro complex **48I** (364 nm, 295 nm) and that of the isolated complex **48f2** (340 nm, 272 nm, 267 nm) are different. The ¹³C-NMR shows very broad peaks

and elemental analysis failed to confirm the proposed structure. Crystallization attempts in various solvents and temperature did not afford suitable crystals.

The complex **48f3** was prepared in refluxing THF by addition of NaOAc to a yellow–brownish solution of complex **48I** in THF at reflux. The colour of the solution changes from yellow to orange at the end of the reaction. Filtration and evaporation of solvent gave an orange yellow solid which was characterized by MS(ESI+) : m/z 728 [M+2THF]⁺, IR and UV–Vis spectrum. The ¹H- and ¹³C-NMR spectra were recorded but it resulted in broad peaks, probably the samples were contaminated with paramagnetic iron residues. Elemental analysis did not fit the expected results. Crystallisation attempts at RT and at low temperature (-20°C) were done without satisfactory results. In the infrared spectrum of the orange solid **49f2**, the absorptions at 1632 cm⁻¹, could be as previously assigned to the vibrations of the carboxylate groups, however the MS(ESI+) spectrum doesn't show any peak ascribable to the molecular peak.

12.4. Preparation of iron(II) containing cyclopentadienyl ligands



Scheme 51. Synthesis of complexes **93** and **94**.

Table 14. Reactions conditions used for the synthesis of complexes **93** and **94**.

Exp	Cp (mmol)	[Fe] (mmol)	Solvent (ml)	Temp. [°C]	Time [hours]	Yield [%]	UV-VIS [nm]
1	(0.6)	48I (0.5)	THF(20)	-78°C to RT	8	93 (68)	420; 365; 334
2		49I (0.5)				94 (60)	402;357; 297

We make reacted one equivalent of sodium cyclopentadienyl (0.5 M in THF) with complex **48I** in THF at -78°C to RT for 8 hours. Filtration and evaporation of the solvent gave an orange-yellowish solid **93**. The UV-Vis spectra exhibit a large band at 420 nm and two others at 365 nm and 324 nm (figure 48); for comparison, the ferrocene shows two absorption bands at 484 nm and 239 nm. The product was characterized by ¹H- and ¹³C-NMR techniques. Indeed, this compound seems to be a diamagnetic complex. In the carbon spectrum, the signal between 165 ppm and 162 ppm was attributed to the resonance of the iron-carbene. The proton and carbon spectra are represented in the figure 49 and 51. All the expected peaks are

presents. Unfortunately, the mass (ESI+) spectrum and the elemental analysis do not furnish the expected results. All crystallizations attempts until now failed.

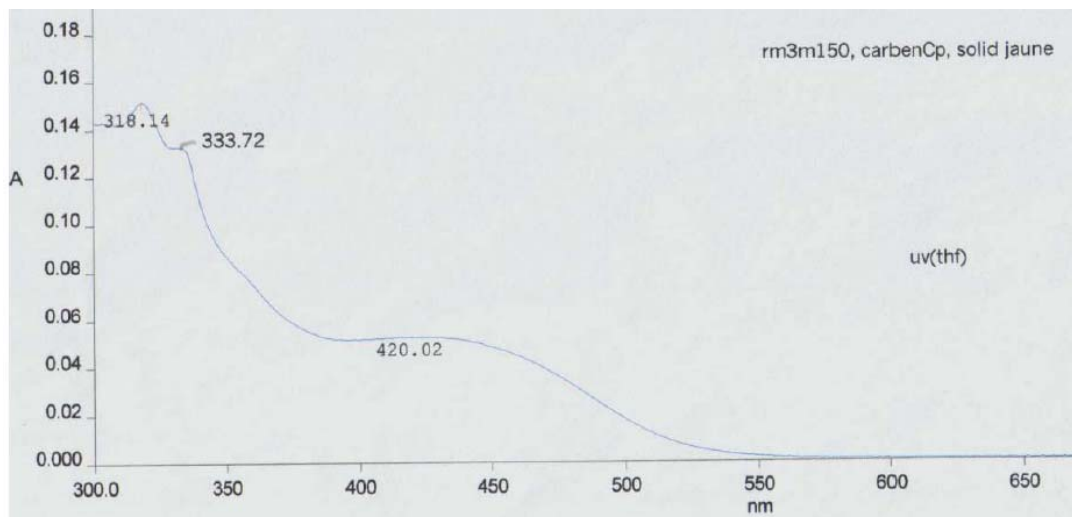


Figure 48. The UV–Vis spectrum of complex **93** in THF.

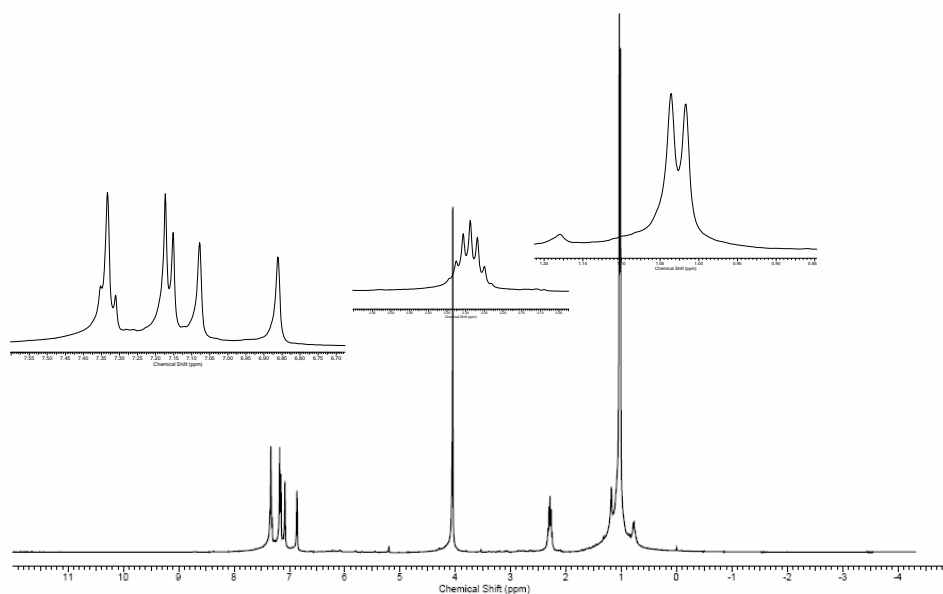


Figure 49. $^1\text{H-NMR}$ (500 MHz) spectrum of complex **93** in CD_2Cl_2 .

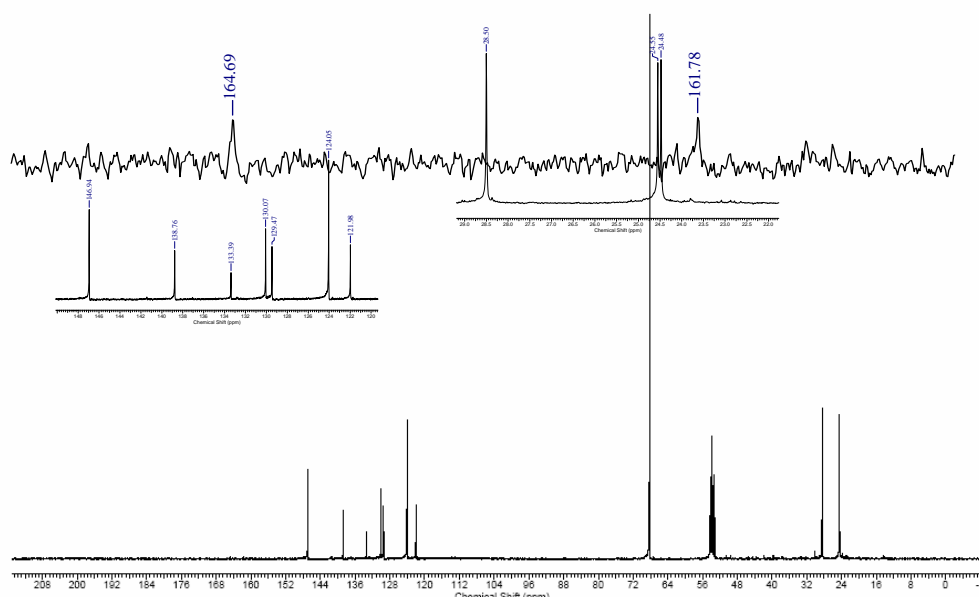


Figure 50. ^{13}C -NMR (125 MHz) spectrum of complex **93** in THF-d_8 .

Despite the presence of all the expected peaks in the ^1H -NMR spectrum, the integral values are slightly beside those awaited. Moreover, a qualitative analysis of the peaks in the ^{13}C -NMR spectrum shows that the peak at 69 ppm, attributed to the cyclopentadienyle, is about four times larger than those situated between 24–32 ppm assigned to the methyl on the isopropyl moieties. These considerations combined with the observations of the ^1H -NMR spectrum suggests the probable presence of ferrocene in the sample, however the mass spectrum of the product does not show any peak ascribable to ferrocene.

Moreover, we exclude the presence of the bisimidazolium salt in the sample based on the absence of the peak corresponding to the proton HC(2) in the spectrum ^1H -NMR. Furthermore, a comparison of the proton spectra of **93** with that of free biscarbene shows that certain peaks (imidazole core) are moved about 0.1 towards low field, but this can also be due to the fact that the peaks in **93** are slightly broader. Additionally, in the ^{13}C -NMR spectrum the peak of the carbon carbenoid differs by approximately 60 ppm.

We also compared the spectra of protons and carbon of the **93** with those obtained for the silver complexes, where a weak difference in the chemical shifts is visible. All these data, is certainly not sufficient to confirm the structure of compound **93**, but they enable us to exclude certain assumptions as previously enounced.

The iron complex **49I** was also reacted with one equivalent of sodium cyclopentadienyl under the same conditions described before for the synthesis of **93**. An orange–yellow solid **94** was

isolated in a good yield (68%), after treatment of the solution. The UV–Vis spectrum of this compound shows absorption bands at 402 nm, 357 nm and 297 nm (figure 51); as previously observed with **93**, this complex also seems to be diamagnetic, thus we were able to record the ^1H - and ^{13}C -NMR spectra. However, in contrast to the complex **93**, the signal of the iron-carbene did not appear in the ^{13}C -NMR spectrum (figure 53). The MS (ESI+) spectrum was done but the obtained results are not in agreement with those expected. All crystallisation attempts failed.

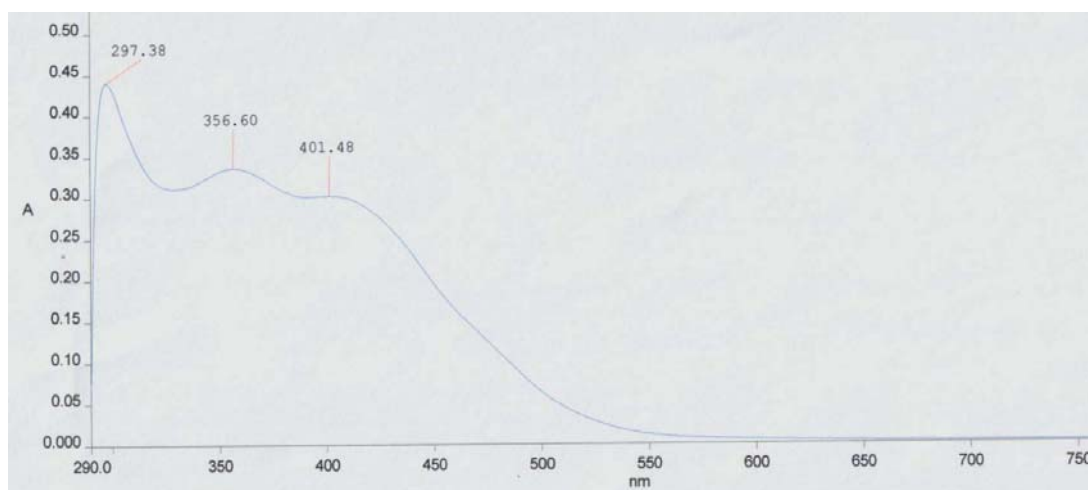


Figure 51. The UV–Vis spectrum of complex **94** in THF.

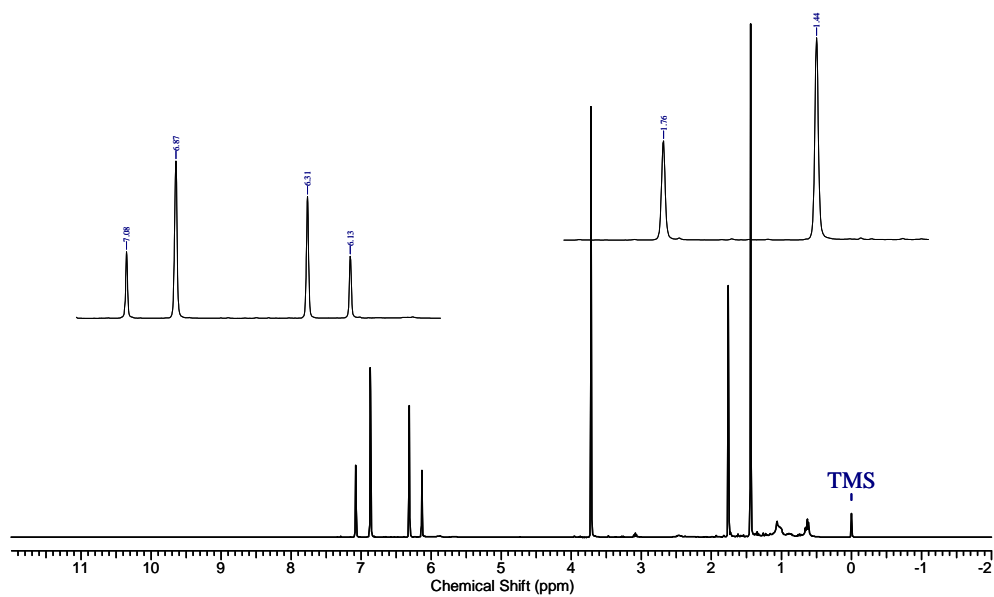


Figure 52. $^1\text{H-NMR}$ (500 MHz) spectrum of complex **94** in C_6D_6 .

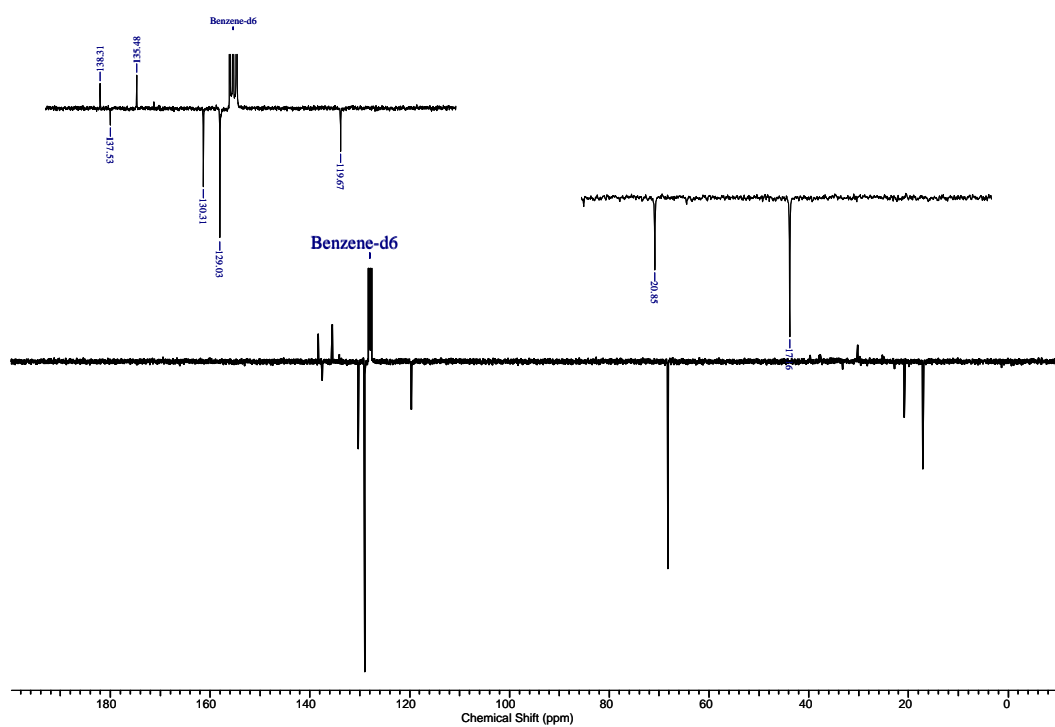
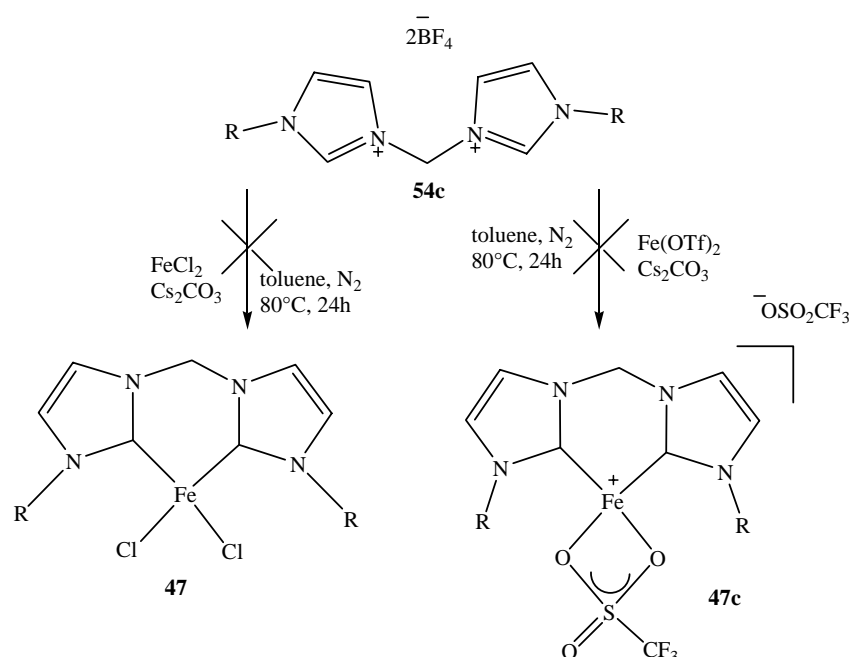


Figure 53. APT $^{13}\text{C-NMR}$ (125 MHz) spectrum of complex **94** in C_6D_6 .

12.5. Attempted synthesis of Iron(II) complexes via “*in situ*” formation of free carbene

In situ deprotonation of phenylimidazolium salt **54c** with the mineral base Cs₂CO₃ followed by complexation with FeCl₂ or Fe(OTf)₂ has been attempted but did not lead to an identifiable complex. On the contrary, we recovered the starting ligand intact. We suppose that the failure of this reaction is due to the poor solubility of the starting materials in toluene (Cs₂CO₃ and the iron (II) sources).



Scheme 52. “*In situ*” attempt using Cs₂CO₃ as base.

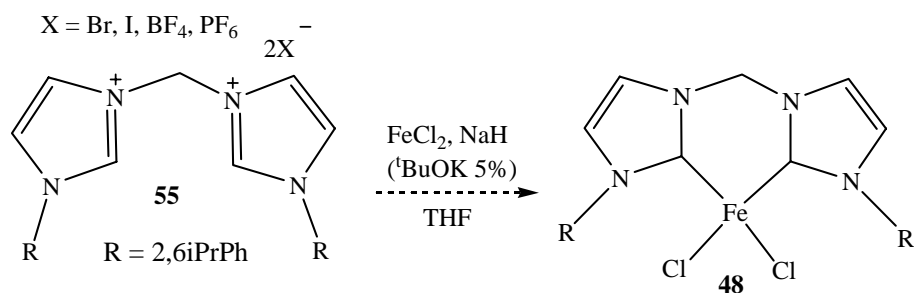
Table 15. The use of Cesium carbonate as base.

Exp	54c (mmol)	[Fe] (mmol)	Cs ₂ CO ₃ (mmol)	Solvent (ml)	Temp [°C]	Time [h]	UV-Vis [nm]
1	0.6	0.6 ^a	4.2	Tol (20)	RT- 80	24	-
2		0.6 ^b					

^a FeCl₂, ^b Fe(OTf)₂

We also tried a “one pot” reaction of imidazolium salts **55a-d** with NaH/(^tBuOK 2%) in the presence of FeCl₂ at RT. Red brownish solids were recovered after filtration over Celite and

evaporation of the solvent. The ^1H - and ^{13}C -NMR spectra were not recorded because of the strong paramagnetism of the obtained materials. The MS spectra (ESI+) did not show any desired peak; products were placed at low temperature in order to provoke crystallization but no crystals formed. The UV-Vis spectra in THF of the isolated compounds show only a singular absorption in the range of 298-300 nm.



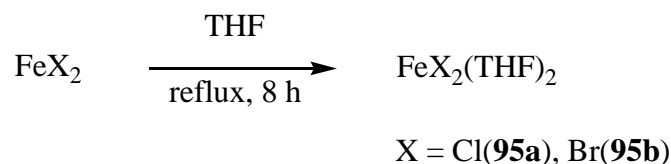
Scheme 53. Attempted preparation of **48** via “one pot” reaction.

II-6. Synthesis of iron(II) precursors

13. Synthesis of Iron (II) precursors soluble in THF ($\text{FeX}_2(\text{THF})_2$) and $\text{FeX}_2(\text{PPh}_3)_2$

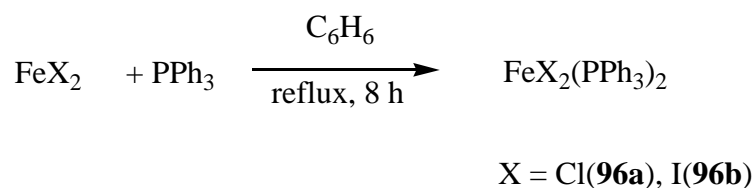
As part of our effort to synthesize the iron(II) biscarbene imidazol-2-ylidene complexes **47-49**, we have investigated the synthesis of new iron (II) precursors which would be soluble in common solvents such as THF or toluene. Thus, we have prepared and employed a series of bis(halidetetrahydrofuran)iron(II), $\text{FeX}_2(\text{THF})_2$ **95**, and bis(halidetriphenylphosphine) iron(II), $\text{FeX}_2(\text{PPh}_3)_2$ **96**, complexes.

The $\text{FeBr}_2(\text{THF})_2$ (**95a**) was prepared by refluxing FeBr_2 in dry THF for 8 hours (scheme 54). Cooling this solution at room temperature give faint yellow crystals whose mass spectrum shows the desired product $\text{FeBr}_2(\text{THF})_2$, together with other oligomers: $[\text{FeBr}_2(\text{THF})_2]_2$, $\text{FeBr}_2(\text{THF})_3$, probably formed under MS conditions. $\text{FeCl}_2(\text{THF})_2$ (**95b**) was also prepared in a same way. These compounds are sensitive to the air that is visible by through rapid changes of their colour, which went from pale-beige to yellow and then orange-red. Nevertheless, it is possible to weigh them quickly in air.



Scheme 54. Synthesis of $\text{FeX}_2(\text{THF})_2$ **95**.

The $\text{FeCl}_2(\text{PPh}_3)_2$ **96a** was prepared following a reported procedure⁷⁸, by reaction of anhydrous FeCl_2 with PPh_3 in dried benzene at reflux. Hot filtration of the reaction mixture permits to recover a yellowish solution, which was allowed to stand for 1 day at room temperature affording pale-green crystals in a good yield. The isolated crystals were analysed by X-ray diffraction and the molecular structure shows a *trans*-dichloro iron(II) complex (figure 54).



Scheme 55. Bishalide bistrisphenylphosphine iron (II) synthesis.

In the same manner we tried to prepare the $\text{FeI}_2(\text{PPh}_3)_2$ **96b** compound. However, the X-ray diffraction of isolated brownish-clear crystals shows a phosphine oxide complex **97** (figure 55).

The X-ray analysis of **95a** and **97**

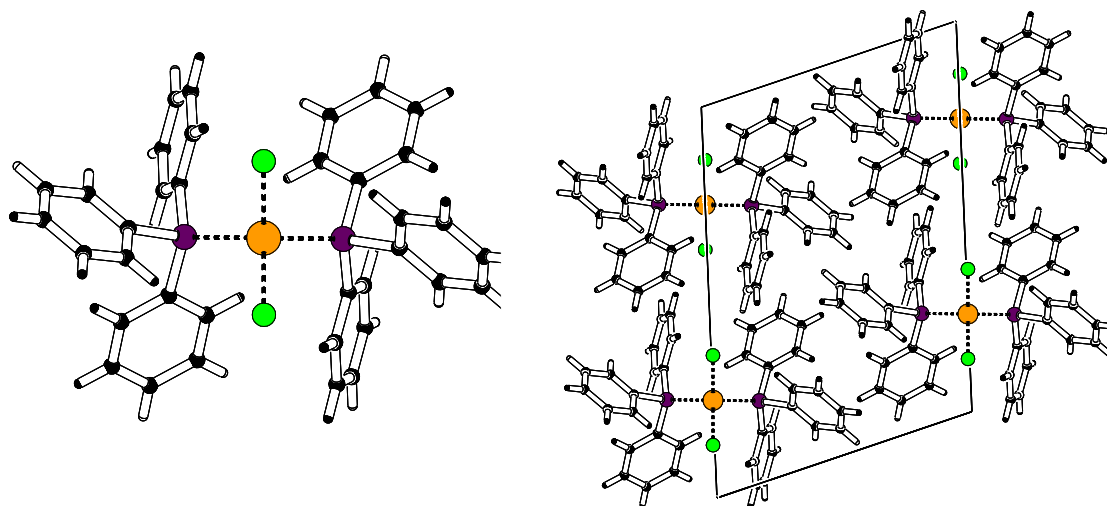


Figure 54. X-ray structure of complex **95a** and his crystal packing arrangement projected along the *a*-axis.

Table 16. Selected bond lengths [\AA] and angles [$^\circ$] for **95a**.

Fe(1)-Cl(1)	2.218(5)	Fe(1)-P(1)	2.453(5)
Fe(1)-Cl(2)	2.218(5)	Fe(1)-P(2)	2.453(5)
P(1)-C(1)	1.819(18)		
P(1)-C(7)	1.814(18)		
P(1)-C(13)	1.817(18)		
Cl(1)-Fe(1)-Cl(1a)	124.2(3)	Fe(1)-P(1)-C(7)	115.8(6)
P(1)-Fe(1)-Cl(1)	104.7(18)	Fe(1)-P(1)-C(13)	118(6)
P(1)-Fe(1)-P(1a)	111.6(2)	C(1)-P(1)-C(7)	104.5(8)
P(1)-Fe(1)-Cl(1a)	105.9(17)	C(1)-P(1)-C(13)	104.1(8)
Fe(1)-P(1)-C(1)	108.3(6)	C(7)-P(1)-C(13)	104.8(8)

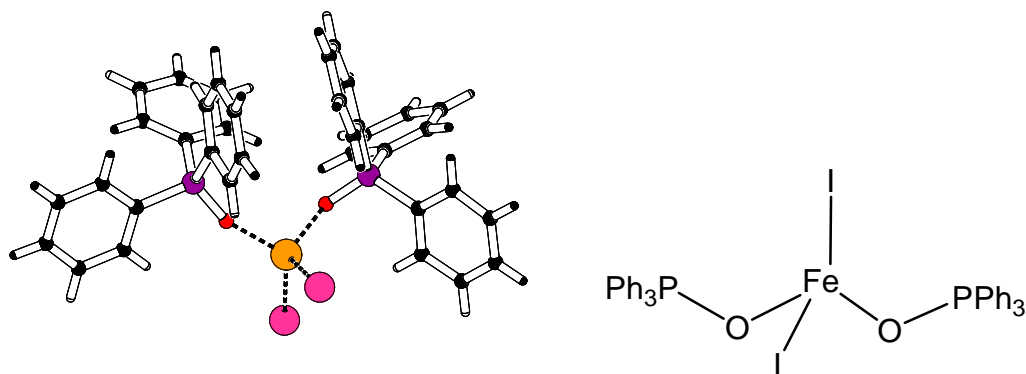


Figure 55. X-ray structure of tetrahedral complex **97**.

Table 17. Selected bond lengths [\AA] and angles [$^\circ$] for **97**.

Fe(1)-I(1)	2.616(13)	Fe(1)-O(1)	1.963(6)
Fe(1)-I(2)	2.608(12)	Fe(1)-O(2)	1.988(7)
P(1)-O(1)	1.489(6)	P(2)-O(2)	1.458(7)
P(1)-C(1)	1.772(9)	P(1)-C(7)	1.794(9)
P(1)-C(13)	1.798(9)		
I(2)-Fe(1)-I(1)	111.6(4)	P(1)-O(1)-Fe(1)	159.6(5)
O(1)-Fe(1)-O(2)	102.0(3)	P(2)-O(2)-Fe(1)	144.3(4)
O(1)-Fe(1)-I(2)	109.1(19)	O(1)-P(1)-C(1)	109.6(4)
O(1)-Fe(1)-I(1)	116.6(2)	O(1)-P(1)-C(7)	110.9(4)
O(2)-Fe(1)-I(1)	103.4(19)	O(1)-P(1)-C(13)	113.7(4)
O(2)-Fe(1)-I(2)	113.8(2)	C(1)-P(1)-C(7)	106.2(4)

The oxygen incorporated in the structure of **97** can come from several sources:

- 1) The solvent used could contain traces of water and/or oxygen, but this assumption is to be excluded since the same solvent was employed to prepare complex **95a**.

- 2) Leaking-in moisture if admitting that the system was not tight but then this product should be a minor one besides the desired product.
- 3) The most plausible assumption, relies on the fact that the commercial triphenylphosphine contains a small amount of its oxidized form. In this case **97**, which crystallizes first, is simply a minority product of our reaction.

To justify the difference in behavior of FeCl₂ and FeI₂ towards the used triphenylphosphine, it is necessary to regard upon the concept of hard-soft acid-base (HSAB). In FeI₂, iodine being a soft ligand in the coordination sphere. Stabilizing iron requires a ligand containing hard atoms like oxygen, that explains the preference for phosphine oxide rather phosphine.

The structure depicted in figure 54 shows that the molecule is planar with little deviation from an idealised geometry, and the iron atom is on a symmetry center. This distortion of the tetragonal geometry is normally ascribed to a combination of steric bulkiness and of the relatively low ligand field–strength of triphenylphosphine. Selected bond length and angle are summarized in the annexe. The Fe—P (2.453(5)Å) is shorter as compared to those observed in analogous iron(III) complexes FeCl₃(PPh₃)₂ (Fe—P in the range 2.654Å)¹²⁵. However, the shortness of Fe—Cl bonds is similar in both complexes (average bond Fe—Cl (2.218(5)Å)). The Cl—Fe—P average angle (105.858(17)°) is less than the Cl—Fe—Cl angle (124.20(3)°) in the same molecule, however both values are far away from the ideal tetrahedral value, 109.5°. A projection diagram viewed down the *b* axis in figure 54 illustrates the orientation of the phenyl groups and the absence of Cl---H interactions in the unit cell.

The molecular structure of complex **97** is tetrahedral, the O—Fe—I average angle is 109.06(19)° and the C—P—O average angle is 109.06(19)° (figure 56). The observed Fe—O mean bond distance of 1.95Å is shorter as compared to those reported for the analogous octahedral FeCl₂(OPPh₃)₄ (2.12Å)¹²⁶. The Fe—I mean distance of 2.616Å is larger than the distance of 2.217Å calculated by Wang¹²⁷. The P—C mean distance of 1.179Å is slighter shorter than the expected 1.87Å from the sum of the single bond covalent radii. As shown in figure 56, the crystal packing of the molecules shows intramolecular hydrogen bonds between iodine and the HC(18) atom that stabilizes the molecule internally [I---H18a 2.992Å and

H18a – C(18) 0.950(4)Å]; There are no interactions due to H---O bonds in the molecular structure of **97**.

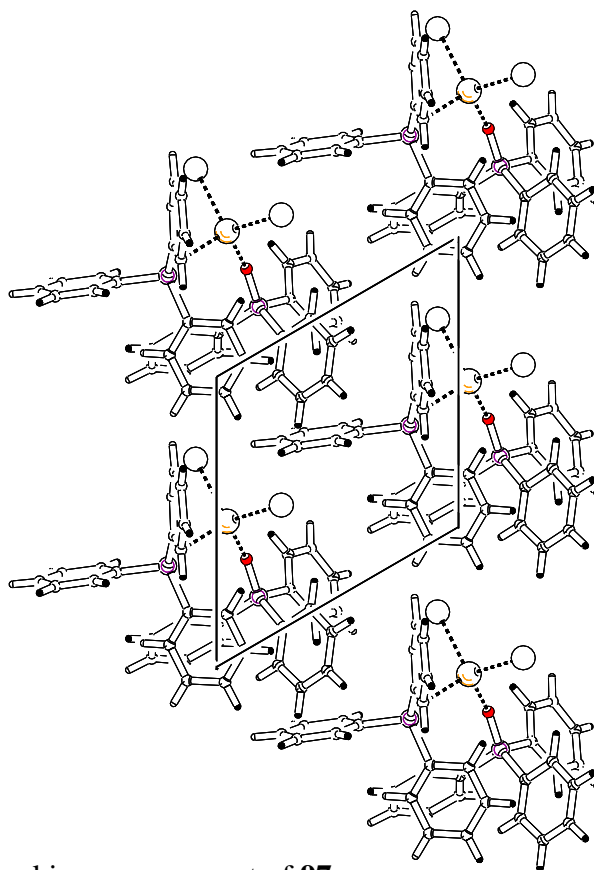
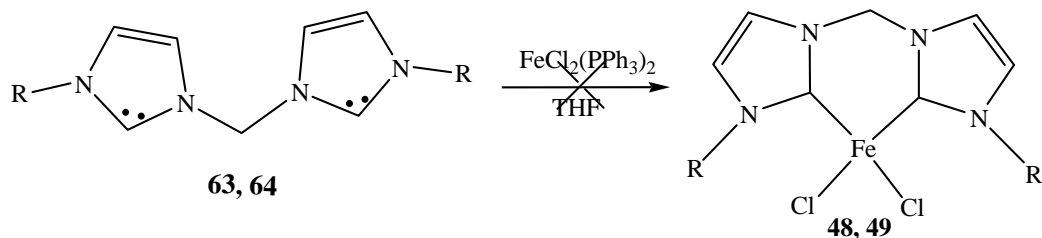


Figure 56. Crystal packing arrangement of **97**.

13.1. Reaction of free biscarbene imidazole-2-ylidenes **63** and **64** with $\text{FeCl}_2(\text{PPh}_3)_2$



Scheme 56. Reaction of iron phosphine with free carbene.

Table 18. Reactions conditions

exp	Carbene (mmol)	$\text{FeCl}_2(\text{PPh}_3)_2$ (mmol)	solvent	Temp. [°C]	Time [hours]	48, 49 yield [%]	UV – Vis [nm]
1	63 (0.4)	0.2	THF (20 ml)	RT	24	-	320
2	64 (0.4)					-	324

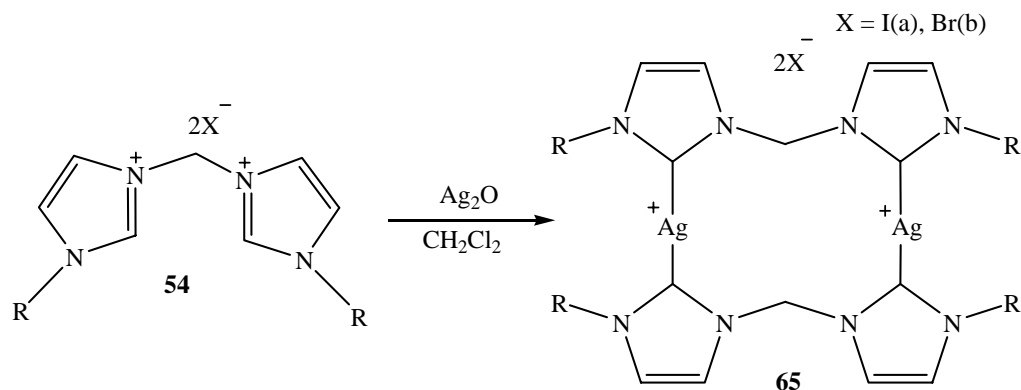
Reaction of $\text{FeCl}_2(\text{PPh}_3)_2$ with free carbene **63** or **64** (2 equivalents) in THF at room temperature leads in both cases to a brown oily-solid after evaporation of THF and several extraction with toluene. Unfortunately, we were not able to identify any product. Indeed, not all analytical and spectroscopic measurement gave expected signals, except for the UV–Vis, where absorption bands were observed at 320 nm and 324 nm, respectively. A NMR spectrum was not recorded because the sample was expected to be paramagnetic. Colourless crystals were grown in THF solution. The X-ray diffraction of them showed triphenylphosphine, probably released during the reaction.

II-7. Silver complexes

14. Silver biscarbene imidazole-2-ylidene as intermediates for a synthesis of iron(II) complexes

In this chapter we describe the synthesis and use of silver N-heterocyclic carbene complexes as ligand transfer reagents for the preparation of the corresponding iron(II) complexes. In fact, the use of silver carbenes instead of free NHC carbenes is becoming common^{128,129}, both as a method to avoid unselective deprotonation of N-functionalised NHC's, and due to the tolerance to air and moisture of the silver complexes. Furthermore, some of them are even not light sensitive.

14.1. Synthesis of the bis(N-(1,1')-bisphenyl-3,3'-methylenebisimidazolyl-2-ylidene) silver complex

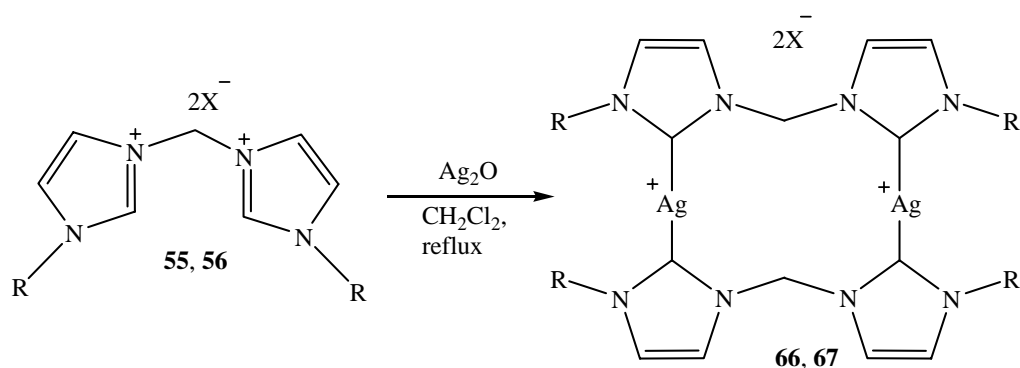


Scheme 57. Synthesis of silver carbene complex **65**.

The bisimidazolium salts **54a-b** were readily deprotonated upon treatment with Ag₂O in the presence of activated molecular sieves 4Å to afford silver complexes **65a-b** at RT in CH₂Cl₂ (scheme 57). The black–grey mixture was stirred overnight to produce a yellowish solution and some grey-white solid. Filtration and evaporation of the solvent afforded the silver carbene complexes **65a-b** as a pale-yellow solid in 60% yield. The formation of the carbene complex **65a-b** was established by the absence of the resonance for the H-C(2) imidazolium proton in the ¹H-NMR spectra. The ¹³C-NMR spectra show all the expected peaks except the resonance of a carbenoid carbon. The UV-Vis spectrum of the product **65a** in dichloromethane shows absorptions bands at 292 nm and 279 nm. The yellowish-pale solid was recrystallized from pentane-dichloromethane to give a colorless crystalline product. The X-ray analysis was not possible because of an insufficient quality of crystals. Furthermore,

these crystals seemed to be light sensitive. Indeed, they darkened when taken out of the yellowish solution. The dimeric nature of the structure was confirmed by MS(ESI+) analysis.

14.2. Bis(N-(1,1')-bis(2,4,6-trimethylphenyl) and bis(N-(1,1')-bis(2,6diisopropylphenyl)-3,3'-methylenebisimidazol-2-ylidene) silver complexes (**66** and **67**)

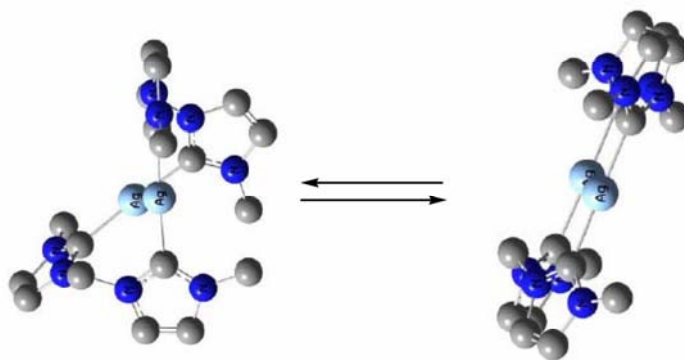


Scheme 58. Silver carbene complexes **66** and **67**.

Silver complexes **66a-b** and **67a-b** were prepared in CH_2Cl_2 at RT using the previously reported method for the synthesis of **65** (scheme 58). After filtration, the solution was evaporated to yield about 30% of beige solid in both cases. The low yield observed under these conditions has prompted us to change the procedure. Thus, the reaction was still done in CH_2Cl_2 but at reflux instead of RT. Filtration and evaporation of the solvent followed by several washings with diethyl ether and pentane afforded **66a-b** and **67a-b**, as white-beige solids in 86 % yield. The absence of the proton resonance for the H-C(2) imidazolium in the $^1\text{H-NMR}$ spectra, permit again to establish the formation of carbene complexes. As already noted in literature¹³⁰⁻¹³³, the $^1\text{H-NMR}$ spectra points also to the formation of a rigid conformation of **67** in solution (figure 57), with two methylene C-H resonances. Supplementary evidence of this structural rigidity is visible by the number of CH_3 -aryl signals: three instead of two for **66**, and by the methyl signal in the isopropyl group, which appears as two doublets for **67**. This is a good indication for hindered rotation of the aryl-rings.

In the $^{13}\text{C-NMR}$ spectrum the mesityl complexes show two doublets at 182.1 ppm and 183.5 ppm for **66**, and 179.5 ppm and 181.5 ppm for **67** (figure 58) for the carbene carbon, due to well resolved silver – carbon couplings ($^1J_{107\text{Ag-C}} = 183\text{ Hz}$ and $^1J_{109\text{Ag-C}} = 212\text{ Hz}$), suggesting that the structures **66** and **67** do not experience rapid exchange of labile silver – carbene bonds

in solution. There are only few examples in the literature concerning this observation, as in most cases sharp singlet ^{13}C -NMR signals are reported, generally taken as evidence of fluxionality in solution (scheme 59)¹³⁰.



Scheme 59. Schematic rotational barriers on silver carbene imidazole-2-ylidene complexes, hydrogens and aryl substituents are omitted¹³⁰.

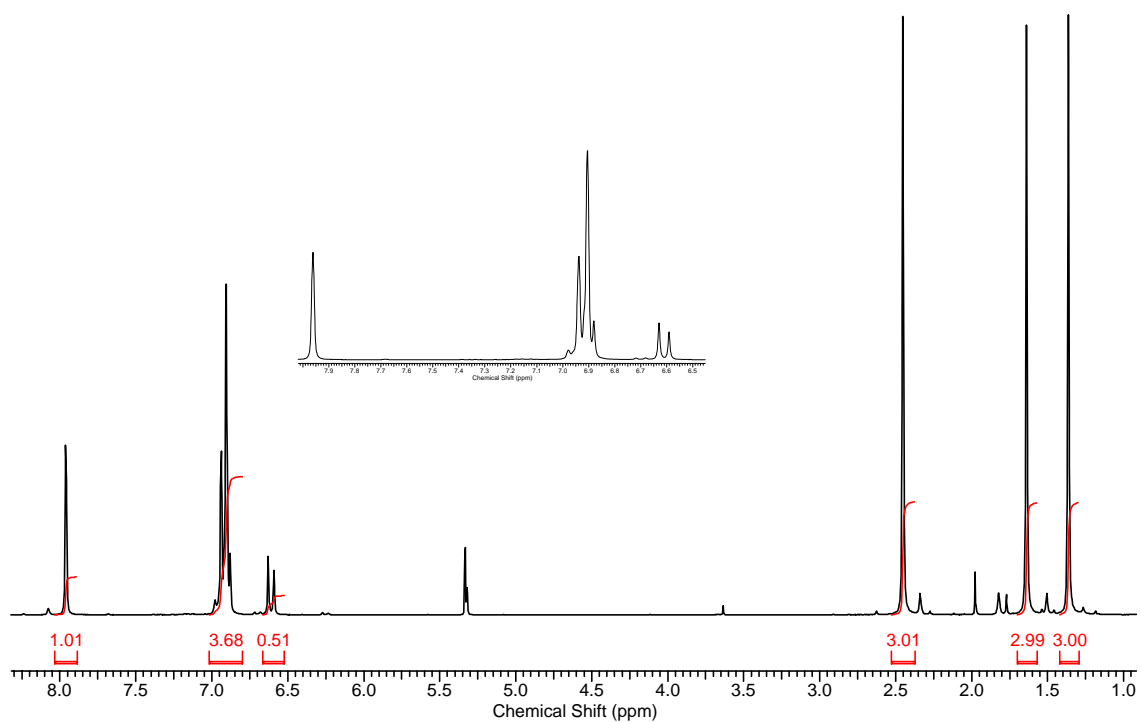


Figure 57. The ^1H -NMR (500 MHz) spectrum of silver complex **67**.

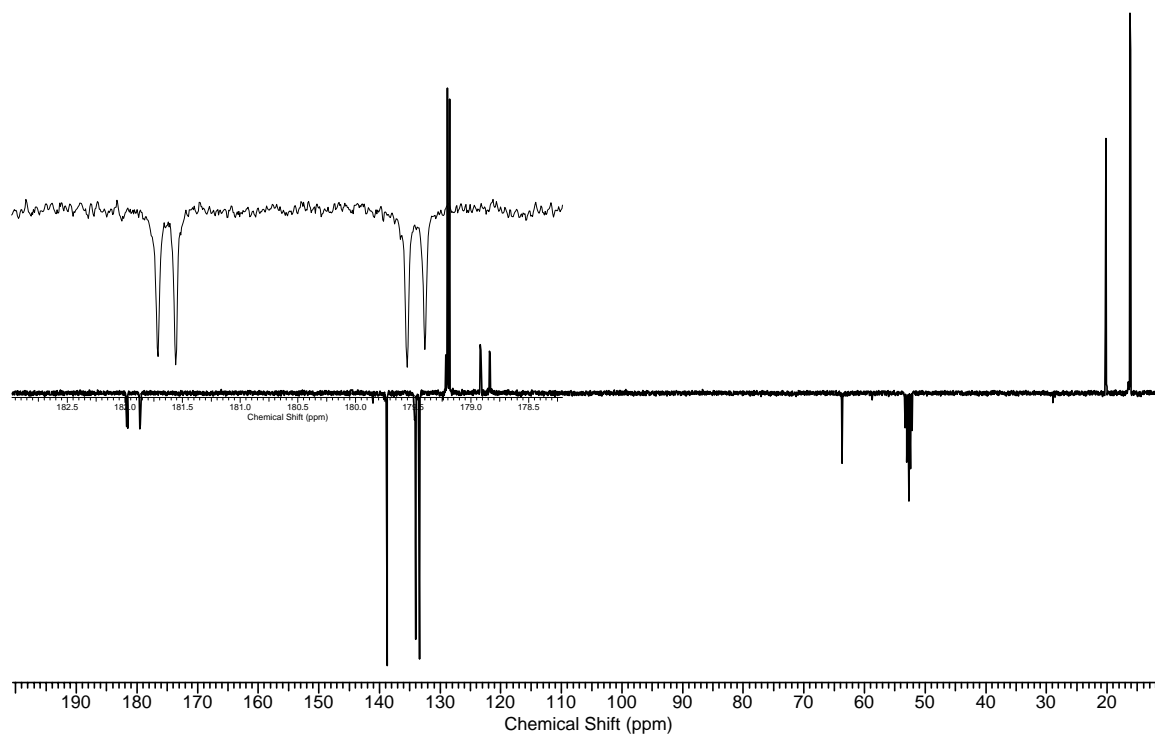


Figure 58. The APT ^{13}C -NMR (125 MHz) spectrum of silver complex **67**.

The UV-Vis spectra of **66** and **67** in dichloromethane show several absorptions at 291 nm, 264 nm and 245 nm; the absorption at 245 nm could be attributed to a probable argentophilic interaction due to the spin-allowed ($d_{\sigma^*}-p_{\pi}$) transition¹³²⁻¹³⁸. Electrospray mass spectrometry MS(ESI+) confirms the dimeric nature of these compounds. Definitive prove of the dimeric structure was obtained by X-ray analysis of colorless crystals grown from dichloromethane (figures 59 and 61).

N-heterocyclic silver carbene complexes with anionic coligands such as tetrafluoroborate (**66d-e**) and hexafluorophosphate (**67c-d**) were also prepared by reaction of the respective bisimidazolium salts with silver oxide in dichloromethane or in acetonitrile at reflux. In all cases, light and air stable white solids were isolated after filtration and evaporation of the solvent. As before two doublets appear in the ^{13}C -NMR spectrum for the N-C(2)-N carbene carbon in the same region (180-182 ppm); the UV-Vis spectra of these products in dichloromethane show two absorption bands at 264 nm and 219 nm. Suitable colorless crystals for **66d** and **67d** were grown in dichloromethane or acetonitrile at room temperature; X-ray diffractions were done and the obtained structures are depicted in the figures 59, 64 and 66.

X-ray structures

In general, the X-ray diffraction analysis of these silver complexes revealed a biscarbene-bridged dimer (figures 59, 61, 64 and 66), each metal ion being coordinated with two carbenoid carbon atoms, and each carbene center stemming from a different ligand. This differs from the other structurally characterized Ag bis-NHC complexes, which are either monomeric or polymeric with terminal¹³¹ or bridging halide ligands¹³², respectively. In all of our silver complexes, the pronounced tendency to force a stretched configuration around silver prevents the formation of small rings with bidentate chelating ligands. Therefore, the system switches to a bisargentocycle structure with twelve ring atoms in a twisted boat-like or chair like conformation (figure 59 and 61).

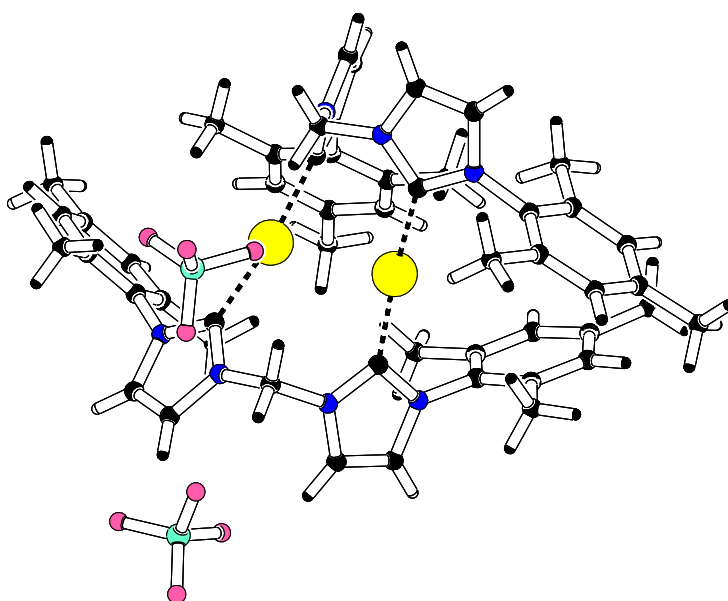


Figure 59. Crystal representation of complex **67c**.

Table 19. Selected bond lengths [Å] and angles [°] for **67c**.

Ag(1)- C(2)	2.070(5)	N(2)- C(2)	1.354(6)
Ag(1)- C(27)	2.074(4)	N(3)- C(1)	1.443(6)
Ag(2)- C(14)	2.082(5)	N(5)- C(26)	1.450(6)
Ag(2)- C(39)	2.084(5)	N(5)- C(27)	1.343(6)
Ag(2)- Ag(1)	3.199(6)	N(6)- C(27)	1.357(6)
N(3)- C(1)	1.443(6)	N(7)- C(26)	1.448(7)
N(1)- C(2)	1.355(7)		
<hr/>			
C(14)- Ag(2)- C(39)	173.6(2)	N(3)- C(1)- N(1)	110.5(4)
C(2)- Ag(1)- C(27)	172.0(2)	N(5)- C(27)- N(6)	104.0(4)
N(2)- C(2)- N(1)	103.9(4)	N(7)- C(26)- N(5)	108.8(4)

In the molecular structure of **67c** the silver atoms are bi-coordinated with carbenoid carbons. The average Ag–C bond lengths of 2.070(5) to 2.084(5) Å is at the upper end of the C(sp³)-Ag bond distance range, and is confirming the weakness of any π -character in the bond¹³³⁻¹³⁸. Nevertheless, the Ag—C bond distances of the biscarbene-silver complexes are shorter than those reported for monocarbene silver complexes¹³⁰. Complex **67c** could be considered as a nearly-linear compound with C-Ag-C angles of 172.0(2) to 173.6(2)°, these values are within the normal range for published silver NHC complexes. The Ag(1)—Ag(2) separation of 3.199(6)Å is considerably smaller than the van der Waals contact distance of 3.44Å and is used for a diagnostic of argentophilic interactions. From the literature only few mixed-ligand NHC combined with other donor ligands are reported and few of them contain [AgX₂]⁻ anions¹³⁰. We found only one example with such interactions involving an Ag center coordinated exceptionally with a carbene ligand¹²⁹. However, these kinds of interactions between d¹⁰ metals are well documented for gold¹³⁴. Another interesting feature of this geometry is the twist (76.5°) of the bulky mesityl substituents towards the imidazole rings, probably to minimize interactions. The planes of the two imidazole rings are twisted by 46.5° from coplanarity. The mesityl substituents are also involved in face-to-face interactions with an inter-planar separation of 3.536(6)Å (figure 62). All counter anions are non-coordinated,

and located far away from the metal center as shown in the crystal packing (figures 60 and 65).

The twelve atoms of the bisargentocycle adopt a C-2 symmetric twisted-boat conformation with both CH₂ tethers projected away from the Ag₂ core in one direction. This observation is in contrast to the complex **66c** which is chair-like and unlike most reported bis(NHC) silver dimers which show serpentine, helical or polymeric structures^{132,133}.

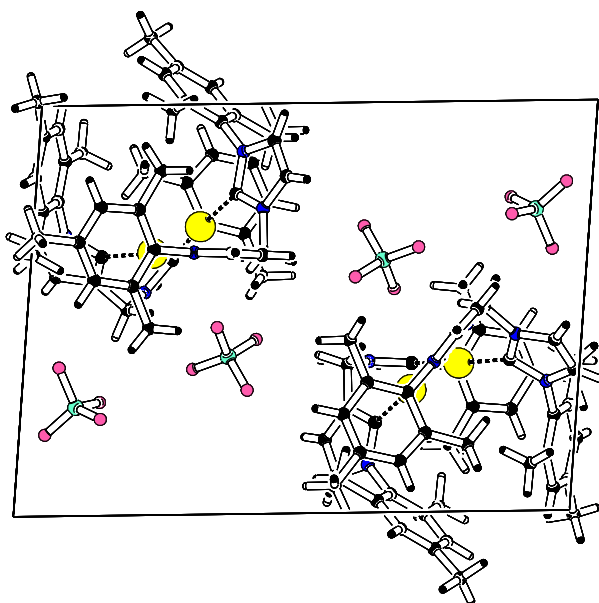


Figure 60. Crystal packing diagram of complex **67c** viewed along the *b*-axis.

X-ray structure of 66c

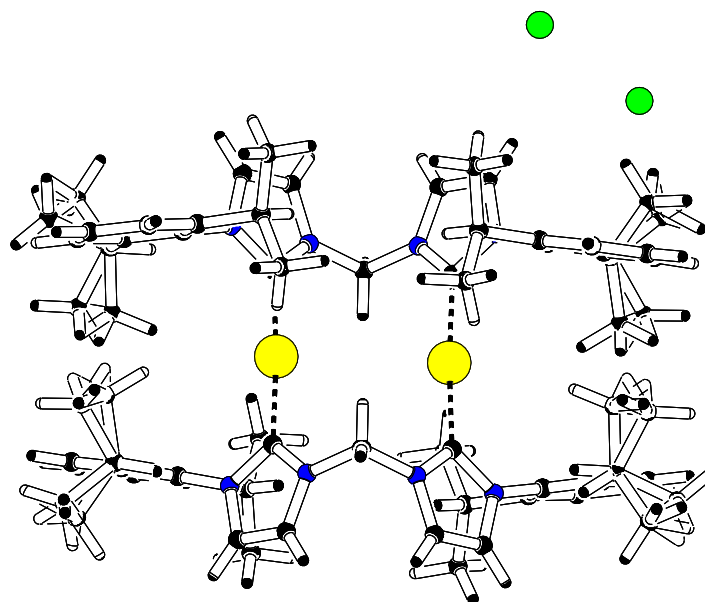


Figure 61. Crystal representation of silver complex **66c**.

Table 20. Selected bond lengths [\AA] and angles [$^\circ$] for **66c**.

Ag(1)- C(2)	2.079(6)	N(3a)- C(17a)	1.348(6)
Ag(1)- C(17a)	2.089(6)	N(4a)- C(17a)	1.367(6)
Ag(1a)- C(17)	2.089(6)	N(2a)- C(2a)	1.351(6)
Ag(1a)- C(2a)	2.079(6)	N(1a)- C(2a)	1.346(6)
Ag(1a)- Ag(1)	3.816(5)	N(3)- C(1)	1.347(8)
N(1)- C(2)	1.348(8)	N(1)- C(1)	1.351(8)
N(2)- C(2)	1.367(9)		
C(2)- Ag(1)- C(17a)	175.9(2)	N(3a)- C(17a)- N(4a)	103.7(4)
C(2a)- Ag(1a)- C(17)	175.9(2)	N(3)- C(17)- N(4)	104.1(5)
N(1)- C(2)- N(2)	103.8(5)	N(2a)- C(2a)- N(1a)	104.1(4)
N(1)- C(1)- N(3)	110.9(5)		

In the solid-state structure of **66c** (figure 61), the silver atoms are essentially linearly and bi-coordinated with carbene carbons. The angles of $175.9(2)^\circ$ for C—Ag—C and the average Ag-C bond lengths of 2.079(2) to 2.089 (2) Å are consistent with the values described for the previously discussed complex **67c**. These values clearly indicate the typically large σ -donor and low π -donor nature of the imidazole-2-ylidene ligand-to-silver interaction¹³²⁻¹³⁴. In the complex **66c** the twelve membered ring adopts a chair like conformation with both CH₂ tethers projected in opposite directions. The bite angle of the chelating ligand is $110.9(5)^\circ$, in the same range of that observed with the complex **67c** ($110.3(2)^\circ$). However, the value of 3.816(5) Å for the Ag(1)—Ag(2) separation in **66c** is different from that observed in complex **67c** (3.199(6) Å). The imidazole rings in the structure exhibit typical features of coordinated NHC ligands. Specifically, the C_{carbene}—N bond distance average, increased from 1.326 Å in the imidazolium salt **55** to 1.367 Å in **66c**. The N—C_{carbene}—N angles are significantly decreased from 108.5° in **55** to 104.1° in **66c**. Such changes are well documented in the literature and have been attributed to the decrease of π delocalization in the five membered-ring and increase of the σ character of the carbenoid carbon¹³⁹. In order to minimize the steric congestion around the metal center, the 2,6-diisopropylphenyl substituents adopt an orthogonal position with respect to the imidazol-2-ylidene rings. A projection diagram viewed down the *b* axis illustrates the arrangement of the silver complex **66c** (figure 62).

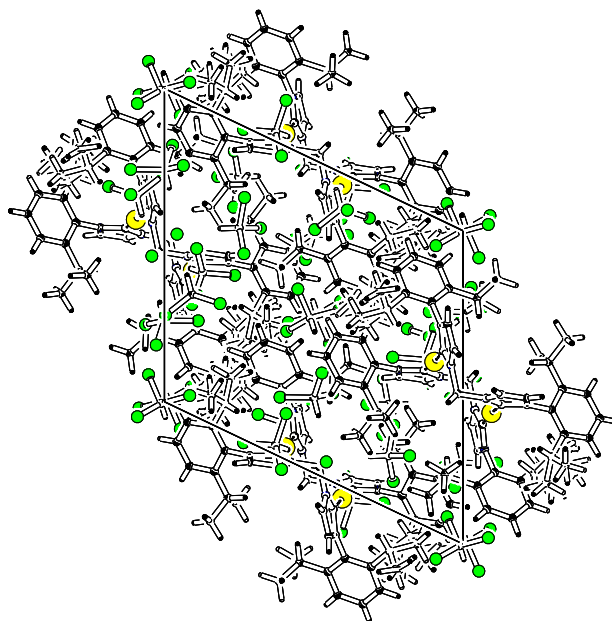


Figure 62. Crystal packing arrangement of **66c**.

The X-ray structure of **66c** shows isolation of a chloro complex instead of the expected iodo starting counter ion. The source of chloride could be probably the dichloromethane solvent. Exchange of bromide and chloride was reported when the reaction of imidazolium bromide or iodide with Ag_2O was carried out in chlorinated solvents under reflux; Lin¹⁴⁰ has observed the iodide-chloride exchange even at room temperature. These results indicate a lower activation energy of exchange of iodide for chloride.

Theoretical calculations carried out by Slaughter¹³⁰ on analogues N-methyl substituted had shown that the boat conformation is more favored as compared to the chair form by 3.4 kcal/mol ($E_a = +153.25$ kcal/mol).

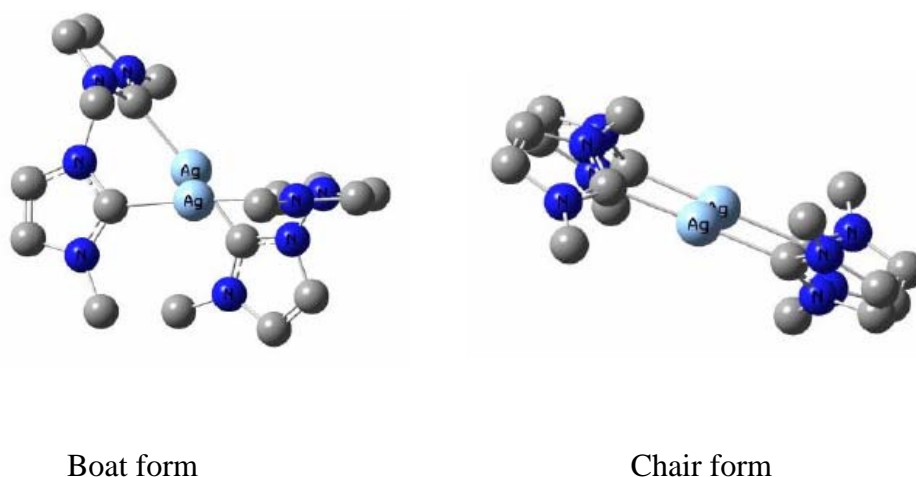


Figure 63. Boat and chair form of twelve-membered silver carbene complexes. Aryl groups were replaced with methyl¹³⁰.

Mesityl N- substituents increase this difference to 9.6 kcal/mol due to unfavorable intra-ligand $\text{CH}_3\cdots\text{CH}_3$ contacts in the chair form and result in a close Ag—Ag approach in the boat form (3.43\AA), that is near the observed distance. However, our observed results with complexes **66** and **67** contrast with the theoretical calculations of Slaughter. Indeed, 2,6-diisopropylphenyl is normally regarded as being more sterically hindered as compared to 2,4,6-trimethylphenyl, and according to that it was normal to expected a boat-conformation for complex **66**.

A comparison of complexes **66** and **67** allows us to attributes their structural differences exclusively to the nature of the 2,6-diisopropyl and 2,4,6-trimethylphenyl N-substituents. The

role of counter anions could be neglected since both are uncoordinated, and the complexes were prepared under the same conditions (dichloromethane at reflux). According to these results, we can conclude that the substituents on the nitrogen atom of the imidazole ring play an important role in the conformational preference of these twelve membered metallacycles. With more hindered substituents, such as 2,6-bis(isopropyl)aryl, the chair like conformation is more favorable, while with mesityl substituents the compound adopts a twist-boat conformation.

X-ray analysis of **66d** and **67d**

The structure of silver carbene complex **67d** with a PF_6^- counter-anion is shown in figure 64; important bond lengths and angles are given in the table 21. The coordination around the silver atom is nearly linear with a C—Ag—C angle comprised between $169.9(2)^\circ$ and $172.9(2)^\circ$. There is no intermolecular interaction of the PF_6^- anions with silver atoms. The value of $3.207(5)\text{\AA}$ for the Ag—Ag distance is not significantly higher as compared to that observed in **67c** ($3.199(6)\text{\AA}$), but enough to confirm the argentophilic interaction. The complex adopts a twisted-boat conformation as previously described for complex **67c**. The other bond lengths and angles are in the normal range for this type of compounds.

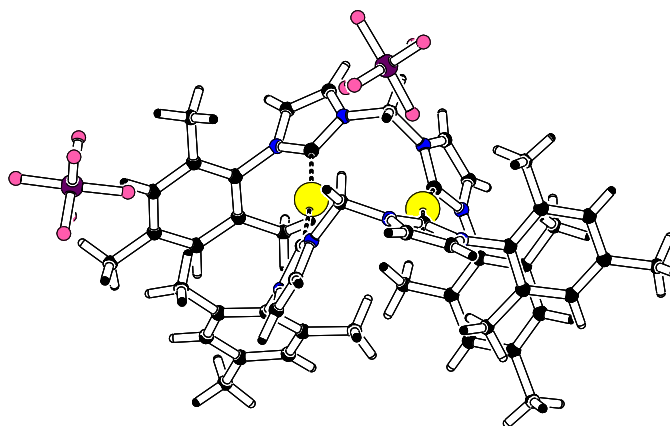


Figure 64. X-ray structure of PF_6^- silver biscarbene complex **67d**.

Table 21. Selected bond lengths [\AA] and angles [$^\circ$] for **67d**.

Ag(1)- C(2)	2.087(5)	N(3)- C(14)	1.352(6)
Ag(1)- C(27)	2.087(4)	N(4)- C(14)	1.358(6)
Ag(2)- C(14)	2.087(5)	N(5)- C(27)	1.357(6)
Ag(2)- C(39)	2.095(4)	N(6)- C(27)	1.354(6)
Ag(2)- Ag(1)	3.207(5)	N(7)- C(39)	1.357(6)
N(1)- C(2)	1.357(6)	N(8)- C(39)	1.348(6)
N(2)- C(2)	1.338(6)		
<hr/>			
C(2)- Ag(1)- C(27)	169.9(2)	N(5)- C(27)- N(6)	104.4(4)
C(14)- Ag(2)- C(39)	172.9(2)	N(3)- C(14)- N(4)	104.2(4)
N(1)- C(2)- N(2)	104.1(4)	N(7)- C(39)- N(8)	104.9(4)
N(1)- C(1)- N(3)	110.3(4)		

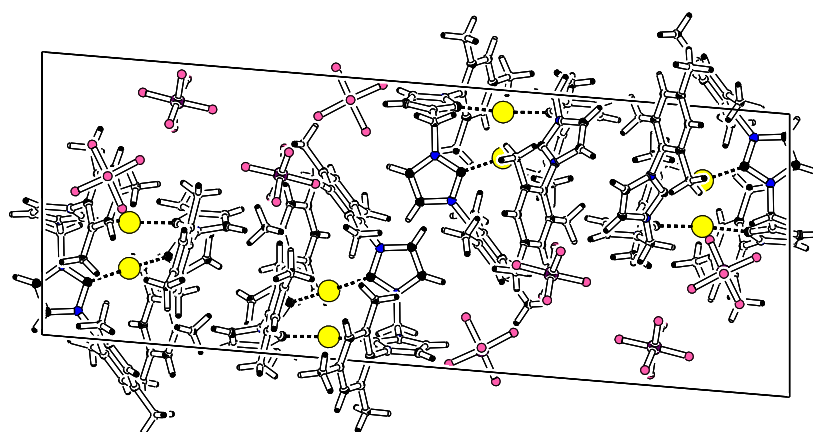


Figure 65. Crystal packing of PF_6^- **67d**.

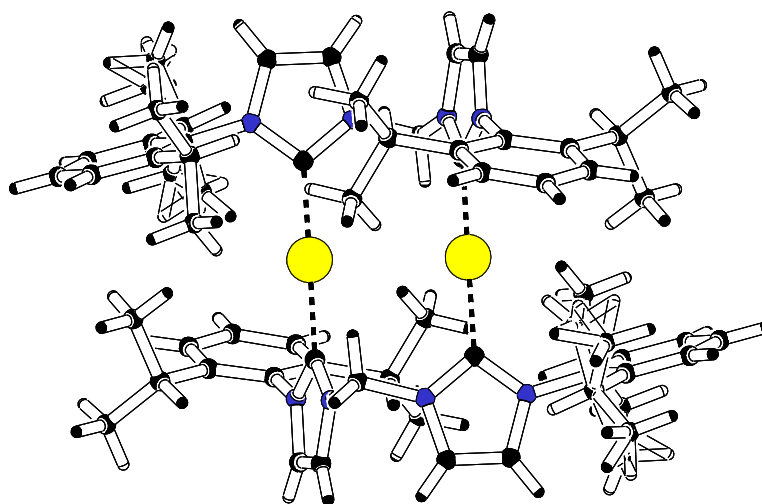


Figure 66. Crystal structure of silver carbene complex **66d**, the counter anions BF_4^- were omitted for clarity.

Table 22. Selected bond lengths [\AA] and angles [$^\circ$] for **66d**.

Ag(1)- C(2)	2.093(5)	N(3a)- C(17a)	1.353(6)
Ag(1)- C(17a)	2.102(5)	N(4a)- C(17a)	1.362(6)
Ag(1a)- C(2a)	2.093(5)	N(3)- C(17)	1.352(6)
Ag(1a)- C(17)	2.101(5)	N(4)- C(17)	1.363(6)
Ag(2)- Ag(1)	3.788(4)	N(1a)- C(2a)	1.359(6)
N(1)- C(2)	1.359(6)	N(2a)- C(2a)	1.363(6)
N(2)- C(2)	1.362(6)		
C(2)- Ag(1)- C(17a)	176.1(2)	N(3a)- C(17a)- N(4a)	103.6(4)
C(2a)- Ag(1a)- C(17)	176.1(2)	N(3)- C(17)- N(4)	104.2(4)
N(1)- C(2)- N(2)	103.3(4)	N(1a)- C(2a)- N(2a)	103.28(4)
N(1)- C(1)- N(3)	110.5(4)		

Crystallographic data of complex **66d** (figure 66) are given in the table 22. As for the previous complex **66c**, this compound exhibits a chair like conformation. The observed Ag—Ag interactions of $3.788(4)\text{\AA}$ is much higher than all previously reported values for mesityl

silver compounds **71c** and **71d**, but in the same range as compared with that observed for complex **66c**. The perpendicularity of the bulky aryl substituents towards the imidazole rings is also observed and there is no interaction between counter anions with silver atoms as shown in crystal packing figure 67.

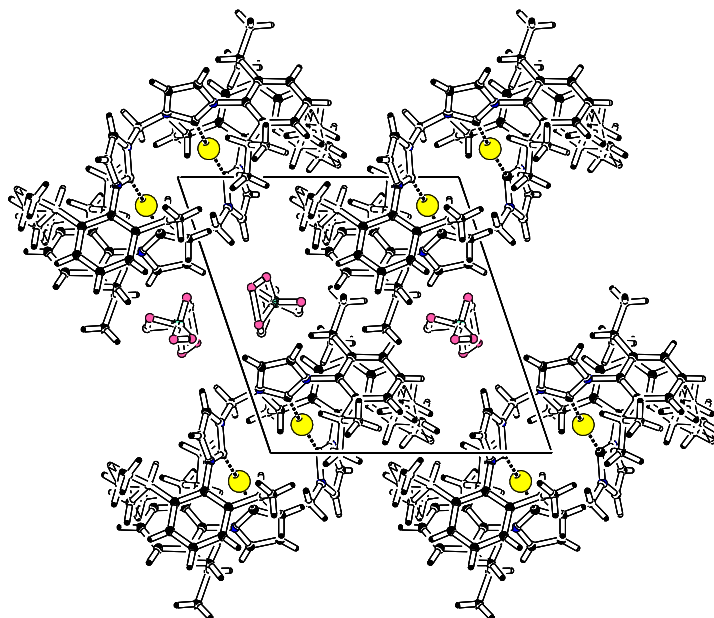


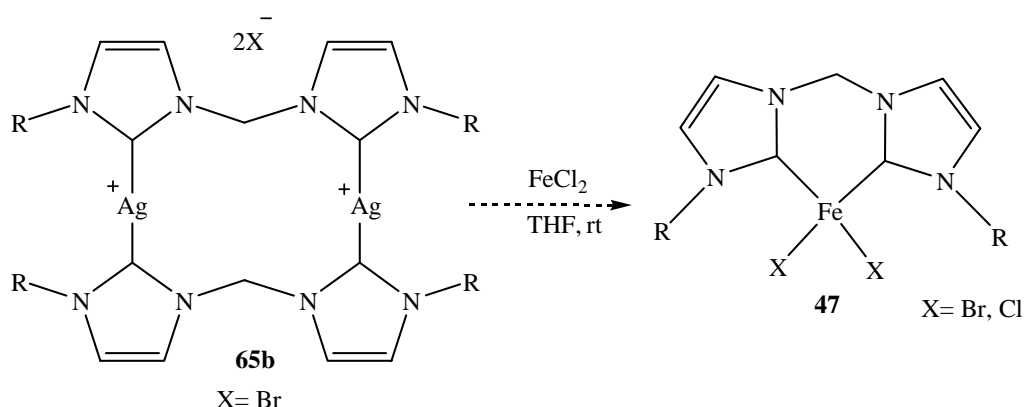
Figure 67. The packing diagram of complex **66d** viewed along the *b*-axis.

II-8. Transmetallation reactions

15. Silver bisaryl N-heterocyclic biscarbene complexes as transfer agents for the synthesis of iron(II) and Ni(II) complexes

Silver complexes **65–67** should be ideal vehicles for the transfer of the carbene N-heterocyclic moiety to other metals using the driving force of silver halide precipitation. Thus we reacted all our silver carbene complexes with different sources of iron in order to get iron(II) complexes.

15.1. Reaction of silver complex **65b** with $\text{FeCl}_2(\text{THF})_2$



Scheme 60. Transmetalation reaction of **65b** with FeCl_2 .

The reaction of silver complex **65b** with $\text{FeCl}_2(\text{THF})_2$ was done in THF at RT for 48 hours. During this time a grey yellow precipitate was formed and the solution became slightly yellow. The precipitate was filtered off, and the recovered solution was evaporated under vacuum affording an orange red solid **47I**. The UV-Vis spectrum of this solid in THF is depicted in figure 68 and shows absorption bands at 364 nm, 295 nm, and 241 nm (sh). Very broad peaks were observed in the NMR. This solid was dissolved in THF and stored at RT in order to crystallize but no crystals were observed. Further crystallization attempts were made by slow diffusion of toluene into THF solution of isolated product but did not afford crystals. The Electrospray mass spectrometry (ESI+) was measured too but we did not find recognizable peaks.

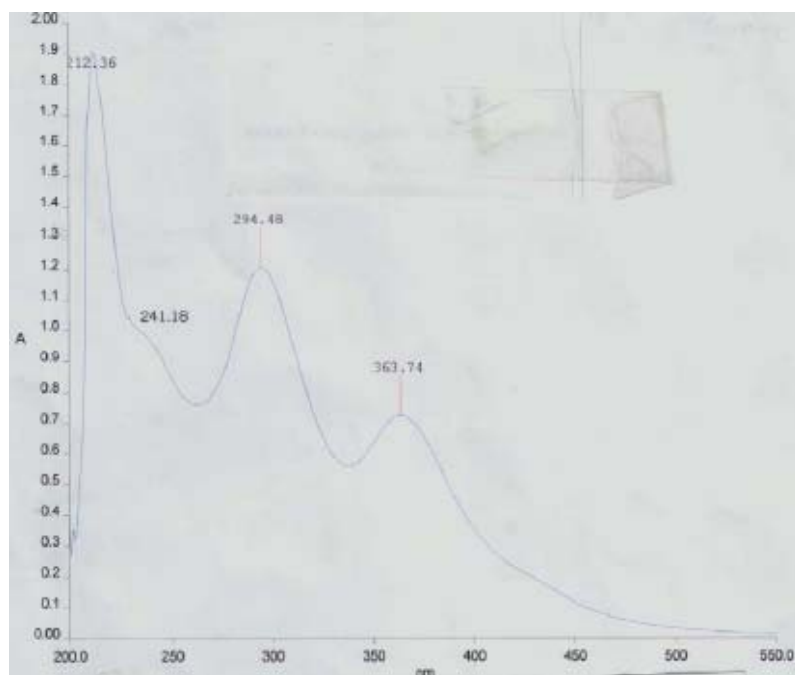
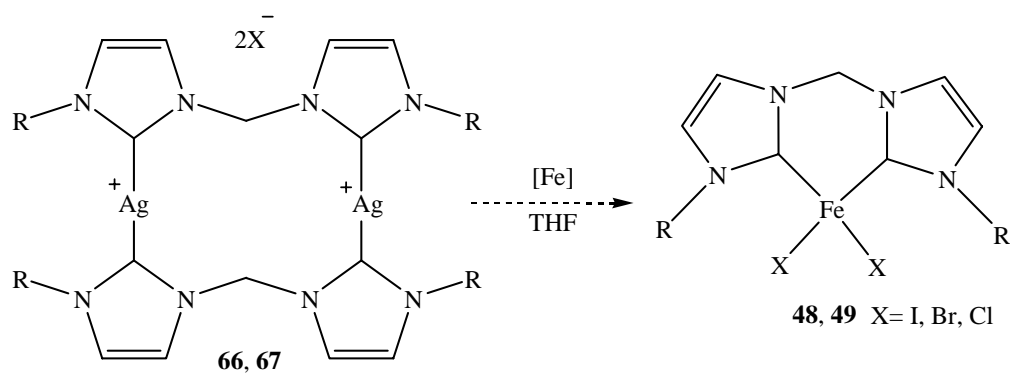


Figure 68. The UV-Vis spectrum of **47I** in THF.

15.2. Reaction of silver complexes **66** and **67** with iron(II) in different solvents



Scheme 61. Reaction of silver carbene with iron(II).

Table 23. Experimental conditions and obtained results.

Exp	Complex(Ag) (mmol)	Fe(II) source (mmol)	Solvent (ml)	Temp. [°C]	Time [hours]	Product [mg]	UV- Vis [nm]	
1	66b (0.2)	FeCl ₂ (0.4)	DCM (20)	RT	6	48IV	362, 317	
2	67b (0.3)	FeCl ₂ (0.6)			24	49II	359, 311	
3	66a (0.5)	FeCl ₂ (1.0)	THF (20)	RT	24	48V	365, 319	
4	66a (0.5)	FeCl ₂ (1.0)		Reflux	24	48VI	358, 315	
5	66b (0.5)	FeBr ₂ (THF) ₂ (1.0)		Reflux		48VII	364, 318	
6	66b (0.1)	FeBr ₂ (THF) ₂ (0.2)		-10°C to RT		48VIII	367; 295	
7	66d (0.38)	FeBr ₂ (0.75)		RT		48IX	365, 294	
8	66e (0.16)	FeBr ₂ (0.32)			48X	363, 315		
9	67b (0.3)	FeBr ₂ (THF) ₂ (0.6)		THF (20)		2	49III	365, 310
10	66d-e (0.1)	Fe(OTf) ₂ (0.2)		THF/DCM (15)	RT - reflux	72	-	-
11	67c-d (0.2)	Fe(OTf) ₂ (0.4)	RT - reflux		72	-	-	

15.2.1. Reaction in dichloromethane

The reaction of silver carbene **66b** with a suspension of iron chloride (1:2) in CH₂Cl₂ at RT for 6 hours, give a yellow-green solid (**48IV**) after filtration and elimination of the solvent under vacuum (entry 1). The UV-Vis spectrum in THF shows two maxima at 362 nm and 317 nm. The ¹H-NMR spectra show only broad peaks, the signal of the carbene was not observed in the ¹³C-NMR. The MS(ESI+) doesn't show any recognizable peak. Recrystallization in different solvent was also attempted without success (entry 1).

When **67b** reacts with a suspension of FeCl₂ in CH₂Cl₂ at RT for 24 hours, a yellow-green solid **49II** was obtained after filtration and evaporation of the upper solution; this product is very air sensitive (entry 2). Taking an NMR was not possible because of the paramagnetism and the rapid decomposition observed during the NMR experiment. However, we were able to collect an UV-Vis spectrum in THF. It shows two absorption maxima at 359 nm and 311 nm. The fact that the product decomposes rapidly in dichloromethane, recommends the necessity of an supplementary coordinating ligand in order to stabilize the complex. In fact, dichloromethane is known to be a weakly coordinating ligand.

15.2.2. Reaction in tetrahydrofuran

Reaction of **66a** with FeCl₂ (1:2) in THF at RT gives a red-brownish solid (**48V**, entry 3). This reaction proceeds fast, as immediately silver halides precipitates in the reaction medium. The UV-Vis spectra of this compound **48V** in THF and in toluene (poorly soluble) shows two maxima around 358 nm and 315 nm; The fact that the UV-Vis spectra in both solvent give the same absorption bands could suggest no influence of solvent in the coordination sphere of the metal. The recorded ¹H- and ¹³C-NMR spectra resulted in broad peaks. A crystallization attempt by slow diffusion of toluene or hexane into the THF solution of isolated product was unsuccessful, degradation was observed. However, when the reaction was done at reflux in THF, an orange-yellowish solid (**48VI**) was obtained after filtration and evaporation of the solvent (entry 4). Some yellow crystals were obtained from slow diffusion of toluene into the THF solution of complex **48VI**. Crystallographic diffraction analysis shows an bisimidazolium tetrachloroferrate complex **98a**, its structure is depicted in figure 69. The UV-Vis spectrum of crystals dissolved in THF show two absorptions bands at 365 nm and 315

nm, similarly to that observed with previous complexes. Here again, the ^1H - and ^{13}C NMR spectra were not recorded due to the paramagnetism of this product, and the MS (ESI+) failed to show any expected or recognizable peaks.

We also reacted silver complex **66b** with $\text{FeCl}_2(\text{THF})_2$ in THF which afforded an orange yellow solid **49VII** after filtration and evaporation of the solvent (entry 5). Crystallization attempts by slow diffusion of diethylether into a THF solution of the isolated product gave yellow crystals. The X-Ray analysis shows a bisimidazolium salt with tetrabromoferrate $[\text{FeBr}_4]^{2-}$ as counter anion **98b** (figure 70) as previously.

X – ray structure of **98a** and **98b**

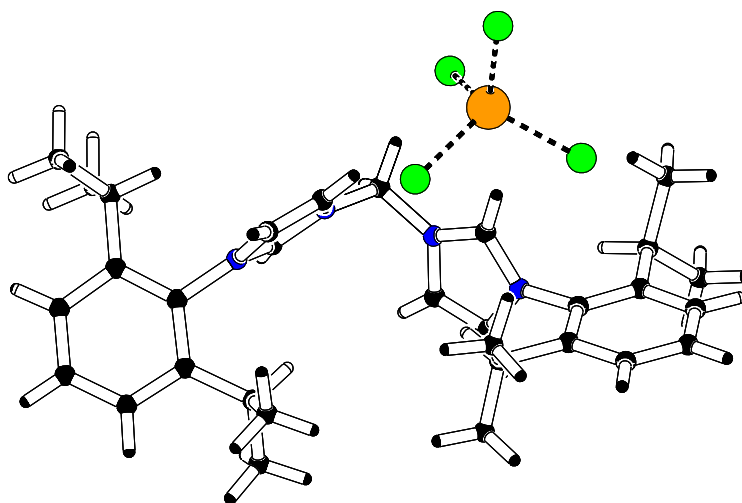


Figure 69. Crystal structure of imidazolium tetrachloroferrate complex **98a**.

Table 24. Selected bond lengths [\AA] and angles [$^\circ$] for **98a**.

Fe-Cl(1)	2.178(9)		
Fe-Cl(2)	2.187(1)		
Fe-Cl(3)	2.157(1)		
Fe-Cl(4)	2.212 (9)		
N(1)-C(2)	1.337(3)	N(2a)- C(4a)	1.385(6)
N(2)- C(2)	1.326(3)	C(3a)- C(4a)	1.345(4)
N(1)- C(3)	1.382(3)	N(1)- C(1)	1.460(3)
N(2)- C(4)	1.385(3)	N(1a)- C(1)	1.463(5)
C(3)- C(4)	1.344(4)	N(2)- C(5)	1.451(3)
N(1a)- C(2a)	1.337(3)	N(2a)- C(5a)	1.451(4)
N(1a)-C(3a)	1.382(6)	N(2a)- C(2a)	1.326(3)
N(1)- C(2)- N(2)	108.2(2)	C(10)- C(5)- N(2)	117.9(2)
N(1a)- C(2a)- N(2a)	108.9(2)	C(6a)- C(5a)- N(2a)	117.9(2)
N(1)- C(1)- N(1a)	108.7(3)	C(10a)- C(5a)- N(2a)	117.4(2)
C(6)- C(5)- N(2)	117.4(2)		

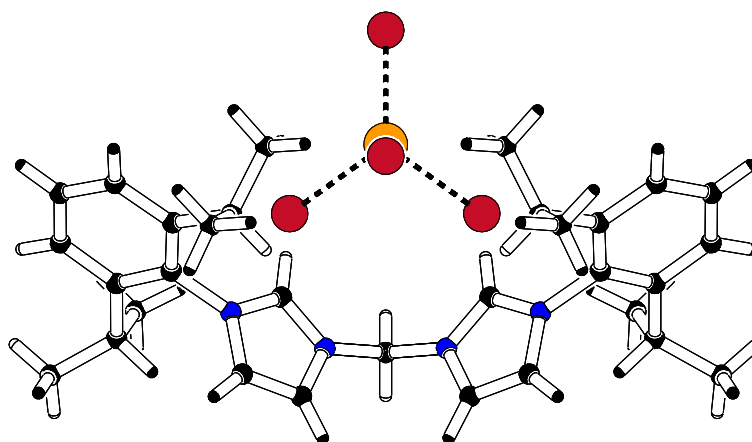


Figure 70. Crystal structure of imidazolium iron tetrabromo complex **98b**.

Table 25. Selected bond lengths [Å] and angles [°] for **98b**.

Fe-Br(1)	2.499(8)		
Fe-Br(2)	2.499(8)		
Fe-Br(3)	2.399(1)		
Fe-Br(4)	2.419 (1)		
N(1)-C(2)	1.338(6)	N(2b)- C(4b)	1.383(6)
N(2)- C(2)	1.325(6)	C(3b)- C(4b)	1.352(1)
N(1)- C(3)	1.370(6)	N(1)- C(1)	1.463(5)
N(2)- C(4)	1.383(6)	N(1a)- C(1)	1.463(5)
C(3)- C(4)	1.353(6)	N(2)- C(5)	1.456(6)
N(1b)- C(2b)	1.337(6)	N(2a)- C(5a)	1.456(8)
N(1a)-C(3b)	1.371(9)	N(2b)-C(2b)	1.326(6)
N(1)- C(2)- N(2)	107.6(4)	C(10)- C(5)- N(2)	117.6(4)
N(1b)- C(2b)- N(2b)	107.6(4)	C(6b)- C(5b)- N(2b)	117.6(5)
N(1)- C(1)- N(1a)	112.0(5)	C(10a)- C(5a)- N(2a)	117.8(5)
C(6)- C(5)- N(2)	117.7(4)		

In the structures depicted in figures 69 and 70, both imidazole rings are orientated in the same direction as observed with bisimidazolium salt **55b**. Formal charge balance consideration would require an iron(II) configuration for the resulting complex **98a**. However, the bond valence sum calculation observed here is in the range of 2.157(11) \AA to 2.212(9) \AA for Fe—Cl, this value seems to support an iron(III) species. Indeed, the typical bond lengths for tetrahedral iron chlorine bond is 2.301 \AA for iron(II) and 2.195 \AA for iron(III)¹¹⁵. Interesting are the Fe—Br bond lengths values in complex **98b** (2.399(12) to 2.499(8) \AA), which were in the same range of those reported for iron(II) species (2.40 to 2.50 \AA)¹¹⁵.

The packing diagram of **98a** in figure 71 confirm the presence of iron(III), in fact there are two $[\text{FeCl}_4]^-$ anions for each bisimidazolium salt. The packing of **98a** and **98b** (figure 71 and 72 respectively), emphasizing also, the orientation of the cations around the $[\text{FeX}_4]^-$ anions, as may be seen, the bisimidazolium cation and the iron tetrahalide anions occupy alternate layers along the crystallographic *a*-axis. There appears no significant cation—anion interaction as shown in the crystal packing.

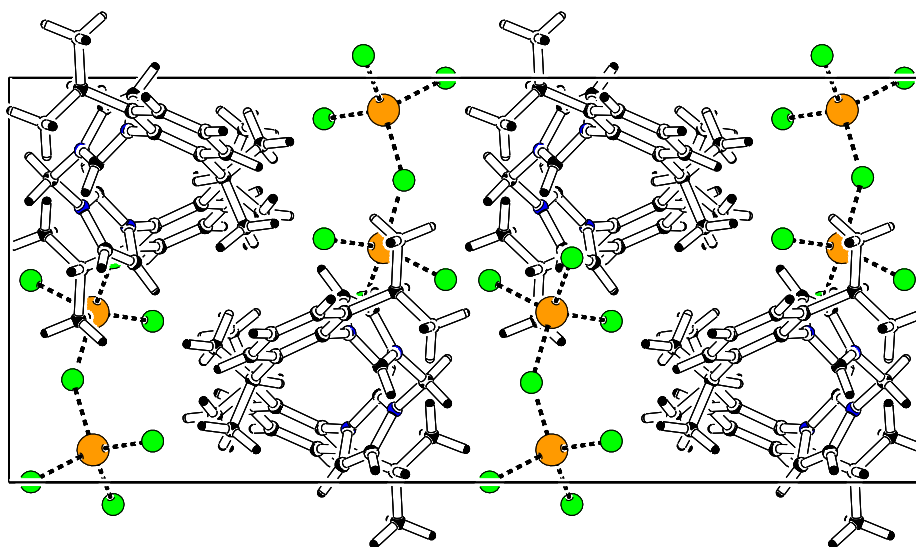


Figure 71. Crystal packing of **98a**, viewed along the *c*- axis.

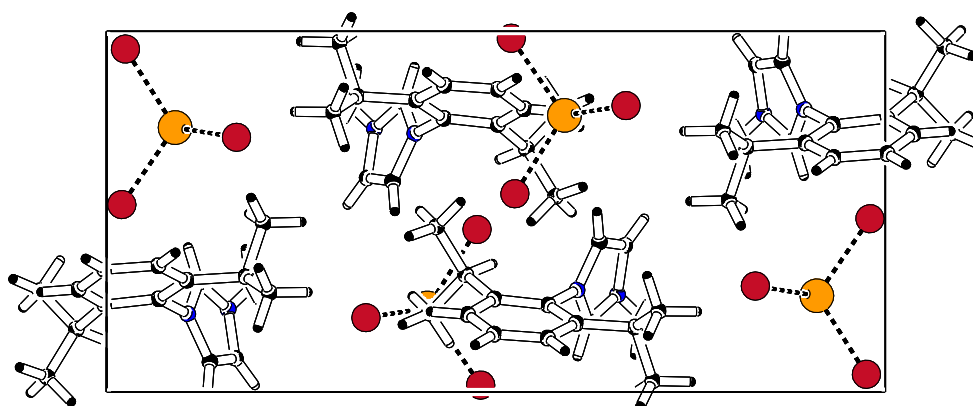
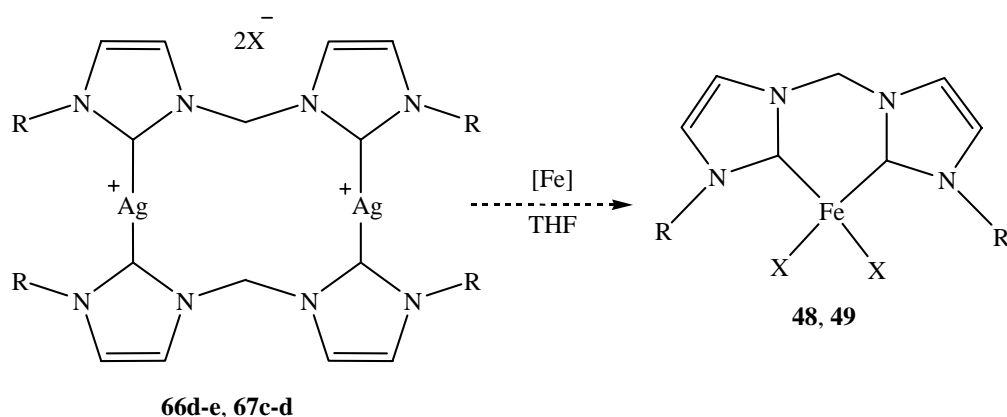


Figure 72. Crystal packing of **98b** viewed along the $\frac{1}{2} b$ -axis.

In order to analyse the role of temperature on the transmetalation reaction of **66b** with $\text{FeCl}_2(\text{THF})_2$, we did the experiment at -10°C (entry 6). After 12 hours, the orange red solution was filtered and the solvent evaporated affording a red solid **48VIII**. Unfortunately, analytical tools such as elemental analysis, MS, ^1H - and ^{13}C -NMR did not permit the identification of products. Attempts to crystallise the isolated compounds did not work either.

The reaction of silver carbene complex **67b** with $\text{FeBr}_2(\text{THF})_2$ in THF at room temperature gave an orange solid **49III** after work-up (entry 9). This product is a high-spin Fe(II) compound. Thus, it is very difficult to assign the ^{13}C -NMR spectrum due to extreme broadening and missing peaks. The mass spectra (ESI+) did not show the expected peaks, but a peak corresponding to the imidazolium starting ligand was found. This outlines the possible presence of a bisimidazolium tetrabromoferrate complex **99**, similar to **98b**. The UV-Vis spectrum in THF shows two absorption maxima at 365 nm and 310 nm. Crystallization attempts of the obtained product from THF/MeCN or from diethylether/THF did not work.

15.2.3. Reaction of silver BF₄ and PF₆ with iron(II) precursors



Scheme 62. Transmetalation using silver BF₄ and PF₆.

In a similar manner, the tetrafluoroborate and hexafluoroborate silver bis-carbene complexes **66d-e** were reacted with FeBr₂(THF)₂ in THF affording brown solids (scheme 62). Crystallization was attempted by slow diffusion of diethylether in a THF solution of the product, and we were able to isolate red-brown crystals from the tetrafluoroborate derivative **48IX**. Unfortunately, their size, sensitivity to air and poor quality did not permit an X-ray analysis with good resolution and the obtained structure is not satisfactory due to the low quality of material. However, we can conclude that the structure **98c** is quite the same as obtained before for **98b** (figure 73).

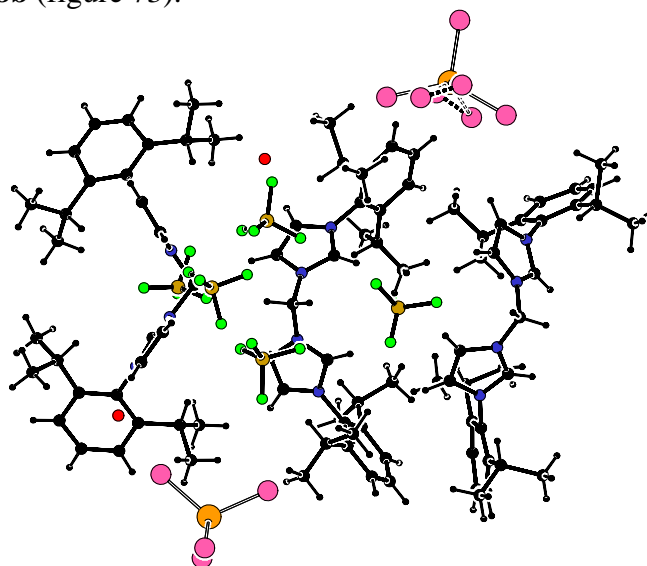


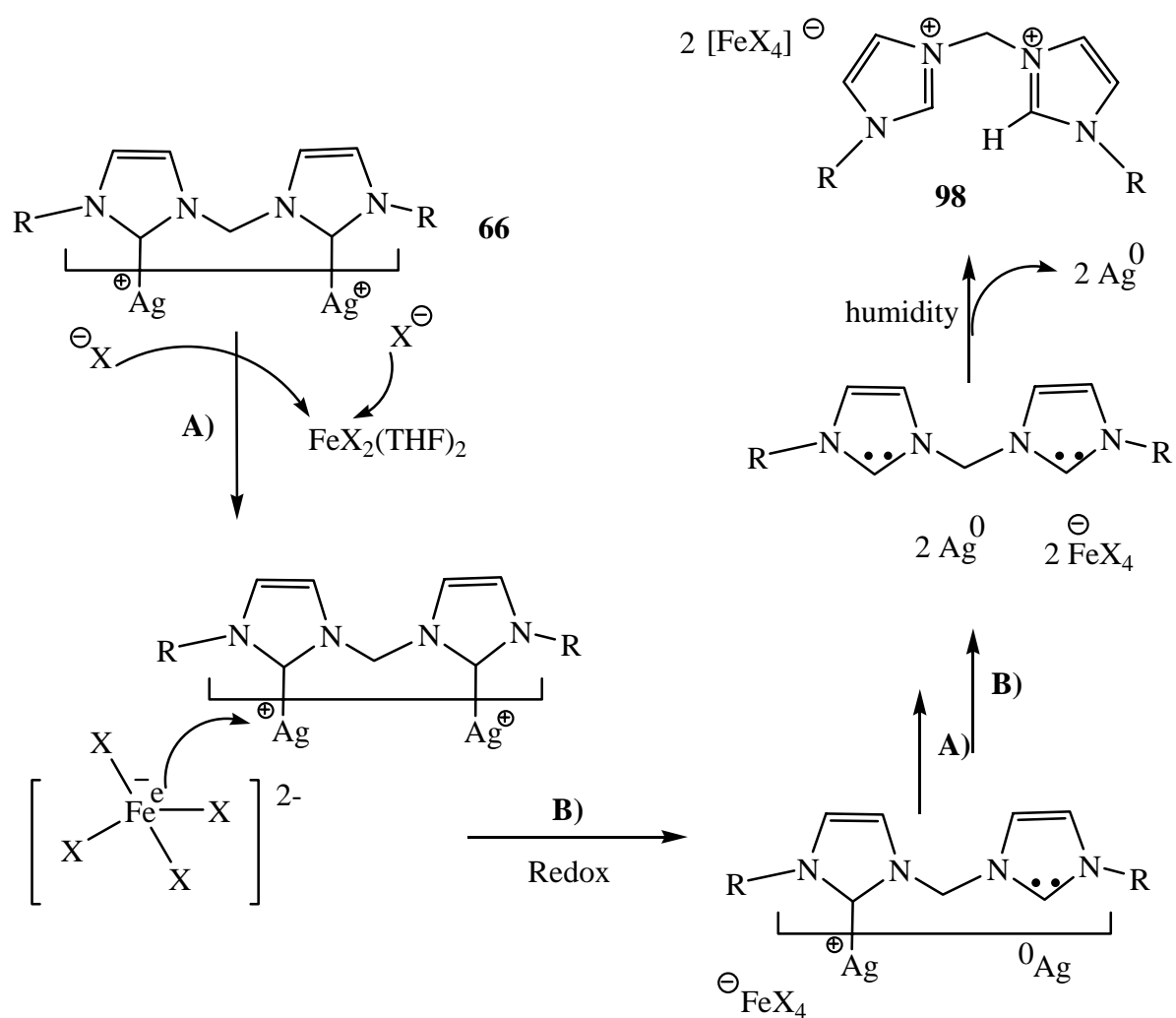
Figure 73. X-ray representation of complex **98c**.

Analyse such as ^{13}C -NMR, MS(ESI+), CHN were attempted. Nevertheless, in all cases the expected results were not obtained.

The reaction of the silver carbenes complexes **70d-e** and **71c-d** with $\text{Fe}(\text{OSO}_2\text{CF}_3)_2$ in THF / CH_2Cl_2 (1:2) has been performed as well, first at RT for 72 hours and then at reflux for 96 hours (entry 10-11). After cooling to RT, the product was filtered over Celite. Evaporation of the solvent gives a white yellowish solid. The ^1H - and ^{13}C -NMR spectra show only the peaks corresponding to the starting silver complexes. We believe that the strong $\text{Ag}-\text{X}$ bond formed in the previous reactions must act as a significant thermodynamic driving force leading to the transmetallation.

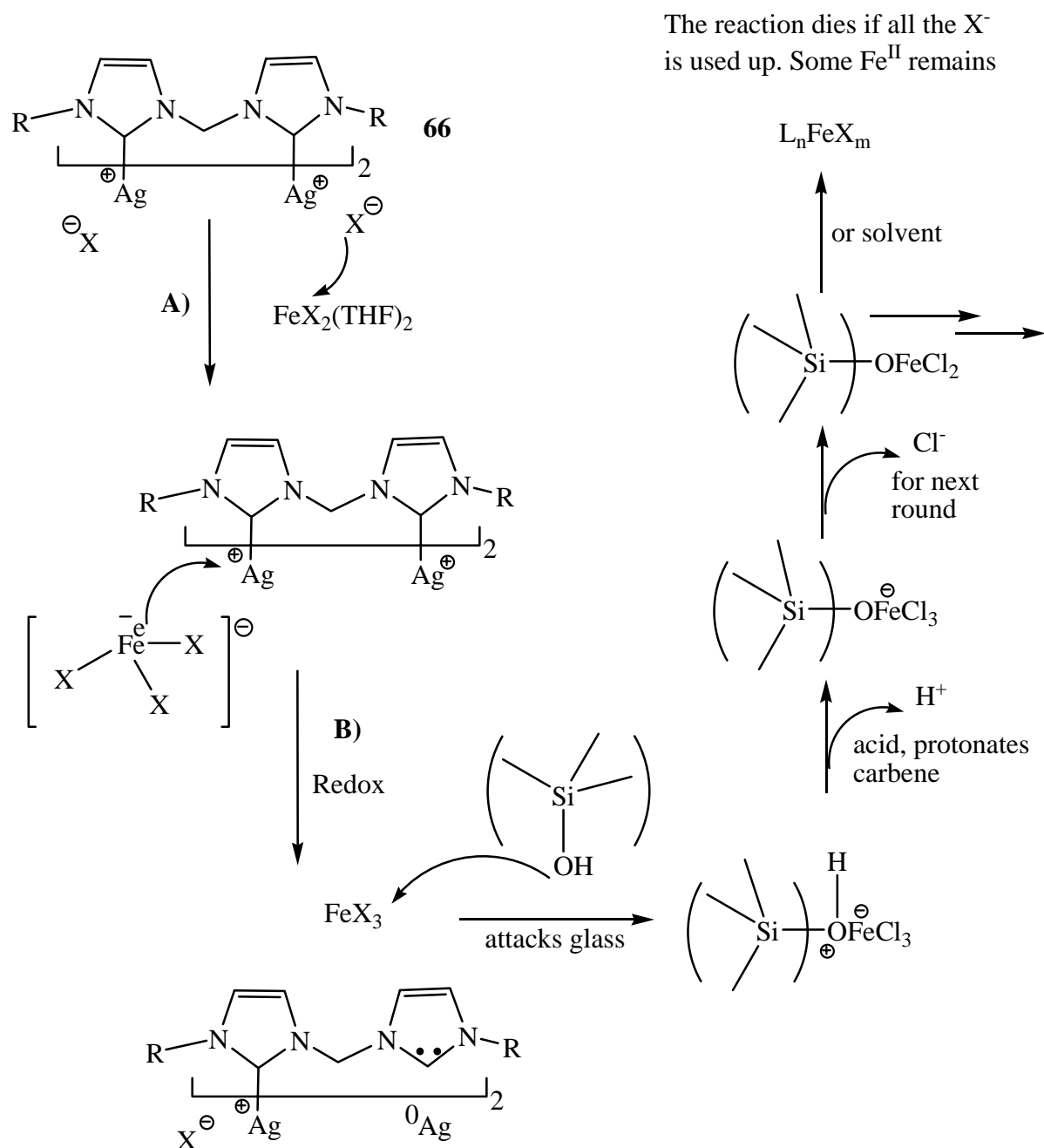
15.2.4. Tentative mechanism for formation of tetrahalideferrates complexes

The formation of the cationic imidazolium iron(III)tetrahalogenate complex **98** is probably initiated by nucleophilic attack of halide anions at the iron(II) atom to yield a $[\text{FeCl}_4]^{2-}$ complex ion. In a second step, decomposition of the silver carbene complex occurs to form silver chloride and releasing free carbene ligands. Under these conditions, a redox reaction takes place between silver chloride and FeCl_2 which is present in solution to yield $\text{Ag}(0)$ and FeCl_3 (Lewis acid) that can react with a chloride anion from another molecule of silver carbene complex to produce $[\text{FeCl}_4]^-$ anion or $[\text{FeCl}_2(\text{THF})_4]^+[\text{FeCl}_4]^-$. The traces of water from THF solvent or humidity in the reaction medium or during work-up could explain the protonation of free carbene bisimidazol-2-ylidene to the respectively bisimidazolium species. A proton source could also be the glass wall of the reaction vessel.



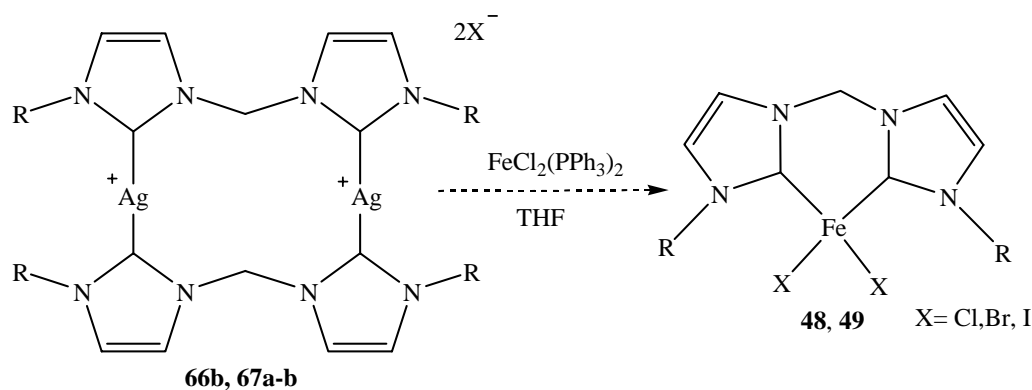
Scheme 63. Probably mechanism for a formation of bisimidazolium iron tetrahalogenate complexes.

If only one halide is transferred, first one obtains:



Scheme 64. Mechanism for a formation of bisimidazolium iron(III) tetrahalogenate complexes, based on a singular halide transfer.

15.3. Reaction of silver complexes with $\text{FeCl}_2(\text{PPh}_3)_2$

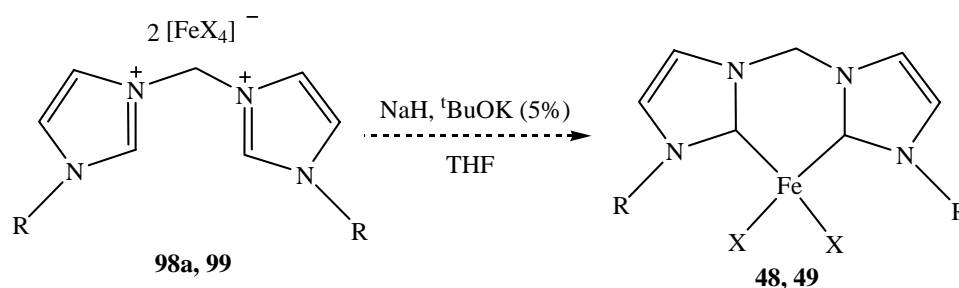


Scheme 65. Transmetalation reaction of **66** and **67** with $\text{FeCl}_2(\text{PPh}_3)_2$.

The reaction of silver complexes **66b** and **67a-b** with $\text{FeCl}_2(\text{PPh}_3)_2$ was done at room temperature in THF. In the case of **66b** the mixture was then heated at reflux until the color of the solution changed from yellow to green. The upper colorless solution was removed and the left green-brown solid was washed with toluene in order to remove PPh_3 released during the reaction. Purification attempts of this solid were difficult due to its insolubility in many organic solvents. Treatment of the resulting mixture by filtration followed by evaporation of the solvent afforded a green-brown solid. The MS (FAB) analysis was done without success. In the case of the silver carbene complexes **67a-b** no reaction took place at room temperature, even after two days. However, when the mixture was refluxed, an untreatable green solid formed in solution. Purification attempts by washing in different solvents was unsuccessful, indeed this product shows again poor solubility in many organic solvents (chloroform, hexane, toluene, xylene, DMSO, methanol). This problem prevented spectroscopic analyses.

15.4. Deprotonation attempts of bisimidazolium iron tetrahalogenate complexes with different bases

15.4.1. Deprotonation using sodium hydride (NaH)



Scheme 66. Deprotonation of bisimidazolium complexes with sodium hydride.

Table 26. Experimental conditions used in the synthesis of iron complex **48** and **49**.

Exp	[Fe] (mmol)	NaH (mmol)	solvent (ml)	Temp. [°C]	Time [h]	UV – Vis [nm]
1	98a (0.1)	0.45	THF (20)	0 to RT	8	360, 315
2	98a (0.1)	0.45	THF (20)	reflux	8	364, 290
3	99 (0.1)	0.45	THF(20)	RT	8	292

Treatment of complex **98a**, at that time assumed to be a Fe(II) complex, with NaH in THF at 0°C to RT, gave a yellow brown solid after filtration and evaporation of the solvent. The ¹H- and ¹³C-NMR spectra were not recorded because of the paramagnetism of the samples. The MS(ESI+) and elemental analyses were done, but the results were not according to expected values. The slow crystallization from diethylether/THF gave yellow crystals. However, the X-ray analysis showed that this structure corresponds to the starting material **98a**. This result permits us to conclude that no reaction took place at or below room temperature.

Changing temperature conditions (THF at reflux), an orange solid was isolated after work up. Mass spectroscopic analyses (MS (ESI+) and FAB) were done, but no signal corresponding to the expected product was found. The results of the elemental analysis do not correspond with the theoretical values; the isolated compound is paramagnetic and its ^{13}C -NMR shows broad signals. Suitable crystals for X-ray analysis were grown in a mixture of THF and diethylether at RT. Surprisingly the structure of this new complex **100a** was much different from that expected one. The X-ray structure of trans-dichlorotetraimidazolaryliron(II) is represented in the figure 74 and the most important bond distances and angles are listed in the annexe.

X-Ray analysis of complex **100a**

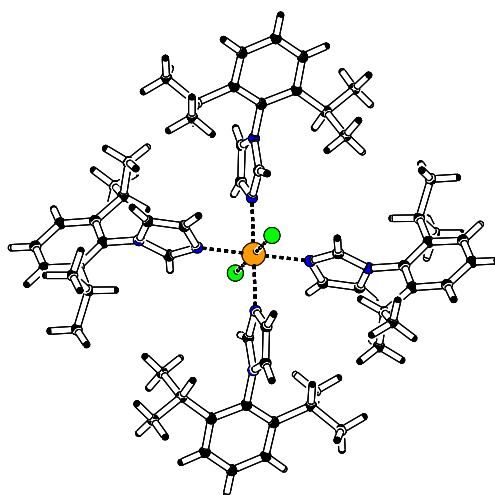


Figure 74. ORTEP representation of complex **100a**.

Table 27. Selected bond lengths [Å] and angles [°] for **100a**.

Fe-Cl(1)	2.536(8)	Fe-N(1)	2.189(2)
Fe-Cl(2)	2.536(8)	Fe-N(3)	2.162(2)
N(1)-C(1)	1.313(3)	N(3)-C(16)	1.307(3)
N(1)- C(2)	1.364(3)	N(3)- C(17)	1.370(3)
N(2)- C(1)	1.344(3)	N(4)- C(16)	1.342(3)
C(2)- C(3)	1.350(3)	C(17)- C(18)	1.359(3)
N(2)- C(4)	1.437(3)	N(4)- C(19)	1.442(3)
Cl- Fe- Cl	180.0(1)	N(1)- Fe- N(1a)	180.0(1)
N(1)- Fe- Cl(1)	89.6(6)	C(1)- N(1)- C(2)	105.1(2)
N(1)- Fe- Cl(1a)	90.4(6)	C(16)- N(3)- C(17)	105.3(2)

Neutral and cationic complexes of iron(II) chloride and bromide with nitrogen bases are well known for imidazole, pyridine and pyrazoles. However, analogous arylimidazoles have not been reported so far.

The iron(II) adopts a trans-octahedral geometry with a FeCl_2N_4 core. Four arylimidazole molecules are coordinated to iron ion through their tertiary N atom. The trans-Fe(II)—Cl bond distance is 2.5360(8) Å, this value is significantly longer than those found for non substituted analogues *trans*-imidazole complexes which were structurally characterized (average Fe – Cl 2.355(2) Å)¹⁴², indicating a substantial decrease in the covalency of the bond. As expected, based upon steric arguments, the Fe—N bond distances (2.162(2)-2.189(2) Å) in **100a** are longer than those measured for the $[\text{FeCl}_2(\text{imidazole})_4]$ ¹⁴³ derivatives (average Fe—N 2.125(5) Å) and shorter than those observed for pyridines analogues (mean value of 2.206(4) Å)¹⁴⁴. However, these Fe—N bond distances measured in compound **100a** are in agreement with the Fe(II)—N pyrazoles distances (mean value of 2.158(3) Å) for mononuclear six-coordinated iron(II) complexes with a high spin configuration¹⁴⁴. This lengthening of the Fe—Cl bonds and concomitant shortening of the Fe—N bonds may be

because the chlorines atoms are subjected to the steric pressure of the isopropyl groups in order to accommodate both ligands in the coordination sphere of the iron. All four imidazole rings are perfectly aligned so that they are perpendicularly to the Cl(1)—Fe—Cl(2) axis, as expected for an octahedral geometry at a metal center (average angle for the four *cis* N—Fe—N arrangement is 90°). However, the associated aryl substituents are slightly twisted-off from the imidazole axis (13.6°) and are located in an up-up-down-down fashion and not in an up-down-up-down manner with respect to the basal Fe—N₄ plane. This must somewhat increase the steric repulsions within the ligands, since it brings the 2,6-diisopropylphenyl substituents on the same side of adjacent imidazole rings.

Analysis of the packing diagram of molecules in the unity cell reveals that the individual molecules of **100a** are well separated from each other with essentially no intermolecular contact distances (figure 75).

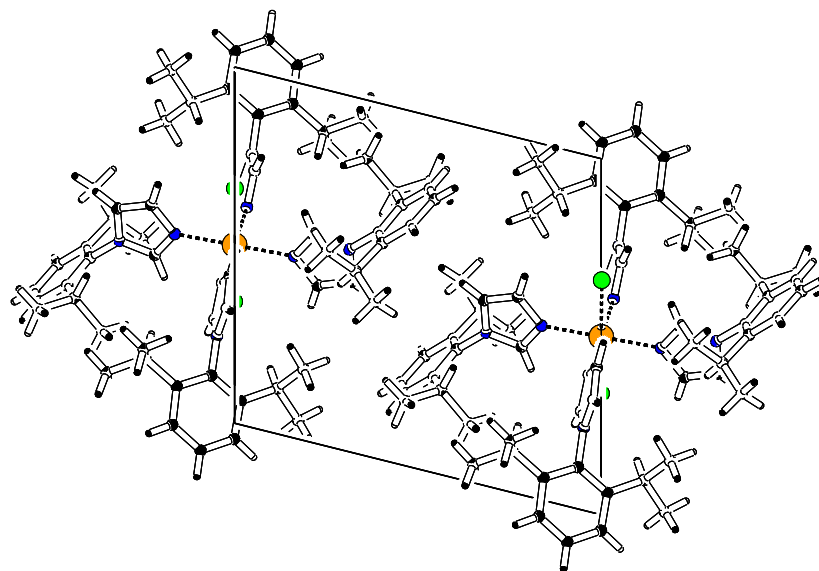


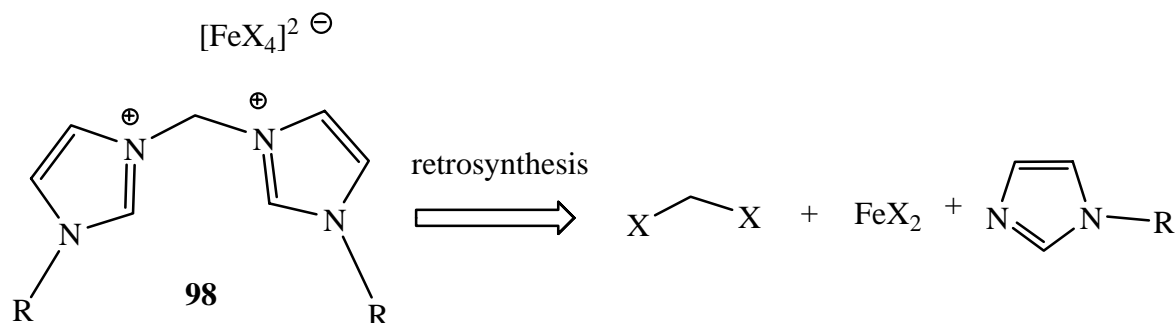
Figure 75. Diagram packing of complex **100a**.

Assuming that the isolated complex **99** is similar to the obtained bisimidazolium iron(III) tetrahalogenate **98a**, we have tried a deprotonation of **99** with NaH in THF at 0°C to RT, which afforded a yellow brown solid after filtration and evaporation of the solvent. The ¹³C-NMR was not possible because the sample is again paramagnetic; MS(ESI+) and CHN analyses were done, but the obtained results are not according to expected values. The UV-Vis spectrum shows only one maximum at 292 nm, this is different compared to that observed with the starting complex where two maxima are visible at 365 nm and 310 nm. Unfortunately, no crystals were obtained.

15.4.2. Tentative mechanism of formation of tetraarylimidazolbishalide iron(II) complexes

The main result in the structure of **100a** is the loss of the bridge methylene, probably as dichloromethane. Thus, two independent imidazole groups are formed for each starting ligand. Additionally, this result demonstrates a possible fragility of these ligands when used in harsh reaction conditions.

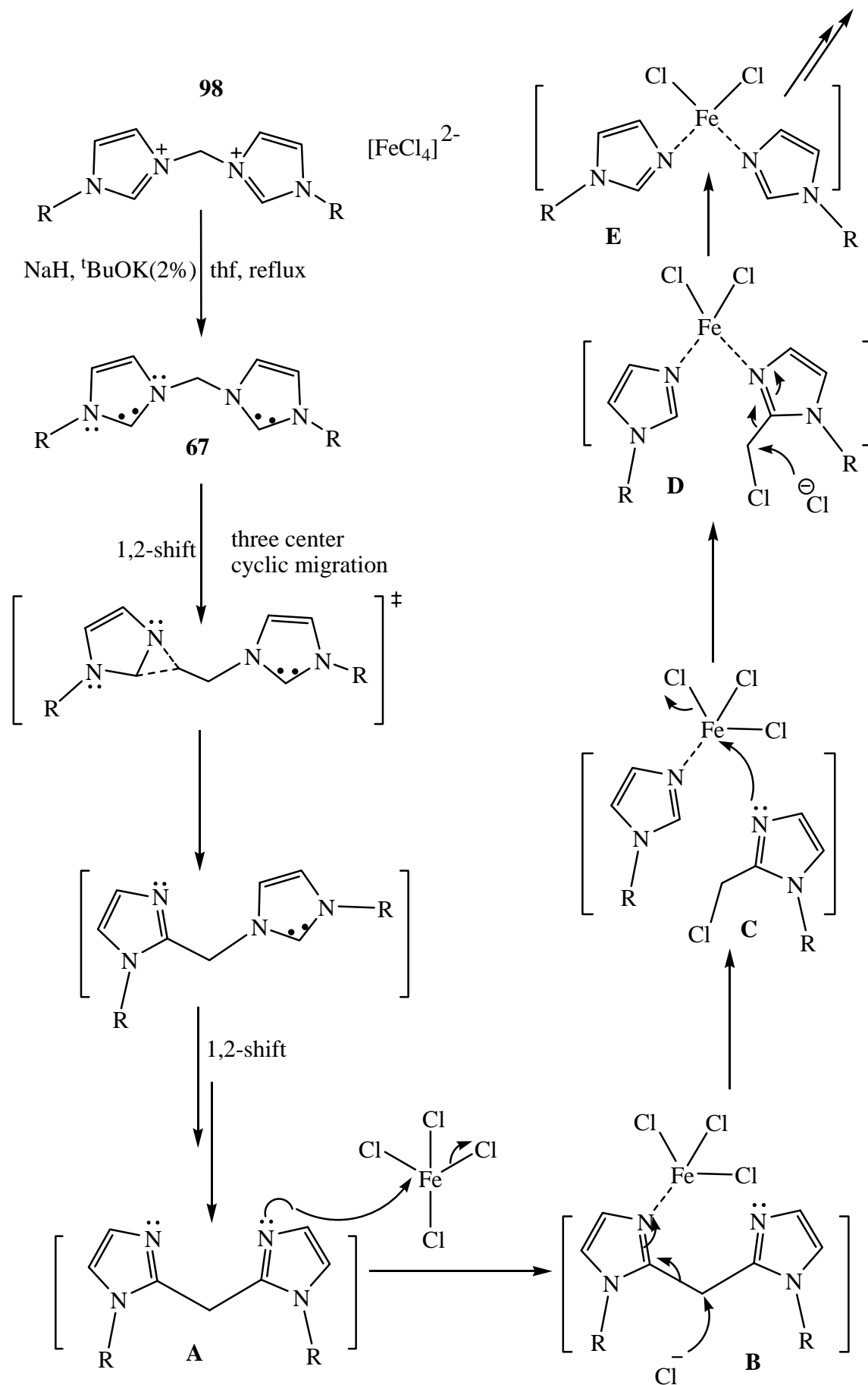
The mechanism of formation of complex **100a** can be regarded as a return in direction of starting N-1-arylimidazol with a loss of the methylene bridging group; it is a kind of retrosynthesis (schema 64). It remains to elucidate the reduction of Fe(III) to Fe(II).



Scheme 67. Proposed pathway.

Alternatively, the formation of **100** could be explained as a two fold 1,2-migration reaction of the methylene bridge in free carbene **66** to form the intermediate **A** (scheme 68). Indeed, it is now well established that 1,2-migration is a fundamental reaction for carbenes and occurs via an unimolecular concerted mechanism⁸⁸.

In the next step, the unsubstituted nitrogen atom of the imidazole ring reacts with iron to give the intermediate **B**, which rearranges and affords the FeCl_3 -imidazole **C** and C(2)-chloromethylimidazole **D**. This latter was described in the literature as intermediate in the preparation of C(2)-olefins¹⁴⁵. Attack of **D** to the iron moiety of **C** makes it possible to form the bis-substituted imidazole complex **E** and to release the dichloromethane. These series of reactions continue until the stable complex **100** is obtained.



Scheme 68. Proposed mechanism II: 1,2-shift.

An analogous compound of **100a** was also isolated when [bisimidazolium]²⁺[FeBr₄]²⁻ complex was reacted with NaH in similar conditions as before (complex **100b**, figure 76).

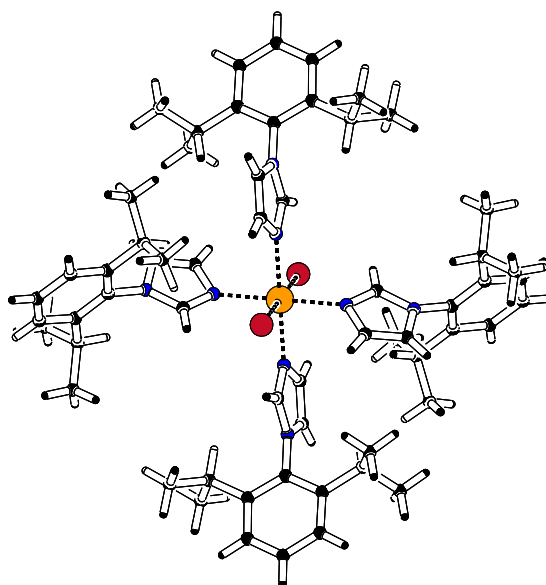


Figure 76. ORTEP representation of complex **100b**.

Table 28. Selected bond lengths [Å] and angles [°] for **100b**.

Fe-Br(1)	2.742(3)	Fe-N(1)	2.188(2)
Fe-Br(2)	2.742(3)	Fe-N(3)	2.178(2)
N(1)-C(1)	1.324(2)	N(3)-C(16)	1.317(2)
N(1)- C(2)	1.374(2)	N(3)- C(17)	1.381(2)
N(2)- C(1)	1.348(2)	N(4)- C(16)	1.349(2)
C(2)- C(3)	1.357(2)	C(17)- C(18)	1.350(3)
N(2)- C(4)	1.438(2)	N(4)- C(19)	1.359(2)
Br- Fe- Br	180.0(8)	N(1)- Fe- N(1a)	180.0
N(1)- Fe- Br(1)	89.9(4)	C(1)- N(1)- C(2)	105.7(1)
N(1)- Fe- Br(1a)	90.1(4)	C(16)- N(3)- C(17)	105.4(1)

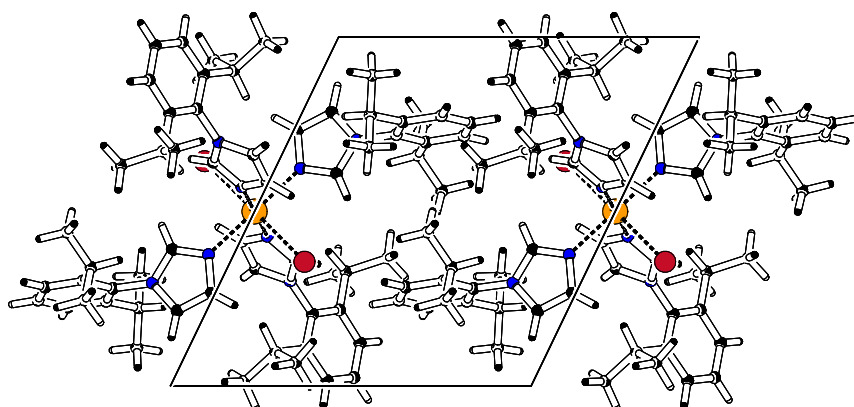


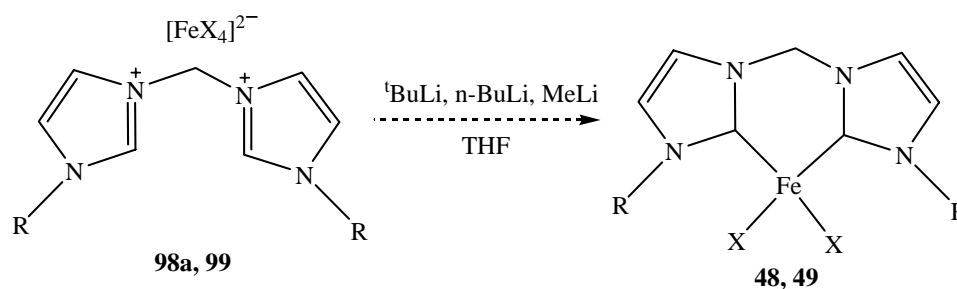
Figure 77. Crystal packing of complex **100b**, viewed along the *a*-axis.

The isolation of complex **100a** permits us to conclude that :

- The cleavage of the bridged biscarbene/imidazolium ligand requires halide ions and perhaps a Lewis acid catalysis;
- Not all the iron was oxidized to Fe(III) during the formation of **98a**.

15.4.3. Deprotonation of complexes **98** and **99** with lithium bases (MeLi, ^tBuLi and ⁿBuLi)

There are few examples in the literature concerning the reduction of Fe^{III} compounds to their Fe^{II} analogue by lithium bases¹⁴⁶. In our case, the base plays both the roles of a reducing and a deprotonating agent.



Scheme 69. Synthesis of **48, 49** from the reaction of imidazolium salts and lithium bases.

Table 29. Experimental conditions

Exp	[Fe] (mmol)	Base (mmol)	THF (ml)	Temp. [°C]	Time [hours]	UV – Vis [nm]
1	98a (0.10)	^t BuLi (0.25)	20	-78 to 0	4	240
2		ⁿ BuLi (0.25)		-		
3		MeLi (0.25)		-78 to RT	12	431, 362, 314, 241
5	99 (0.1)	MeLi (0.25)		470, 363, 287		

Addition of ^tBuLi at -78°C to the yellow solution of complex **98a** causes immediately colour changes of the solution to red-brown. The temperature was allowed to rise and kept at 0°C for 4 hours. At the end of the reaction, the colour of the solution turned yellowish-brown. Filtration at -78°C and evaporation of the solvent permitted us to recover a yellow brownish solid. This solid was again extracted with toluene at 0°C and the solvent was evaporated, yielding a yellow brown solid. The NMR spectra it was not possible to record because of decomposition of the isolated compound, which occurs in few minutes. As before, the mass spectrum shows many peaks but not the expected signals. Compared with the previous complexes, here only one band at 240 nm was observed in the UV–Vis spectrum. ⁿBuLi also was used as base for a synthesis of complex **48** without success.

The reaction of **98a** with MeLi in THF was done from -78°C to RT. After filtration and evaporation of the solvent, a yellow-brown solid was obtained which was treated by extraction with toluene affording again an yellow-brown solid. The recorded UV-Vis spectrum in toluene shows three absorption bands at 362 nm, 314 nm and 241 nm with shoulders at 431 nm (figure 80). The ¹H-NMR shows broad signals but we were able to record a carbon ¹³C-NMR in which we observed two broad signals at 178.8 ppm and 168.2 ppm, which could be assigned to the iron-carbene bond resonance, by comparison with the

reported $[\text{FeCp}(\text{CO})_2(\text{imid})]^+$, where the Fe-carbene was found at 172.5 ppm³¹ (figure 78). The MS (ESI+) and the CHN analysis of the yellow-brown solid do not show the expected results. Furthermore, the degradation of the isolated compound was observed to occur rapidly in solution.

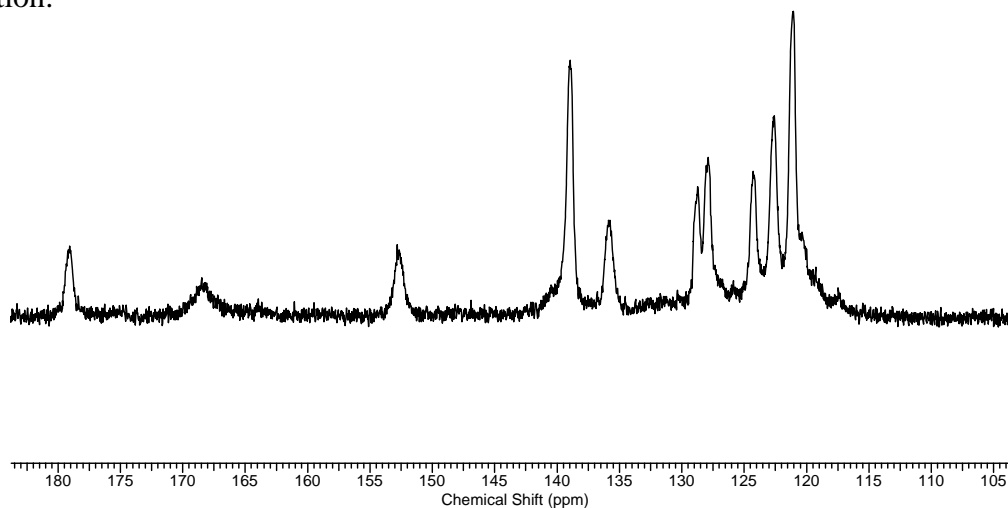


Figure 78. The down field ^{13}C -NMR (125 MHz) spectrum of complex **48** in THF- d_8 .

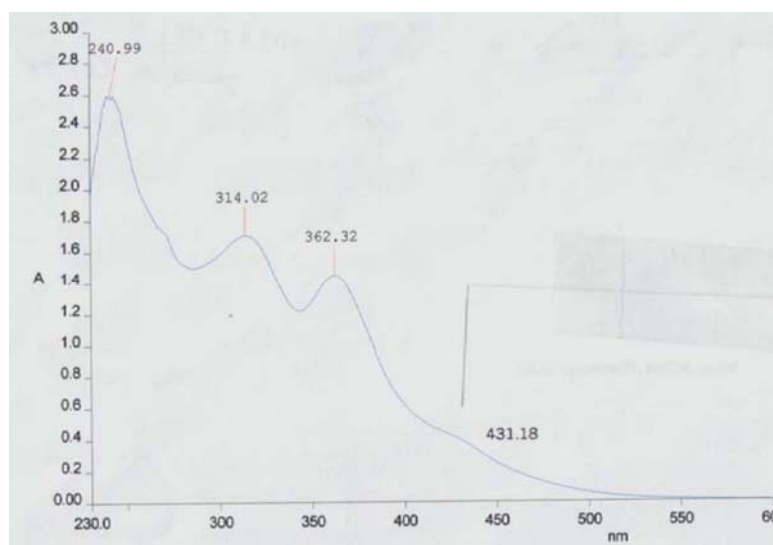


Figure 79. The UV-Vis spectrum of complex **48** in THF.

The reaction of **99** with MeLi in THF at low temperature permits the isolation of a yellow-brown solid. Crystallization by slow diffusion in THF/ether gave orange crystals but their quality was not sufficient for X-ray analysis, furthermore rapid degradation was observed. The MS (ESI+) and the CHN analysis of the yellow-brown solid do not show the expected results. However, the broad ^{13}C -NMR spectrum in THF- d_8 shows one signal at 169.4 ppm

which was assigned as previously to the resonance of a Fe—carbenoid (figure 80). In the UV-Vis spectrum, two absorption maxima at 363 nm and 287 nm were detected with a shoulder at 470 nm (figure 81).

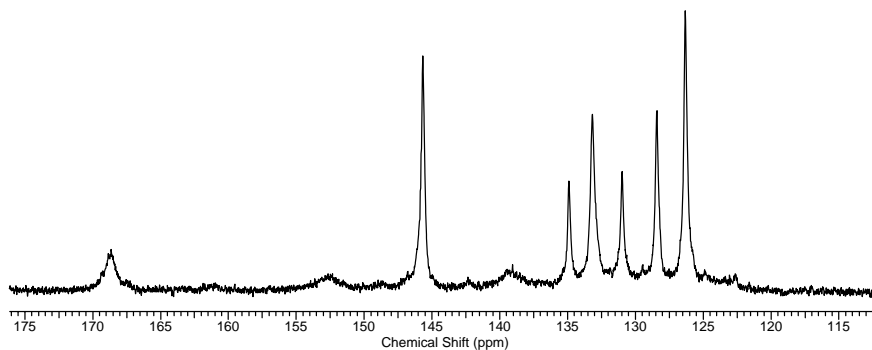


Figure 80. The down field ¹³C-NMR (125 MHz) spectrum of complex **49**.

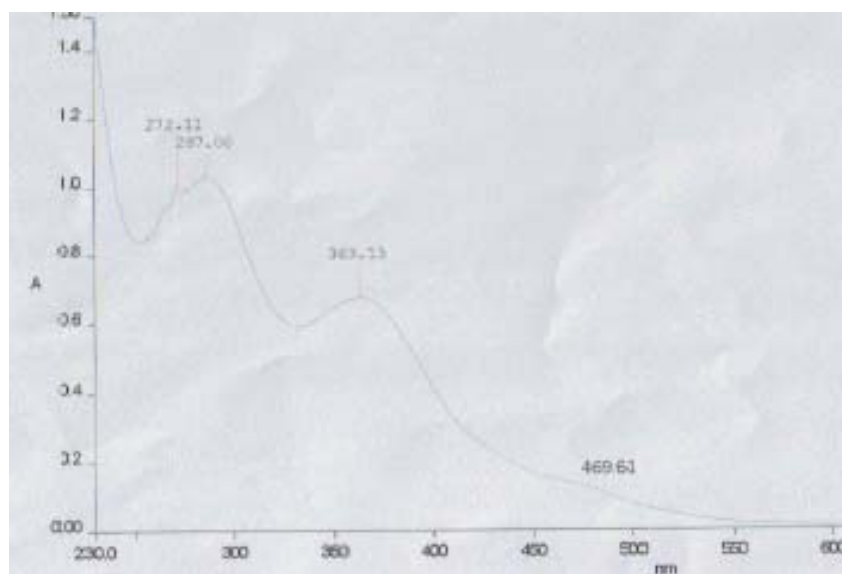
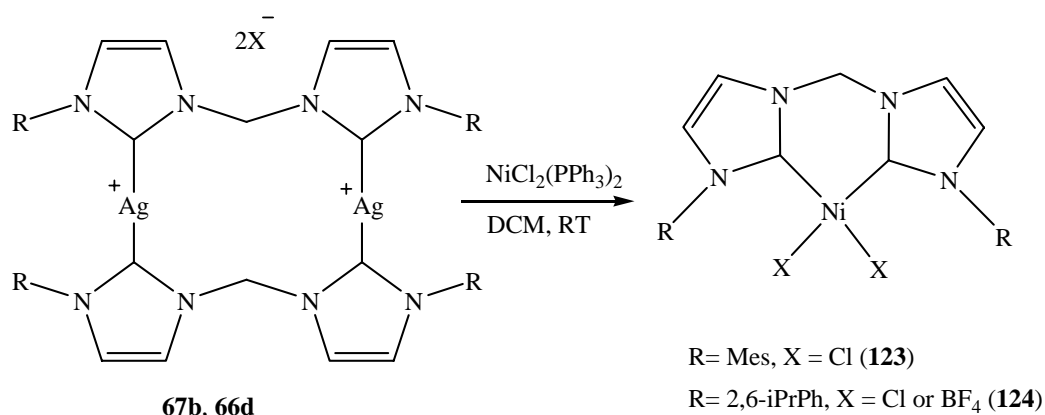


Figure 81. The UV-Vis spectrum of complex **49** in THF.

15.5. Reaction of silver complexes with NiCl₂(PPh₃)₂

We were also interested in a possible use of other metals as catalyst for polymerization of olefins and, we plan to make comparison of their catalytic activity with that observed in iron complexes. Our choice moved towards nickel (II) since a certain number of complexes of this

metal are very active in the catalytic polymerization of olefins. However, no systematic investigation was carried out on the synthesis of the Ni(II) complexes with the ligands bisimidazol-2-ylidene and of course their applications.



Scheme 70. Synthesis of Nickel bisNHC complex **123** and **124**.

Thus, the reaction of silver complex **67b** with two equivalents of $\text{NiCl}_2(\text{PPh}_3)_2$ in dichloromethane at RT was done (scheme 70). The starting black solution turns yellow-green after few minutes. The upper green was take-off and the left yellow solid was washed with benzene or toluene in order to remove the released triphenylphosphine. The yellow solid, was then dissolved in methanol and filtrate over celite, this operation permit to remove the formed AgI. Evaporation of the solvent permits the isolation of yellow solid in 73% yield. The UV-Vis spectrum in methanol of the product shows five absorptions maxima at 769, 529, 441, 374 and 319 nm; for comparison the UV-Vis spectra in methanol of the starting $\text{NiCl}_2(\text{PPh}_3)_2$ shows two absorptions at 474 and 354 nm. The carbene-nickel appears at 171.7 ppm in the ^{13}C -NMR. The product was also characterized by MS(ESI+) : m/z 513 $[\text{M}+1]^+$ and 385 $[\text{M}+1-\text{NiCl}_2]^+$. Suitable yellow crystals for X-ray diffraction were grown by slow diffusion of diethylether into the methanol solution of the product. Despite the poor quality of these crystals, the skeletal arrangement is in the same line of NMR analysis. The structure in the figure 82 shows clearly that, the chelate ligand adopts a *cis* arrangement around the nickel atom; there is also an C_2 symmetry at the nickel center. The aryl substituents on the NHC imidazole are twisted and that resulting in a favourable steric arrangement with the nickel center.

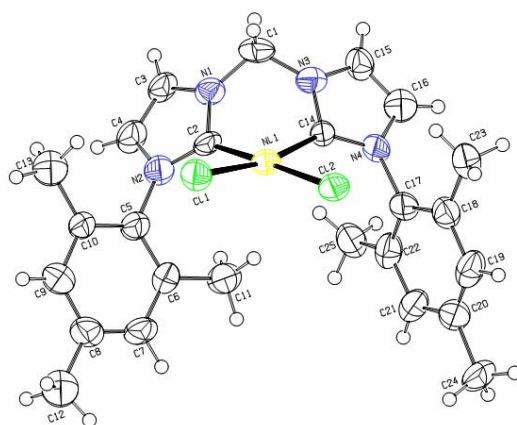


Figure 82. ORTEP representation of nickel complex **123**.

The reactivity of silver biscarbenes imidazole-2-ylidene **66d** was also tested with $\text{NiCl}_2(\text{PPh}_3)_2$. Reaction was done in CH_2Cl_2 at room temperature. The colour of mixture changes fairly from black to red-purple in few minutes and a yellowish precipitate appears after 2 hours. The upper red solution was filtrate and the left yellow solid was washed with benzene and methanol then dried under vacuum, affording the product **124** as a red-brown solid in a good yield (76%). The formation of carbene-nickel compound was confirmed by ^1H - and ^{13}C -NMR; in carbon NMR the signal at 172.7 ppm was assigned to the resonance of carbene C(2)-Nickel bound. The UV-Vis spectrum of the product shows two maxima at 385 and 257 nm. The peak at m/z 469 in the MS(ESI+) spectrum was assigned to the $[\text{M}+1-\text{NiCl}_2]^+$. Crystallization by slow diffusion of diethylether into the methanol solution of **124** affords red crystals. The structure obtained by X-ray diffraction is depicted in the figure 83.

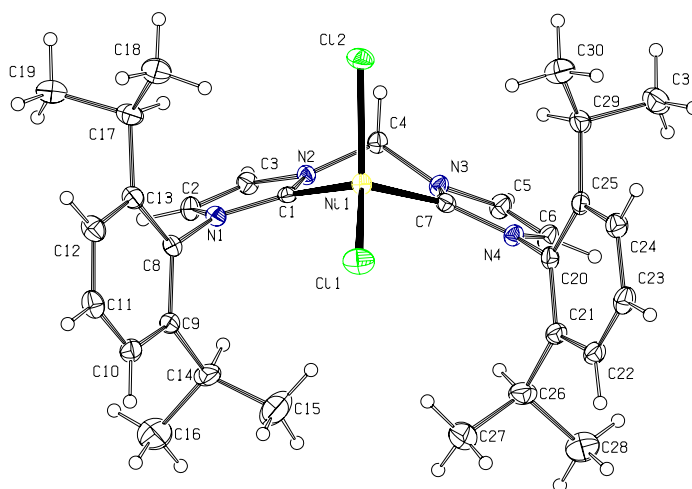


Figure 83. ORTEP representation of nickel complex **124**.

Table 30. Selected bond lengths [Å] and angles [°] for **124**.

Ni-Cl(1)	2.2307(6)	Ni-C(1)	2.989(2)
Ni-Cl(2)	2.2624(6)	Ni-C(7)	2.984(2)
N(1)-C(1)	1.350(2)	N(3)-C(4)	1.449(3)
N(1)- C(2)	1.389(3)	N(3)- C(7)	1.360(3)
N(2)- C(1)	1.359(2)	N(4)- C(6)	1.384(3)
C(2)- C(3)	1.339(3)	C(5)- C(6)	1.342(3)
N(2)- C(4)	1.446(3)	N(3)- C(5)	1.382(3)
Cl- Ni- Cl	124.85(2)	C(7)- Ni- Cl(2)	102.83(6)
C(1)- Ni- C(7)	91.97(8)	N(2)- C(4)- N(3)	111.68(16)
C(1)- Ni- Cl(2)	97.91(8)	N(3)- C(1)- N(2)	103.48(17)

The formation of the six-membered chelate ring distorts the coordination of the nickel from the ideal tetrahedral geometry, with the C—Ni—C bite angle being reduced to 91.97(8)° and Cl—Ni—Cl to 124.85(2)°. The Ni-carbene bond lengths lie in the range 1.984(2)Å and 1.989(2)Å and are similar to those reported for the mono substitute imidazol-2-ylidene [NiCp(NHC)Cl] (1.8748(11)Å, NHC = 2,6-diisopropylphenylimidazol-2-ylidene)^{160a} and [Ni(Py(CH₂)NHC)₂]²⁺ (1.851(4)Å, NHC = 1-Benzylimidazol-2-ylidene)^{160b,c}.

Very interesting is the behaviour of the related complex **124**, which acts like a sensor of oxygen or moisture. Indeed in absence of any moisture and oxygen the product is red-brown in colour, while when exposed to air the product becomes yellow-clear in a few minutes; this system is reversible even after several weeks (figure 84 and 85). Moreover, complex **124** is completely colourless in the acetonitrile, while it is yellow in methanol.

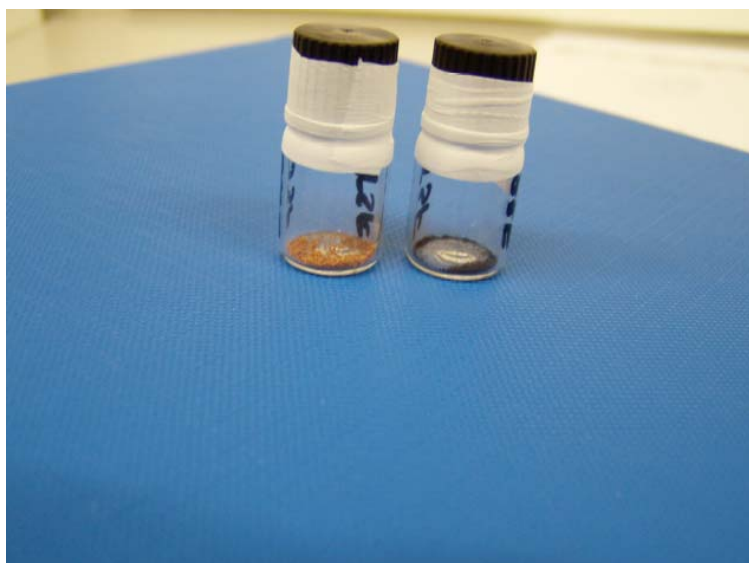


Figure 84. Picture of complex **124**. left: sample exposed to air. Right: sample under argon.

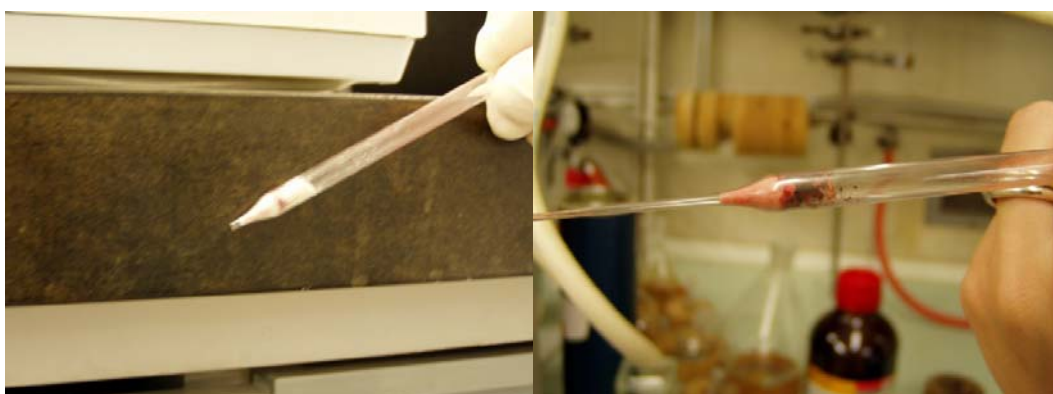


Figure 85. Picture of complex **124**. left: sample exposed to air. Right: sample under argon.

II-10. Analytical Tools

16. Analytical tools

16. 1. Electronic absorption spectroscopy of isolated iron complexes

16.1.1. Iron(II) benzyletherfuran complex **50**

The electronic spectra of the iron(II) benzyletherfuran complex **50** and its respective ligand were recorded in tetrahydrofuran. According the reported studies of Lambert¹⁴⁷ on substituted iron–arene complexes and of Palaniandavar¹⁴⁸ on iron-Phenolate complexes, the absorbance in the range of 300-400 nm could be attributed to a metal to ligand charge transfer or ligand to metal charge transfer (MLCT or LMCT). For our experiment, we did first the UV–Vis spectrum of the ligand that permitted us to observe the shift or the appearance of new absorption bands during the complexation.

The UV–Vis spectrum of the benzyletherfuran ligand **53** is dominated by two absorptions in the UV region of the spectra (220 nm and 263 nm), which is characteristic for $\pi-\pi^*$ transitions (figure 86).

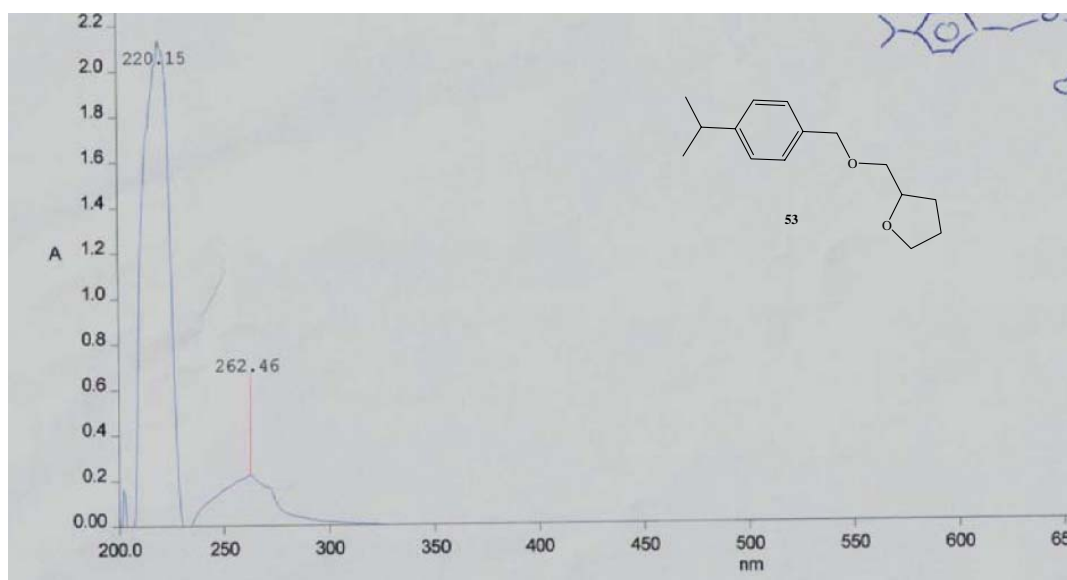


Figure 86. The UV–Vis spectrum of benzyletherfuran ligand **53** in THF.

In the THF UV-Vis spectrum of complex **50** (figure 87), four absorptions bands are observed at 360 nm, 310 nm, 238 nm and 212 nm. Such bands have been already observed for iron

allybenzylether complexes prepared by Raemy. He correlated them with the observed catalytic activity in hydrogenation and acetylen polymerization⁸⁶. According to the literature^{148,149}, the majority of μ -oxo complexes of iron show typical absorption bands in the region of 312 nm and 358 nm. In our case, the metal to ligand charge transfer (MLCT) is found at 364 nm and the position of this band demonstrates the high-spin state of complex **50**. However, the values observed here are lower as those normally observed in others systems such as iron oxo- or amido-pyridine complexes, which usually display a MLCT band in the visible region (*ca.* 410 nm) in polar solvent such as tetrahydrofurane, methanol or acetonitrile¹⁵⁰. Moreover, there is no *d-d* transition observed in the spectrum of **50**. These transitions are reported to appear near the infrared region of the spectrum.

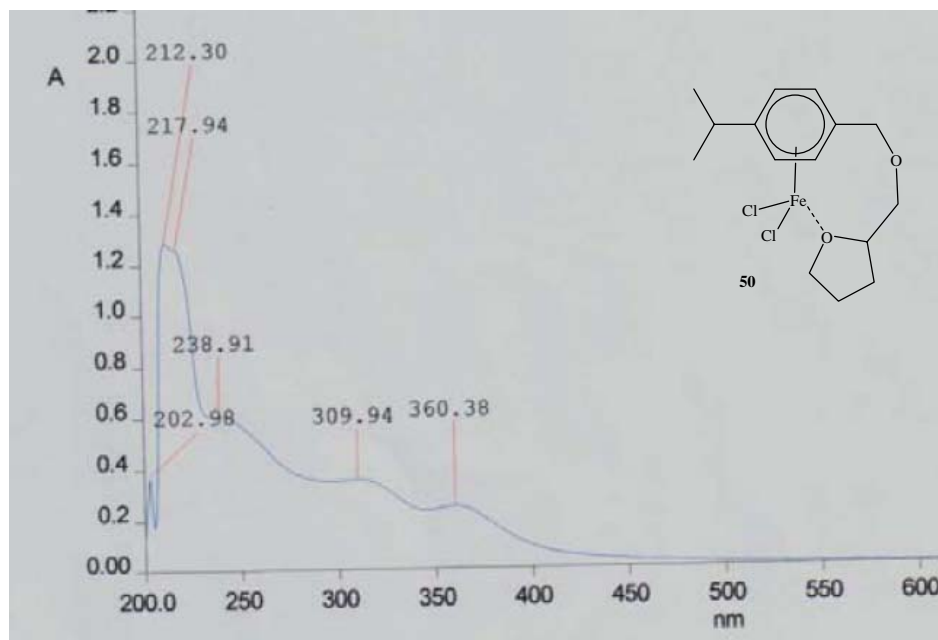


Figure 87. The UV-Vis spectrum of complex **50** in THF.

For purpose of comparison, the UV–Vis spectrum of FeCl_2 in THF was also recorded under the same conditions, as is shown in the figure 88, the absorption maximum is at 336 nm.

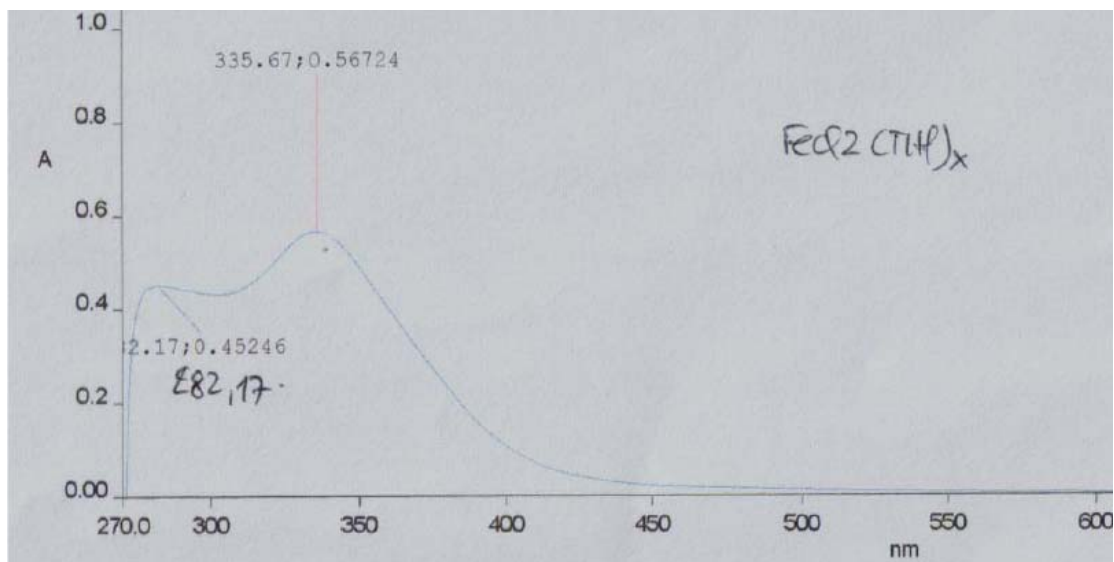


Figure 88. The UV–Vis spectrum of $\text{FeCl}_2(\text{THF})_2$ in THF.

16.1.2. Iron(II) methylenebisimidazol-2-ylidene complexes

The electronic spectra of the iron(II) methylene bisimidazol-2-ylidene complexes **48** and **49**, and their respective ligands were recorded in tetrahydrofurane figure 89 and 90).

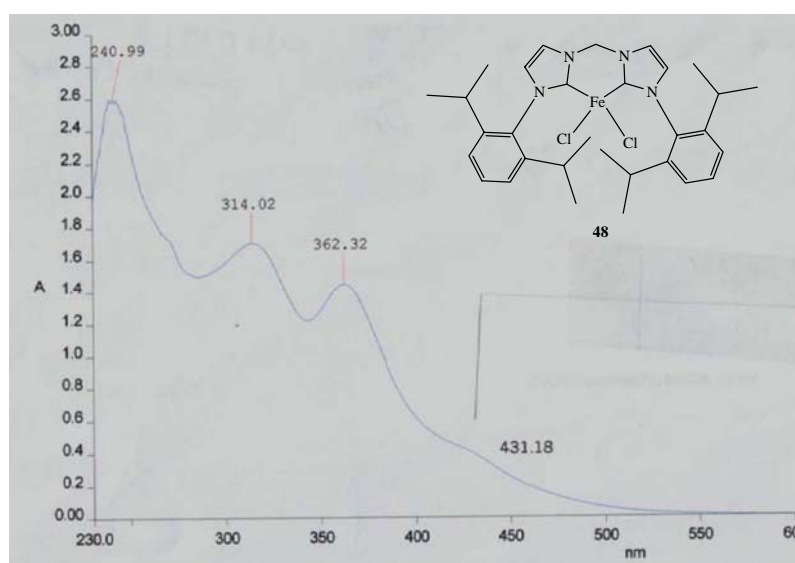


Figure 89. The UV–Vis spectrum of iron imidazole-2-ylidene complexes **48** in THF.

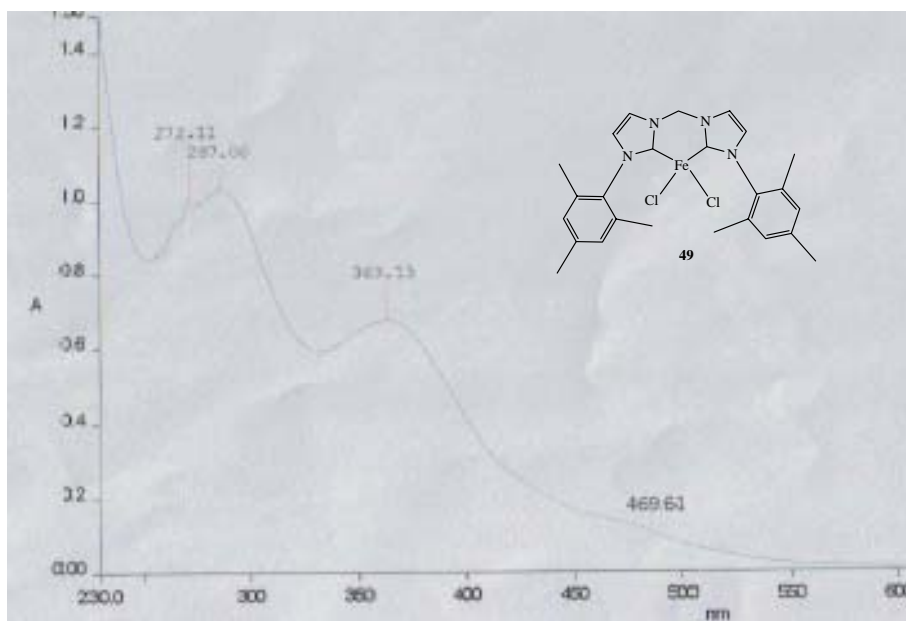


Figure 90. The UV–Vis spectrum of iron imidazole-2-ylidene complex **49** in THF.

We first thought that the broad and weak shoulder in the visible region could be attributed to a charge transfer transition from the coordinated halide to the metal. Nevertheless, our data should be compared to those reported for similar ferrous complexes, but unfortunately, there are no electronic data concerning iron imidazol-2-ylidene complexes. We also checked the literature for Fischer carbene complexes of iron but we did not find a real electronic study. Thus, we compared our results with those reported for N,N',N''-tris(2-pyridylmethyl)ethane-1,2-diamine type ligands^{121b, 150, 151}. In such complexes a similar broad band at 400 nm is assigned to a MLCT between the Fe(II) t_{2g} orbitals and the π^* pyridine orbitals. The origin of the absorptions in our series of compounds might be the same. The spectrum of **48** exhibits ligand centered $n-\pi^*$ and $\pi-\pi^*$ absorptions at 362 nm, 314 nm and 240 nm; the smaller weak and broad band at 431 nm could be assigned again to the MLCT transition.

In the complex **49**, ligand centered $n-\pi^*$ and $\pi-\pi^*$ transitions are also observed in the UV region (363 nm and 287 nm). Nevertheless, the striking feature in this complex is the significant weakening of the broad absorption. In addition, this weak signal is shifted to the visible region with respect to the one in complex **48**; the shoulder is now recorded at 470 nm. Actually, we have no explanation of this noticeable difference between **48** and **49**; in fact, we

exclude a possible difference in the ligand field around the metal and consequently a difference in the coordination sphere, since both ligands are very similar.

The comparison of the absorption bands for the MLCT in iron bischlorobenzyletherfuran complex **50** (363 nm), with that observed in iron bischloro methylenebisimidazol-2-ylidene complexes (431 nm (**48**) and 470 nm (**49**)), illustrates that, substitution of a π donor aryl, which stabilizes the t_{2g} set of orbitals, with a strong σ -donor and weak π -acceptor NHC-carbene, which destabilizes the t_{2g} set, will decrease the gap between the t_{2g} metal orbitals and the imidazole π^* orbitals, resulting in a shift of the λ_{max} of the MLCT to higher wavelengths.

The influence of exogenous ligands on the metal centre in the charge transfer transition is well reflected in the iron(II) biscarbene complexes containing charged formiate or triflate ligands. It is expected that, since these ligand stabilize the t_{2g} set of orbitals, the metal to ligand charge transfer will occur at higher energy in comparison with the bischloro iron NHC complex **49**. Furthermore when the exogenous ligand is a better σ -donor, it provokes the lowering of the iron formal oxidation state^{150,151} and by consequence the MLCT will occur at higher energy as compared to complex **49**.

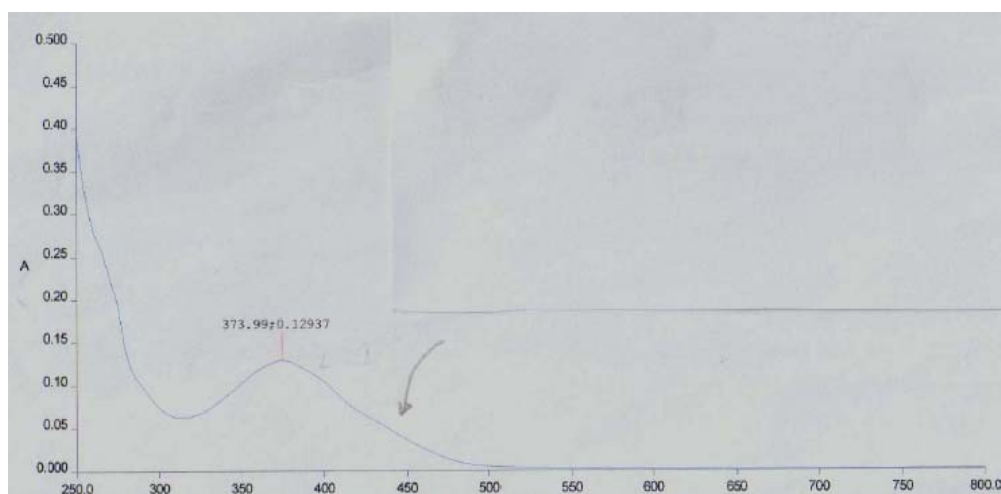


Figure 91. The UV-Vis spectrum of iron(NHC) triflate complex **49e** in THF.

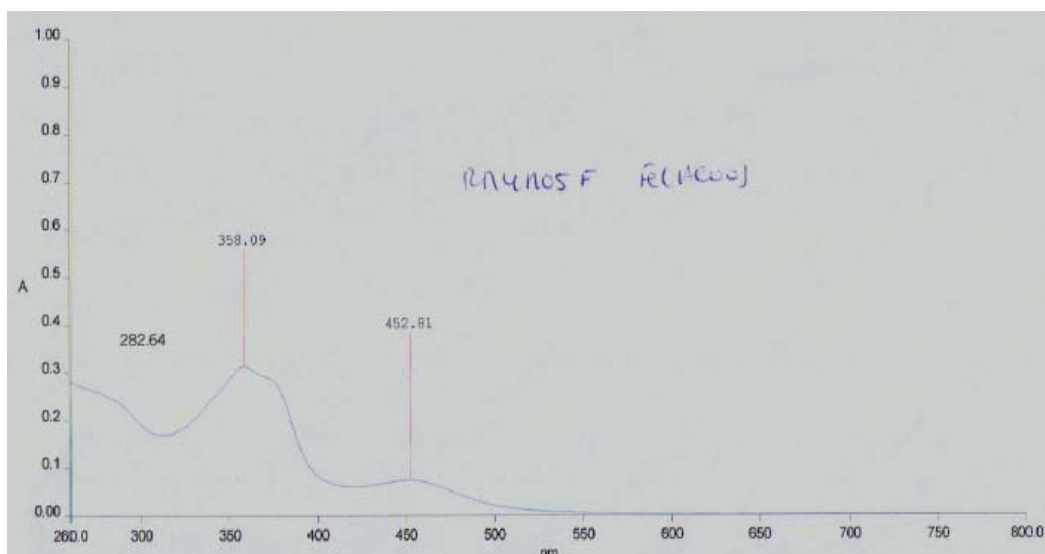


Figure 92. The UV-Vis spectrum of iron(NHC) formiate complex **49d** in THF.

The UV-Vis spectrum of iron biscarbeneformiate complex **49d** with the maximum absorption at 453 nm (figure 91) and that of iron biscarbenetriflate **49e** at 350 nm (weakening, figure 91) confirm this expectation. The position of the band is differently affected in going from formiate to triflate towards the bisimidazol-2-ylidene ligand **64**.

16.1.3. Reactivity of complexes **48**, **49** and **50** towards H_2O_2 as oxidant

The reactivity of complexes **48**, **49** and **50** with an excess of H_2O_2 was studied in THF from low temperature to RT. In fact, it was reported that reaction of Fe^{II} complexes with excess H_2O_2 forms a transient red purple species, and comparison of UV-Visible spectra of these complexes with other $\text{Fe}^{\text{III}}-\mu_1-\text{OOH}$ systems support the formulation of the purple species as the low-spin Fe^{III} -hydroperoxo compounds¹⁵².

For this purpose, the addition of 100 equivalents of 30% H_2O_2 to a THF solution of **48** and **49** at -10°C was done and resulted in the appearance of a weak band at 985 nm in the UV-Vis spectrum. Such absorption could be attributed to a metal $d-d$ transition¹⁵³. We did not find any hydroxoperoxo-to- Fe^{III} charge transfer transition, which was reported to appear in the range of 530 nm (figure 93)¹⁵². We also observed a quickly degradation of the sample.

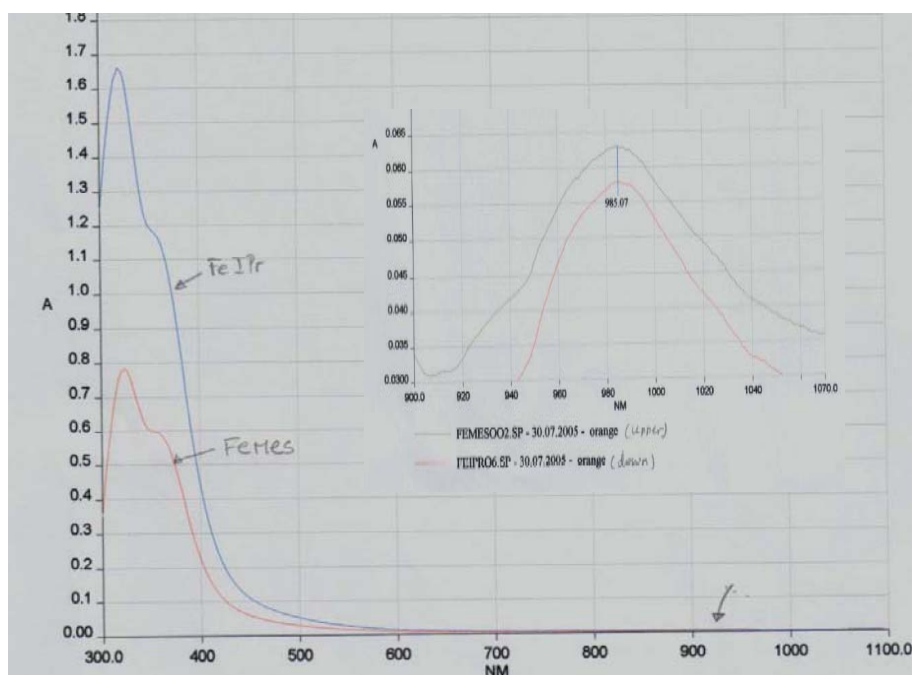


Figure 93. The UV–Vis spectra resulted from the reaction of complexes **48** and **49** with H_2O_2 in THF.

The complex **75** was also reacted under the same conditions, again no band around 530 nm was observed in UV–Vis spectrum even though it adopts a structure in solution similar to that of complexes **48** and **49**. That is probably due to the steric congestion provided by the aryl groups in the imidazole-2-ylidene complexes or to the benzyletherfuran ligand around the metal atom, which prevents the coordination of the hydroperoxo moiety on the metal center. Moreover, we observed a rapid degradation of the complexes to rust. The same reaction carried out with FeCl_2 and FeCl_3 did not afford any expected results.

16.2. The ^1H - and ^{13}C -NMR in solution

The electron count of complexes **48** and **49** suggests an electronically deficient compound, i.e. a compound with 14 electrons; this configuration reflects a high-spin ferrous state. Moreover, other purely theoretical factors make it possible to envisage a high-spin complex: the chloride and bromide ions are low-field ligands, and their size exerts sufficient steric constraint to push the imidazole-2-ylidene ligand away from the metal center. Thus, the ^1H - and ^{13}C -NMR

spectra of complexes **48** and **49** reflect the high-spin state for iron, with very broad signals (figure 94) compared to the spectra of where the ligand halide was replaced by more stabilizing ligands (formiate, triflate, cyclopentadienyle).

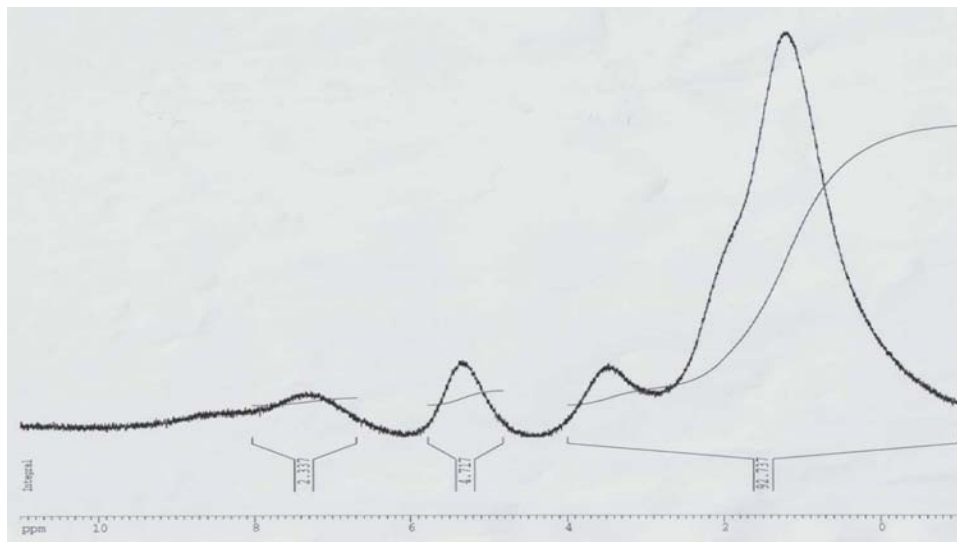


Figure 94. Example of $^1\text{H-NMR}$ (360 MHz) spectrum obtained for complex **49** in THF-d_8 solution.

Furthermore, the coordination of methanol and acetonitrile to the metal has been considered in **49**. Thus, the $^1\text{H-NMR}$ spectrum of complex **49** was taken in deuterated methanol, CH_3OD (figure 95 and 96).

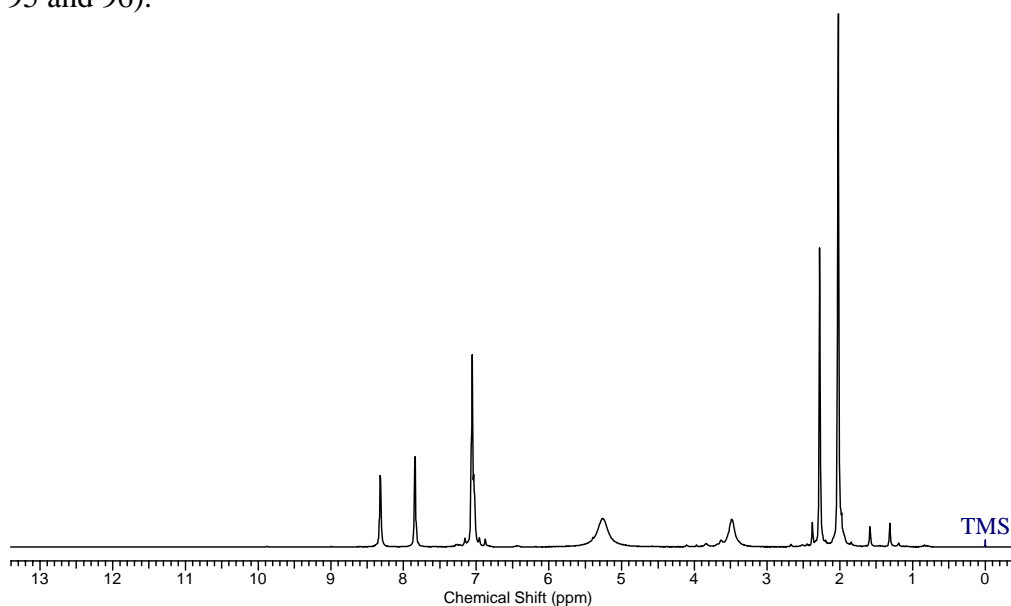


Figure 95. The $^1\text{H-NMR}$ (500 MHz) spectrum obtained for complex **49** in the MeOD solution.

In this solvent, all the expected peaks are visible, even if they are still broad. The integral of the peak situated at 1.8 ppm gives six protons corresponding to the two *ortho*-methyl groups and the three protons at 2.1 ppm were assigned to the *para*-methyl of the aromatic substituent. The signals of the aromatic protons appear in the down field region located between 6.5 and 7.0 ppm at the same place as the two protons of the bridging methylene. The two remaining signals at 7.7 and 8.1 ppm were attributed to the two protons on the imidazole ring. The solvent methanol gives two signals at 5.1 and 3.49 ppm. We did the same experiments as before with the complex **49** in deuterated acetonitrile and we observed broad peaks for both ^1H - and ^{13}C -NMR spectra (figure 97 and 98). The ^{13}C -NMR spectrum shows all peaks except for the carbenoid carbon. In contrast to the previous experiment with methanol- d_4 , the proton spectrum shows very large peaks, however we can distinguish the aromatic protons at 7.1 ppm and the imidazole protons at 8.3 and 10.1 ppm.

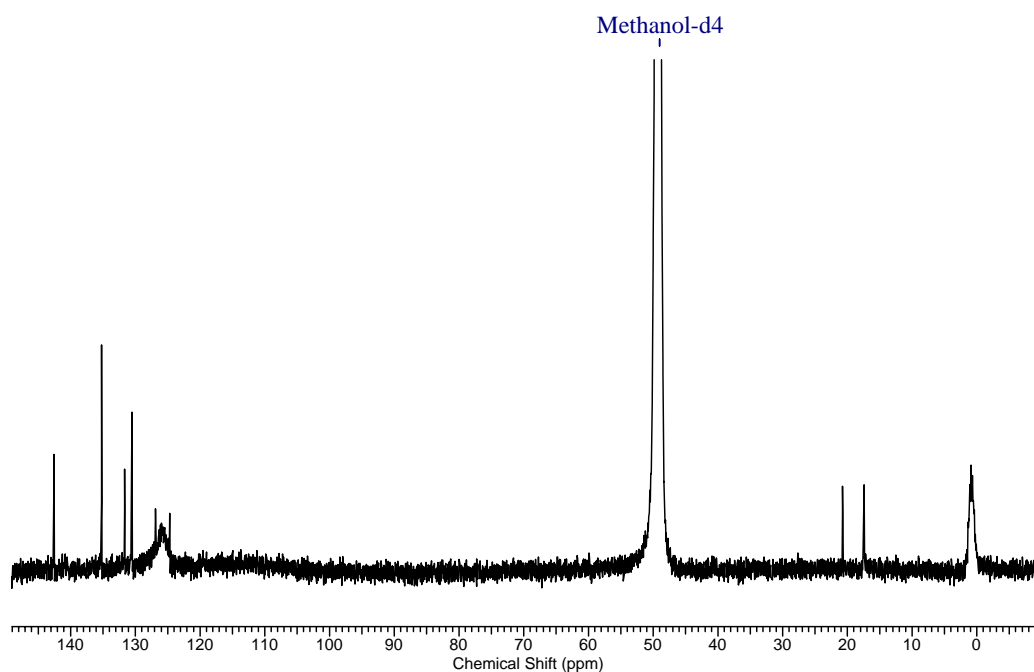


Figure 96. Example of ^{13}C -NMR(125 MHz) spectrum obtained for complex **49** in the MeOD solution.

The ^{13}C -NMR spectrum measured in methanol (figure 96) shows that the aromatic peaks of *N*-substituted aryls are only slightly influenced by the paramagnetism of the metal center. However, the zone corresponding to the resonance of the carbons on the imidazole ring is very broad. Another broad peak appears between 0.5 and 2.0 ppm, which could correspond to

the methyl of metal coordinated methanol. Unfortunately, we do not see any peaks assignable either to the carbon carbenoid nor to methylene bridged. The carbon spectrum measured in other solvents such as THF or dichloromethane gives very broad peaks. It is important to note that degradation of the products occurs after a short time (< 48 hours). The same observations were made for the complex **48**.

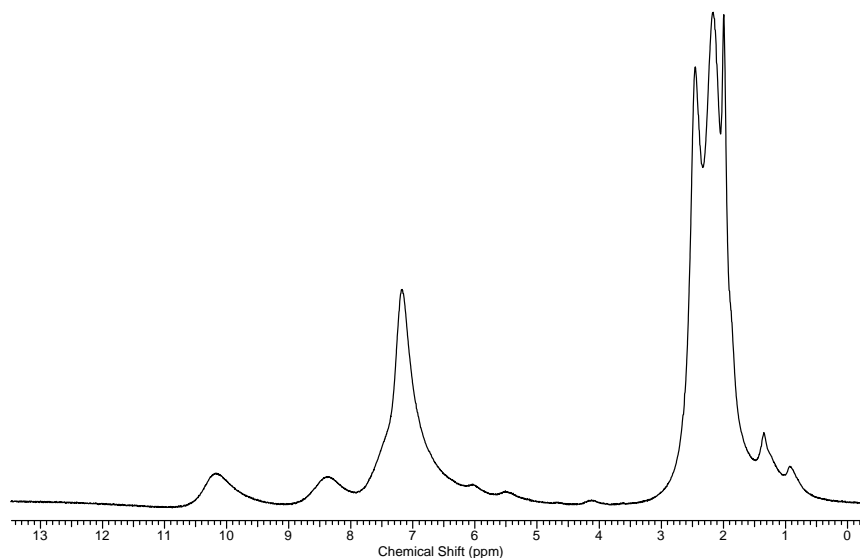


Figure 97. Example of ¹H-NMR (500 MHz) spectrum obtained for complex **48** in the CD₃CN solution.

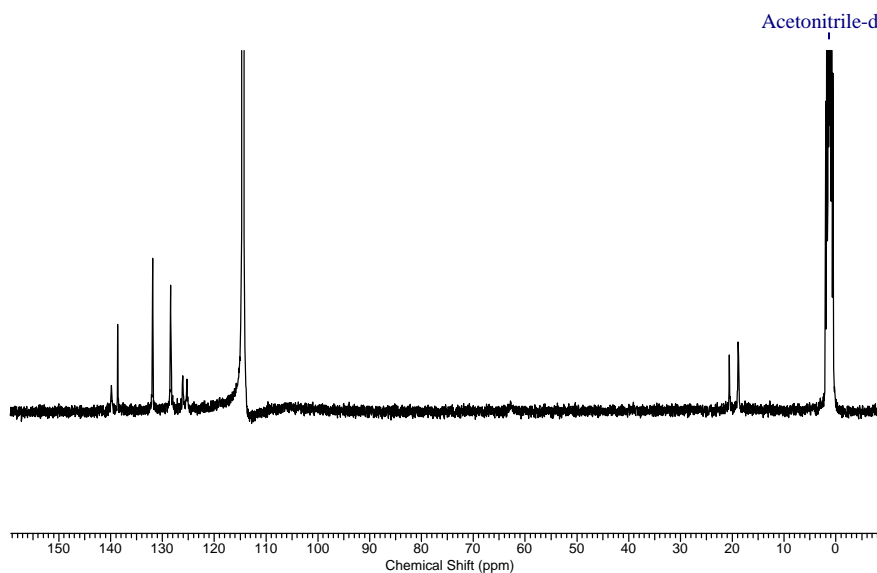


Figure 98. Example of ¹³C-NMR (125 MHz) spectrum obtained for complex **48** in the CD₃CN solution.

The ^1H -NMR spectrum of complex **50** is also typical for a high-spin ferrous compound and is difficult to be interpreted because of the absence of distinct signals (figures 99 and 100).

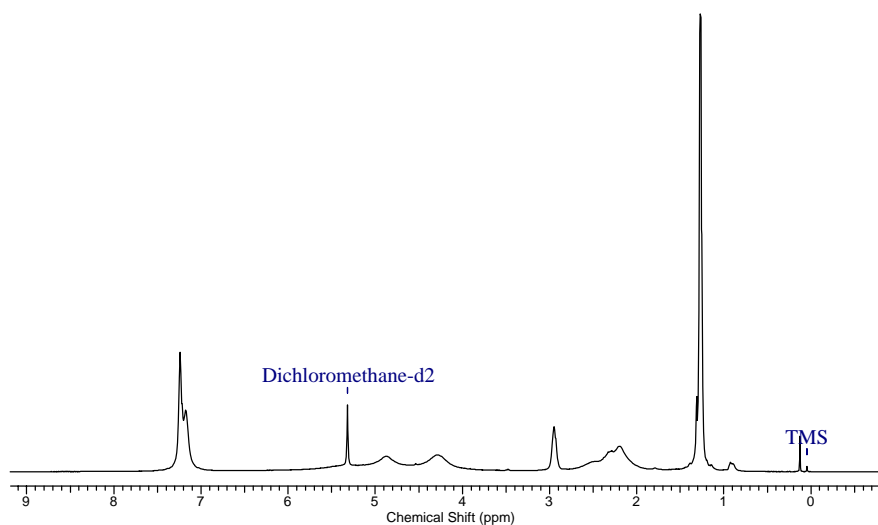


Figure 99. The ^1H -NMR (500 MHz) spectrum of complex **50**.

However, the signals corresponding to the alkyl-protons are easily identifiable *via* the integration of the peaks situated at 1.3 and 3.0 ppm respectively giving six and one protons attributed to the isopropyl moiety on the aromatic group (figure 99). The remained peaks, whose integrals do not correspond to the numbers of the protons, could be assigned to the benzyl and furfuryl protons. The same assumption is valid for the ^{13}C -NMR spectrum (figure 100).

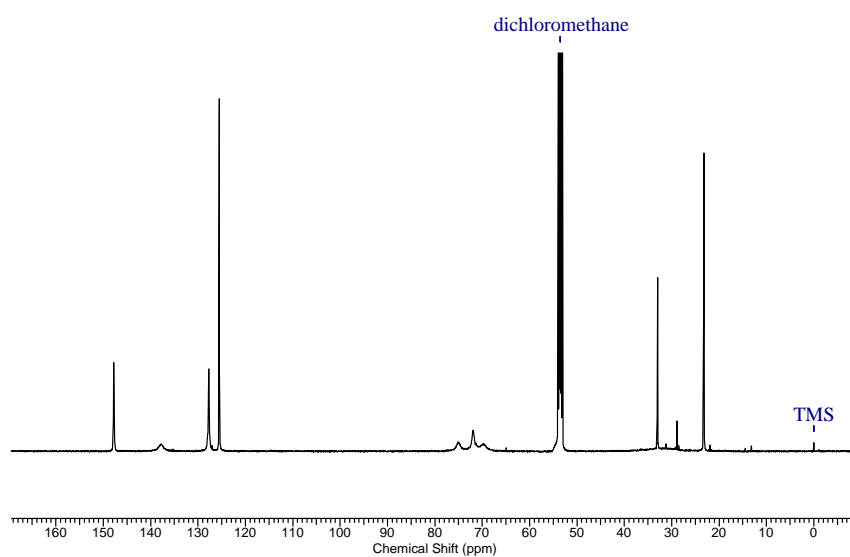
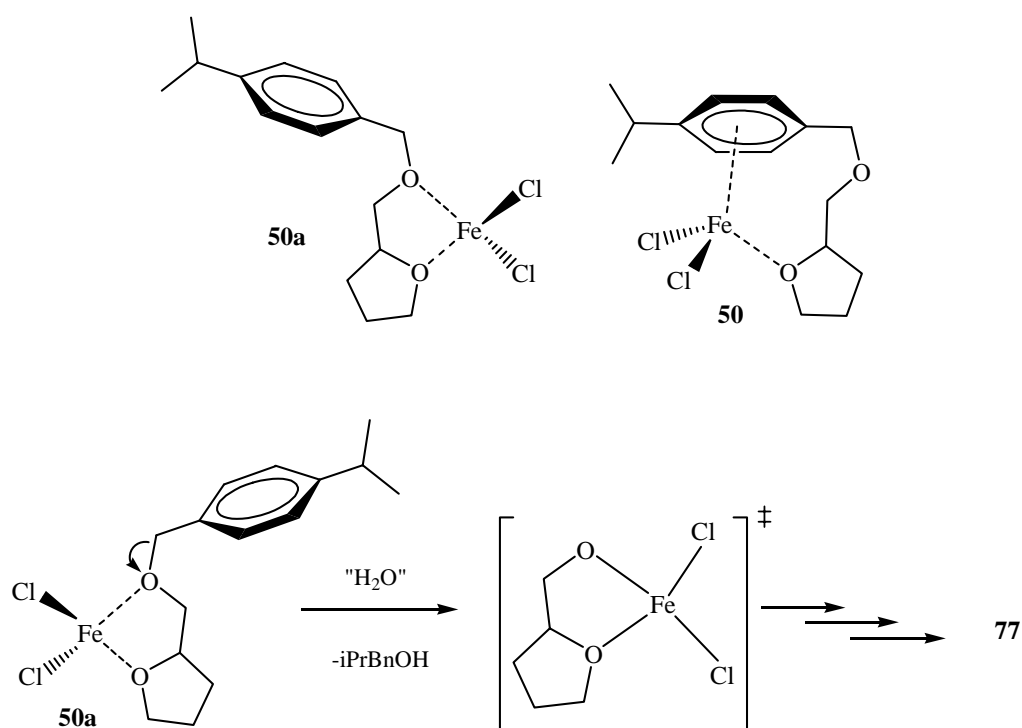


Figure 100. The ^{13}C -NMR (125 MHz) spectrum of **50**.

In the ^{13}C -NMR spectrum of **50** (figure 100), it is interesting to note that, excepted the peak located at 138.2 ppm and attributed to the carbon bearing benzylic linker, all the other aromatic peaks are only less influenced by the paramagnetism of the metal center, that is in contrast to the furfuryle carbon signals located between 64–76 ppm.

The previous observation can lead us to formulate the hypothesis according to which in the complex **50** the aromatic ring is not complexed directly with the metal atom, the connection will be done somewhat *via* the oxygen atoms. Consequently, only the carbon bearing benzyl linker, which is near to the complexed oxygen atom, is influenced by this paramagnetic effect of iron.



Scheme 71. Probably structures of complex **50** and tentative mechanism leading to the multinuclear complex **77**.

Another direct consequence of this formulation is that the oxygen atom connected to the iron becomes very acidic and, could thus be stabilized by losing the aromatic moiety; for example as isopropylphenol compound, if some water traces exist in solution (scheme 71). This mechanism could explain the formation of surprising multinuclear iron complex **77** (figure 21).

16.3. The mass spectrometry (MS)

The ESI and the FAB mass spectra in different solvents of the halide complexes (**48** and **49**) were systematically recorded. We were unfortunately unable to identify any peaks attributable to species in which a biscarbene imidazole-2-ylidene ligand is coordinated to FeX_2 ($\text{X} = \text{Cl}, \text{Br}$).

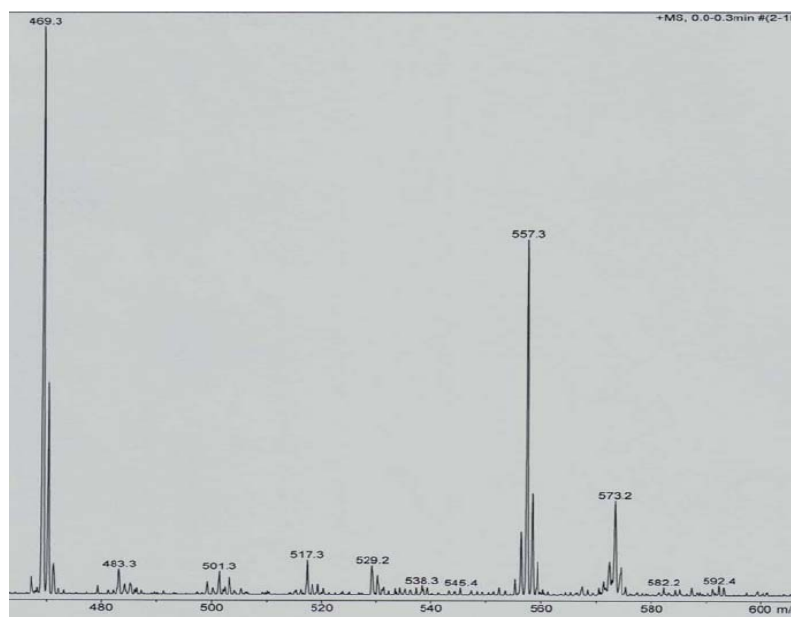


Figure 101. Example of the obtained ESI+ spectrum for complex **48**.

We think that the pronounced sensitivity of these compounds with respect to moisture or solvents employed in the preparation of the samples is at the origin of these failures. Instead, the spectra often indicate the peaks corresponding to the monoprotonated free ligand at $m/z = 469$ (figure 103) or to the ligand in the form of adduct with the counter anions halides or the solvent (figure 102 and 103). These observations could be interpreted either as the signal of the desired complex after losing one FeX_2 entity (in this case that could imply that the formed complex is not stable under the conditions of the mass spectrometry experiment), or quite simply as the result of pre-sampling degradation.

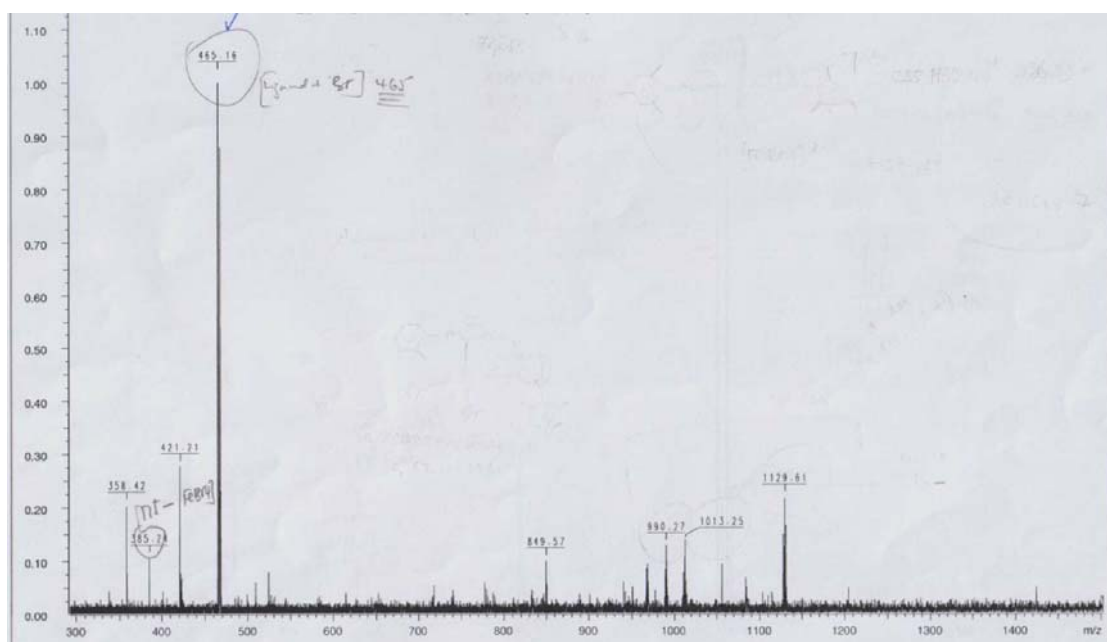


Figure 102. The MS(ESI+) spectrum of complex **49** showing the formation of adduct with the counter anion bromide ($m/z = 465$).

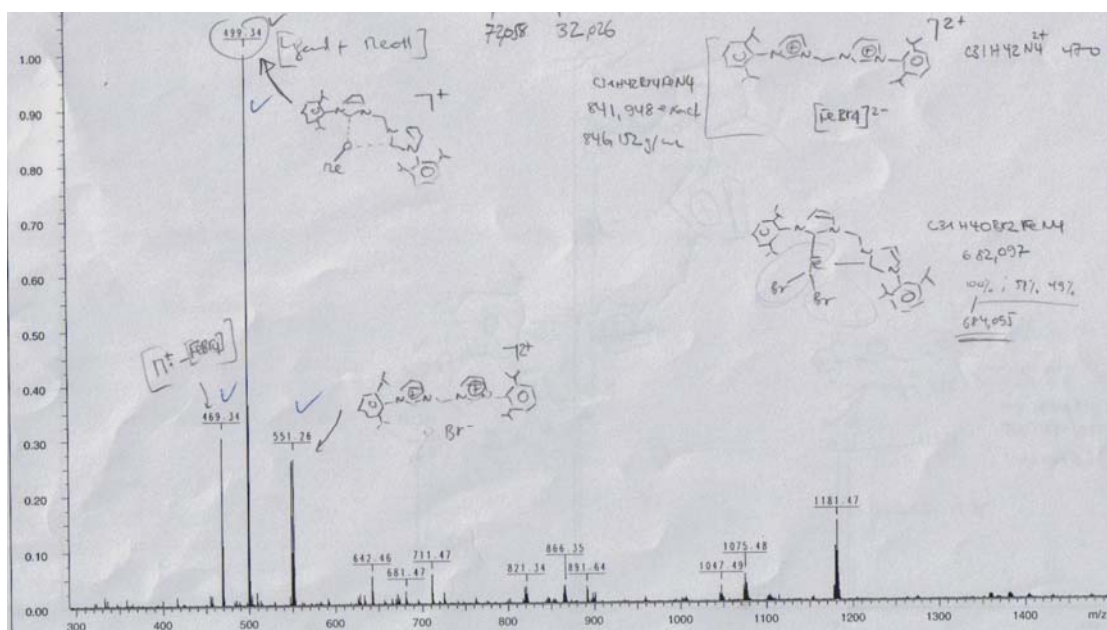


Figure 103. The MS(ESI+) spectrum of complex **48** showing the formation of adduct with MeOH ($m/z = 499$) and with counter anion bromide ($m/z = 551$).

No matter what the explanation is, we checked the reliability of the second assumption by applying the FAB-MS spectrometry. This technique does not require the dilution of the product in a solvent but rather in a matrix. The result seems to be the same one as under ESI-MS, as only the peak of the ligand are present among several others (figure 104).

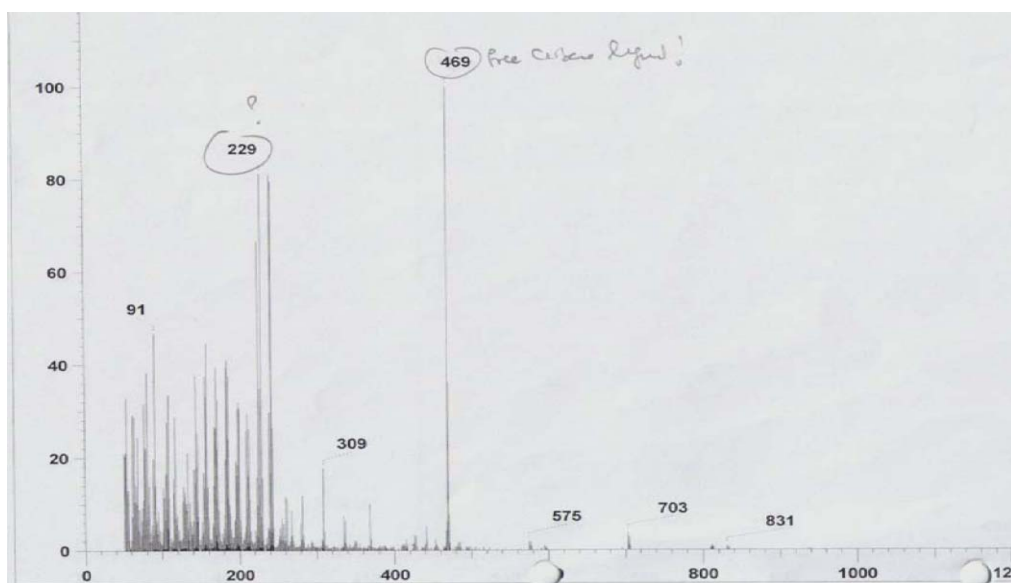


Figure 104. FAB-MS spectrum of complex **48** showing the peaks corresponding to the monoprotonated free ligands.

Finally, we do not dismiss the following assumption: The desired complexes could be a minority in the sample and thus, its signal passes unperceived in the mass spectrum. However, that goes contrary to what we observed in the ^{13}C -NMR spectrum (figure 78 or 80).

The MS(ESI+) spectrum of **50** exhibits four major peaks at $m/z(\%) = 594.2(100)$, $558.4(5)$, $432.1(\sim 5)$, $360(30)$ and $269.99(25)$. These features correspond to the $[\text{FeCl}_2(\text{L})_2]^+$, $[\text{FeCl}(\text{L})_2]^+$, $[\text{FeCl}_2(\text{L})+\text{THF}]^+$ $[\text{FeCl}_2(\text{L})]^+$ and $[\text{FeCl}_2(\text{THF})_2]^+$ ions, respectively. The corresponding isotopic patterns of these ions fully agreed with those calculated for the given formulations (figure 105).

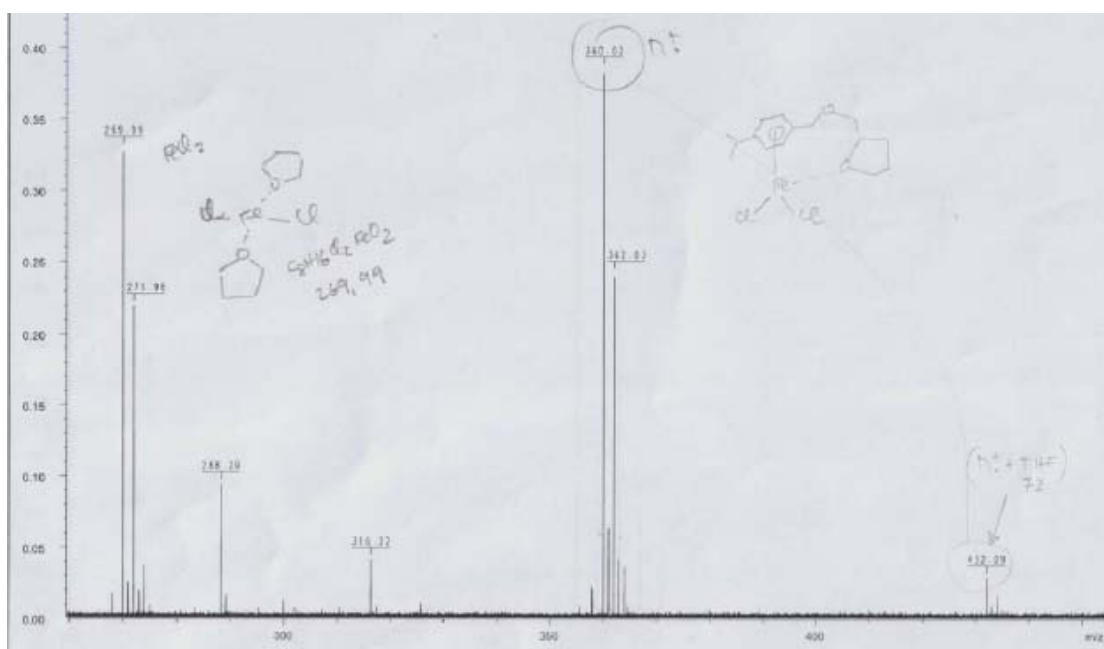


Figure 105. The MS(ESI+) spectrum of complex **50** in THF.

III. Catalytic Reactions

17. Catalytic reactions

Over the last ten years, many transition metal complexes of Pd, Rh, Ir, Ni, Ti, Co ... were introduced for catalytic hydrogenation and polymerization of olefins. In contrast to the great variety of applications for these metals, only few of them treat iron(II). Otherwise, the number of substrates, which could be hydrogenated or polymerized is limited and these reactions require high hydrogen pressure (30-100 bar) and/or elevated temperatures (150-180°C)^{2b,86}.

17.1. Hydrogenation

As previously evoked, our original approach for development of new types of iron catalysts for polymerization involves the screening of iron complexes for homogeneous hydrogenation activity, since both reaction types have similar elementary steps. This reliability between both reactions was observed by Raemy⁸⁶ and Sieber⁸⁷. It is important to note that, in Sieber's approach the catalysts were obtained by addition of the precatalyst solution into an activator suspension, whereas in Raemy's approach the active catalyst was obtained after addition of an activator into the precatalyst suspension, in both cases the nature of the precatalyst has never been elucidated.

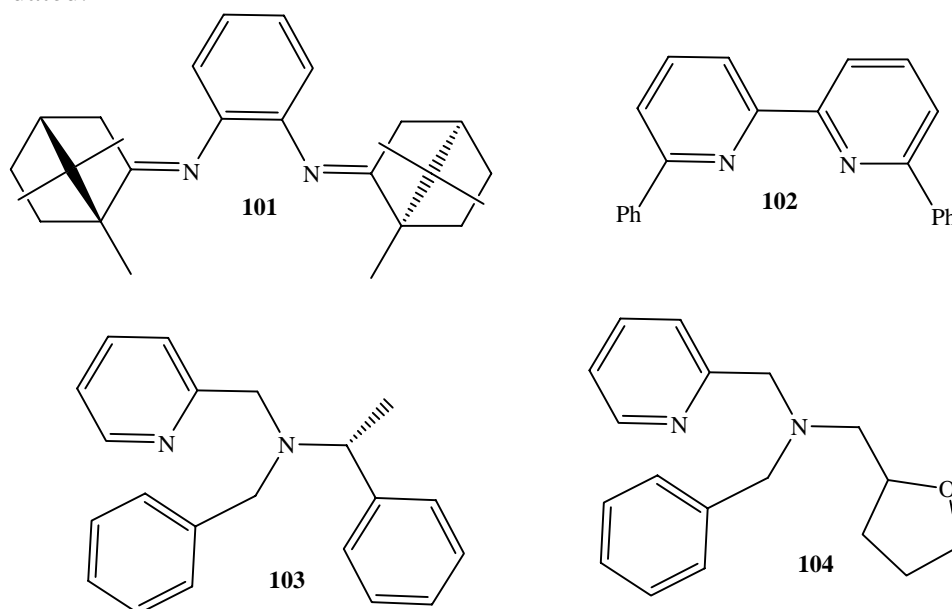
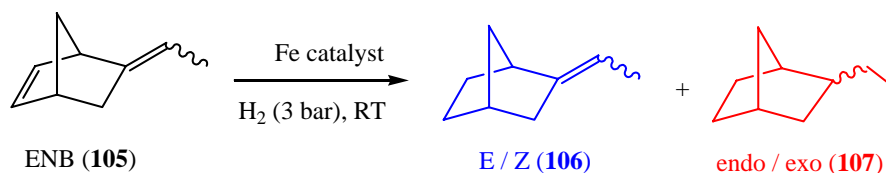


Figure 107. Diimine and pyridyl ligands employed by Sieber and Raemy in the preparation of iron(II) precatalyst solution for hydrogenation of 5-ethylidene-2-norbornene(ENB).

Moreover, the system requires an additional “diene dummy ligand” present in the mixture in order to ensure the catalytic hydrogenation activity. Sieber has suggested that the supplementary diene acts as stabilizing ligand for coordinatively unsaturated catalyst intermediates; thus among many dienes tried, norbornadiene (NBD) shows best suitability for this purpose. Some of Raemy and Sieber’s results are summarize in table 30 and represent a good point for comparison with our experiments.



Scheme 72. Hydrogenation of **ENB**.

Table 31. Summary of the Raemy-Sieber hydrogenation catalysts performance^a.

Entry	Ligand L	Time [h]	Additive	Conversion [%]
1	101	90	NBD	88(107)
2	102	112		92(107)
3	103	24 ^b		100(106)
4	104	16		100(106)
5	FeCl ₂	16	--	100(107)

a) Reaction conditions : ENB 0.5 M in Benzene, NBD 0.5 M, precatalyst 10%, iron / ligand 1:1, iron/LAH 1:4, RT, 3 bar H₂. *b)* The absence of NBD increases the time duration of reaction to about 150 hours.

During their work, they investigate the influence of different parameters such as ligands, additives, activators and iron(II) sources. Interesting is the result of Raemy, who found that the FeCl₂ itself (without any ligand) works faster than all others catalyst prepared under the same activation conditions. The best result was observed with DIBAH in toluene. However, there is no chemo- and stereoselectivity observed when alkenes with different substituted double bond such as ENB, are engaged as substrates (Schema 72). This result is in contrast to that observed when FeCl₂ diimine or pyridyl complexes were used, in which the less

substituted cyclic double bond is always converted fast leading to *E*- and *Z*-5-ethylidene-2-norbornane with almost the same ration *E/Z* (3:1); in fact, ENB is commercially available in racemic form as a 3:1 mixture of *E*- and *Z*-isomers. Calculated turn-over-frequency (TOF) was about 10 h^{-1} when ligands **101** and **102** were used for preparation of catalytic active species.

Raemy has also performed some preliminary hydrogenation experiments of ENB using iron(II) complexes bearing allyl- and allylbenzyl ether ligands **108**, **109** and **110** (figure 108). The precatalyst system consists in a refluxed mixture of the ligand and FeCl_2 in toluene. The best results obtained with these complexes are given in table 32.

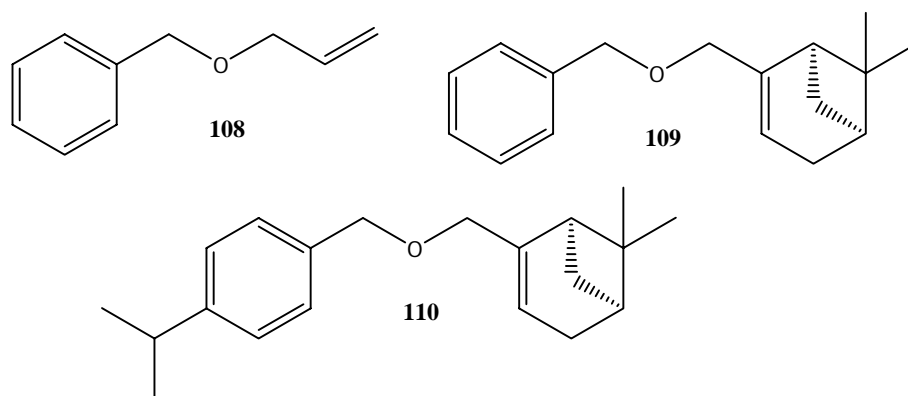


Figure 108. Allyl- and allylaryl ligands employed by Raemy in hydrogenation of **ENB 105**.

Table 32. Hydrogenation of ENB **105** using allyl- and allylbenzyl ether.

Entry	Ligand L	Time [h]	Additive	Activator	Conversion [%]
1	108	40	NBD	$n\text{BuLi}$	92(106)/(107)
2	109				100(106)
3	110				100(106)

Reaction conditions: ligand 0.5 M in cyclohexane, 0.5 mmol FeCl_2 in 2 ml of THF, ENB 0.5 M, NBD 0.5 M, iron/activator 1:4, RT, 3 bar H_2 .

The best result was obtained with the ligand bearing the less substituted allyl group **108**, with small conversion of the exocyclic double bond, whereas with the other ether ligands the hydrogenation stopped when the cyclic double bond had been reduced.

17.1.1 Hydrogenation reactions with iron methylenebisimidazol-2-ylidene complexes

The iron(II) bisimidazol-2-ylidene complexes **48** and **49** were preliminary investigated in the hydrogenation of 5-ethylidene-2-norbornene (ENB) with DIBAH or n-BuLi as activator reagents. For clarity, we assume the structure **48I**, **49I**, resulted from the reaction of respective free biscarbenes species with iron(II) in THF and, the structure **48** and **49** as the product obtained after deprotonation of respective complexes tetrachloro iron bisimidazolium with MeLi (figure 109). It is also important to note that these complexes are less soluble in toluene; yellowish solutions were obtained in both cases.

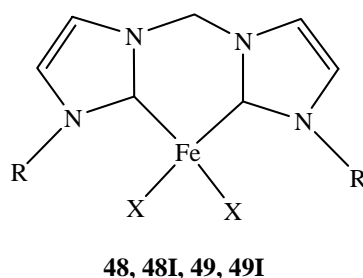
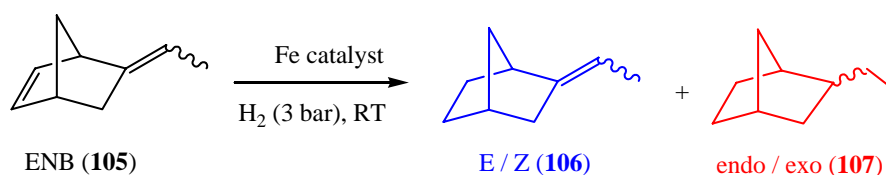


Figure 109. Assumed structures of complex Iron(II) bisimidazol-2-ylidene, used as precatalyst for the hydrogenation of alkenes and alkynes.

Hydrogenation of ENB

At the beginning, the hydrogenation was performed following Raemy's reaction conditions, namely addition of substrate to the yellowish solution of precatalyst in toluene. Then the mixture is set under 3 bar hydrogen pressure prior to the activation step. Table 33 shows that **48**, **48I** and **49**, **49I** are all active catalysts.



Scheme 73. Hydrogenation of **ENB** with iron bisimidazol-2-ylidene complexes.

Table 33. Hydrogenation of cyclic alkene with Iron(II) biscarbenes complexes

Exp	Precat. (0.1 mmol)	Solvent (ml)	Substrate (equiv)	Activator (mmol)	Additive	Time[h]	Conversion (%)
1	--	Toluene (20 ml)	105 (15)	DIBAH	--	24	--
2	--			n-BuLi (0.1)	--		--
3	49, 49I			--	--		--
4	48, 48I			--	--		--
5	49, 49I			--	--		--
6	48, 48I			--	NBD		--
7	49, 49I	Toluene (20 ml)	105 (15)	DIBAH	NBD	4	100(106) + NB-H ₄
8	49, 49I			n-BuLi (0.1)			--
9	48, 48I			DIBAH			100(106) + NB-H ₄
10	48, 48I			n-BuLi (0.1)			--
11	49, 49I	Toluene (20ml)	105 (15)	DIBAH (0.1)	--	4	100(106)
12	49, 49I			n-BuLi (0.1)	--	4	--
13	48, 48I			DIBAH (0.1)	--	4	100(106)
14	48, 48I			n-BuLi (0.1)	--	24	--

The catalytic hydrogenation was performed in a 75 ml Schlenk tube. The complex and the solvent were mixed in the Schlenk tube followed by introduction of the substrate, then the Schlenk was pressurized with 3 bar of H₂. At the end, the activator was added. DIBAH activated precatalyst solutions showed the best catalytically activity.

No hydrogenation activity is observed in blank experiments pointing out the necessity of the precatalyst as well as the activation step (entries 1-6 versus entries 7-14). Very good hydrogenation activity was observed with complex **48**, **48I** and **49**, **49I** in the presence of DIBAH. Furthermore, chemo-selectivity toward the less substituted cyclic double bond was observed. This means that the hydrogenation stopped after the cyclic double bond has been reduced. Additionally, we also observed the reduction of the dummy ligand NBD to the corresponding alkane NB-H₄. Further, we performed some experiments without additive NBD and we found that contrary to Raemy and Sieber, diene additive is not necessary in the reaction mixture for the catalytic hydrogenation activity. The activation with n-BuLi led not to an active catalyst. Increasing the time duration of reaction or addition of large excess of activator does not change the progression of reaction.

During the addition of activator into the precatalyst mixture (**48**, **48I**, **49**, **49I**), the color of solution changes from yellowish to dark brown–black homogeneous solution, but this black color of solution stay only for few minutes, and then the reaction becomes yellowish as before the addition of activator. However, this short time seem to be sufficient to hydrogenate the cyclic double bond. Supplementary addition of substrate **105** and activator affords again **106**. According to Raemy⁸⁶ and Kauffmann¹⁵⁴ who have observed the same phenomena, these black heterogeneous slurry mixtures suggest the formation of colloidal iron clusters that may be the active catalyst. In fact, the activation with ^sBuLi generate super-ate complexes of iron(II) (^sBu₂Fe, ^sBu₃FeLi, ^sBu₄FeLi), which are known to promote cross-coupling reactions, hence they may also be able to catalyze the hydrogenation reaction, although no secured information as to their structure or mode of action could be obtained¹⁵⁵. Fürstner¹⁵⁶ at his turn suggest that the black slurry suspension could be an Fe(-II) species. In order to prove this fact, he prepared a freshly, highly dispersed and nonpassivated metallic Fe(0) powder by reduction of FeCl₃ with potassium, then he used it without any other activation in the cross-coupling reaction of alkyl Grignard with aryl and heteroaryl chlorides, tosylates or triflates without observing any activity. However, he found that the suspension of this finely dispersed iron(0) particles, slowly dissolved on treatment with an excess of Grignard reagent (n-C₁₄H₂₉MgBr) leading to a formally assumed iron(-II) species [(Fe(MgBr)₂]. The resulting black homogeneous solution catalyzes the cross coupling reaction. As consequence, to date are no details about the mechanism or structure information whatsoever.

We also tested the ability of commercial available iron(0) as precatalyst in the hydrogenation of alkenes (ENB) and made comparison with FeCl₂. Results of these experiments are summarized in the table 34.

Table 34. Use of powdered iron(0) as precatalyst in hydrogenation of alkenes (3 bar H₂).

Exp	Precat. (mmol)	Solvent (ml)	Substrate 105 (mmol)	Activator DIBAH (mmol)	Additive	Duration (hrs)	Conversion (%)
1	Fe(0) (0.1)	Toluene (10)	(1.5)	--	--	120	--
2	Fe(0) (0.1)			(0.1)	--	4	--
3	Fe(0) (0.1)			(0.4)	--		100(106)
4	FeCl ₂ (0.1)	Toluene (10)	(1.5)	(0.1)	--	4	100(106)
5	FeCl ₂ (0.1)			(0.4)	--		100(107)
6	FeCl ₂ (THF) ₂ (0.1)	Toluene (10)	(1.5)	(0.1)	--	4	--
7	FeCl ₂ (THF) ₂ (0.1)			(0.4)	--		--

Table 34 shows that, the active catalyst was obtained when fine powder iron(0) was activated with excess DIBAH (entries 2 and 3), however the hydrogenation stopped after the reduction of cyclic double bond and this catalyst mixture can be activated many times with success. However, we never observed the reduction of the exocyclic double bond. The most interesting result here is the dependence of the FeCl₂ catalyst toward the amount of activator (entries 4 and 5), when one molar equivalent of activator was used only the less substituted double bond **106** was hydrogenated, while the use of four equivalents of activator leads to the higher conversion of both double bond (**107**). There is no activity when FeCl₂(THF)₂ was employed as precatalyst (entries 6 and 7).

Hydrogenation of alkenes using “in situ” formation of catalyst from bisimidazolium salts (**55d** and **56c**) and the bisimidazolium tetrahalogenate iron (**106** and **108**)

Since the isolation and characterization of the real catalyst species is difficult, information about the origin of the catalytic activity was studied by systematic modification of the composition of the reaction mixture. In this section, we investigate the ability of “in situ” formed catalyst from reaction of FeCl₂ with imidazolium salt (**55d**, **56c**) and from isolated tetrahalogenate iron imidazolium (**98a**, **99**).

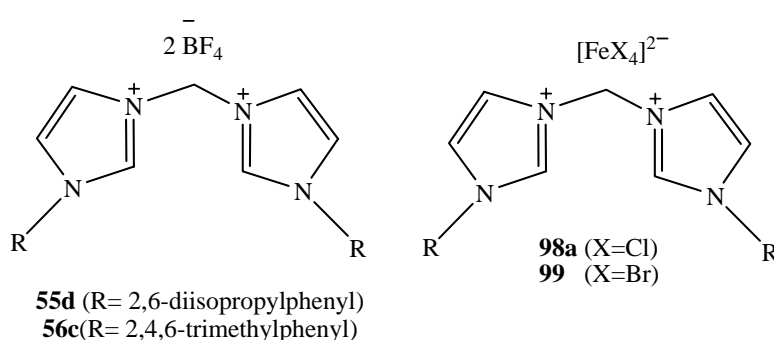


Figure 110. Imidazolium salts employed in the hydrogenation attempt of alkenes.

Procedure I: with imidazolium salts **55d** and **56c**.

The typical procedure is that, a mixture of ligand **56d** or **57c** and FeCl₂ in toluene was placed in a Schlenk tube under 3 bar hydrogen pressure, then the activator was added.

Procedure II: with tetrahalogenate iron imidazolium complexes (**94a**, **95**)

Bisimidazolium tetrahalogenate iron **98a** or **99** and the substrate were dissolved in toluene and placed in a Schlenk tube under 3 bar hydrogen pressure, and then the activator was added at RT. The obtained results are summarized in the table 35.

Table 35. The '*in situ*' activation from imidazolium salts and FeCl₂.

Exp	Precat. (mmol)	Solvent (ml)	Substrate 105 (mmol)	Activator DIBAH (mmol)	Additive	Duration	Conversion (%)
1	55d (0.1)	Toluene (10)	(1.5)	(0.3)	--	8	--
2	55d (0.1) + FeCl ₂ (0.1)				--	12	--
3	56c (0.1)	Toluene (10)	(1.5)	(0.3)	--	2	--
4	56c (0.1) + FeCl ₂ (0.1)				--	12	--
5	98a (0.1)	Toluene (10)	(1.5)	(0.3)	--	8	--
6	98a (0.1) + FeCl ₂ (0.1)				--	12	--
7	99 (0.1)	Toluene (10)	(1.5)	(0.3)	--	2	--
8	99 (0.1) + FeCl ₂ (0.1)				--	12	--

Here the activator plays a double role: the deprotonating agent for the formation of free carbene and activator for the formation of catalyst. In all of these experiments, we never observed the formation of black slurry material in solution. We conclude that, the presence of bisimidazolium ligand inhibited the activity of FeCl₂, even when a large excess of activator was added, that means previous formation of a precatalyst is needed for the success of the reaction.

Hydrogenation of alkenes, study of solvent effect

We have analyzed the role of solvent in our catalytic reaction. Three solvents namely THF, toluene and pentane were compared in the iron catalytically hydrogenations of ENB. These solvents are considered as coordinative, less coordinative and non coordinative, respectively. Among of them only THF solubilizes our precatalysts complexes. The evolution of the reaction was followed by GC – MS and obtained results are summarized in the table 36.

Table 36. The solvent effect (1-3 bar H₂).

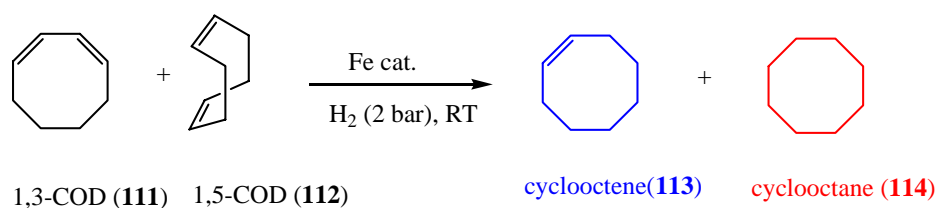
Exp	Precat. (mmol)	Solvent (ml)	Substrate 105 (mmol)	Activator DIBAH (mmol)	Additive	Duration	Conversion (%)
1	FeCl ₂ (0.1)	Toluene (10)	(1.5)	(0.1)	--	4	100(106)
2	49I (0.1)				--		100(106)
3	48I (0.1)				--		100(106)
4	FeCl ₂ (0.1)	pentane (10)	(1.5)	(0.1)	--	4	30(106)
5	49I (0.1)				--		--
6	48I (0.1)				--		--
7	FeCl ₂ (0.1)	THF (10)	(5)	(0.4)	--	8	--
15	49I (0.1)			(0.1)	--	8	--
16	48I (0.1)			(0.1)	--	8	--

According to this table, toluene seems to be a better solvent for these experiments (entries 1-3). The use of pentane as solvent works only in the case of FeCl₂ as precatalyst but, the conversion is very low (entry 4). In THF where our precatalysts species are soluble, no

hydrogenation takes place, even in the presence of a large excess of activator. The results of table 36 confirm also those previously obtained for FeCl₂ when the activator is used in stoichiometric amount, namely the hydrogenation stopped after the reduction of the cyclic double bond, no trace of **107** was observed in the GC-MS.

Hydrogenation of alkynes and others alkenes

To generalize the utility of these compounds as catalysts in hydrogenation, a selected range of alkenes and alkynes with different substitution patterns were investigated. The typical hydrogenation experiments were carried out with 1.5 mmol of substrate in toluene solutions and others solvent such as THF, fewer than 3 bar hydrogen pressure, varying the time duration. Only 1-2 % of precatalyst were used in the presence of n-BuLi or DIBAH as activators.



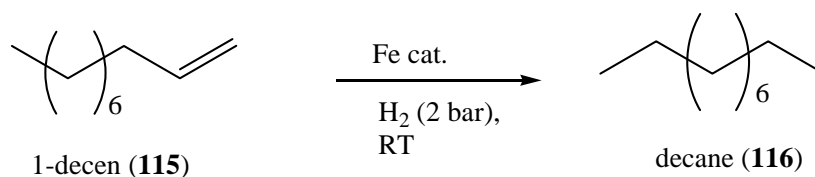
Scheme 74. Hydrogenation of 1,3- and 1,5-cyclooctadiene.

The iron(II) bisimidazol-2-ylidene complexes **48I** and **49I** were successfully tested in the hydrogenation of mixture of 1,3-cyclooctadiene (1,3-cod, **111**) and 1,5-cyclooctadiene (1,5-cod, **112**) using DIBAH as activator. The total reduction of double bonds occurred after 24 hours of reaction without supplementary addition of activator. The use of ⁿBuLi as activator reagents failed.

Table 37. Iron(II) complexes **48I** and **49I** catalyzed hydrogenation of cyclic alkenes.

Exp	Precat. (mmol)	Solvent (ml)	Substrate (equiv)	Activator (mmol)	Time [h]	Conversion (%)
1	49I (0.01)	Toluene (20)	111 + 112 (20)	n-BuLi (0.2)	24	--
2	49I (0.02)			DIBAH (0.2)	4	72(113) 28(114)
3	48I (0.02)			DIBAH (0.1)	4	61(113) 39(114)

Use of 1-decen as substrate in the hydrogenation reaction



Scheme 75. Hydrogenation of 1-decene.

To understand the role of steric effects on substrates in our hydrogenation experiment, a terminal and long chain alkene (1-decen) was used as substrate and the catalytic hydrogenation in the presence of **48I** and **49I** and FeCl₂ was analyzed. As depicted in table 37, the reaction take place, only when FeCl₂ was used, otherwise **48I** and **49I** are inactive. Our conclusion is that less reactive terminal olefins seem to be insensible to hydrogenation in our conditions.

Table 38. Iron(II) complexes catalyze hydrogenation of 1-decene (3 bar H₂).

Exp	Precat. (mmol)	Solvent (ml)	Substrate 115 (mmol)	Activator (mmol)	Time [h]	Conversion (%)
1	FeCl ₂ (0.1)	Toluene (10)	(1.5)	--	24	--
2	FeCl ₂ (0.1)			(0.1)	4	100(116)
3	48I (0.1)			(0.1)	10	--
4	48I (0.1)			(0.4)		--
5	49I (0.1)			(0.1)		--
6	49I (0.1)			(0.4)		--

Hydrogenation of functionalized alkenes

Iron(II) complexes **48**, **48I** and **49**, **49I** were also investigated in the hydrogenation of functionalized alkenes using DIBAH as activator reagents, under 2 bar hydrogen pressure and at RT.

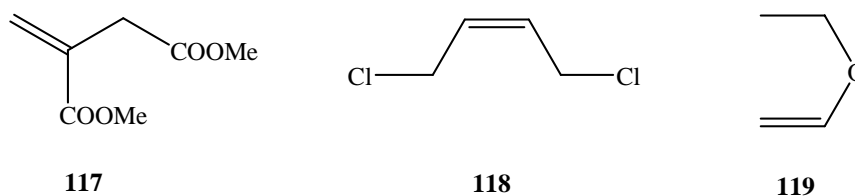
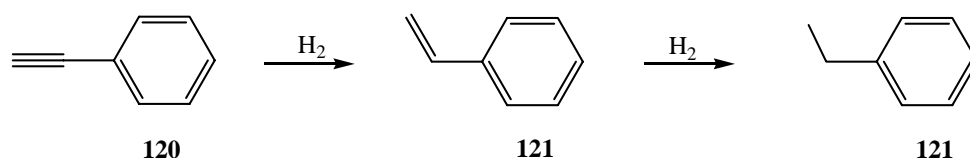


Figure 111. Functionalized alkenes.

The reduction of olefins containing carbonyl (**117**) and chlorides (**118**) groups failed, because in these cases the activation reagent reacts with the substrate instead of precatalyst to form the catalytic species. Particularly, in the case of **118**, neither the starting material nor the expected hydrogenated products were detected in GC-MS spectra.

Vinyl ether **119** was not hydrogenated; this result is according to that observed by Sieber, however it is contrary to Raemy's work in which he observed the occurrence of hydrogenation when the amount of DIBAH is raised to an eight fold excess with respect to iron.

Precatalysts **48I** and **49I** also show ability to reduce aromatic alkynes when activated with default amount of DIBAH. Phenylacetylene **120** was quickly reduced (10 minutes) to its corresponding alkane. The finding about the amount of activator used contrast Raemy work where the reduction occurs only when the ratio Fe/DIBAH is at least (1:4). Furthermore, we did not observe the formation of oligo- or polymerization side product during our experiment.



Scheme 76. Hydrogenation of phenylacetylene.

17.1.2. Catalytic hydrogenation of alkenes with iron(II) benzyletherfuran complex **50**

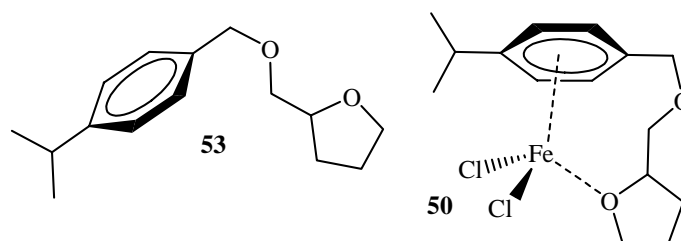
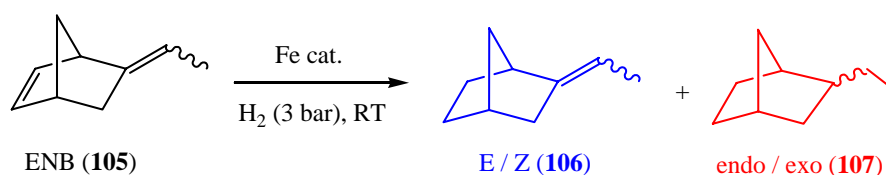


Figure 112. Ligand and complex iron(II) benzyletherfuran.

Preliminary experiments were performed with the isolated complex benzyletherfuran iron(II) **50** as precatalyst for hydrogenation of ENB. As previously with imidazol-2-ylidene iron(II) precatalyst, we were also interested by the influence solvent and the *in situ* generation of catalytic species.



Scheme 77. Hydrogenation of ENB with complex **50**.

The role of solvent

The activation of the precatalyst **50** with one equivalent of activator in toluene generates an active catalyst and the reduction of double bonds occurs in short time, but the exocyclic double bond remained untouched (table 39). This result is comparable to that observed with FeCl₂ (entries 1 and 2).

When the catalytic reaction was done in pentane (entries 3 and 4), precatalyst **50** gave better result (70% of conversion), than FeCl₂ (30% of conversion) and imidazol-2-ylidene complexes **48I** and **49I**. Solubility effect could be responsibly for this result; indeed, precatalyst **50** is much more soluble in pentane than FeCl₂, **48I** and **49I**. No activity was observed in THF, but this finding fits the observation with all others experiments in the same solvent (entries 5 and 6).

Table 39. The solvent effect (3 bar H₂).

Exp	Precat. (mmol)	Solvent (ml)	Substrate 105 (mmol)	Activator DIBAH (mmol)	Duration	Conversion (%)
1	FeCl ₂ (0.1)	Toluene (10)	(1.5)	(0.1)	4	100(106)
2	50 (0.1)					100(106)
3	FeCl ₂ (0.1)	pentane (10)	(1.5)	(0.1)	4	30(106)
4	50 (0.1)					70(106)
5	FeCl ₂ (0.1)	THF (10)	(1.5)	(0.4)	8	--
6	50 (0.1)					--

The *in situ* preparation of a precatalyst-catalyst by mixing the ligand **53** and FeCl₂ in toluene under hydrogen pressure, followed by addition of activator was done (table 40). Only 10% conversion of the cyclic double bond was observed, however this constitutes the best result if compared with FeCl₂ and bisimidazolium salts where no reaction took place. Increasing the

amount of activator does not change dramatically the yield of conversion (entry 3). Results are summarized in table 40.

Table 40. The “*in situ*” activation from ligand **53** and FeCl₂ (3 bar H₂).

Exp	Precat. (mmol)	Solvent (ml)	Substrate 105 (mmol)	Activator DIBAH (mmol)	Additive	Duration	Conversion (%)
1	53 (0.1)	Toluene (10)	(1.5)	(0.3)	--	2	--
2	53 (0.1) + FeCl ₂ (0.1)			(0.1)	--	12	10(106)
3	53 (0.1) + FeCl ₂ (0.1)			(0.5)	--	12	23(106)

According to the results obtained in this section, we conclude that toluene seems to be a better solvent for these reactions. The use of pentane as solvent works only in the case of aryl ether precatalyst **50** and FeCl₂. The use of THF does not work, even in the presence of a large excess of activator. As before, the previous formation of precatalyst is necessary to ensure the catalytic activity.

17.2. Polymerization

During the development of the precatalysts it was always question to apply it in the polymerization of alkenes, among them olefins such as ethylene, 1,3-butadiene and isoprene were tried as substrate. Our original approach, compared to many reported polymerization reaction is based on the use of very mild conditions, namely ambient temperature, low pressure (1-1.5 bar for ethylene), reduced amount of catalyst in mixture and if necessary the activator is different to the commonly used MAO or MMAO.

Since our starting work hypothesis was the reliability between hydrogenation and polymerization; indeed, very similar mechanisms were assumed for hydrogenation and polymerization respectively, a catalyst displaying hydrogenation activity can be imagined as potentially polymerization catalyst too⁸⁶. Since it was found that complexes of iron

bisimidazol-2-ylidene (**48**, **48I**, **49**, **49I**) and benzyetherfuran (**50**) are active in hydrogenation screening reaction under strong base activation; these results prompted us to investigate their capability as catalysts precursors for alkenes and alkynes polymerization. It has to be noted that our lacking of appropriate equipment and experience for this kind of reactions prevented the synthesis of freestanding polymers films, and only simple qualitative experiments were performed. Nevertheless, interesting results were obtained in these attempts.

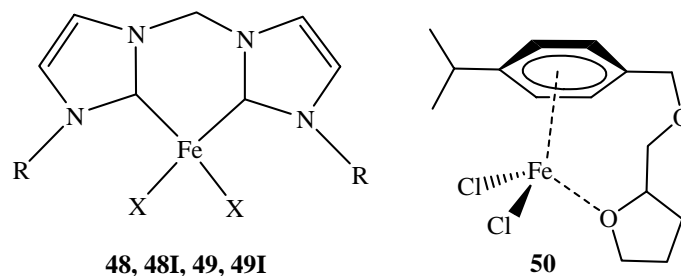


Figure 113. Assumed structure of precatalyst used in polymerization reaction.

17.2.1. The ethylene polymerization reaction

We used two strategies for the preparation of a catalyst mixture. In the first approach, the activator was added in large excess (1-100 equivalents) into a solution of precatalyst, and then ethylene was introduced at 0.5-1.5 bar pressure. The resulting solution was stirred at ambient temperature for a fixed reaction time, after that MeOH/HCl was added to terminate the polymerization. As for hydrogenation activation, in the case of precatalysts **48**, **48I** and **49**, **49I**, we observe the formation of black-brown solution during the addition of DIBAH (activator), but the color change rapidly to orange.

The second approach consists in addition of an activator to a mixture of precatalyst and substrate under ethylene pressure. Here again, we observe the formation of black-brown material in a catalytic mixture for complexes **48**, **48I** and **49**, **49I**, with DIBAH.

Using reaction conditions on the table 41 no polymerization took place for all activator used; even MAO, the best know activator for polymerization failed. The use of iron(II) benzyetherfuran complex **50** in the same conditions reactions as for **48** and **49** does not lead to any polymer.

Tableau 41. Ethylene polymerization with iron complexes

Exp	Precat. (mmol)	Solvent (ml)	Ethylene (pressure, bar)	Activator (equiv.)	Additive	Time[h]	Conversion Y/N		
1	--	Toluene (10 ml)	(1.5)	n-BuLi (10)		24	--		
2	--			DIBAH (10)	--		--		
3	--			MAO(10)	--		--		
4	48, 48I (0.05)			n-BuLi (10)	--		--		
5	48, 48I (0.07)			DIBAH (10)	--		--		
6	48, 48I (0.1)			MAO (10)			--		
8	49, 49I (0.05)	Toluene (10 ml)	(1.5)	n-BuLi (10)		4	--		
9	49, 49I (0.1)			DIBAH (10)			--		
10	49, 49I (0.05)			MAO (10)			--		
11	50 (0.1)	Toluene (10ml)	(1.5)	n-BuLi (10)	--	24	--		
12	50 (0.05)			DIBAH (10)	--	24	--		
13	50 (0.1)			MAO(500)	--	48	--		
11	FeCl₂ (0.1)	Toluene (10ml)	(1.5)	n-BuLi (10)	--	24	--		
12	FeCl₂ (0.1)			DIBAH (10)	--	24	--		
13	FeCl₂ (0.08)			MAO(300)	--	48	--		

Preliminary polymerization tests of ethylene were also carried out with nickel complex **123** in toluene using DIBAH as activator at mild conditions (1.5 bar ethylene pressure, RT). Polyethylene was obtained after 2 days reaction and quenching the mixture with ethanol/HCl (figure 114). Under the same conditions, the complex alone did not produce any polymer. Moreover, the use of MAO as activator failed to perform this reaction.



Figure 114. Picture of polyethylene in a yellow solution of Ni(II) catalyst.

We also tested the polymerization of ethylene still with the complex **123**, but this times the activation was done with a silver salt AgBF_4 (1 eq.). After treatment of the reaction mixture with ethanol/HCl, we successfully isolate another polymer, whose texture differs from the precedent (figure 115).



Figure 115. Picture of obtained polymer under AgBF_4 activation.

To date, no characterization was carried out with these two isolated polymers and we think that much remains to be exploited in this new open field. However, to our knowledge, this is the first time where this kind of bisimidazol-2-ylidene nickel (II) complexes were reported and exhibit activity toward polymerization of ethylene.

17.2.2. Polymerization of 1,3-Butadiene and isoprene with iron complexes

The ability of our complexes to polymerize butadiene and isoprene was checked in a few experiments. Contrary to previous reactions with ethylene, we have adopted only the second approach for the preparation of catalyst, which consist to add the activator into a mixture of precatalyst and substrate.

When the mixture of complex **48**(2%) and butadiene was reacted with 300 equivalents of *n*-BuLi in toluene, the color of the solution turned to yellow–brownish. Then the resulting solution was stirred at ambient temperature for over night, to terminate the polymerization a mixture of MeOH/HCl was added. The precipitated material was dried under vacuum affording insoluble pale yellow elastic material (**P0**, in the figure 116). The coloration is probably due to the some contamination with iron.

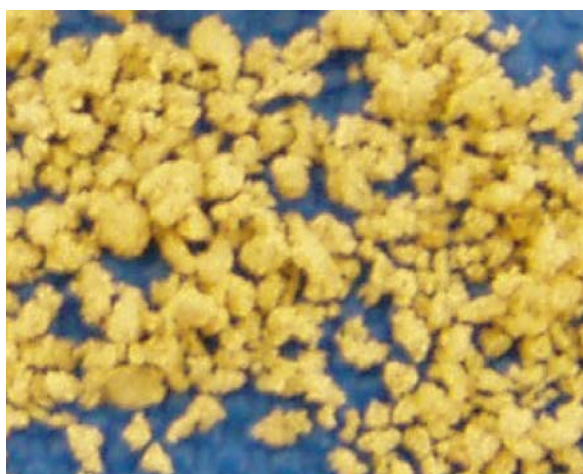


Figure 116. Photography of obtained polybutadiene **P0**.

The solid-state NMR (^{13}C -CP-MAS) spectrum was measured and shows four signal groups (figure 117). The two large signals between 24-30 ppm could indicate terminal and non-terminal alkyl carbons, whereas the three signals group between 120-130 ppm could represent different sp^2 carbons. There is probably a mixture of terminal and non-terminal double bonds in the secondary growth chain or in the linear chain.

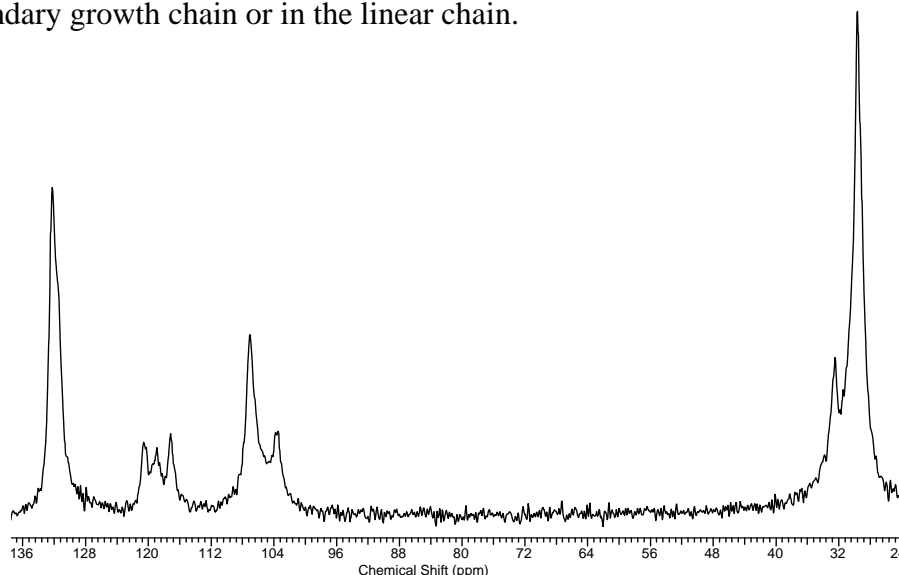


Figure 117. Solid-state ^{13}C -CP-MAS-NMR spectra of isolated polybutadiene polymer **P0**.

Supplementary data about this polymer was obtained with resonance Raman spectroscopy (figure 118), where different absorptions are visible on the region of 1060 cm^{-1} and 1500 cm^{-1} which are assigned to the double bond stretching mode (ν_1) and to the single bond stretching mode (ν_3)¹⁵⁷.

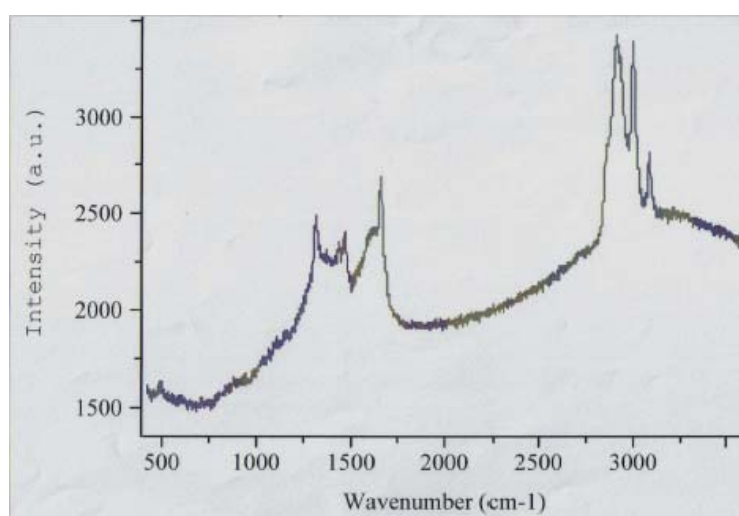


Figure 118. Raman spectra of isolated polybutadiene polymer **P0**.

In our case, the Raman spectrum of the obtained material exhibited three interesting bands at 1280 cm^{-1} , 1400 cm^{-1} and 1650 cm^{-1} respectively. Particularly, the band at 1650 cm^{-1} can be assigned to the C=C stretching vibration of cis-1,4-polybutadiene and the formation of a shoulder at 1607 cm^{-1} can be explained in terms of cross linking, which reduces the population of the C=C bonds and concomitant formation of molecular species having vibrations at slightly different frequencies¹⁵⁷. The low frequency signal at 1280 cm^{-1} is most likely due to polybutadiene segments coupled to modified hydrocarbon chains¹⁵⁸. The fact that we have several bands in this region implies probably the presence of different types of double bonds, which come to reinforce the idea about the branched nature of this polymer.

We also did the mass spectrum analysis (MALDI) using different matrices without success. That implies we are in presence of an amorphous polymer, in which the present double bounds are inside and that the exterior is consisted of the saturated chains; This argument corroborates with the morphology of the polymer, as is showed in the picture on the figure 116, the product have the form of slightly round granules.

The test of polymerization of butadiene in presence of catalyst **49** was carried out using the same reaction conditions described previously. After 48 hours of reaction, the solution is neutralized with a mixture MEOH-HCl and the phases are separate. The organic phase is dried with MgSO_4 then the solvent is evaporated furnishing brownish oil. This color is probably due to the presence of impurities coming from the catalyst. Redissolution in toluene then filtration trough Celite, allowed us to recover a yellowish oily solid (**P1**, in the figure 119).

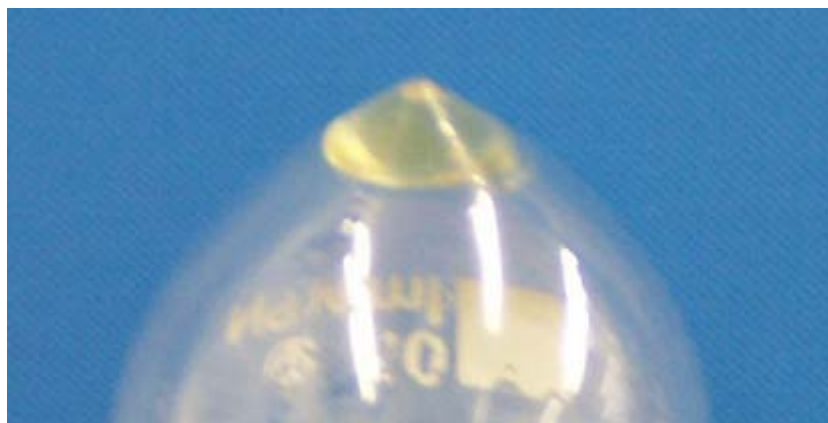


Figure 119. Picture of obtained polybutadiene **P1**.

The isolated oily solid was analyzed by ^{13}C -NMR and Raman spectroscopy. In the spectrum ^{13}C -NMR of the product carried out in toluene and in comparison with that of butadiene, one sees many new resonances towards 30 ppm, which can be attributed to the resonance of alkyl carbons. Then the resonances located between 110 ppm and 130 ppm can be assigned to the resonances of sp^2 carbons (figure 120).

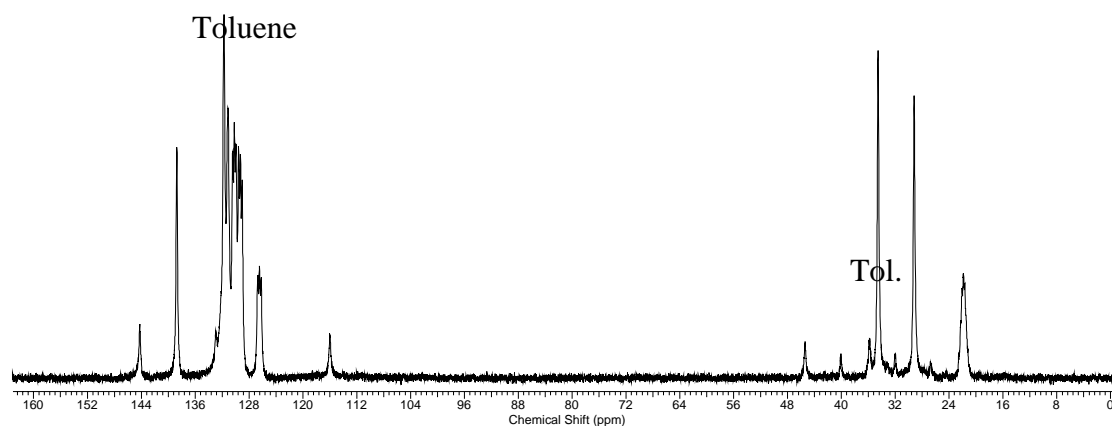


Figure 120. The ^{13}C spectrum of polybutadiene **P1**.

Analysis of the Raman spectrum shows mainly absorption bands between 1500 cm^{-1} and 1700 cm^{-1} , such absorptions were published in the literature for polybutadiene polymers with very low molecular weight¹⁵⁹ (figure 121).

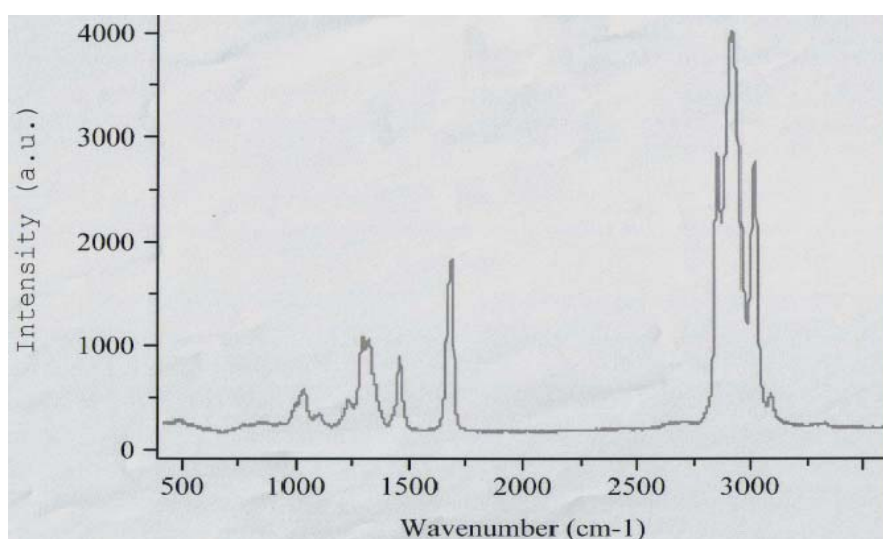


Figure 121. Raman spectra of linear polymer **P1**.

Polymerization attempts using styrene as substrate did not afford any polymer material; The complexes benzyletherfuran **50** was inactive toward the polymerization of 1,4- butadiene and isoprene.

17.2.3. Catalytic hydrogenation of isolated polymers **P0**

We wanted to analyze the reactivity of the double bound in this polymer. For that, the obtained branched polybutadiene **Po** was subjected to the catalytic hydrogenation in toluene with a modified Wilkinson catalyst $(PPh_3)_3(CO)RhH$ in toluene under 3 bar pressure hydrogen. However, due to the insolubility of the polymer we did not observed any reaction after 6 days reaction. The obtained solid spectra ^{13}C -CP-MS NMR corresponds exactly to that of the starting product.

IV. Conclusions

18. Conclusions

We have successfully synthesized several new complexes of iron(II) and iron (III) following three synthetic pathways: the first by direct reaction between an adequate iron (II) source with free biscarbene ligands obtained by reaction of the corresponding imidazolium salt with a strong base such as sodium hydride and potassium *tert*-butoxide.

Further, we prepared a series of new dimeric complexes of silver bisimidazol-2-ylidene, which were useful agents for the transfer of bisimidazol-2-ylidene ligand to iron. This reaction enabled us to isolate an intermediate complex, the tetrahalogenate ferrate bisimidazolium, which at its turn was deprotonated with methyl lithium to give the expected complex.

In order to prepare stable iron complexes, we tried to replace halides ligands on the metal center by much more coordinating ligands such as the formiate, the carboxylate and the triflate. For this, we employed two strategies; one of them is the ligand exchange, which involves the halogens iron bisimidazol-2-ylidene and formiate or acetate salts. Another is the “*in situ*” reaction of bisimidazolium salts with iron(II) sources which already carries ligand coordinators in the presence of a strong base such as sodium hydride or potassium *tert*-butoxide.

This works was slightly handicapped by the available analytical tools, as we could only draw very little information from the routine techniques such as the ^1H -, ^{13}C -NMR, MS, UV-Vis, IR and elemental analysis. On one side, this is due to the paramagnetism of the isolated compounds or because the sample contained traces of FeCl_2 . On the other side, the sensitivity with respect to minor traces of moisture and the degradation observed in many organic solvents, did not allow us to achieve a good purification of our complexes. That explains the absence of the results in MS spectrometry and in elements analysis.

The exploitation of the UV-Vis spectra remains very marginal, indeed several other complexes of Fe(II) or Fe(0) gave similar spectra compared to that we observed with our complexes. However, there is no sufficient data at hand to specify how ligands such as benzyletherfuran and bisimidazol-2-ylidene carbenes affect the environment of a metal center. Although the assignments of these absorption bands remain largely equivocal, we thus suggest that they originate from ligand-centered as well as ligand-to-metal and metal-to-ligand charge transfer transitions.

The only thing which is certain, is that the UV-Vis spectra of the isolated complexes are different as compared to the iron(II) sources employed as starting material.

Assuming the structures **48** and **49** are as the one of the obtained product, we showed that these complexes are very active in hydrogenation of olefinic hydrocarbons and alkynes compounds under very soft conditions (1-3 bars hydrogen pressure, RT). In contrast to FeCl₂, the complexes obtained show a chemio-selectivity during the reduction of ENB, in the sense that they react only with the cyclic double bond. Several other parameters of this reaction were studied, thus we have concluded that the best solvent is toluene; attempts to hydrogenate ENB by in situ preparation of catalyst starting from imidazolium salt, FeCl₂ and the activator didn't lead to the awaited reduction. That means the active precatalyst complex must be prepared previously.

Applications of these complexes in polymerization were tested in a preliminary way. Thus, in the presence of n-BuLi as activator, the complexes iron(II) bisimidazol-2-ylidene **48** and **49** perform the polymerization of butadiene to a branched polybutadiene material. We think that optimization of the reaction conditions could lead to very effective catalysts for the polymerization of olefins.

With the aim of taking on Raemy's assumption about the ability of iron(II) allyletheraryle bidentate complexes to carry out the catalytic hydrogenation and polymerization of olefins, we have successfully prepared and tested the activity of a iron benzyletherfuran complex **50** in hydrogenation of ENB when activated with an alkylaluminium reagent in different solvents. Furthermore, complex **50** is showing a greater activity than FeCl₂ in pentane; in toluene, we find the same chemio-selectivity as that of the imidazole-2-ylidene precatalysts with respect to the ENB endo- and exocyclic double bonds. Unfortunately, no polymerization took place neither with butadiene nor with ethylene under our mild reaction conditions. Moreover, we were able to isolate a new hepta-core iron complex coming probably from the degradation of **50**.

In one period where one speaks more about "Green Chemistry", we are convinced that the synthesis and applications of biscarbenes imidazolylidene Fe(II) complexes is a new challenge in organometallic chemistry and homogeneous catalysis. Indeed, it is a question to combine a not poisoning, physiologically and environmentally friendly metal (Fe) with the ability and the potential of the imidazole ligand in the catalysis, which was already shown several times with other metals.

Taken in this direction the work carried out here is pioneering in this field. Thus, the optimization of these syntheses, especially concerning the purification of the products obtained, remains an interesting task to achieve and will make it possible to correctly determine the structure. Once the structure is determined, it will be much easier to rationalize in term not only of catalytic performances in hydrogenation and polymerization reactions, but also on the possible modifications to be made on the ligand. Indeed, the selected ligands offer a multitude of choices to be tuned, as we announced at the beginning of this work; and for the moment, we were satisfied only to look at the effect of the substituted groups on the nitrogen located in N-1 position.

In order to compare the reactivity of silver complexes with others metals, we prepared and characterized two new complexes of Ni(II) (**123** and **124**). In contrast to its $\text{FeCl}_2(\text{PPh}_3)_2$ homologous, the transmetallation reaction of silver complexes with $\text{NiCl}_2(\text{PPh}_3)_2$ was carried out successfully. Preliminary polymerization tests of ethylene were successfully carried out with complex **123** in toluene using DIBAH or AgBF_4 as activator at mild conditions. On the other side, complex **124** seems act like a sensor of oxygen or moisture. We are convicted that, the results obtained with this thesis constitute the basis of several other future projects.

V. Experimental part

19. General considerations

Reactions were generally performed under argon or dry nitrogen atmosphere. Most of the chemical reagents were purchased from Fluka, Merck, Acros or Strem, and used without further purification if not stated otherwise. THF, dichloromethane, toluene and ether were dried by passing them, under argon atmosphere, through activated Alox columns, a safe purification system similar to that proposed by Grubbs¹³¹. Ethanol, methanol, were also purged with argon for 15 minutes and kept over molecular sieves.

Ultrasound irradiation reactions were performed on a TPC-40 Telsonic Ultrasonics equipped with a heat controller.

Thin-layer chromatography analysis (TLC) were performed using aluminium sheets coated with silica gel 60 F-254 (0.2 mm) (Merck). Product were revealed with UV-light (254 nm) or by spraying the TLC with either KMNO₄-solution or a HNO₃/KSCN combination. Column chromatographic purifications were performed with Merck 230-400 mesh silica gel or Macherey-Nagel silicagel 60 (0.063-0.2 mm (70-230 mesh ASTM)).

NMR spectra were recorded either on a Bruker Avance DRX-500 (¹H: 500 MHz and ¹³C: 125 MHz), on a Bruker DPX-360 (¹H: 360 MHz and ¹³C: 91 MHz) and on a Varian Gemini 200 (¹H: 200 MHz and ¹³C: 50 MHz). Chemical shifts are given in ppm relative to tetramethylsilane (TMS) or the residual proton signal of the deuterated solvent employed. The NMR signals were assigned using APT, HETCOR and COSY techniques. Solid-state NMR were recorded on a Bruker Avance 400 (¹³C: 100 MHz) equipped with a MAS probe head.

UV-Vis spectra were recorded on a Perkin-Elmer Lambda 40 diode array spectrophotometer. The infrared (IR) was acquired on FTIR Unicam Mattson 5000 spectrometer. Raman spectra were measured on a Dilor Labram1 300 spectrometer with the assistance of Raoul Buffat and Dr. Jean-Nicolas Aebischer (EIF-Fribourg).

Mass spectra were recorded either on a Vacuum Generators Micromass VG 70/70E (FAB ionisation) or on a Bruker 4.7T BioApex II FT/ICR mass spectrometer (EI). Analysis of volatil compounds were carried out on a Thermoquest Finnigan Voyager GC-MS Trace GC 2000 series equipped with a Zebron ZB1 capillary column (30m L x 0.25mm ID x 0.25 μm df, 100% methyl polysiloxane).

.

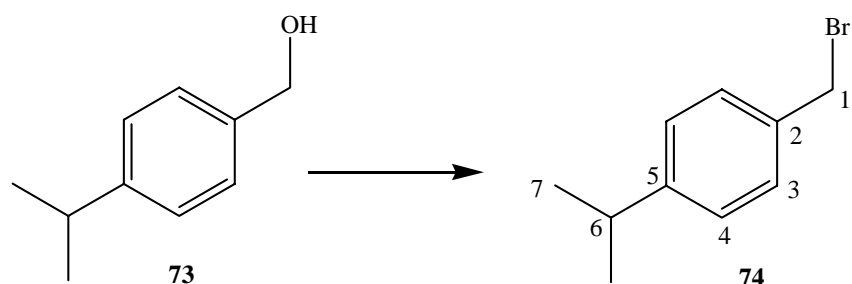
The X-ray analysis was measured at the University of Neuchâtel by Prof Helen Stoeckli-Evans, Dr Antonia Neels and Dr Gael Labat. The structures were solved by direct methods using the program SHELXS-97¹ and refined by full matrix least squares F^2 with SHELXL-97. The figures were drawn with PLATON99 and Mercury 1.4.

Synthesis of organic substrates

20. Synthesis of organic substrates

20.1. 2-(4-isopropyl-benzyloxymethyl)-tetrahydrofuran 53

4-isopropylbenzylbromide 74



To a solution of 4-isopropylbenzylalcohol (3.0 g, 20 mmol) in diethylether at 0°C was added dropwise tribromophosphine (5.4 g, 20 mmol), then the temperature was allowed to RT and the mixture was left to react for 2 hours. After addition of a saturated aqueous solution of NaHCO₃ (50 ml), the mixture was extracted with diethylether (2 x 100 ml). The organic phases was washed with a saturated solution of NaCl (50 ml) and dried over MgSO₄. After evaporation of the solvent under vacuum, a yellowish oily product was obtained. A flash column chromatography (SiO₂, pentane/diethylether (1:1), R_f = 0.92), permitted the isolation of pure product **74** as a slightly yellow oil (2.9 g, 68%).

¹H-NMR (360 MHz, CDCl₃): δ 7.32 (*d*, J = 7.7, 2H, HC(4)), 7.20 (*d*, J = 7.7, 2H, HC(3)), 2.90 (*hept*, J = 7.1, 1H, HC(6)), 4.49 (*s*, 2H, H₂C(1)), 1.24 (*d*, J = 7.1, 6H, H₃C(7)).

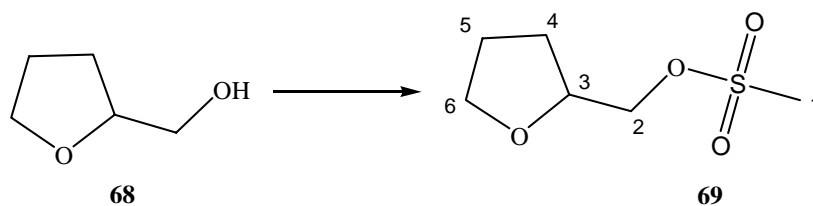
¹³C-NMR (91 MHz, CDCl₃): δ 149.7 C(5), 135.6 C(2), 129.5 C(3), 127.3 C(4); 34.3 C(6), 34.2 C(1), 24.3 C(7).

IR (NaCl film, 4000-400 cm⁻¹): 2960s, 2871w (sh), 1610w, 1514m, 1463m, 1419m, 1226m, 1053m, 837m, 665m.

UV-Vis (THF, 200 nm–800 nm): 235

MS (EI): *m/z* 212 [M]⁺.

(Tetrahydrofuran-2-yl)methyl 4-methanesulfonate **69**

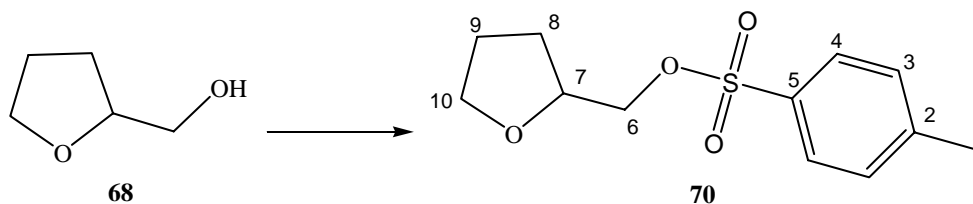


A 500 ml round bottomed flask was charged with furfuryl alcohol (1.0 ml, 10 mmol), triethylamine (2.7 ml, 20 mmol) and 30 ml of dichloromethane at 0 °C. To this solution was added methanesulphonyl chloride (1.1 ml, 15 mmol). Then the mixture was warmed to RT, stirred for 3 hours, diluted with 2 x 20 ml of CH₂Cl₂ and washed sequentially with 10 ml of aqueous HCl 20%, 10 ml of water, and 10 ml of saturated aqueous solution of NaHCO₃. The extracted organic layer was dried over MgSO₄ and concentrated in vacuum to give a yellow liquid. The purification by flash column chromatography (SiO₂, diethylether/pentane (1:1) R_f = 0.7) afford mesylate **69** as yellow oil (1.5 g, 85 %).

¹H-NMR (360 MHz, CDCl₃): δ 4.29-4.24 (*m*, 1H, HC(3)), 4.22-4.15 (*m*, 2H, H₂C(6)), 3.91-3.88 (*m*, 1H, HC(2)), 3.87-3.81 (*m*, 1H, HC(2)), 3.07 (*s*, 3H, H₃C(1)), 2.09-1.02 (*m*, 1H, HC(5)), 1.98-1.90 (*m*, 2H, H₂C(4)), 1.74-1.65 (*m*, 1H, HC(5)).

MS (EI): *m/z* 150 [M - 30]⁺.

(Tetrahydrofuran-2-yl)methyl 4-methylbenzenesulfonate **70**

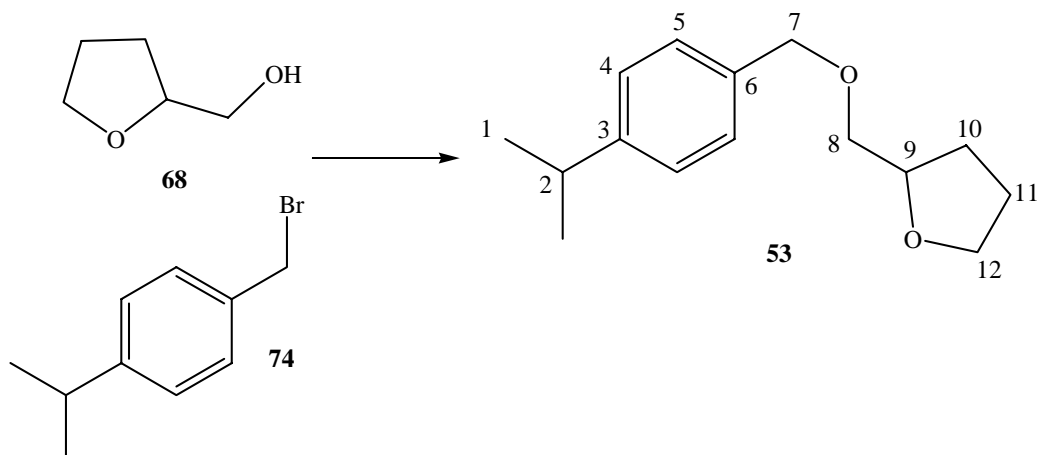


A 500 ml round bottomed flask was charged with furfuryl alcohol (1.0 ml, 10 mmol), triethylamine (2.7 ml, 20 mmol) and 30 ml of dichloromethane at 0 °C. To this solution was added *p*-toluenesulfonyl chloride (2.86 g, 15 mmol). Then the mixture was warmed to RT, stirred for 3 hours, diluted with 2 x 20 ml of CH₂Cl₂ and washed sequentially with 100 ml of aqueous HCl 20%, 10 ml of water, and 10 ml of saturated aqueous of NaHCO₃. The extracted organic layer was dried over MgSO₄ and concentrated in vacuum to give a yellow liquid. The purification by flash column chromatography (SiO₂, diethylether/pentane (1:1) R_f = 0.5) afford tosylate **70** as yellow oil (2.50 g, 100%).

¹H-NMR (360 MHz, CDCl₃): *d* 7.80 (J = 7.8, 2H, HC(4)), 7.35 (*d*, J = 7.8, 2H, HC(3)), 4.09 (*m*, 1H, HC(7)), 4.12-3.97 (*m*, 2H, H₂C(10)), 3.82-3.70 (*m*, 2H, H₂C(6)), 2.45 (*s*, 3H, H₃C(1)), 1.99-1.99 (*m*, 1H, HC(9)), 1.89-1.80 (*m*, 2H, H₂C(8)), 1.69-1.1.64 (*m*, 1H, HC(9)).

MS (EI): *m/z* 257 [M + 1]⁺.

2-(4-Isopropyl-benzyloxymethyl)-tetrahydrofuran 53



To a two necked flask equipped with a bubbler was charged with 140 mg, (2.1 mmol) of NaH (60 % in mineral oil washed three times with pentane and dried under vacuum), then a solution of alcohol **68** (0.22 g, 2.1 mmol) in THF (10 ml) was added dropwise over a period of 15 minutes. Stirring was continued until gas evolution ceased. After addition of KI (0.08 g, 0.5 mmol), benzylbromide **74** (0.50 g, 2.3 mmol) dissolved in 1 ml of THF was added over a period of 15 minutes. The reaction mixture was stirred overnight and then mixed with 5 ml of water and saturated NaCl solution (5 ml). The aqueous phase was extracted three times with CH₂Cl₂ and the combined organic phases were washed with 20 ml of water and dried over MgSO₄. After evaporation of the solvent, the obtained yellow oil product was purified by flash column chromatography (diethylether/pentane (1:1), R_f = 0.7) affording 0.5 g (92 %) of **53** as a pale-yellow liquid.

¹H-NMR (360 MHz, CD₂Cl₂): δ 7.23 (*d*, 2H, J = 8.2, HC(4)), 7.20 (*d*, 2H, J = 8.2, HC(5)), 4.48 (*s*, 2H, H₂C(7)), 4.03-4.00 (*m*, 1H, HC(9)), 3.85-3.3.79 (*m*, 1H, H_bC(12)), 3.74-3.68 (*m*, 1H, H_aC(12)), 3.44 (*d*, 2H, J = 5.4, H₂C(8)), 2.90 (*sept* 1H, J = 6.8, HC(2)), 1.98-1.80 (*m*, 3H, H_bC(10, 11)), 1.65-1.57 (*m*, 1H, HC(10)), 1.23 (*d*, 6H, J = 6.8, H₃C(1)).

¹³C-NMR (91 MHz, CD₂Cl₂): δ 149.1 C(3), 136.9 C(6), 128.6 C(4), 127.1 C(5), 78.8 C(9), 73.9 C(8), 73.8 C(12), 68.9 C(7), 34.7 C(2), 29.0 C(11), 26.5 C(10), 24.6 C(1).

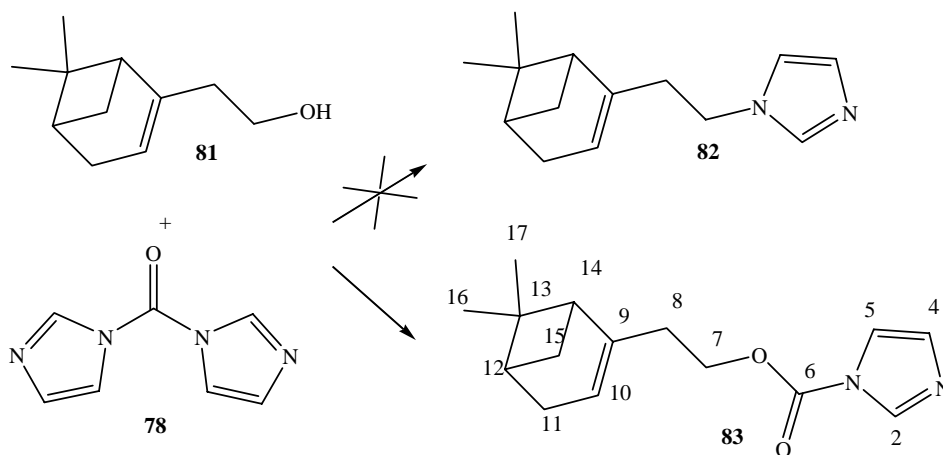
UV-VIS (THF, 200-800 nm): 220, 263.

IR (NaCl film, 4000-400 cm⁻¹): 2960m, 2928m, 2868m, 1462w, 1088m, 818w.

MS (EI): *m/z* 234 (25) [M]⁺, 191(14), 149(43), 133(100), 117(27), 71(46).

20.2. Synthesis of alkyl and arylimidazole

(2-(6,6-Dimethylbicyclo[3.1.1]hept-2-en-2-yl)ethyl)-1H-imidazole-1-carbamate **83**



To a freshly distilled (50°C, 10 mmHg) solution of nopol (0.75 g, 5.0 mmol) in acetonitrile (40 ml) was added CDI (2.20 g, 13.5 mmol) and the mixture was stirred at reflux for 24 hours. After the solution was cooled, 100 ml of aqueous saturated solution of K₂CO₃, 200 ml of diethylether were added, and the layers were separated. The aqueous solution was extracted with 2 x 20 ml of diethylether. The combined organic phases were washed with 2 x 100 ml of water, dried over MgSO₄ and evaporated under reduced pressure. Purification was accomplished by flash column chromatography (SiO₂, CH₂Cl₂/MeOH (20:1), R_f = 0.5) affording 0.90 g of an colourless oil product. The MS (ESI+), ¹³C-NMR and infrared spectra indicate only the presence of carbamate product **83** in a 90 % yield.

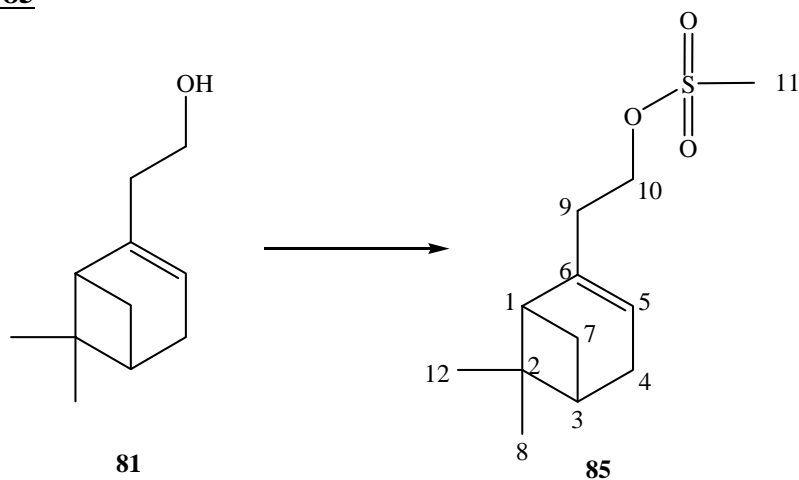
¹H-NMR (360 MHz, CDCl₃): δ 8.12 (*s*, 1H, HC(2)), 7.41 (*s*, 1H, HC(5)), 7.29 (*s*, 1H, HC(4)), 5.37 (*br*, 1H, HC(10)), 4.43 (*t*, 2H, J = 7.3, HC(7)), 2.45-2.39 (*m*, 3H); 2.25-2.17 (*m*, 2H); 1.28 (*s*, 3H, H₃C), 1.17 (*d*, J = 8.2, 1H), 0.82 (*s*, 3H, H₃C).

¹³C-NMR (91 MHz, CDCl₃): δ 149 C(2), 143.5 C(9), 131 C(2), 120.2 (C(5, 4)), 117.5 C(10), 66.8 C(7), 46 C(8), 41 C(11), 36.2 C(11), 32.1 C(7), 31.7 C(12), 31.3 C(14), 26.6 (C(15, 16)), 21.5 (C(15, 16)).

IR (NaCl film, 4000-400 cm⁻¹): 1769 (C=O stretch vibration).

MS (ESI+): *m/z* 261 [M]⁺

Nopylmesylate **85**



A 500 ml round bottomed flask was charged with nopol (4.0 g, 24.0 mmol), triethylamine (6.8 ml, 48.0 mmol) and 30 ml of dichloromethane at 0 °C. To this solution was added methanesulphonyl chloride (2.8 ml, 35.5 mmol). Then the mixture was warmed to RT, stirred for 2 hours, diluted with 2x100 ml of CH₂Cl₂ and washed sequentially with 100 ml of aqueous HCl 20%, 100 ml of water, and 10 ml of saturated aqueous solution of NaHCO₃. The extracted organic layer was dried over MgSO₄ and concentrated in vacuum to give a yellow liquid. The purification by flash column chromatography (SiO₂, pentane/diethylether (1:1) R_f = 0.8) afford mesylate **85** as yellow oil (4.6 g, 96 %).

¹H-NMR (360 MHz, CDCl₃): δ 5.23 (*s*, 1H, HC(5)), 4.22 (*t*, 2H, J = 7.3, HC(10)), 3.00 (*s*, 3H, HC(11)), 2.41-2.15 (*m*, 5H), 2.14-2.00 (*m*, 2H), 1.28 (*s*, 3H, HC(8)), 1.21 (*d*, J = 8.5, 1H, HC(7)), 0.84 (*s*, 3H, HC(12)).

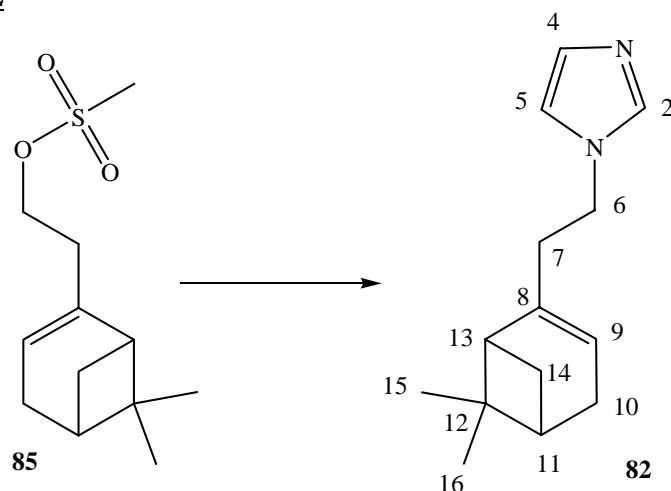
¹³C-NMR (50 MHz, CDCl₃): δ 143.1 C(6), 120.4 C(5), 68.4 C(10), 46 C(1), 41.1 C(5), 38.5 C(2), 37.9 C(11), 36.8 C(14), 32 (C(4, 7)), 31.8 (C(7, 4)), 26.6 (C(12, 8)), 21 (C(8, 12)).

UV-VIS (THF, 200-800 nm): 220, 263.

IR (NaCl film, 4000-400 cm⁻¹): 2915s, 1450m, 1356s, 1175s, 950s, 920m (sh), 800m.

MS (ESI+): *m/z* 267 [M + Na]⁺. **MS (EI)**: *m/z* 244 [M]⁺.

1-nopylimidazole **82**



A Schlenk tube equipped with septum was charged with NaH 60 % in mineral oil (0.44 g, 11.0 mmol, washed three times with pentane) and 10 ml of THF at 0°C. To this suspension was added dropwise a solution of imidazole (0.74 g, 11.0 mmol) in 10 ml of THF. Then a mixture was warmed to RT and stirred until gas evolution ceased. After that a solution of nopylmesylate **85** (2.31 g, 10.0 mmol) in THF (5 ml) was added at RT and the mixture was heated to reflux under argon atmosphere for 8 hours. After the solution was cooled, 50 ml of saturated aqueous solution of Na₂CO₃, 2 x 50 ml of diethylether was added, and the layers were separated. The aqueous solution was extracted with 2 x 20 ml of diethylether. The combined organic phases were dried over MgSO₄, and evaporated under reduced pressure. Purification was accomplished by flash column chromatography (SiO₂, CH₂Cl₂/MeOH (20:1), R_f = 0.5) affording 1.72 g (94 %) of nopylimidazole **82** as pale yellow oil.

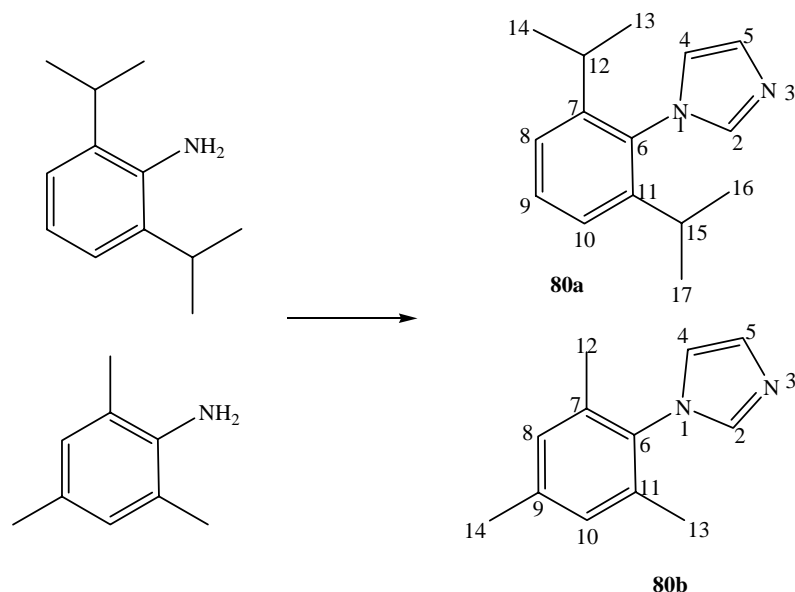
¹H-NMR (360 MHz, CDCl₃): δ 7.45 (*s*, 1H, HC(2)), 7.04 (*s*, 1H, HC(4)), 6.91 (*s*, 1H, HC(5)), 5.26 (*br*, 1H, HC(9)), 3.95 (*t*, 2H, J = 7.3, HC(6)), 2.46-2.27 (*m*, 5H), 2.22-2.01 (*m*, 2H), 1.29 (*s*, 3H, H₃C), 1.12 (*d*, J = 8.5, 1H), 0.82 (*s*, 3H, H₃C).

¹³C-NMR (50 MHz, CDCl₃): δ 144.2 C(8), 137.4 C(2), 129.7 (C(5, 4)), 119.8 (C(4, 5)), 119.1 C(9), 46 C(13), 45.6 C(6), 41.1 C(11), 38.9 C(7), 38.5 C(12), 32.1 (C(16, 10)), 31.7 C(16), 26.7 (C(15, 16)), 21.6 (C(15, 16)).

IR (NaCl film, 4000-400 cm⁻¹): 3419w, 3109w, 2983s, 2916s, 2833m (sh), 1674w, 1506m, 1454m, 1366m, 1229m, 1078m, 900w, 820w, 760w, 680m.

MS (ESI+): *m/z* 217 [M + H]⁺. **MS (EI)**: *m/z* 216 [M]⁺

Synthesis of N-1-arylimidazoles **80a** and **80b** : General procedure



A two-necked 500 ml round-bottomed flask was charged with 100.0 ml (174.7 mmol) of glacial acetic acid, 30.0 ml (40.0 mmol) of formaldehyde 40% in water, and 46 ml (100.7 mmol) of aqueous glyoxal. The mixture was heated to 70 °C, and a solution of 100.0 ml (174.7 mmol) of glacial acetic acid, 30.8 g (399.6 mmol) of ammonium acetate, 20.0 ml water (to solubilize the ammonium acetate) and 400 mmol of amine was added dropwise over a period of 30 min. The mixture was stirred overnight at 70 °C. After cooling, the solution was dripped into a stirred solution of 300 g of NaHCO₃ in 3 l of water. A precipitate formed was filtered, washed with water, and dried under vacuum to yield 94 % of the brownish product in both cases. Both **80a** and **80b** were isolated as off white crystals in 87 % yield after sublimation under vacuum (0.1 bar, 130°C).

1-(2,6-Diisopropylphenyl) -1H-imidazole **80a**

¹H-NMR (360 MHz, CDCl₃): δ 7.45-7.41 (*m*, 2H, HC(2, 9)), 7.27 (*d*, 2H, *J* = 7.7, HC(8, 10)), 7.17 (*s*, 1H, HC(5)), 6.96 (*s*, 1H, HC(4)), 2.38 (*hept*, *J* = 6.8, 2H, HC(12, 13)), 1.12 (*d*, *J* = 6.8, 12H, HC(13, 14, 16, 17)).

¹³C-NMR (91 MHz, CDCl₃): δ 147.3 (C(7, 11)), 132 C(2), 134 C(6), 130.6 (C(5, 4)), 129.5 C(9), 124.5 (C(8, 10)), 28.9 C(12), 24.9 (C(13, 14)), 23 (C(13, 14)).

IR (NaCl film, 4000-400 cm⁻¹): 2960m, 2928m, 2868m, 1462w, 1088m, 818w.

MS (EI): *m/z* 228 [M]⁺.

1-(2,4,6-Trimethylphenyl)-1H-imidazole **80b**

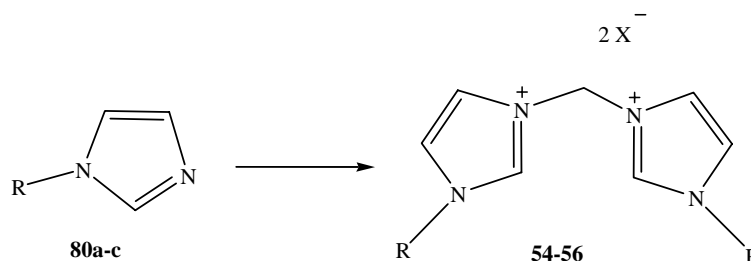
¹H-NMR (360 MHz, CDCl₃): δ 7.40 (*s*, 1H, HC(2)), 7.17 (*s*, 1H, HC(5)), 6.98 (*s*, 2 H, HC(8, 10)), 6.91 (*s*, 1H, HC(4)), 2.32 (*s*, 3H, H₃C(14)), 1.97 (*s*, 6H, H₃C(12, 13)).

¹³C NMR (91 MHz, CDCl₃): δ 139.6 C(9), 138.2 C(2), 136.2 (C(7, 11)), 134.9 C(6), 129.9 C(5), 129.6 C(4), 129.5 (C(8, 10)), 120.9 C(3), 21.5 C(14), 18.1 (C(12, 13)), 17.9 (C(13, 12)).

IR (NaCl film, 4000-400 cm⁻¹) : 3114m, 3095s, 2922s, 1769w, 1644w, 1595w, 1500s, 1496m, 1380w, 1313m, 1284m, 1237s, 1097s, 1068s, 1036m, 936w, 906s, 870s, 816s, 782s, 671s, 581m, 555w, 425w.

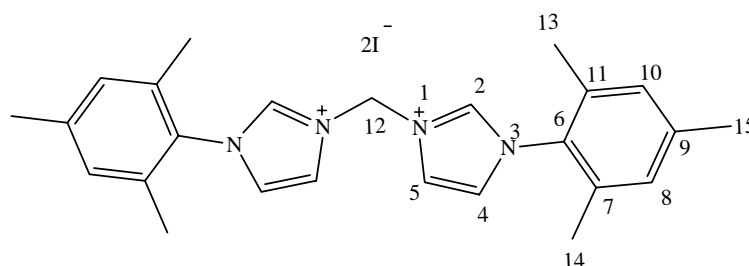
MS (EI): *m/z* 186 [M]⁺.

20.3. Synthesis of Bisimidazolium salts: Typical procedure



A typical procedure was followed: A solution of 1-mesitylimidazole **80b** (1.0 g, 4.4 mmol) in 20 ml of xylene (mixture of isomers) and CH₂I₂ (0.6 g, 2.2 mmol) was heated at 150 °C for 24 h. The formed precipitate was collected by filtration and recrystallized from hot methanol to RT yielding 2.76 g (98%) of **56a** as colourless crystal.

Diodide methylene bis(N-mesityl) bisimidazolium **56a**



¹H-NMR (360 MHz, CD₂Cl₂) : δ 10.87 (*s*, 1H, HC(2)), 8.82 (*s*, 1H, HC (4)), 7.52 (*s*, 1H, HC(5)), 7.13 (*s*, 2 H, HC(8, 10)), 7.06 (*s*, 2H, H₂C(12)), 2.36 (*s*, 3H, H₃C(15)), 2.09 (*s*, 6H, H₃C(13, 14)).

¹³C-NMR (91 MHz, CD₂Cl₂): δ 146.6 C(9), 139.7 C(2), 134.6 (C(7, 11)), 131.2 (C(6)), 130 (C(8, 10)), 129.8 (C(8, 10)), 124.9 (C(4, 5)), 123.1 (C(4, 5)), 58.8 C(12), 21 C(15), 17.5 (C(13, 14)).

MS (ESI+): *m/z* 511(100) [M - I]⁺.

Bisbromide methylene bis(N-mesityl) bisimidazolium **56b**

¹H-NMR (360 MHz, CD₂Cl₂) : δ 10.87 (*s*, 1H, HC(2)), 8.82 (*s*, 1H, HC (4)), 7.52 (*s*, 1H, HC(5)), 7.13 (*s*, 2 H, HC(8, 10)), 7.06 (*s*, 2H, H₂C(12)), 2.36 (*s*, 3H, H₃C(15)), 2.09 (*s*, 6H, H₃C(13, 14)).

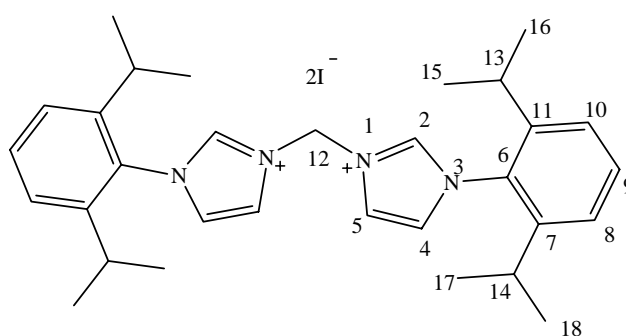
¹³C-NMR (91 MHz, CD₂Cl₂): δ 146.6 C(9), 139.7 C(2), 134.6 (C(7, 11)), 131.2 (C(6)), 130 (C(8, 10)), 129.8 (C(8, 10)), 124.9 (C(4, 5)), 123.1 (C(4, 5)), 58.8 C(12), 21 C(15), 17.5 (C(13, 14)).

UV-VIS (THF, 200-800 nm): 220, 263.

IR (KBr film, 4000-400 cm⁻¹) : 3446w, 3157w, 3055s, 2955s, 1780w, 1608w, 1545s, 1486m, 1444m, 1376m, 1205s, 1163m, 1072m, 1035w, 936w, 856m, 771m, 754m, 668m, 617w, 580m, 447w.

MS (ESI+): *m/z* 467(100) [M - Br]⁺, 1013 (25) [2M - Br]⁺.

Diodide methylene bis(N-2,6-diisopropylphenyl) bisimidazolium **55a**, off-white crystals



¹H-NMR (360 MHz, DMSO-*d*₆) : δ 9.92 (*s*, 1H, HC(2)), 8.38 (*s*, 1H, HC (4)), 8.31 (*s*, 1H, HC(5)), 7.69 (*t*, *J* = 7.7, 1H, HC(9)), 7.47 (*d*, *J* = 7.7, 2H, H₂C(10, 8)), 6.93 (*s*, 1H, HC(12)), 2.26 (*hept*, *J* = 6.8, 2H, HC(13, 14)), 1.18 (*d*, *J* = 6.8, 12H, HC(15-18)).

¹³C-NMR (91 MHz, DMSO-*d*₆): δ 145.2 C(7, 11), 139.4 C(2), 132.2 C(9), 130.6 C(6), 126.3 (C(4, 5)), 125.2 (C(8, 10)), 123.7 (C(4, 5)), 59.9 C(12), 28.4 (C(13, 14)), 24.3 (C(15-14)), 24.1 (C(15-18)).

IR (NaCl film, 4000-400 cm⁻¹): 3441m, 3047s, 2964s, 1628w, 1537m, 1462m, 1366m, 1188s, 1070m, 808m, 765m, 671m.

MS (ESI+): *m/z* 469 [M-2I]⁺.

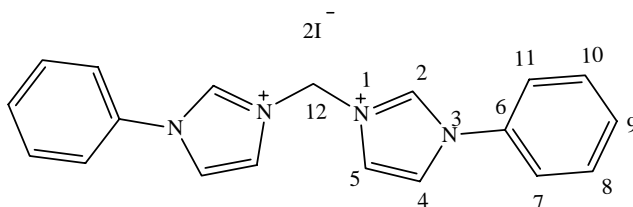
Bisbromide methylene bis(N-2,6-diisopropylphenyl) bisimidazolium 55b, off-white crystals

¹H-NMR (360 MHz, DMSO-*d*₆): δ 9.92 (*s*, 1H, HC(2)), 8.38 (*s*, 1H, HC(4)), 8.31 (*s*, 1H, HC(5)), 7.69 (*t*, *J* = 7.7, 1H, HC(9)), 7.47 (*d*, *J* = 7.7, 2H, H₂C(10, 8)), 6.93 (*s*, 1H, HC(12)), 2.26 (*hept*, *J* = 6.8, 2H, HC(13, 14)), 1.18 (*d*, *J* = 6.8, 12H, HC(15-18)).

¹³C-NMR (91 MHz, DMSO-*d*₆): δ 145.2 C(7, 11), 139.4 C(2), 132.2 C(9), 130.6 C(6), 126.3 (C(4, 5)), 125.2 (C(8, 10)), 123.7 (C(4, 5)), 59.9 C(12), 28.4 (C(13, 14)), 24.3 (C(15-14)), 24.1 (C(15-18)).

MS (ESI+): *m/z* 469 [M-2Br]⁺.

Diiodide methylenebis(N-phenyl)bisimidazolium 54a, colourless crystals



¹H-NMR (360 MHz, DMSO-*d*₆): δ 10.29 (*s*, 1H, HC(2)), 8.46 (*s*, 1H, HC(4)), 8.37 (*s*, 2H, HC(2, 5)), 7.82 (*d*, 4H, *J* = 7.8 Hz, HC(7, 11)), 7.75 (*dd*, 4H, *J* = 7.3, *J* = 7.8, HC(8, 10)), 7.67 (*t*, 2H, *J* = 7.3, HC(9)), 6.82 (*s*, 2H, H₂C(12)).

¹³C-NMR (91 MHz, DMSO-*d*₆): δ 138.09 C(6), 127.43-128.92 C(5-11), 127.43-128.92 C(2), 127.43-128.92 C(4), 119.82 C(5), 59.14 C(12).

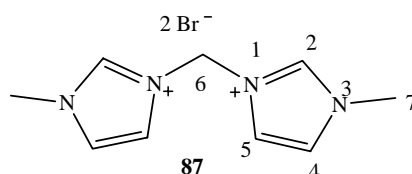
UV-VIS (THF, 200-800 nm): 220, 263.

IR (NaCl film, 4000-400 cm⁻¹): 2960m, 2928m, 2868m, 1462w, 1088m, 818w.

MS (ESI+): *m/z* 151 (25), 301(40) [M-1]⁺, 429(100) [M-I]⁺, 707(10), 985(40) [2M-I]⁺.

20.4. Solvent free sonochemical preparation of bisimidazolium salts: Typical procedure

A 75 ml Schlenk tube was charged with a mixture of 1-methylimidazole (1.2 g, 14.8 mmol) and 1.2 g (7.2 mmol) of dibromomethylene and the mixture was placed in a sonication bath. After 2 h, the formation of ionic liquid could be visibly monitored as the reaction contents turned from a clear solution to opaque (emulsification) and finally a clear viscous phase or separation of solids occurred. Then the mixture was washed with 2 x 20 ml of diethylether and the solvent take off by filtration. The remaining solid was dried under vacuum, affording 4.7 g (93 %) of the desired bisimidazolium salt **87** as a white solid. Recrystallization in hot MeOH gave colourless crystals. Methylene bisphenylbisimidazolium iodide **54a** was also prepared in 16% yield, using the same procedure as described above.



¹H-NMR (360 MHz, DMSO-*d*₆): δ 9.72 (*s*, 1H, HC(2)), 8.42 (*s*, 1H, HC(4)), 8.39 (*s*, 2H, HC(2, 5)), 6.82 (*s*, 2H, H₂C (12)), 3.54 (*s*, 3H, HC(7)).

MS (ESI+): *m/z* 178 [M – 2Br]⁺.

20.5. The counter-ion exchange

Tetrafluoroborate derivatives : Typical procedure

A typical procedure for a counter-anion exchange was followed: To a solution of diiodobisimidazolium mesityl **56a** (0.35 g, 0.6 mmol) in CH₃CN (40 ml) was added AgBF₄ (0.26 g, 1.4 mmol). The mixture was stirred at RT for 15 minutes. After completion, the reaction mixture was filtered, the solvent was evaporated under vacuum and the resulting solid was washed with diethylether. Drying under vacuum afford the desired product **56c** as white-grey solids (0.23 g, 98 %). If necessary, they were purified by recrystallization from saturated solution of dichloromethane and diethylether.

Bistetrafluoroborate methylenebis(N-mesityl) bisimidazolium **56c** white crystals (98 %)

¹H-NMR (360 MHz, CD₂Cl₂) : δ 9.16 (*s*, 1H, HC(2)), 8.03 (*s*, 1H, HC (4)), 7.59 (*s*, 1H, HC(5)), 7.11 (*s*, 2 H, HC(8, 10)), 6.70 (*s*, 2H, H₂C(12)), 2.33 (*s*, 3H, H₃C(15)), 2.04 (*s*, 6H, H₃C(13, 14)).

¹³C-NMR (91 MHz, CD₂Cl₂): δ 143 C(9), 139.2 C(2), 134.3 (C(7, 11)), 130.4 (C(6)), 130.3 (C(8, 10)), 130.1 (C(8, 10), 125.5 (C(4, 5)), 123.1 (C(4, 5)), 59.3 C(12), 21.1 C(15), 17.3 (C(13, 14)).

UV-VIS (THF, 200-800 nm): 220, 263.

IR (KBr film, 4000-400 cm⁻¹) : 3437m, 3147m, 1610w, 1546m, 1204s, 1085s, 1076s, 1053s, 1018s, 920w, 758w, 660w.

MS (ESI+): *m/z* 193(25), 385(100) [M-2BF₄]⁺, 473(45) [M - BF₄]⁺, 753(20), 1034(20) [2M-BF₄]⁺.

Bistetrafluoroborate methylene bis(N-2,6-diisopropylphenyl) bisimidazolium **55d** colourless crystals (94 %)

¹H-NMR (360 MHz, CD₃CN) : δ 9.92 (*s*, 1H, HC(2)), 8.38 (*s*, 1H, HC (4)), 8.31 (*s*, 1H, HC(5)), 7.69 (*t*, J = 7.7, 1H, HC(9)), 7.47 (*d*, J = 7.7, 2H, H₂C(10, 8)), 6.93 (*s*, 1H, HC(12)), 2.26 (*hept*, J = 6.8, 2H, HC(13, 14), 1.18 (*d*, J = 6.8, 12H, HC(15-18)).

IR (KBr film, 4000-400 cm^{-1}) : 3432w, 3166s, 3097s, 2926m, 1632m, 1608m, 1562m, 1543m, 1487m, 1458m, 1404w, 1380m, 1290w, 1204s, 1192s, 1076s, 1052s (sh), 1020s (sh), 856m, 758m, 671m, 578m, 523m.

MS (ESI+): m/z 186(30), 235(60) $[\text{M}-2\text{BF}_4]^+$, 557(100) $[\text{M}-\text{BF}_4]^+$, 879(20), 1201(10) $[2\text{M}-\text{BF}_4]^+$.

Bistetrafluoroborate methylene bis(N-phenyl)imidazolium **54c**: slightly grey solid (67 % yield)

$^1\text{H-NMR}$ (360 MHz, DMSO-D_6): 10.29 (*s*, 1H, HC(2)), 8.46 (*s*, 1H, HC(4)), 8.37 (*s*, 2H, HC(2, 5)), 7.82 (*d*, 4H, $J = 7.8$, HC(7, 11)), 7.75 (*dd*, 4H, $J = 7.3, J = 7.8$, HC(8, 10)), 7.67 (*t*, 2H, $J = 7.3$, HC(9)), 6.82 (*s*, 2H, H_2C (12)).

Hexafluorophosphate derivatives : Typical procedure

To a solution of diiodo bisimidazolium mesityl **56a** (0.90 g, 1.6 mmol) in water or methanol (30 ml) was added NH_4PF_6 (0.77 g, 4.7 mmol). The mixture was stirred at RT for 48 hours. After completion, the aqueous phase containing NH_4Cl was filtered off, and the remaining precipitate was washed with water (2 x 10 ml), diethylether (2x 15 ml) and dried under vacuum affording 0.88 g (90%) of **56c** as white solids. If necessary, they were purified by recrystallization from saturated solution of acetonitrile and diethylether.

Bishexafluorophosphate methylenebis(N-mesityl) bisimidazolium **56c**

$^1\text{H-NMR}$ (360 MHz, CD_2Cl_2) : δ 10.74 (*s*, 1H, HC(2)), 8.53 (*s*, 1H, HC (4)), 7.48 (*s*, 1H, HC(5)), 7.21 (*s*, 2 H, HC(8, 10)), 7.08 (*s*, 2H, H_2C (12)), 2.36 (*s*, 3H, H_3C (15)), 2.12 (*s*, 6H, H_3C (13, 14)).

$^{13}\text{C-NMR}$ (91 MHz, CD_2Cl_2): δ 139.8 C(9), 137.4 C(2), 133.6 (C(7, 11)), 130.2 (C(6)), 130 (C(8, 10)), 129.5 (C(8, 10), 124.8 (C(4, 5)), 122.7 (C(4, 5)), 59 C(12), 19.4 C(15), 16.9(C(13, 14)).

IR (KBr film, 4000-400 cm^{-1}) : 3446w, 3162s, 2929w, 1608m, 1590m (sh), 1545s, 1487m, 1452m, 1423m, 1202s, 1163s, 1115m, 1070m, 1034m, 850vs, 772m, 739m, 671w, 557s.

MS (ESI+): m/z 193 (35), 385(100) $[\text{M}-2\text{PF}_6]^+$.

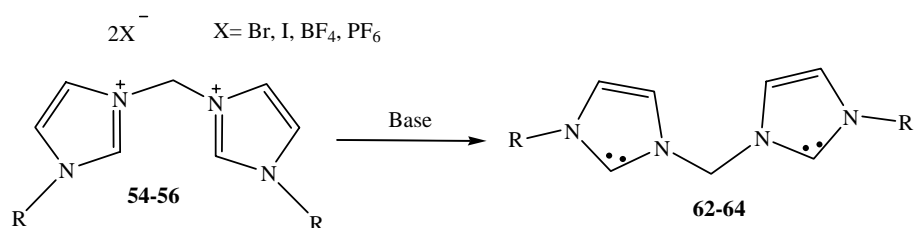
Bis(hexafluorophosphate methylenebis(N-2,6-diisopropylphenyl) bisimidazolium 55e. White crystals (98 % yield)

¹H-NMR (360 MHz, DMSO-d₆) : δ 10.07 (*s*, 1H, HC(2)), 8.51 (*s*, 1H, HC (4)), 8.41 (*s*, 1H, HC(5)), 7.75 (*t*, J = 7.6, 1H, HC(9)), 7.48 (*d*, J = 7.7, 2H, H₂C(10, 8)), 6.95 (*s*, 1H, HC(12)), 2.31 (*hept*, J = 6.8, 2H, HC(13, 14)), 1.20 (*d*, J = 6.8, 12H, HC(15-18)).

¹³C-NMR (91 MHz, DMSO-d₆): δ 147.4 C(7, 11), 139.8 C(2), 131.9 C(9), 130.4 C(6), 127.3 (C(4, 5)), 125.2 (C(8, 10)), 124 (C(4, 5)), 59.7 C(12), 28.4 (C(13, 14)), 25.1 (C(15-14)), 24.9 (C(15-18)).

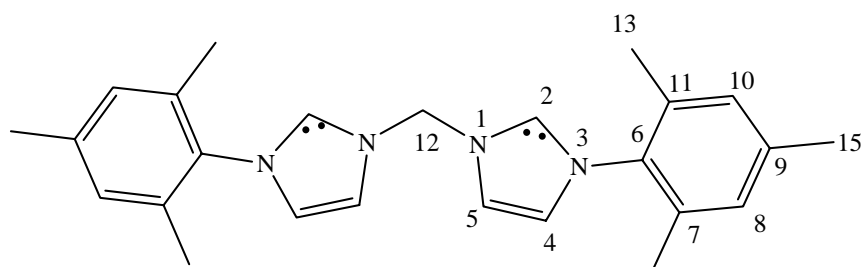
MS (ESI+): *m/z* 469(100) [M-2PF₆]⁺.

20.6. Synthesis of free carbene bisimidazol-2-ylidenes: Typical procedure



A 75 ml Schlenk tube was charged with 30 ml of THF, dibromobisimidazoliummesityl salt **56** (1.00 g, 2.0 mmol), 0.20 g (4.0 mmol) of NaH 60% (washed three times with pentane) and KO^tBu (0.03 g, 0.3 mmol). The Schlenk tube was capped with a septum and the rate of hydrogen evolution was monitored by oil-filled bubbler. The colour of the solution turned immediately to yellow and changed finally to orange. The stirring continues until gas evolution ceased. The solvent was removed under vacuum, the residue was extracted into warm toluene (30 ml, 70°C), and filtered hot through celite. Evaporation of the solvent afforded 0.62 g (80%) of biscarbene **64** as a yellow solid.

Methylene bis(N-mesityl) bisimidazol-2-ylidene **64**: yellow solid (80% yield)

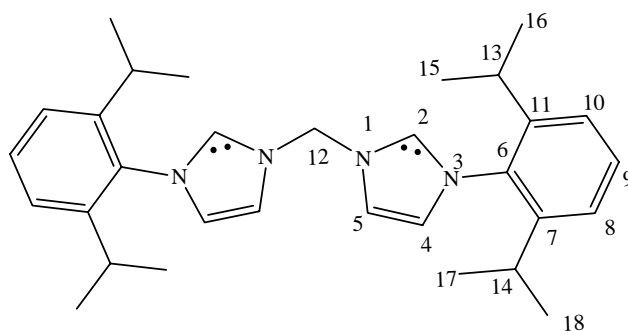


¹H-NMR (360 MHz, THF-*d*₈) : δ 7.58 (*s*, 1H, HC (4)), 7.16 (*s*, 1H, HC(5)), 6.99 (*s*, 2 H, HC(8, 10)), 6.96 (*s*, 2H, H₂C(12)), 2.30 (*s*, 3H, H₃C(15)), 1.98 (*s*, 6H, H₃C(13, 14)).

¹³C-NMR (91 MHz, THF-*d*₈): δ 141.4 C(9), 137.8 C(2), 134.3 (C(7, 11)), 130.2 (C(6)), 130.1 (C(8, 10)), 129.6 (C(8, 10), 125.3 (C(4, 5)), 122.9 (C(4, 5)), 59.3 C(12), 19.9 C(15), 16.6 (C(13, 14)).

UV-VIS (THF, 200-800 nm): 213, 242.

Methylene bis(N-2,6-diisopropylphenyl) bisimidazol-2-ylidene **63** : Yellowish solid (80% yield)

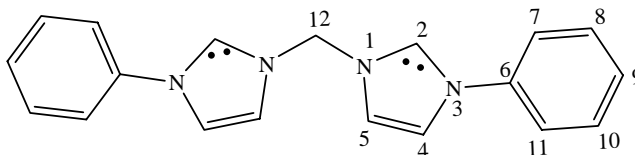


¹H-NMR (360 MHz, THF-*d*₈) : δ 7.58 (*s*, 1H, HC (4)), 7.42 (*t*, J = 7.7, 1H, HC(9)), 7.28 (*d*, J = 8.1, 2H, H₂C(10, 8)), 7.15 (*s*, 1H, HC(5)), 7.04 (*s*, 1H, HC(12)), 2.38 (*hept*, J = 6.8, 2H, HC(13, 14)), 1.18 (*dd*, J = 6.8, J = 1.8, 12H, HC(15-18)).

¹³C-NMR (91 MHz, THF-*d*₈): δ 213.9 C(2), 146.8 C(7, 11), 138.7 C(12), 133.8 C(6), 129.9 (C(4)), 129.4 C(9), 123.9 (C(8, 10)), 121.7 C(5), 28.4 (C(13, 14)), 24.1 (C(15-18)).

UV-VIS (THF, 200-800 nm): 246.

Methylene bis(N-phenyl) bisimidazol-2-ylidene **62**: Brown solid (76% yield)

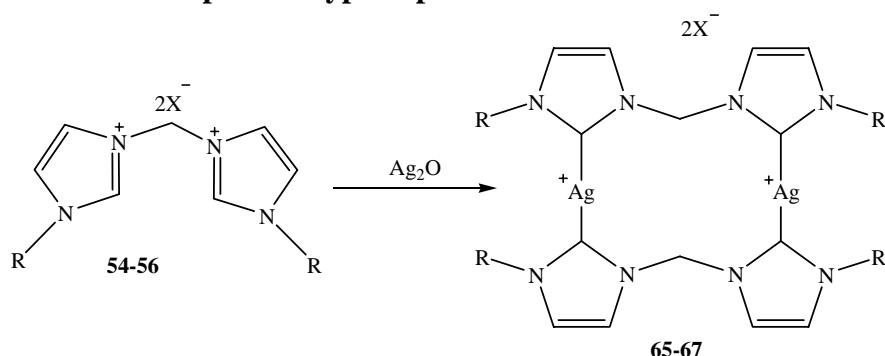


¹H-NMR (360 MHz, DMSO-*d*₆): δ 7.66 (*d*, 2H, *J* = 7.7, HC(4, 5)), 7.54-7.11 (*m*, 5H, HC(7-11)).

¹³C-NMR (91 MHz, DMSO-*d*₆): δ 137.19 C(6), 114.16-130.16 (C(7-11)), 114.16-130.16 2 C(4), 114.16-130.16 C(5).

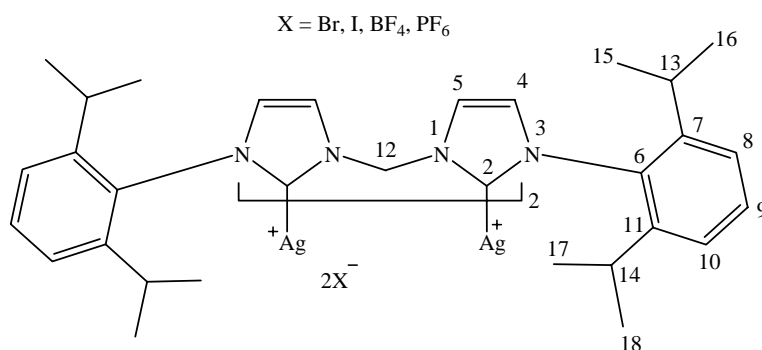
Silver complexes

21. Synthesis of silver complexes: Typical procedure



A Schlenk tube was charged with 30 ml of CH_2Cl_2 , diiodidebisimidazolium 2,6-diisopropylphenyl salt **55** (1.6 g, 2.0 mmol), Ag_2O (0.5 g, 2.0 mmol) and molecular sieves (4Å). The resulted black suspension was heated at reflux for 8 hours. After cooling, the mixture was filtered, and the solvent was removed under vacuum yielding 2.5 g (86 %) of silver complex **66a** as white-beige solid. Suitable colourless crystals for X-ray diffraction were grown after 48 hours in dichloromethane solution.

2,6-Diisopropylaryl derivatives



Iodide 66a: white-beige solid (86% yield)

$^1\text{H-NMR}$ (500 MHz, CD_2Cl_2): δ 7.9 (*s*, 1H, HC (5)), 7.52 (*t*, $J = 7.7$, 1H, HC(9)), 7.26 (*d*, $J = 7.7$, 2H, HC(8, 10)), 7.10 (*s*, 1H, HC(4)), 6.67 (*s*, 1H, HC(12)), 2.32 (*hept*, $J = 6.8$, 2H, HC(13, 14)), 1.20 (*d*, $J = 6.8$, 6H, HC(15-18)), 1.10 (*d*, $J = 6.8$, 6H, HC(15-18)).

$^{13}\text{C-NMR}$ (125 MHz, CD_2Cl_2): δ 183 (2 d, $^1J_{107\text{Ag-C}} = 183$, $^1J_{109\text{Ag-C}} = 210$ Hz, $\text{AgC}(2)$), 147.3 (C(7, 11)), 135.9 C(6), 131.3 C(9), 128.5 C(4), 125 (C(8, 10)), 124.5 C(5), 64.8 C(12), 29.1 (C(13, 14)), 25 (C(15-18)), 25 (C(15-18)).

UV-VIS (THF, 200-800 nm): 291, 264, 219.

MS (ESI+): m/z 1475(100) $[\text{M}+\text{CH}_2\text{Cl}_2]^+$, 1331(40) $[\text{M}-58]^+$, 469(50) $[\text{ligand}]^+$.

Bromide 66b : white-beige (98%)

¹H-NMR (500 MHz, CD₂Cl₂) : δ 7.96 (*s*, 1H, HC (5)), 7.52 (*t*, J = 7.7, 1H, HC(9)), 7.30 (*d*, J = 7.7, 2H, HC(8, 10)), 7.08 (*s*, 1H, HC(4)), 6.65 (*s*, 1H, HC(12)), 2.35 (*hept*, J = 6.8, 2H, HC(13, 14)), 1.19 (*d*, J = 6.8, 6H, HC(15-18)), 1.10 (*d*, J = 6.8, 6H, HC(15-18)).

¹³C-NMR (125 MHz, CD₂Cl₂): δ 183.6 C(2), 182.1 C(2), 146.9 (C(7, 11)), 135.9 C(6), 130.5 C(9), 128.5 C(4), 125.3 (C(8, 10)), 124.5 C(5), 65 C(12), 29.1 (C(13, 14)), 25 (C(15-18)), 25 (C(15-18)).

Tetrafluoroborate 66d : white solid (92% yield)

¹H-NMR (500 MHz, CD₃CN) : δ 8.01 (*s*, 1H, HC (5)), 7.56 (*t*, J = 7.6, 1H, HC(9)), 7.42 (*s*, 1H, HC(4)), 7.30 (*d*, J = 7.6, 2H, HC(8, 10)), 6.38 (*br*, 1H, HC(12)), 5.87 (*br*, 1H, HC(12)), 2.53 (*br*, 2H, HC(13, 14)), 1.09 (*d*, J = 6.8, 12H, HC(15-18)).

¹³C-NMR (125 MHz, CD₃CN): δ 183.7 C(2), 182.2 C(2), 146.9 (C(7, 11)), 135.7 C(6), 132.3 C(9), 128.5 C(4), 126.1-125.8 (C(8, 10)), 123.2 C(5), 66.8 C(12), 29.9 (C(13, 14)), 23.1 (C(15-18)), 25 (C(15-18)).

MS (ESI+): *m/z* 1239(100) [M-BF₄]⁺, 469(10) [ligand]⁺.

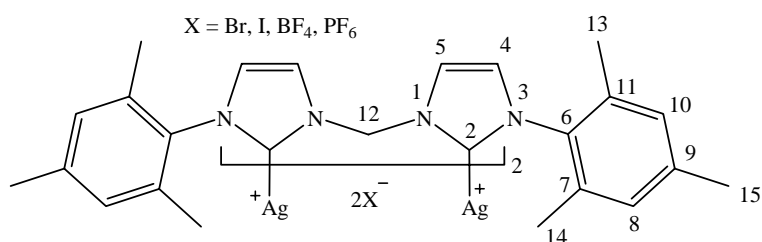
Hexafluoroborate 66e : white solid (90% yield)

¹H-NMR (500 MHz, CD₃CN) : δ 8.42 (*s*, 1H, HC (5)), 7.70 (*t*, J = 7.6, 1H, HC(9)), 7.48 (*s*, 1H, HC(4)), 7.35 (*d*, J = 7.6, 2H, HC(8, 10)), 6.30 (*br*, 1H, HC(12)), 5.88 (*br*, 1H, HC(12)), 2.53 (*br*, 2H, HC(13, 14)), 1.12 (*d*, J = 6.8, 12H, HC(15-18)).

¹³C-NMR (125 MHz, CD₃CN): δ 183 C(2), 183.1 C(2), 148.2 (C(7, 11)), 136.4 C(6), 132.3 C(9), 129 C(4), 126.1-125.6 (C(8, 10)), 124.1 C(5), 65.7 C(12), 30 (C(13, 14)), 23.5 (C(15-18)), 25 (C(15-18)).

MS (ESI+): *m/z* 2020(30), 1295 (100) [M-PF₆]⁺, 469(30) [ligand]

2,4,6-trimethylphenyl derivative



Iodide 67a : white-beige solid (86% yield)

¹H-NMR (500 MHz, CD₂Cl₂): δ 8.41 (*s*, 2H, HC(5)), 7.57 (*d*, *J* = 13.7, 1H, HC(12)), 7.15 (*d*, *J* = 13.7, 1H, HC(12)), 6.86-6.79 (*m*, 8H, HC(4, 8, 10)), 2.43 (*s*, 6H, HC(15)), 1.70 (*s*, 6H, HC(13,14)), 1.33 (*s*, 6H, HC(13, 14)).

¹³C-NMR (125 MHz, CD₂Cl₂): δ 183.2 (2 *d*, ¹*J*_{107Ag-C} = 183, ¹*J*_{109Ag-C} = 212, C(2)), 139.5 (C(7, 11)), 136.2 (C(11, 7)), 136.1 C(6), 135 C(9), 130.2 (C(8, 10)), 129.7 (C(10, 8)), 124.3 (C(4, 5)), 124 (C(5, 4)), 66.1 C(12), 21.8 C(15), 18.8 (C(13, 14)), 17.8 (C(14, 13)).

UV/VIS (THF, 200-800 nm): 213, 242.

IR (NaCl film, 4000-400 cm⁻¹) : 3082m, 2916m, 1608w, 1585w, 1489s, 1452m, 1379m, 1238vs, 1220w, 1032w, 853m, 745s, 583w.

MS (ESI+): *m/z* 1251(50) [M - 13]⁺, 1029(100) [M-AgI]⁺, 792(10), 492(20).

Bromide 67b : white-beige solid (86% yield)

¹H-NMR (500 MHz, CD₂Cl₂): δ 8.45 (*s*, 2H, HC(5)), 7.54 (*d*, *J* = 13.7, 1H, HC(12)), 7.20 (*d*, *J* = 13.7, 1H, HC(12)), 6.81-6.78 (*m*, 8H, HC(4, 8, 10)), 2.43 (*s*, 6H, *p*-HC(15)), 1.71 (*s*, 6H, HC(13, 14)), 1.33 (*s*, 6H, HC(13, 14)).

¹³C-NMR (125 MHz, CD₂Cl₂): δ 183.6 (2 *d*, ¹*J*_{107Ag-C} = 182, ¹*J*_{109Ag-C} = 210 Hz, AgC(2)), 139.2 (C(7, 11)), 135.9 (C(11, 7)), 135.6 C(6), 134.7 C(9), 129.8 (C(8, 10)), 129.3 (C(10, 8)), 123.9 (C(4, 5)), 123.6 (C(5, 4)), 65.3 C(12), 21.4 C(15), 18.2 (C(13, 14)), 17.4 (C(14, 13)).

UV/VIS (THF, 200-800 nm): 213, 242.

MS(ESI+) : *m/z* 1063(10), 1019(100), 340(10)

Tetrafluoroborate 67c : white solid (90% yield)

¹H-NMR (500 MHz, CD₂Cl₂): δ 8.46 (*s*, 2H, HC(5)), 7.54 (*d*, *J* = 13.7, 1H, HC(12)), 7.01 (*d*, *J* = 13.7, 1H, HC(12)), 6.7-6.62 (*m*, 8H, HC(4, 8, 10)), 2.40 (*s*, 6H, HC(15)), 1.93 (*s*, 6H HC(13, 14)), 1.23 (*s*, 6H, HC(14, 13)).

MS (MALDI) : *m/z* 1071(100) [M-BF₄]⁺, 983(30) [M-2BF₄]⁺.

Hexafluorophosphate Silver 67d : white solid (90%)

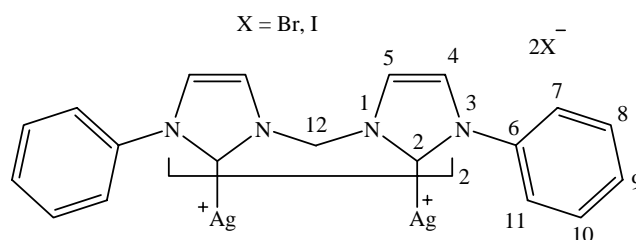
¹H-NMR (500 MHz, CD₂Cl₂): δ 8.01 (*s*, 2H, HC(5)), 7.67 (*d*, *J* = 13.7, 1H, HC(12)), 7.01 (*d*, *J* = 13.7, 1H, HC(12)), 6.83-6.69 (*m*, 8H, HC(4, 8, 10)), 2.39 (*s*, 6H, HC(15)), 1.95 (*s*, 6H HC(13, 14)), 1.36 (*s*, 6H, HC(13, 14)).

¹³C-NMR (125 MHz, CD₂Cl₂): δ 182.3 (2 *d*, ¹*J*_{107Ag-C} = 180, ¹*J*_{109Ag-C} = 208 Hz, AgC(2)), 140.8 (C(7, 11)), 135.7 (C(11, 7)), 135.6 C(6), 134.9 C(9), 130.5 (C(8, 10)), 130.2 (C(10, 8)), 125.1 (C(4, 5)), 122.9 (C(5, 4)), 65.4 C(12), 21.8 C(15), 17.7 (C(13, 14)), 17.5 (C(14, 13)).

IR (KBr film, 4000-400 cm⁻¹) : 3155w, 2920w, 1610m, 1591w, 1587w, 1489m, 1467m, 1398m, 1240m, 1200m, 1180w, 1100w, 1050w, 841s, 743m, 557m.

MS (ESI+) : *m/z* 1129(100) [M-PF₆]⁺, 565(15), 531(15), 492(20) [1/2(M-2PF₆)].

Phenyl derivatives



Iodide 65a : pale-yellow solid (60% yield)

$^1\text{H-NMR}$ (360 MHz, CD_2Cl_2): δ 8.16 (s, 2 H, HC(4, 5)), 7.70 – 7.20 (*m*, 6H, HC(7-12)).

$^{13}\text{C-NMR}$ (91 MHz, CD_2Cl_2): δ 184.2 C(2), 140.9 (C(6)), 130.2-129.9 (C(8, 10)), 128.1 C(9), 127.1 C(5), 125 (C(7, 11)), 119 C(5), 64.7 C(12).

UV-Vis (CH_2Cl_2 , 200-800 nm), 292, 279, 242.

MS (ESI+): m/z 996(100), 775(30), 633(70), 352(10).

Bromide 65b : pale-yellow solid (60% yield)

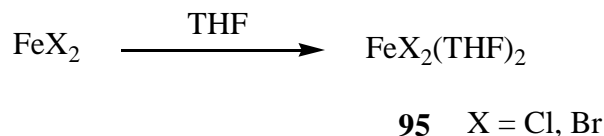
$^1\text{H-NMR}$ (360 MHz, THF-d_8): δ 8.21 (s, 2 H, HC(4, 5)), 7.70 – 7.20 (*m*, 6H, HC(7-12)).

$^{13}\text{C-NMR}$ (91 MHz, THF-d_8): δ 141.4 (C(6)), 130-128.7 (C(8, 10)), 127.8 C(9), 127 C(5), 124.6 (C(7, 11)), 120.3 C(5), 65 C(12).

Iron(II) precursors

22. Synthesis of iron precursors

22.1. Iron(II) bishalidesbistetrahydrofurane $\text{FeX}_2(\text{THF})_2$ (X = Cl, Br)



$\text{FeCl}_2(\text{THF})_2$ **95a**:

A Schlenk tube was charged with 1.0 g (7.9 mmol) of anhydrous FeCl_2 and 20 ml of THF under argon. The obtained suspension was heated to reflux for 8 hours. Then the mixture was allowed to cool down to RT and the upper yellowish solution was filtered. After evaporation of solvent and drying under vacuum, 1.5 g (68% yield) of pale yellow solid was obtained. The isolated product is air sensitive, it turns red – brown if in contact with air.

UV –Vis (THF, 200-800 nm): 335

IR (KBr film, 4000-400 cm^{-1}): 1599s, 598m.

MS (ESI+): m/z 433 (96), 371(70), 323(50), 279(50), 270(100) $[\text{M}]^+$.

$\text{FeBr}_2(\text{THF})_2$ **95b**:

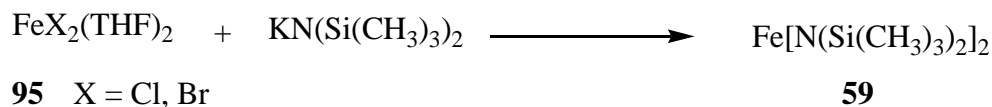
A Schlenk tube was charged with 1.0 g (4.7 mmol) of FeBr_2 anhydrous and 20 ml of THF under argon. The obtained suspension was heated to reflux for 8 hours. Then, the orange solution was allowed to cool to RT; yellowish crystals of $\text{FeBr}_2(\text{THF})_2$ precipitate already at 40 °C. The upper orange solution was filtered off and the remained yellowish crystal were washed with 2 x 10 ml of cold THF and dried under vacuum affording 1.0 g (60 % yield) of $\text{FeBr}_2(\text{THF})_2$ as grey crystals. The product is air sensitive, in contact with air it become dark red.

UV–Vis (THF, 200-800 nm): 328

IR (KBr film, 4000-400 cm^{-1}): 1630s, 1604s, 577w, 467w.

MS (ESI+): m/z 926(10), 713(10), 677(20), 515(50), 497(100), 464(20), 299(10), 279(20), 250(15).

22.2. Bis[bis(trimethylsilyl)amido] iron (II) **59**



A Schlenk tube was charged with 0.30 g (1.0 mmol) of $\text{FeCl}_2(\text{THF})_2$ in 20 ml of diethylether. To this suspension was added 2.1 ml (2.0 mmol) of $\text{KN}(\text{SiMe}_3)_2$ (1 M in THF), the colour of solution changes immediately to pale green, and the mixture was stirred for 12 hours at 0°C. Solvent was removed under reduced pressure, and the brown-green residue was extracted with pentane (2x10 ml). The red solution was filtered and the filtrate was taken to dryness leaving a dark oil that was distilled using a Kugelrhor apparatus at 110°C / 10⁻² mmHg, affording 0.33 g (87 %) of product as a green-yellow oil. This oil solidified to a green-yellow solid in the freezer.

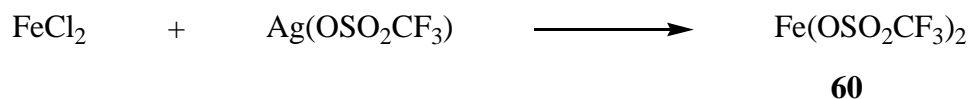
UV-Vis (THF, 200-800 nm): 272.

IR (KBr film, 4000-400 cm⁻¹): 2958m, 1445w, 1257s, 1410 (sh), 1051s, 937s, 839s, 825m, 783w, 665m.

MS (ESI+): *m/z* 898(20) [2M + 2 THF]⁺, 651(100), 471(30), 307(10).

Elemental analysis (CHN): calculated for C₁₂H₃₆FeN₂Si₄: C 38.27, H 9.63, N 7.44. Found: C 17.40, H 4.17, N 0.90.

22.3. Bistriflate iron(II) $\text{Fe}(\text{OSO}_2\text{CF}_3)_2$ **60**

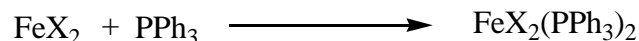


A 75 ml Schlenk tube was charged with 0.3 g (2.4 mmol) of anhydrous FeCl_2 in 20 ml of THF under argon. To this suspension was added 1.2 g (4.8 mmol) of silver trifluoromethanesulfonate, a white precipitate formed immediately (AgCl). The upper yellowish solution was filtered, and the solvent was evaporated under reduced pressure giving a yellow solid. The obtained yellow solid was washed with diethylether (3 x 10 ml) and dried under vacuum affording 0.8 g (94 %) of a white solid.

UV –Vis (THF, 800 nm – 200 nm) : 298

IR (KBr film, 4000-400 cm⁻¹): 1235s, 1197m, 1042s, 945w, 630s, 610w (sh), 595w, 525m

22.4 Iron(II) bischloro(bistriphenylphosphine) FeCl₂(PPh₃)₂ **96 and iron(II) bisiodo(bisoxotriphenylphosphine) FeI₂(OPPh₃)₂ **97****



96 X = Cl

A 250 ml Schlenk tube was charged with 1.4 g (11.0 mmol) of anhydrous FeCl₂ and 10.5 g (40 mmol) of triphenylphosphine in 60 ml of benzene under argon. The mixture was heated to reflux for 8 hours, then filtered while hot and allowed to stand for one day at RT the upper yellow solution was take off by filtration and the precipitate colourless crystal **96** was washed with benzene and dried under vacuum. The yield of the reaction was 60 % (4.2 g). The slightly yellow crystal of FeI₂(OPPh₃)₂ **97** was isolated using the same procedure as described above for the preparation of FeCl₂(PPh₃)₂. The reaction yield in this case was of 65% (6.2 g)

FeCl₂(PPh₃)₂ **96** : colourless crystals (60% yield)

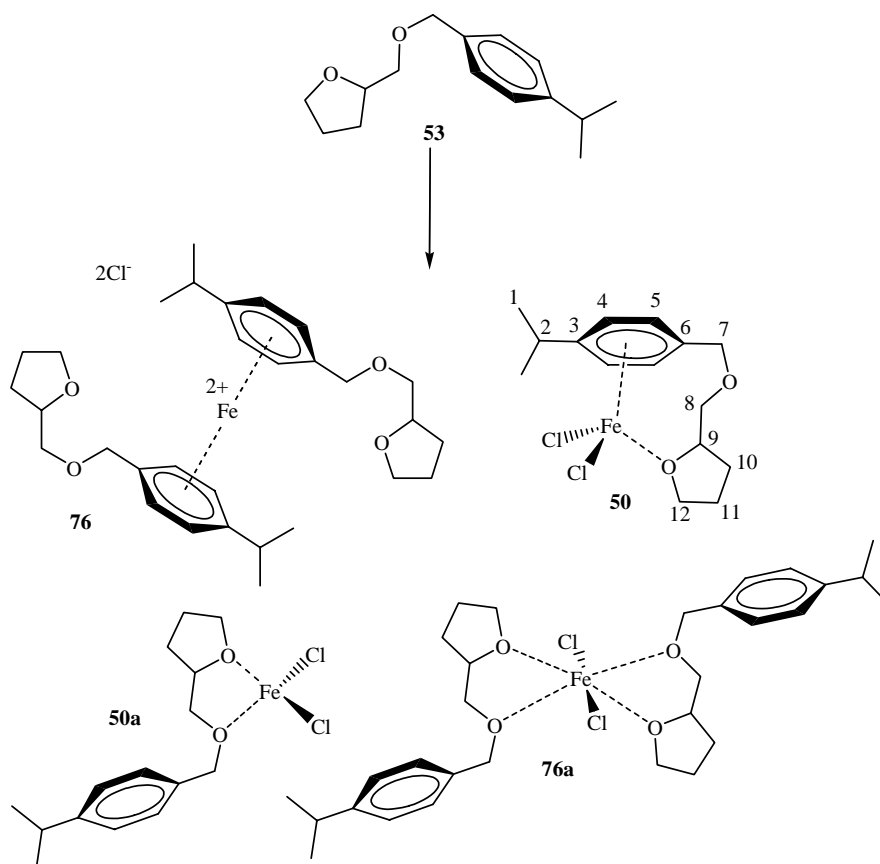
UV-Vis (THF, 200-800 nm): 328

IR (KBr film, 4000-400 cm⁻¹) : 3050m, 1601w, 1480s, 1462vs, 1250m, 1240m, 1120m, 1095vs, 1020s, 1009s, 990w,790vs, 720vs, 520vs, 490vs, 450m.

Elemental analysis (CHN): calculated for C₃₆H₃₀Cl₂FeP₂ : C 66.39, H 4.67. Found: C 68.20, H 4.80.

Iron benzyletherfuran complex

23. Iron (II) bischloro-2-(4-isopropyl-benzyloxymethyl)-tetrahydrofuran (**50**)



To a solution of FeCl_2 (0.11 g, 0.9 mmol) or $\text{FeCl}_2(\text{THF})_2$ (0.25 g, 0.9 mmol) in 15 ml of THF under argon atmosphere was added a solution of benzyletherfuran **53** (0.1 g, 0.4 mmol) in 5 ml of THF. The reaction mixture was allowed to reflux over 8 hours. After reaction cooled at RT, the yellowish solution was filtered through Celite and the solvent was removed in vacuum to give **50** (0.22 g, 60 %) as a yellow oil.

$^1\text{H-NMR}$ (360 MHz, CD_2Cl_2): δ 7.24 – 7.18 (*br m*, 4H, HC(4, 5)), 4.89 (*br*, 1H, HC(7, 9)), 4.30 (*br*, 1H, HC(9, 7)), 2.95 (*br*, 1H, HC(8, 12)), 2.20 (*br m*, 3H, HC(8, 11, 12)), 1.27 (*d*, $J = 3.5$, 6H, $\text{H}_3\text{C}(1, 2)$).

$^{13}\text{C-NMR}$ (91 MHz, CD_2Cl_2): δ 148.1 C(4), 138.2 C(9), 128 (C(5, 6)), 125.8 (C(7, 8)), 75.1 C(12), 72.2 C(11), 70 (C(15, 10)), 33.3 C(3), 29.2 C(14), 23.5 – 23.4 (C(1, 2, 13)).

UV-VIS (THF, 230-800 nm): 369, 324, 281, 237.

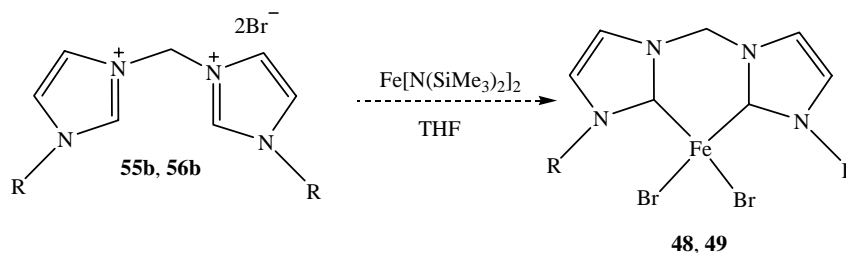
IR (NaCl film, 4000–400 cm^{-1}): 2960s, 2930s, 2875s, 1601m, 1461m, 1364w, 1042m, 876m, 820m.

MS (ESI+): m/z 594(100) [**76**]⁺, 559 [**76** - Cl]⁺, 491 [**76** - 103]⁺, 432 [**50** + THF]⁺, 360(70) [**50**]⁺, 270 [FeCl₂(THF)₂]⁺.

**Synthesis of iron(II) complexes by direct metallation of
bisimidazolium salts**

24. Synthesis of iron(II) complexes by direct metallation of bisimidazolium salts

24.1. Direct metallation of bisimidazolium salts with $\text{Fe}[\text{N}(\text{SiMe}_3)_2]_2$



Methylene Bis(N-Mesityl)bisimidazol-2-ylidene iron bromide **49**

A 75 ml Schlenk tube was charged with 0.11 g (0.3 mmol) of $\text{Fe}[\text{N}(\text{SiMe}_3)_2]_2$ and 0.16 g, (0.3 mmol) of bisimidazolium salt **56b** under argon atmosphere. To this mixture was introduced via cannula 20 ml of cold ($-78\text{ }^\circ\text{C}$) THF and the reaction mixture was stirred at this temperature for 24 hours. Then the temperature was allowed to RT for additionally 48 hours; the colour of solution changes from orange to red purple and a white-yellowish solid precipitate. The upper red purple solution was filtered through Celite and treated by addition of 3 x 10 ml of pentane, which provoke the precipitation of beige solid (0.12 g). The white solid residue that precipitated during the reaction was washed with THF and pentane then dissolved in CH_2Cl_2 (green solution). Evaporation of dichloromethane under vacuum affords orange-yellow oil (50 mg).

UV – Vis (THF, 200-800 nm) : 360, 320

MS (ESI+) : m/z 1041(30), 856(40), 793(30), 717(30), 606 (100) [M-8], 379(40)

Elemental analysis (CHN): calculated for $\text{C}_{25}\text{H}_{28}\text{Br}_2\text{FeN}_4$: C 50.03, H 4.70, N 9.34. Found C 43.26, H 4.99, N 6.96.

Residue: **UV - Vis** (CH_2Cl_2 , 200-800 nm) : 300, 222

Methylene bis(N-2,6-diisopropylphenyl)bisimidazol-2-ylidene iron bromide **48**

A 75 ml Schlenk tube was charged with 0.2 g (0.5 mmol) of $\text{Fe}[\text{N}(\text{SiMe}_3)_2]_2$ and 0.32 g, (0.5 mmol) of bisimidazolium salt **55b** under argon atmosphere. To this mixture was introduced via cannula 20 ml of cold (-78 °C) THF and the reaction mixture was stirred at this temperature for 6 hours. Then the upper red solution was filtered and the solvent evaporated in vacuum to give 0.14 g of orange solid. Another attempt of the reaction was performed at 0°C for 48 hours. After filtration of upper solution and evaporation of THF, an orange solid similarly to that as described above was isolated.

UV-Vis (THF, 200-800 nm) : 358, 322

MS (ESI+) : m/z 1347(10), 1076(15), 1032(10), 1000(5), 968(70), 844(10), 701(20), 685(100), 643(70), 337(15), 301(10).

Synthesis of methylene bis(N-mesityl)bisimidazol-2-ylidene iron bromide **49** in the presence of NaH (^tBuOK 5%)

A 75 ml Schlenk tube was charged with 0.11 g (0.3 mmol) of $\text{Fe}[\text{N}(\text{SiMe}_3)_2]_2$ and 0.16 g, (0.3 mmol) of bisimidazolium salt **56b** under argon atmosphere. To this mixture was introduced via cannula 20 ml of cold (-78 °C) THF and the reaction mixture was stirred at this temperature for 1 hours. Then 40 mg (1.7 mmol) of NaH and 10 mg (0.05 mmol) of ^tBuOK were added, the colour of solution changes rapidly from yellow to red-purple after addition of mineral base. The reaction mixture was allowed to RT and stirred at this temperature overnight, the mixture is still red – purple and, there is a precipitate in solution. After that, the upper solution was filtered through the Celite and treated as previously by addition of pentane affording a yellowish solid (0.16 g) after drying under vacuum. The white solid residue that was formed during this reaction was washed with THF and pentane, then analysed by elemental analysis where no carbon was detected in sample. Probably it is an inorganic product; in fact, it was well soluble in water.

49, UV – Vis (THF, 200-800 nm) : 350, 268

MS (ESI+): m/z 1088(100), 840(50), 794(40), 776(20), 748(20), 621(40), 569(40), 423(70)

Elemental analysis (CHN): calculated for $\text{C}_{25}\text{H}_{28}\text{Br}_2\text{FeN}_4$: C 50.03, H 4.70, N 9.34. Found C 39.58, H 5.12, N 7.54.

Synthesis of methylene bis(N-mesityl)bisimidazol-2-ylidene iron bromide **49** by one pot reaction

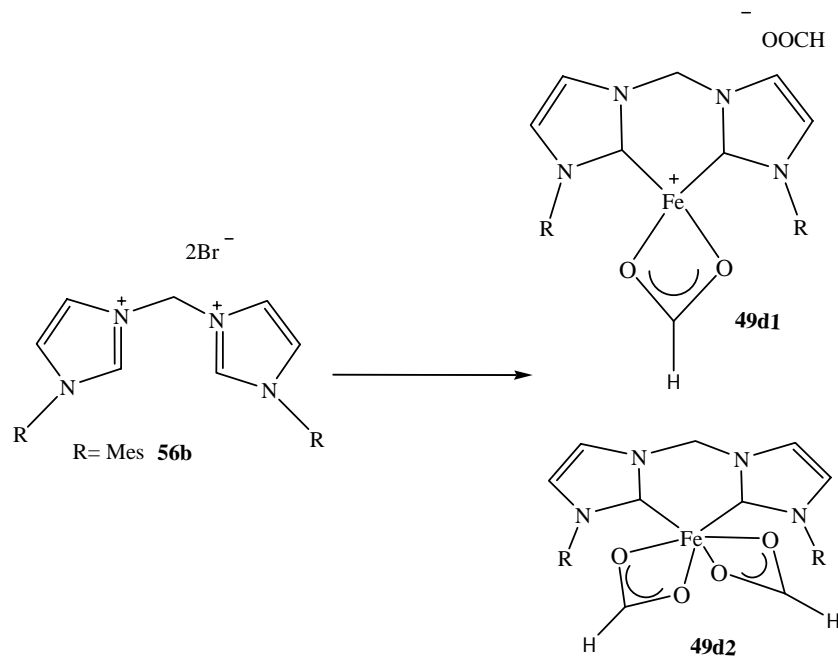
A 75 ml Schlenk tube was charged with 0.27 g (1.0 mmol) of $\text{FeCl}_2(\text{THF})_2$, 0.55 g, (1.0 mmol) of bisimidazolium salt **57b** and 20 ml of THF under argon atmosphere. The reaction mixture was cooled at $-10\text{ }^\circ\text{C}$ followed by dropwise addition of 2.1 ml (2.1 mmol) of $\text{KN}(\text{SiMe}_3)_2$ (1.0 mol in THF), the colour of solution change immediately to slightly green. The reaction mixture was allowed to warm to RT for 48 hours. After that, the red-brown upper solution was recovered by filtration through the celite and the solvent was evaporated under vacuum affording a red-brown solid (0.29 g).

UV-Vis (THF, 200-800 nm) : 360, 320

MS (ESI+) : 1241(40), 1044(30), 968(40), 818(100), 657(80), 401(90)

Single crystal of 85: Colourless crystals of **85** were obtained in THF at RT.

24.2. Direct metallation of bisimidazolium salts with $\text{Fe}(\text{OOCH})_2 \cdot 2\text{H}_2\text{O}$



Synthesis of methylene bis(N-mesityl)bisimidazol-2-ylidene iron formiate **49d1**

A 75 ml Schlenk tube was charged with 20 ml of THF, 0.20 g (0.4 mmol) of bisimidazolium salt **56b** and 0.13 g (0.7 mmol) of $\text{Fe}(\text{OOCH})_2 \cdot 2\text{H}_2\text{O}$ which was overnight dried at $100\text{ }^\circ\text{C}$

under vacuum. The resulting suspension was cooled to -10 °C, then 35 mg (0.7 mmol) of NaH 60% and 4 mg (0.04 mmol) of ^tBuOK were added. The temperature of reaction was allowed to warm slowly, at 0 °C the colour of solution changes to yellow. Stirring was continued for 72 hours at RT and the solution become red. The mixture was filtered and the solvent evaporated affording 0.18 g of red-brown solid. This product was washed and extracted with 4 x 10 ml of pentane, and then the solvent was evaporated yielding 130 mg of yellow solid.

¹³C APT NMR (125 MHz, THF-d₈): 172.1, 171.1, 163.6, 163.3, 162, 150, 144, 143.6, 133.8, 133.2, 132.5, 132.1, 130.6, 129.8, 129.7, 127.8, 127.7, 61.7, 59.3, 58, 57.3, 50.4, 48.4, 45, 21.4, 19.5, 19.4, 19.

UV – Vis (THF, 200–800 nm) : 453, 358, 283

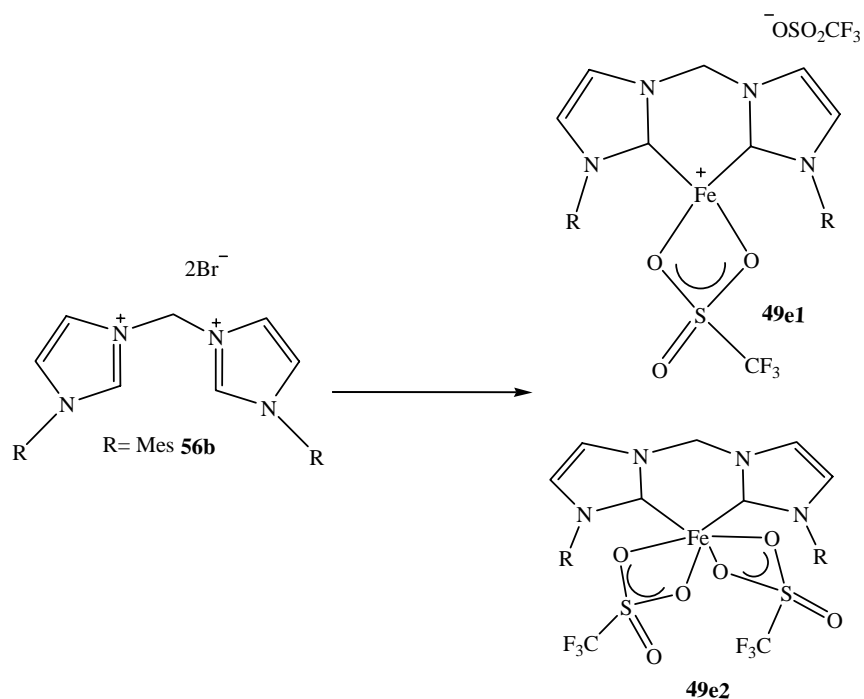
IR (KBr film, 4000–400 cm⁻¹): 3578w, 3518w, 2980vs, 2687w, 2250w, 2050w, 1910w, 1682s, 1452s, 1364m, 1182s, 1059vs, 914vs, 669w.

MS (ESI+): *m/z* 950(10), 850(110), 643(45), 421(30), 421(30), 373(50), 316(50), 288(70).

MS (FAB): *m/z* 421(10), 332(10), 187(100), 136(20)

Elemental analysis (CHN): calculated for C₂₇H₃₀FeN₄O₄ : C 61.14, H 5.70, N 10.56. Found: C 66.75, H 6.68, N 10.31.

24.3. Direct metallation of bisimidazolium salts with $\text{Fe}(\text{OSO}_2\text{CF}_3)_2$



Synthesis of methylene bis(N-Mesityl)bisimidazol-2-ylidene iron triflate **49e1**

A 75 ml Schlenk tube was charged with 20 ml of THF, 0.20 g (0.36 mmol) of bisimidazolium salt **56b** and 0.13 g (0.36 mmol) of $\text{Fe}(\text{OSO}_2\text{CF}_3)_2$ under argon. The resulting suspension was cooled to $-78\text{ }^\circ\text{C}$, then 35 mg (0.72 mmol) of NaH 60% and 4 mg (0.04 mmol) of ${}^t\text{BuOK}$ were added. The temperature of reaction was slowly warming up, at $-10\text{ }^\circ\text{C}$ the colour of solution turned from yellow to orange. Stirring was continued for 1 hour, then the mixture was filtered and the solvent evaporated under vacuum affording 0.20 g of orange-yellowish solid.

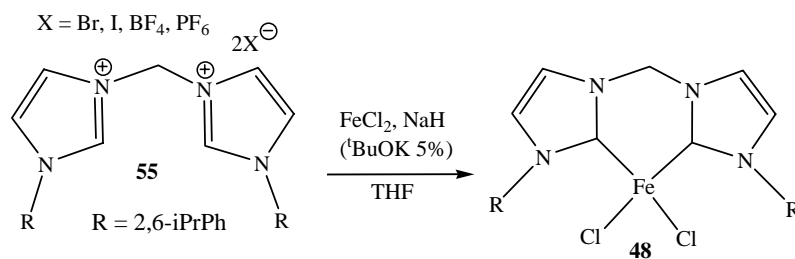
${}^{13}\text{C}$ APT NMR (500 MHz, THF-d_8): 177, 176.7, 164.4, 162.6, 160.7, 152.6, 142.4, 140.9, 139.8, 137.6, 136.1, 132.6, 131, 130.2, 126.4, 125.2, 68.8, 61, 57.6, 21.7, 21.6, 18.5, 18.1, 18, 17.9.

UV-Vis (THF, 200-800 nm): 374

IR (KBr film, $4000\text{--}400\text{ cm}^{-1}$): 1636w, 1283s, 1256s, 1163s, 1032s, 639s

MS (ESI⁺): m/z 968(40), 780(60), 585(100)

24.4. Synthesis of bisimidazol-2-ylidene via “*in situ*” deprotonation reactions



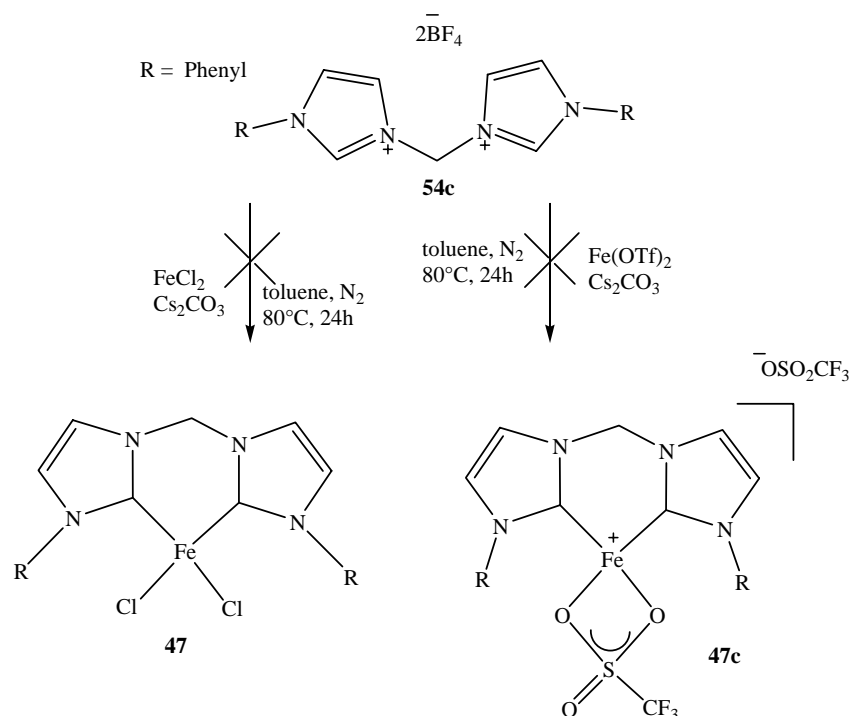
Synthesis of **48** via “*in situ*” deprotonation with NaH (^tBuOK) as base

A typical procedure was the following: A 75 ml Schlenk tube was charged with 20 ml of THF, 0.20 g (1 mmol) of bisimidazolium salt **55b** and 0.13 g (1 mmol) of FeCl₂ under argon. To the resulted suspension was added 97 mg (2 mmol) of NaH 60% and 12 mg (0.1 mmol) of ^tBuOK at RT. The reaction mixture was stirred at RT for 96 hours. After filtration and evaporation of the solvent, a red-brown solid was isolated.

UV-Vis (THF, 200-800 nm) : 300 - 298 nm

MS (ESI+) : *m/z* 682(5), 499(10), 469(100), 333(10), 229(60)

Synthesis of **47** and **47c** via “*in situ*” deprotonation with Cs₂CO₃ as base

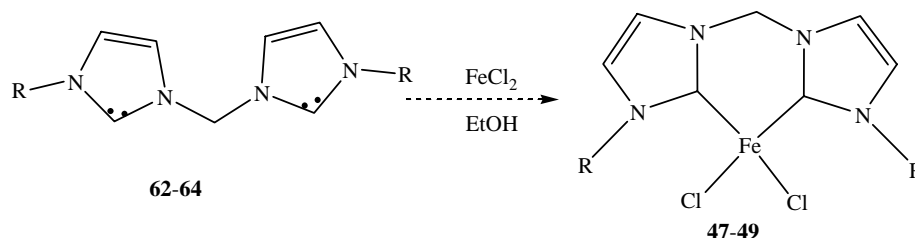


A general procedure was the following: A 75 ml Schlenk tube was charged with 20 ml of toluene, 0.29 g (0.6 mmol) of bisimidazolium salt **54b** and 0.08 g (0.6 mmol) of FeCl₂ or 0.21 g (0.6 mmol) of Fe(OSO₂CF₃)₂ under argon. To the resulted suspension was added 1.37 g (4.2 mmol) of Cs₂CO₃ at RT. Then the reaction mixture was heated at 80°C for 24 hours. After cooling the reaction to RT, the solution was filtered and the solvent was evaporated under vacuum yielding the starting bisimidazolium salt.

Reaction of free biscarbene with iron(II) precursors

25. Reaction of free biscarbene with FeX_2 and modified $\text{FeX}_2(\text{THF})_2$ ($\text{X} = \text{Br}, \text{Cl}$)

25.1. Reaction in ethanol: typical procedure



In a 75 ml Schlenk tube, the FeCl_2 (0.17 mg, 1.3 mmol) was dissolved in 10 ml of ethanol, the formed slightly yellow solution was immediately added under argon to the freshly prepared carbene **62** (0.30g, 1.0 mmol). The mixture was then stirred for 12 hours at RT, and then the dark solution was filtered through Celite followed by evaporation of the solvent under vacuum. The obtained solid was extracted several times with 10 ml of THF and the solvent was evaporated to yield a brown solid. This solution was stored at room temperature in order to crystallize.

47 : Brown solid

UV-Vis (THF, 200-800 nm) : 359, 318

MS (ESI+): m/z 970(10), 802(50), 733(10), 685(100)

48 : brown solid

UV-Vis (THF, 200-800 nm) : 362, 294

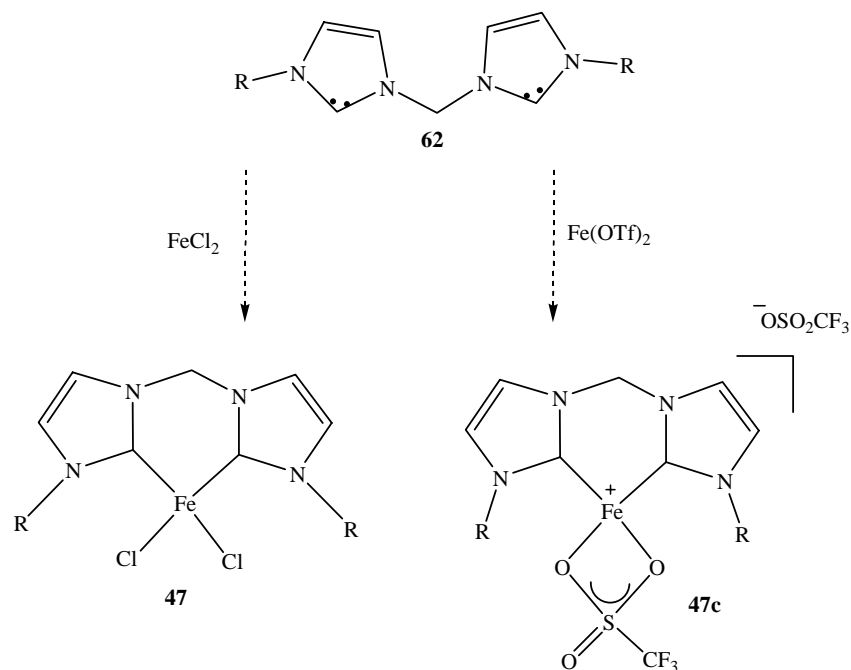
MS (ESI+) : m/z 1344(5), 1315(5), 1262(50), 1182(50), 993(40), 912(100), 668(40), 640(70), 505(40).

49: brown solid

UV-Vis (THF, 200-800 nm): 362, 312

Single X-ray crystals: Attempt to crystallise **47** in DMSO permitted the isolation of red – brown crystals of **88** over 24 hours. Crystals of **89** were isolated as brown-red from the crystallisation attempt of **48** in DMF after 72 hours. The crystallisation attempt of **48** in THF allows to the isolation of ionic complex **90** as oranges crystals.

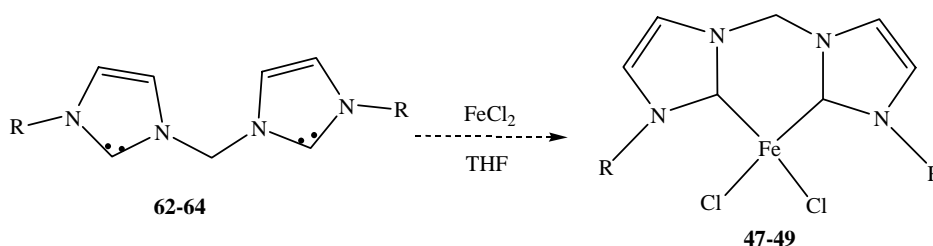
25.2. Reaction in toluene



The reactions were done in Schlenk tube under argon atmosphere. To a solution of FeCl_2 (0.13 g, 1.0 mmol) or $\text{Fe}(\text{OTf})_2$ (0.35 g, 1.0 mmol) in 20 ml of toluene was added at RT, a freshly solution of bis-carbene **62** (0.30 g, 1.0 mmol) in the same solvent. The obtained suspension was heated to 80°C overnight, a solution was red coloured. After cooling down to RT, the solution was filtered through a Celite and the solvent was removed under vacuum affording brown-red oil in both cases (0.37 g of **47** and 0.43 g of **47c**).

47, 47c : UV-Vis (THF) : 298 nm, 242 nm

25.3. Reaction in tetrahydrofuran



The reaction of free biscarbene **62-64** with FeCl_2 was done at different temperatures (-10°C , RT, 67°C) in THF, a typical procedure is the follow: To a solution of FeCl_2 (0.13 g, 1.0 mmol) in 20 ml of THF was added a freshly solution of biscarbene **63** (0.47 g, 1.0 mmol) in the same solvent. The obtained suspension was stirred for 48 hours at adequate temperature (-10°C , RT or 67°C). After warming up or cooling down to RT, the solution was filtered through a Celite and the solvent was removed under vacuum affording brown solid.

48I: reaction at RT, brown solid, 0.48 g (82 % yield)

$^{13}\text{C-NMR}$ (125 MHz, CD_3CN): δ 140.4, 139.1, 132.4, 128.9, 126.6, 125.8, 21.1, 19.4

UV-Vis (THF, 200-800 nm): 363, 316

MS (ESI+): m/z 1149(10), 1095(50), 1041(10), 1014(70), 785(5), 584(10), 421(5), 401(5), 385(100).

48II: reaction at -10°C , brown solid (62 % yield)

$^{13}\text{C-NMR}$ (125 MHz, CD_3CN): δ 168.0, 167.8, 147.8, 140.3, 131.0, 130.6., 125, 122.0, 29.5, 28.8, 26.0, 25.9, 25.7

UV-Vis (THF, 200-800 nm): 36, 316

MS (FAB): m/z 669(2), 634(2), 548, 500(10), 470(40) $[\text{M}+1-\text{FeCl}_2]^+$, 428, 348, 310(5), 242(30), 229(100), 213(109), 154(15), 91(10).

48III: reaction at 67°C , red solid (70 % yield)

UV-Vis (THF, 200-800 nm): 362, 298

49I : reaction at RT, brown solid, 0.34 g (67 % yield)

¹³C-NMR (91 MHz, THF-*d*₈): δ 179.7, 163.1, 153.1, 149.5, 147.7, 142.6, 138.2, 135.4, 133.5, 133, 129.6, 125.1, 123.4, 118.6, 31.2, 29.2, 23.5

UV-Vis (THF, 200-800 nm) : 364, 295, 237

IR (NaCl film, 4000 – 400 cm⁻¹) : 2963s, 2921 sh, 2869 sh, 1679m, 1494s, 1461s, 1364m, 1324w, 1181w, 1106w, 1061s, 964w, 932w, 806m, 762m, 670w.

MS (ESI+): *m/z* 879(10), 650(10), 584(10), 513(100), 421(50), 385(70) [M-FeCl₂]⁺, 256(10), 193(80).

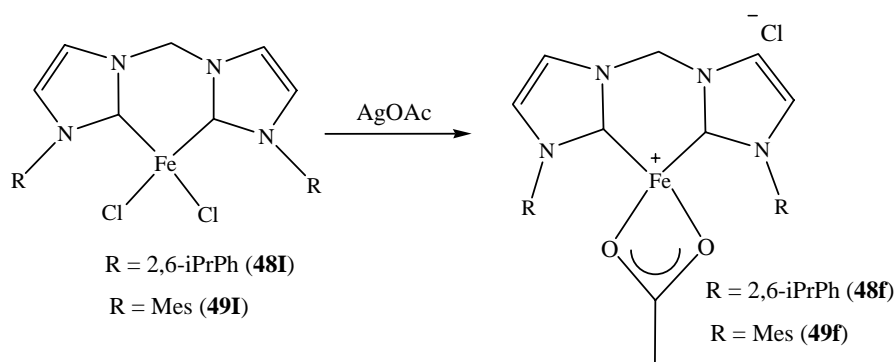
47 : reaction at RT, brown solid (58 % yield)

UV-Vis (THF, 200-800 nm) : 365, 295, 239

MS (ESI+) : *m/z* 1671(10), 1545(10), 1364(30), 1238(30), 1220(30), 1064(30), 1046(30), 919(10), 901(80), 745(20), 597(20), 443(100), 301(30).

26. Synthesis of iron(II) containing bisimidazol-2-ylidene and carboxylate ligands

Reaction of complex **48I** and **49I** with one equivalent of silver acetate



To a solution of **48I** (0.30 g, 0.51 mmol) or **49I** (0.26 g, 0.5 mmol) in 20 ml of THF was added at RT one equivalent of silver acetate (0.08 g, 0.5 mmol), which led to immediate precipitation of a white solid. The orange clear solution was filtered through a Celite and the solvent was evaporated under vacuum yielding orange solids **48f** and **49f**.

48f: orange solid, 0.29 g (94 % yield)

UV-Vis (THF, 200-800 nm) : 368, 300

IR (KBr, 4000 – 400 cm^{-1}): 2965s, 2872 sh, 1682m, 1597m, 1439m, 1111w, 1061w, 806w, 758w, 664w.

MS (ESI+): m/z 968(10), 805(70), 728 $[\text{M}+2\text{THF}]^+$, 469 $[\text{M}-\text{FeOAc}]^+$, 457 (10).

49f: orange-yellowish stick solid, 0.12 g (42 % yield)

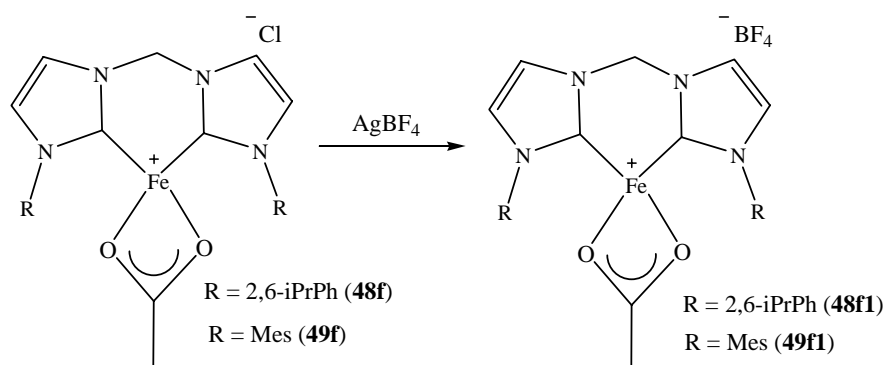
UV-Vis (THF, 200-800 nm): 359

IR (KBr, 4000–400 cm^{-1}): 2965s, 2872w, 1680w, 1632s; 1640 sh; 1453m, 1115w, 1061w, 808w, 760w, 666w, 617w.

MS (ESI+): m/z 1210(5), 1060(5), 984(70), 833(10), 805(40), 677(50), 513(30), 499(100) $[\text{M}-\text{Cl}]^+$, 485(10).

Elemental analysis (CHN), calculated for $\text{C}_{35}\text{H}_{46}\text{FeN}_4\text{O}_4$: C 65.42, H 7.22, N 8.72; Found : C 53.81, H 5.93, N 7.35.

Counter anion exchange in complexes **52f** and **53f**



To a solution of **48f** (0.31 g, 0.5 mmol) or **49f** (0.27 g, 0.5 mmol) in 20 ml of THF at RT was added 0.08 g (0.5 mmol) of silver tetrafluoroborate which led to immediate precipitation of a white solid. The upper orange yellowish solutions were filtered through the Celite and the solvent was evaporated under vacuum yielding orange solids **48f1** and **49f1**.

48f1 : orange solid, 0.20 g (60 % yield)

UV-Vis (THF, 200-800 nm): 360

IR (KBr, $4000 - 400 \text{ cm}^{-1}$): 2967s, 2948 sh, 2876 sh, 1637m, 1523m, 1464m, 1390w, 1074vs, 806w, 762w, 671w, 523w.

MS (ESI+): m/z 984(10), 830(15), 752(20), 728(15) $[\text{M} + 2\text{THF}]^+$, 565(100), 469(20) $[\text{M} - \text{FeOAc}]^+$.

MS (ESI-) : m/z 197(10) $[2\text{BF}_4 + 23]$, 87(100) $[\text{BF}_4]$.

49f1 : reaction at RT, orange-yellowish stick solid, 0.15 g (51 % yield)

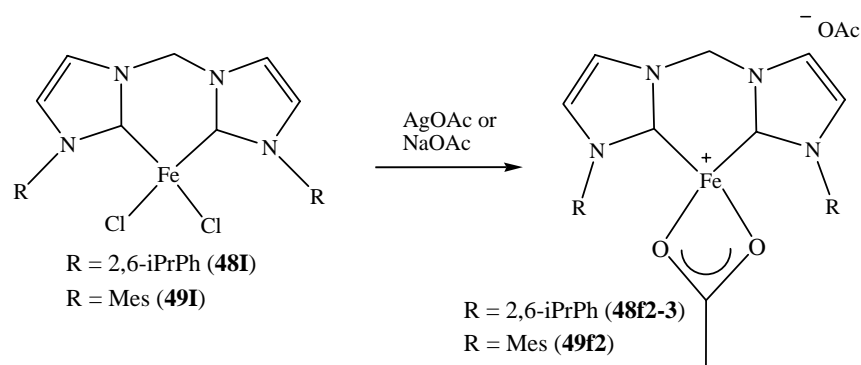
UV-Vis (THF, 200-800 nm): 360

IR (KBr, $4000 - 400 \text{ cm}^{-1}$): 2966s, 2872 sh, 1682 sh, 1636m, 1516m, 1464m, 1390w, 1071vs, 808w, 762w, 671w.

MS (ESI+) : m/z 1210(10), 984(50), 892(10), 805(10), 739(10), 708(20), 513(20), 499(100) $[\text{M} - \text{BF}_4]$, 481(20), 229(30).

MS (ESI-) : m/z 197(50) $[2\text{BF}_4 + 23]$, 87(100) $[\text{BF}_4]$.

Reaction of complex **48I** and **49I** with two equivalents of silver- or sodium acetate



A typical procedure is the follow : To a solution of **48I** (0.18 g, 0.3 mmol) in 20 ml of THF was added at RT two equivalents of silver acetate (0.10 g, 0.6 mmol) or sodium acetate (0.05 g, 0.6 mmol). The reaction was first stirred at RT for 8 hours then heated at 67°C for additionally 8 hours. The orange clear solutions were filtered through the Celite and the solvent was evaporated under vacuum yielding orange solids **48f2** and **48f3**.

48f2: reaction with AgOAc at RT, orange solid, 0.05 g (27 % yield)

$^{13}\text{C NMR}$ (125 MHz, THF- d_8): δ 163.3, 153.3, 147.8, 142.7, 138.4, 133, 131.1, 125.2, 123.5, 118.7, 68.8, 31.3, 29.5, 28.9, 25.1, 24.3, 23.5

UV-Vis (THF, 200-800 nm) : 340, 272, 267, 236

IR (KBr, 4000–400 cm^{-1}): 2963s, 2927s, 1686w, 1601s, 1442s, 1385w, 1061w, 807m, 761w, 671w.

MS (ESI+): m/z 968(5), 950(5), 740(15), 728(100) $[\text{M}+2\text{THF}]^+$, 481(10), 469(50) $[\text{M}-\text{FeOAc}]^+$, 457(10), 243(5), 229(10).

Elemental analysis (CHN), calculated for $\text{C}_{29}\text{H}_{34}\text{FeN}_4\text{O}_4$: C 62.37, H6.14, N 10.03; Found : C49.97, H 6.74, N 7.59.

48f3: reaction with NaOAc at RT, orange solid, 0.08 g (43 % yield)

$^1\text{H-NMR}$ (500 MHz, THF- d_8): δ 8.96–5.57 (*br*), 3.52 (*br*), 2.96 (*br*), 2.70–1.90 (*br*), 1.70 (*br*), 1.21(*br*).

$^{13}\text{C-NMR}$ (125 MHz, THF- d_8): δ 148.3, 142.7, 138.9, 138.5, 133, 131.1, 118.6, 31.4, 29.6, 29, 23.5

UV-Vis (THF, 200-800 nm): 362, 286, 268, 235

IR (KBr, 4000–400 cm^{-1}): 2964s, 2870 sh, 1686s, 1626w, 1602s, 1494m, 1495m, 1442s, 1365m, 1107w, 1061s, 964w, 936w, 807m, 761m, 670w.

MS (ESI+): m/z 968(10), 728(100) $[\text{M}+2\text{THF}]^+$, 499(10), 469(50) $[\text{M}-\text{FeOAc}]^+$, 457(10)

Elemental analysis (CHN), calculated for $\text{C}_{35}\text{H}_{46}\text{FeN}_4\text{O}_4$: C 65.42, H7.22, N 8.72; Found : C53.81, H 5.93, N 7.35.

49f2 : reaction at RT, orange solid, 0.08 g (43 % yield)

UV-Vis (THF, 200-800 nm): 350, 275.

$^1\text{H-NMR}$ (500 MHz, THF-d_8): δ 9.16–5.52 (*br*), 4.00–1.00(*br*).

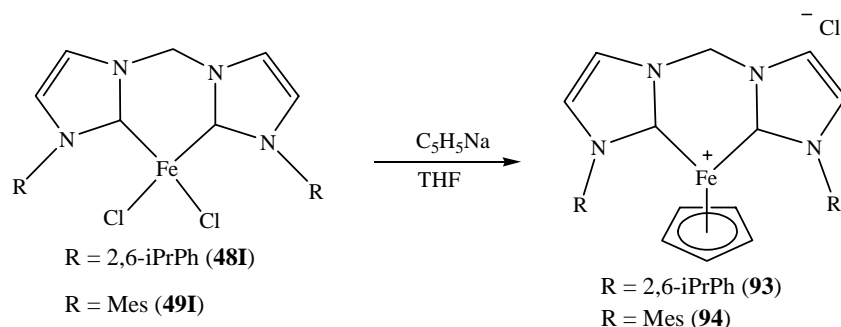
$^{13}\text{C-NMR}$ (125 MHz, THF-d_8): δ 147.9, 140, 134.9, 131, 125, 122.8, 31.4, 29.6.

IR (KBr, 4000–400 cm^{-1}): 2968s, 1680s, 1632m, 1598m, 1413m, 1110w, 1060s, 935w, 765w.

MS (ESI+): m/z 1210(5), 984(60), 719(20), 708(10), 565(50), 513 $[\text{M}+14]$, 485(30).

Elemental analysis (CHN), calculated for $\text{C}_{29}\text{H}_{36}\text{FeN}_4\text{O}_4$: C 65.15, H6.47, N 10.00; Found : C63.34, H 7.28, N 8.49.

27. Synthesis of iron(II) containing cyclopentadienyl ligands



To a solution of **48I** (0.31 g, 0.5 mmol) or **53I** (0.27 g, 0.5 mmol) in 20 ml of THF was added at -78°C one equivalent (0.4 ml, 0.6 mmol) of sodium cyclopentadienyle (solution 2M in THF) and the mixture was allowed to warm to RT. The stirring of reaction mixture was continued at RT for 8 hours. Then the solution was filtered and the solvent removed under reduced pressure yielding orange yellow solid. In order to remove some ferrocene which could be formed during the reaction, the obtained solid was washed several times with pentane then dried under vacuum affording an orange-yellowish solids **93** (0.20 g, 68 %) and **94** (0.16 g, 60 %).

93 : orange yellow solid (68% yield)

¹H-NMR (500 MHz, CD₂Cl₂) : δ 7.45 (*m*, 2H, HC (5, 9)), 7.28 (*d*, J = 7.5, 2H, HC(8, 10)), 7.20 (*br s*, 1H, HC(4)), 6.98 (*s*, 1H, HC(15)), 4.62 (*s*, 5H, Cp), 2.41 (*hept*, J = 6.8, 2H, HC(13, 14)), 1.14 (*d*, J = 6.8, 12H, HC(15-18)).

¹³C-NMR (125 MHz, CD₂Cl₂): δ 164.7 C(2), 161.8 C(2), 146.9 (C(7, 11)), 138.8 C(6), 133.4 C(9), 130.1 C(4), 129.5 C(5), 124.1 (C(8, 10)), 122 C(12), 68.3 Cp, 28.5 (C(13, 14)), 24.5 (C(15-18)).

UV-Vis (THF, 200-800 nm) : 420, 365, 324

MS (ESI+): *m/z* 1185(5), 1046(10), 861(40), 775(60), 730(30), 499(100), 469(70) [M-FeCp]⁺, 235(80).

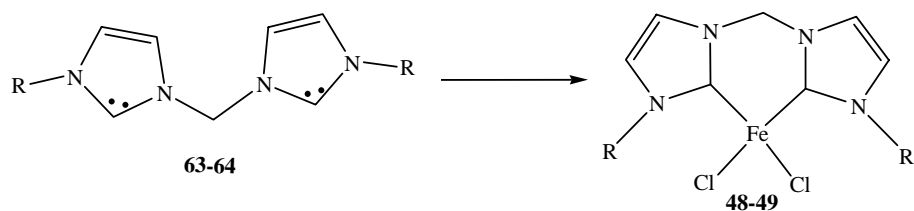
94 : orange yellowish solid (60% yield)

¹H-NMR (500 MHz, CD₂Cl₂): δ 7.08 (*s*, 1H, HC(4)), 6.87 (*s*, 3H, HC(8, 10, 12)), 6.13 (*s*, 1H, HC(5)), 3.72 (*s*, 4H, Cp), 1.76 (*s*, 3H HC(13)), 1.44 (*s*, 6H, HC(13, 14)).

¹³C-NMR (125 MHz, CD₂Cl₂): δ 138.9 (C(7, 11)), 136.1 (C(9)), 134.8 C(6), 130.9 C(5), 129.7 (C(8, 10)), 120.3 (C(5)), 68.9 Cp, 21.5 C(15), 17.8 (C(14, 13)).

UV-Vis (THF, 200-800 nm): 402, 357, 297

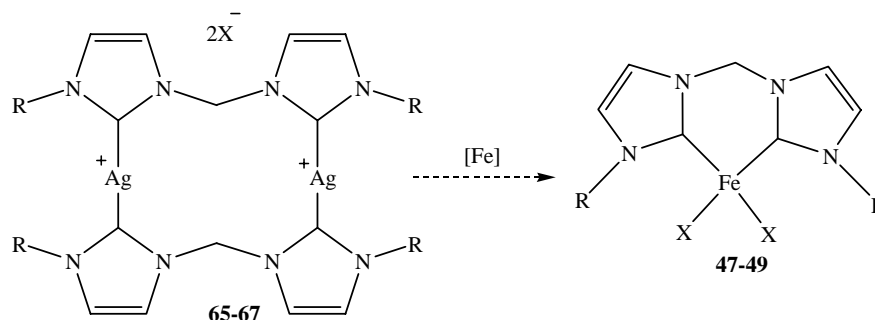
28. Reaction of free biscarbene imidazole-2-ylidenes **63** and **64** with $\text{FeCl}_2(\text{PPh}_3)_2$



To a solution of $\text{FeCl}_2(\text{PPh}_3)_2$ (0.19 g, 0.2 mmol) in 20 ml of toluene was added at RT, a freshly prepared solution of biscarbene **63** (0.19 g, 0.4 mmol) or **64** (0.15 g, 0.4 mmol) in the same solvent. The obtained solution was stirred at RT overnight. The yellow-brown solution was filtered and the solvent was evaporated under vacuum, affording brown-yellowish solid in both cases. These solids were washed several times with toluene in order to remove the PPh_3 released during the reaction and dried in vacuum affording brown-yellow solids. The UV – Vis spectra of these compounds show singular absorption between 320 nm and 324 nm.

Transmetallation reactions

29. Transmetallation reaction of silver complexes 65-67 with iron(II) in different solvents



29.1. Transmetallation in dichloromethane at RT

The general procedure was the followed: To a RT solution of silver complex **66b** (0.26 g, 0.2 mmol) in 20 ml of THF was added 0.05 g (0.4 mmol) of FeCl₂, and the reaction mixture was stirred for 48 hours. During this time, a grey yellowish solid (AgBr) formed and the colour of the solution becomes slightly yellow. The upper yellow solution was filtered and the solvent was evaporated under vacuum yielding a green yellow solid **48IV** (0.21 g, 90 %). The same procedure was used for a reaction of FeCl₂ with silver complexes **67b**.

48IV : green-yellow solid, 0.21 g (90 % yield)

¹H-NMR (360 MHz, CD₂Cl₂): δ 8.47 (*br*), 7.55 – 7.08 (*m br*), 2.23 (*br*), 1.20 (*br*).

¹³C-NMR (91 MHz, CD₂Cl₂): 148, 146.1, 133.2, 131.2, 126, 108.6, 54.7, 31.9, 30.5, 25.8

UV-Vis (THF, 200-800 nm) : 362, 317

MS (ESI⁺): *m/z* 499(5), 469(60) [M-FeCl₂]⁺, 347(5), 333(10), 243(10), 229(100), 213(10).

49II : green-yellow solid (87 % yield)

UV-Vis (THF, 200-800 nm): 359, 311, 266

MS (ESI⁺): *m/z* 1594(10), 1314(5), 1034(60), 753(40), 547(5), 473(100), 400(5).

29.2. Transmetallation in THF

Reaction at RT. The general procedure was the followed: To a RT solution of silver complex **65b** (0.1 g, 0.1 mmol) in 20 ml of THF was added 0.03 g (0.2 mmol) of FeCl₂, and the reaction mixture was stirred for 48 hours. During this time, a grey yellow solid formed and the colour of the solution became slightly yellow. The upper yellow solution was filtered and the solvent was evaporated under vacuum yielding an orange solid **47I** (0.08 g, 94 %). The same procedure was used for a reaction of FeCl₂ with silver complexes **66** and **67**.

47I : orange solid, 0.08 g (94 % yield)

¹H-NMR (360 MHz, (Acetone-d₆): δ 7.94-7.79 (*br*), 1.30 (*br*), 1.20 (*br*), 0.87 (*br*).

UV-Vis (THF, 200-800 nm) : 364, 295, 241

MS (ESI+): *m/z* 460(10), 298(100), 298(100), 294(30), 200(10), 136(90), 107(60).

48V : red - brown solid (94 % yield)

¹³C-NMR (91 MHz, THF-d₈): δ 145.6, 139.9, 130.1, 125, 120.9, 62.7, 27.5, 26.5, 21.6, 14.0

UV-Vis (THF, 200-800 nm): 358, 315

MS (ESI+): *m/z* 1128(10), 879(20), 511(100), 469(35) [M-FeCl₂]⁺, 347(10), 229(10).

IR (KBr, 4000–400 cm⁻¹) : 2967s, 1633w, 1545m, 1462m, 1375m, 1308w, 1188s, 1111w, 1065w, 863w, 808w, 758m, 671w, 617w, 555w, 459w.

49III : orange solid (94 % yield)

UV-Vis (THF, 200-800 nm): 365, 310

MS (ESI+): *m/z* 1130(20), 1023(10), 990(10), 850(5), 465(100) [Ligand+Br], 421(20), 385(10) [M-FeBr₂], 358(10).

48VIII : brown solid, reaction done with FeBr₂ as iron source (50 % yield)

¹H-NMR (360 MHz, THF-d₈): δ 8.00–7.36 (*br*), 3.62 (*br*), 2.52–2.31 (*br*), 2.09 (*s br*), 1.76 (*s br*)

¹³C-NMR (91 MHz, THF-d₈): δ 147.5, 135.5, 133.2, 129.3, 98.5, 98.3, 98.1, 46.1, 45.6, 45.3, 37.2, 32.3, 30.2

UV-Vis (THF, 200-800 nm): 367, 295.

MS (ESI+): m/z 1130(20), 1023(10), 990(10), 850(5), 465(100) [Ligand+Br], 421(20), 385(10) [M-FeBr₂], 358(10).

Elemental analysis (CHN): calculated for C₃₁H₄₀Br₂FeN₄ : C 54.41, H 5.89, N 8.19; found : C 61.68, H 7.79, N 6.49.

Reaction at reflux. The general procedure is followed: To a solution of silver complex **66a** (0.70 g, 0.5 mmol) in 20 ml of THF was added 0.13 g (1 mmol) of FeCl₂ at RT, and the reaction mixture was heated at 67°C for 24 hours. The precipitated silver salt was removed by inverse filtration and the solvent was evaporated in vacuum yielding an orange solid **48VI** (1.11 g, 94%). The same procedure was used for a reaction of FeBr₂(THF)₂ with silver complexes **66b**.

48VI : orange solid, 1.11 g (94 % yield)

¹³C-NMR (91 MHz, THF-d₈): δ 158.4, 146.4, 142, 133.9, 132.9, 131.6, 126.7, 69, 37.8, 35.4, 27.6, 26.8

UV-Vis (THF, 200-800 nm) : 363, 315.

MS (ESI+): m/z 603(2), 587, 490, 468(10), 307(20), 154(90), 136(100), 77(70).

Single crystals for X-Ray analysis. Orange crystals of ionic complex **98a** were obtained by slow diffusion of toluene into the THF solution of isolated orange yellow solid **48VI**. The UV-Vis spectra of crystals dissolved in THF shows two similar absorptions as **48VI** at 365 nm and 315 nm.

48VII : orange-yellowish solid, 90 % yield from the reaction of **66b** with FeBr₂(THF)₂ .

UV-Vis (THF, 200-800 nm): 364, 318

MS (ESI+): m/z 866(10), 726(10), 682(20), 598(20), 551(90) [Ligand+MeOH] [ligand+Br], 526(60), 499(100), 469(20), 243(30).

Elemental analysis (CHN): calculated for C₃₁H₄₀Br₂FeN₄ : C 54.41, H 5.89, N 8.19; found : C 43.03, H 4.84, N 5.78.

Single crystals for X-Ray analysis. Orange crystals of ionic complex **98b** were obtained by slow diffusion of diethylether into the THF solution of isolated orange yellow solid **48VII**.

29.3. Reaction of silver tetrafluoroborate and hexafluorophosphates complexes **66d-e** and **67c-d** with iron (II)

The general procedure is followed: To a RT solution of silver complex **66d** (0.53 g, 0.4 mmol) in 20 ml of THF was added 0.17 g (0.8 mmol) of FeBr₂, and the reaction mixture was stirred for 48 hours. During this time, a beige clear solid formed and the colour of the solution became yellow-brownish. The solution was filtered and the solvent was evaporated under vacuum yielding 0.19 mg of brown solid **48IX**. The same procedure was used for a reaction of FeCl₂ with silver complexes **66e**.

48IX : brown solid, 0.19 g.

¹³C-NMR (91 MHz, THF-d₈): 149.6, 146.5, 133.5, 131.5, 130.7, 126.2, 32.4, 30.7

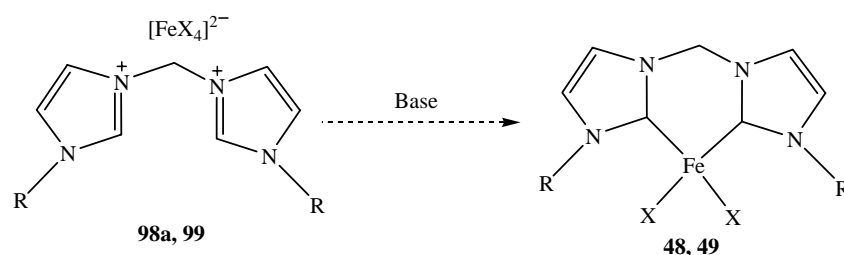
UV-Vis (THF, 200-800 nm) : 385, 320

MS (ESI+): *m/z* 1832(100), 1407(10), 1195(30), 1089(10), 873(60), 557(80), 469(20) [M-FeBr₂]⁺.

Elemental analysis (CHNS) : calculated for C₃₁H₄₀Br₂FeN₄ : C 54.41, H 5.89, N 8.19; found : C 62.10, H 7.53, N 6.92.

Single crystals for X-Ray analysis. Orange crystals of ionic complex **98c** were obtained by slow diffusion of diethylether into the THF solution of isolated brown- yellow solid **48IX**.

30. Deprotonation of bisimidazolium iron tetrahalides complexes



30.1. Deprotonation with sodium hydride (NaH)

Reaction at RT. The general procedure is followed: To a solution of silver complex **98a** (0.34 g, 0.5 mmol) or **99** (0.29 g, 0.5 mmol) in 20 ml of THF was added 0.09 g (2.3 mmol) of NaH 60% and 0.01 g (0.1 mmol) of ^tBuOK at 0°C. The reaction mixture was allowed warm up to RT for 48 hours. The solution was filtered and the solvent was evaporated under vacuum yielding a yellow brown solid in both cases. The UV-Vis spectrum of product isolated from the complex **98a** shows two absorptions at 360 nm and 315 nm and that of the product isolated from the complex **99** shows singular absorption at 292 nm.

Reaction at reflux. The general procedure is followed: To a solution of silver complex **98a** (0.34 g, 0.5 mmol) in 20 ml of THF was added 90 g (2.3 mmol) of NaH 60% and 0.01 g (0.1 mmol) of ^tBuOK, and the reaction mixture was heated at 67 °C for 8 hours. The resulted solution was filtered and the solvent was evaporated under vacuum yielding an orange solid.

UV-Vis (THF, 200-800 nm) : 364, 290

MS (ESI+): *m/z* 1846(30), 1794(30), 1743(10), 1202(40), 1150(25), 880(15), 854(10), 557(100), 505(10), 469(10), 243(25).

Single crystals for X-Ray analysis. Some yellow crystals of **100** were obtained by slow diffusion of diethylether into a THF solution of isolated orange solid.

30.2. Deprotonation of complex with lithium bases (^tBuLi, MeLi and ⁿBuLi)

Reaction with *tert*-butyllithium

To a solution of silver complex **98a** (0.34 g, 0.5 mmol) in 20 ml of THF was added 1.7 ml (2.5 mmol) of ^tBuLi (1.5 M in pentane) at -78 °C, and the reaction mixture was allowed to warm up to 0°C . The stirring of the reaction mixture was continued at this temperature for 4 hours. The obtained yellow brown solution was again cooled down to -78°C and filtered at this temperature. Then, the solvent was evaporated under vacuum yielding 0.14 g (47 %) of yellow brown solid **48**.

UV-Vis (THF, 200-800 nm) : 240

MS(ESI+): *m/z* 780(5), 722(20), 692(100), 669(5), 614(5), 600(5), 557(5), 499(5), 493(5), 410(40), 243(10), 231(10).

MS(FAB): *m/z* 1133(50), 1071(10), 785(30), 491(50), 293(30), 197(100).

Reaction with methyllithium

To a solution of silver complex **98a** (0.34 g, 0.5 mmol) or **99** (0.29 g, 0.5 mmol) in 20 ml of THF was added 1.6 ml (2.5 mmol) of MeLi (1.6 M in hexane) at -78 °C, and the reaction mixture was allowed to warm up to RT. The stirring of the reaction was continued at RT for 12 hours. The yellow brown solution was filtered and the solvent was evaporated under vacuum to give yellow brown solids in both cases. Then, the obtained solids were extracted with 3 x 10 ml of toluene and the solvent was removed under vacuum. 0.15 g (51%) of **48** and 0.14 g (56%) of **49** were obtained as yellow-brown solids for both complexes.

48 : yellow-brown solid

¹³C-NMR (125 MHz, THF-d₈): δ 194.2, 179.1, 168.5, 152.7, 139, 135.8, 132.5, 128.7, 127.9, 125.9, 124.3, 122.6, 121.1, 65.1, 26.3, 24, 22.7, 20.3

UV-Vis (THF, 200-800 nm) : 437, 371, 240

MS (ESI+): *m/z* 1138(10), 910(70), 821.4(5), 726(5), 712(5), 682(100), 551(10), 526(15), 499(70), 469(10) [M-FeCl₂]⁺.

MS(FAB): m/z 871, 707, 642, 535(95), 385(100) $[M-FeCl_2]^+$, 357(20), 187(95), 154(80).

Elemental analysis (CHN): calculated for $C_{31}H_{40}FeN_4$: C 54.41, H 5.89, N 8.19. Found : C 51.81, H 5.88, N 6.95.

49 : yellow-brown solid

^{13}C -NMR (125 MHz, THF- d_8): δ 169.4, 153.3, 146.5, 140.1, 135.7, 133.9, 131.7, 129.2, 127.1, 37.5, 31.8, 31.1, 30.1, 27.0

UV-Vis (THF, 200-800 nm) : 470, 363, 287

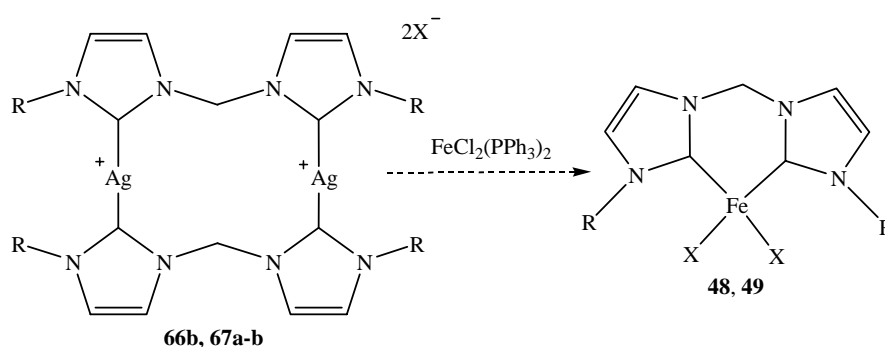
IR(KBr, 4000-400 cm^{-1}) : 3435s, 2968vs, 2874sh, 1626m, 1549m, 1377m, 1308w, 1190s, 1069s, 860w, 808w, 758m, 673w, 617w, 523w, 453w.

MS (ESI+): m/z 698(5), 499(10), 385(100) $[M-FeCl_2]^+$, 275(5), 229(5), 193(10).

MS(FAB): m/z 871, 707, 642, 535(95), 385(100) $[M-FeCl_2]^+$, 357(20), 187(95), 154(80).

Elemental analysis (CHN): calculated for $C_{25}H_{28}FeN_4$: C 50.03, H 4.70, N 9.34. Found : C 49.69, H 6.16, N 6.25.

31. Reaction of silver complexes with $FeCl_2(PPh_3)_2$



To a solution of silver complex **66b** (0.13 g, 0.1 mmol) or **67b** (0.12 g, 0.1 mmol) in 20 ml of THF was added 0.19 g (0.2 mmol) of $FeCl_2(PPh_3)_2$ at RT. Then the reaction mixture was heated to 67°C until the formation of a green solid in both cases. The upper colourless solution was filtered and the remained green solid was washed with 3 x 10 ml of toluene in order to remove the released PPh_3 , and dried under vacuum to yielding uncharacterized green solids in both cases. Indeed, these solids were insoluble in common organic solvent such as hexane, toluene, xylene, DMSO, methanol and chloroform.

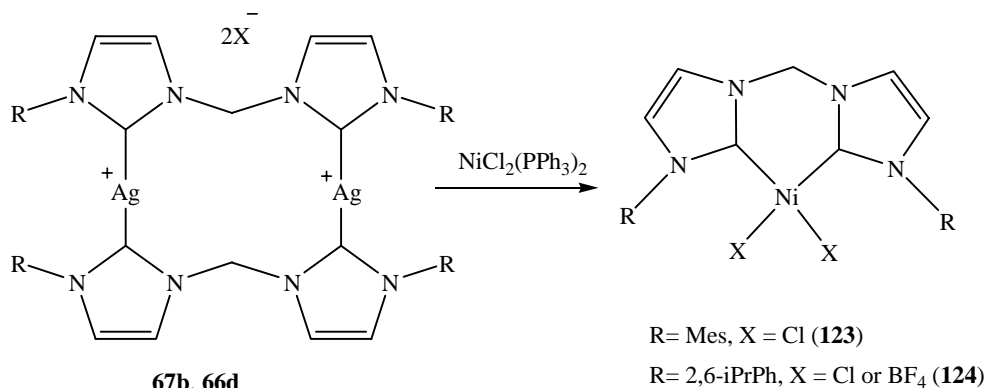
48 :

MS (FAB) : m/z 1021(5), 983(5), 819(10), 649(5), 491(10), 369(60), 262(20), 183(20), 77(45).

49 :

MS (FAB) : m/z 902, 785(20), 635(20), 491(50), 385(30), 197(100).

32. Transmetalation reaction of silver complexes 66d and 67b with NiCl₂(PPh₃)₂



The general procedure was the followed: To a RT solution of silver complex **67b** (0.50 g, 0.4 mmol) in 20 ml of dichloromethane was added 0.58 g (0.9 mmol) of $\text{NiCl}_2(\text{PPh}_3)_2$, and the reaction mixture was stirred for 8 hours. During this time, a yellowish solid formed and the colour of the solution becomes green. The upper green solution was take-off by filtration and the remained yellow solid was washed with 2 x 20 ml of benzene or toluene. Then, the resulted yellow solid was dissolved in 10 ml of methanol and filtrate over Celite. After evaporation of the solvent under vacuum, a yellow solid **48IV** was isolated (0.21 g, 90 %). The same procedure was used for a reaction of $\text{NiCl}_2(\text{PPh}_3)_2$ with silver complexes **67b**, in this case we isolated an red-brown solid **124** in 76% of yield.

123 :

¹H-NMR (360 MHz, MeOH- d_4): δ 8.33 (*br*), 7.92 (*br*), 7.14 (*br*), 6.98 (*br*), 2.35 (*br*), 2.08 (*br*).

¹³C-NMR (91 MHz, MeOH- d_4): 171.7, 142.3, 135.5, 135.3, 134.9, 134.2, 131.6, 21.1, 18.7

UV-Vis (MeOH, 200-900 nm) : 769, 529, 441, 374, 319

MS (ESI+): m/z 513(100) $[\text{M}+1]^+$, 385(80) $[\text{M}+1-\text{NiCl}_2]^+$, 273(10)

124 :

¹³C-NMR (125 MHz, MeOH): 172.7, 147, 139.6, 135.3, 131.7, 130.3, 126.1, 124.8, 82.5, 30.1, 24.6, 24.5

UV-Vis (THF, 200-900 nm): 385, 257

MS (ESI+): m/z 659(60), 633(30), 507(100), 469(85) $[\text{M}+1-\text{NiCl}_2]^+$

Catalytic reactions

33. Catalytic reactions

33.1. General procedures for catalytic hydrogenation reactions

In a dry 75ml Schlenk tube stopped with a septum, was placed a precatalyst source (0.5–1 mmol) in 10-20 ml of solvent under argon atmosphere. Then a substrate (1–1.5 mmol) was added and the mixture was set under 2-3 bar hydrogen pressure, followed by addition of activator reagent (1-10 equivalents). The evolution of catalytic reaction could be analysed by taking some aliquot from the reaction mixture via a septum stopper without pressure release. At the end of the reaction, the mixture was filtered over Alox, the solvent was evaporated under reduced pressure, and the residue was analysed by GC-MS.

In situ generation of precatalyst

In a dry 75 ml Schlenk tube equipped with a septum, were placed the ligand (0.1 mmol), the iron (II) source (0.1 mmol) in 10 ml of solvent under argon atmosphere a RT. The mixture was stirred for 10 minutes, and then 5-50 mmol of substrate was added. The mixture was set under 3 bar hydrogen pressure and the activator reagent (1- 5 equivalents) was added. At the end of the reaction, the mixture was filtered over Alox, the solvent was evaporated under reduced pressure, and the residue was analysed by GC-MS.

34.2. General procedure for polymerization of olefins

In a dry Schlenk tube was placed the precatalyst (0.1–1.0 mmol) in 10 ml of toluene under butadiene or ethylene pressure. Then the activator (1-500 equivalents) was added and the reaction mixture was stirred under substrate pressure. At the end of the reaction, the solution was treated with 5 ml of ethanol/HCl and the solvent was filtered off. In some cases, the resulted material was washed with 2x10 ml of methanol under ultrasound bath in order to remove some catalyst impurities. The resulted material was dried under vacuum.

VI. Annexes

Table 1a.

Identification code	54a	55a	55b	55e
Empirical formula	C ₂₀ H ₂₂ I ₂ N ₄ O {[(C ₁₉ H ₁₈ N ₄)I ₂](CH ₃ OH)}	C ₃₁ H ₄₂ I ₂ N ₄ O {[(C ₃₁ H ₄₂ N ₄)(I ₂)](C ₄ H ₈ O)}	C ₃₃ H ₄₆ C ₁₆ N ₄ {[(C ₃₁ H ₄₀ N ₄)C ₁₂](CH ₂ Cl ₂) ₂ }	C ₃₁ H ₄₂ F ₁₂ N ₄ P ₂ {[(C ₃₁ H ₄₂ N ₄)(PF ₆) ₂]}
Crystal colour	Colourless	Colourless	colourless	brown
Crystal size (mm)	0.50 x 0.50 x 0.50	0.300 x 0.167 x 0.100	0.50 x 0.40 x 0.20	0.500 x 0.500 x 0.500
Crystal system	Triclinic	triclinic	Triclinic	monoclinic
Space group	P -1	P -1	P -1	C 2/c
a(Å)	7.171(2)	9.6892(13)	10.0502(9)	15.846(2)
b(Å)	9.673(5)	14.820(2)	12.5316(10)	23.728(2)
c(Å)	16.350(7)	14.0051(17)	15.7139(14)	9.8341(10)
α(°)	91.80(6)	109.814(9)	78.108(10)	90
β(°)	92.09(4)	90.449(10)	75.886(10)	101.948(10)
γ(°)	103.76(5)	96.601(11)	86.840(10)	90 deg.
Volume(Å ³)	1099.9(8)	1877.1(4)	1878.1(3)	3617.5(7)
Z	2	2	2	4
D _{cal} (g/cm ³)	1.776	1.310	1.258	1.397
Linear Absorption coef. (mm ⁻¹)	2.876	1.700	0.485	0.210
F(000)	568	740	748	1576
θ min. and max. (°)	2.17 to 25.82	1.55 to 29.25	1.93 to 25.91	1.57 to 29.21
Reflections collected/unique	8459/3908	23832/10034	14826/6791	19224/4857
Refinement method	Full-matrix	Full-matrix	Full-matrix	Full-matrix
Final R indices [I>2σ(I)]	R ₁ = 0.0466, wR ₂ = 0.1228	R ₁ = 0.0582, wR ₂ = 0.1153	R ₁ = 0.0637, wR ₂ = 0.1624	R ₁ = 0.0569, wR ₂ = 0.1398
R indices all data	R ₁ = 0.0567, wR ₂ = 0.1274	R ₁ = 0.1732, wR ₂ = 0.1395	R ₁ = 0.0851, wR ₂ = 0.1732	R ₁ = 0.1074, wR ₂ = 0.1573
Goodness-of-fit on F ²	1.080	0.722	0.963	0.939

Table 2a.

Identification code	87	89	90	95a
Empirical formula	C ₅₂ H ₆₄ C ₁₉ Fe ₂ N ₈ {[(C ₂₅ H ₃₀ N ₄) ₂ (Fe ₂ Cl ₅)](CH ₂ Cl ₂) ₂ }	C ₁₈ H ₄₂ C ₁₆ Fe ₃ N ₆ O ₇ {[Fe(CHON(CH ₃) ₂) ₆](Fe ₂ OCl ₆)}	C ₃₅ H ₅₀ C ₁₆ Fe ₂ N ₄ O {[C ₃₁ H ₄₀ N ₄][(FeCl ₃) ₂ O](C ₄ H ₈ O)}	C ₃₆ H ₃₀ Cl ₂ FeP ₂ {FeCl ₂ [P(C ₆ H ₅) ₃] ₂ }
Crystal colour	Colourless	orange	yellow	colourless
Crystal size (mm)	0.300 x 0.217 x 0.050	0.30 x 0.20 x 0.15	0.40 x 0.20 x 0.10	0.150 x 0.117 x 0.100
Crystal system	Monoclinic	Trigonal	Monoclinic	Monoclinic
Space group	P 21/c	R -3	P 21/n	P 2/c
a(A)	a = 13.969(5)	13.9872(15)	10.3775(17)	11.7657(9)
b(A)	14.467(3)	13.9872(15)	26.8249(19)	8.1320(4)
c(A)	14.909(4)	15.766(2)	15.9889(19)	17.0986(13)
α(°)	90	90	90	90
β(°)	103.29(2)	90	108.675(15)	106.397(6)
γ(°)	90	120	90	90
Volume(A ³)	2932.3(14)	2671.2(5)	4216.6(9)	1569.43(19)
Z	2	2	4	2
D _{cal} (g/cm ³)	1.395	1.038	1.391	1.378
Linear absorp. coef. (mm ⁻¹)	0.946	1.132	1.103	0.777
F(000)	1274	856	1832	672
θ min. and max. (°)	1.99 to 25.00	2.12 to 25.94	2.03 to 25.96	1.80 to 25.12
Reflections collected/unique	24252/5131	3927/1155	23909/8062	15172/2796
Refinement method	Full-matrix	Full-matrix	Full-matrix	Full-matrix
Final R indices [I>2σ(I)]	R1 = 0.1050, wR2 = 0.2627	0.0582, wR2 = 0.1478	R1 = 0.0562, wR2 = 0.1254	R1 = 0.0300, wR2 = 0.0812
R indices all data	R1 = 0.1694, wR2 = 0.2977	R1 = 0.1081, wR2 = 0.1719	R1 = 0.2092, wR2 = 0.1834	R1 = 0.0336, wR2 = 0.0829
Goodness-of-fit on F ²	0.974	0.890	0.577	1.047

Table 3a.

Identification code	97	66c	66d
Empirical formula	C ₃₆ H ₃₀ FeI ₂	C ₇₂ H ₉₀ Ag ₂ Cl ₃₂ N ₈ {[Ag ₂ (C ₃₁ H ₄₀ N ₄) ₂ Cl ₂](CHCl ₃) ₁₀ }	C ₆₈ H ₈₉ Ag ₂ B ₂ F ₈ N ₁₁ {[Ag ₂ (C ₃₁ H ₄₀ N ₄) ₂ (BF ₄) ₂](CH ₃ CN) ₃ }
Crystal colour	Colourless	colourless	colourless
Crystal size (mm)	0.150 x 0.117 x 0.100	0.50 x 0.50 x 0.40	0.500 x 0.500 x 0.500
Crystal system	Triclinic	Monoclinic	triclinic
Space group	P 1	P 21/n	P-1
a(Å)	a = 10.0872(15)	15.6288(14)	12.1064(6)
b(Å)	10.2361(13)	22.641(2)	12.9427(7)
c(Å)	10.6629(16)	16.4951(13)	13.5753(7)
α(°)	65.517(10)	90	101.477(4)
β(°)	62.801(10)	115.477(9)	108.780(4)
γ(°)	89.460(11)	90	106.445(4)
Volume(Å ³)	868.9(2)	5269.2(8)	1830.24(16)
Z	1	2	1
D _{cal} (g/cm ³)	1.655	1.524	1.315
Linear Absorption coef. (mm ⁻¹)	2.333	1.224	0.601
F(000)	424	2432	750
θ min. and max. (°)	2.24 to 29.21	2.26 to 25.84	1.67 to 29.52
Reflections collected/unique	9092/7303	37569/9695	35985/10159
Refinement method	Full-matrix	Full-matrix	Full-matrix
Final R indices [I > 2σ(I)]	R1 = 0.0457, wR2 = 0.0833	R1 = 0.0756, wR2 = 0.2054	R1 = 0.0469, wR2 = 0.1364
R indices all data	R1 = 0.0885, wR2 = 0.0922	R1 = 0.1046, wR2 = 0.2209	R1 = 0.0504, wR2 = 0.1388
Goodness-of-fit on F ²	0.816	1.042	1.066

Table 4a.

Identification code	67c	67d	98a
Empirical formula	C ₅₃ H ₆₂ Ag ₂ B ₂ Cl ₆ F ₈ N ₈ {[Ag ₂ (C ₂₅ H ₂₈ N ₄) ₂ (BF ₄) ₂](CH ₂ Cl ₂) ₃ }	C _{52.50} H ₆₂ Ag ₂ Cl ₅ F ₁₂ N ₈ O _{0.50} P ₂ {[Ag ₂ (C ₂₅ H ₂₈ N ₄) ₂ (PF ₆) ₂](CH ₂ Cl ₂) _{2.5} (H ₂ O) _{0.5} }	C ₃₁ H ₄₂ Cl ₈ Fe ₂ N ₄ [(C ₃₁ H ₄₀ N ₄)(FeCl ₄) ₂]
Crystal colour	Colourless	colourless	yellow
Crystal size (mm)	0.50 x 0.50 x 0.50	0.50 x 0.50 x 0.50	0.50 x 0.50 x 0.50
Crystal system	Triclinic	Monoclinic	Monoclinic
Space group	P -1	P 21/n	C 2/c
a(Å)	13.6983(9)	12.4927(8)	14.6803(12)
b(Å)	14.1097(10)	15.8191(12)	25.0403(14)
c(Å)	18.5774(14)	33.0342(18)	11.2759(9)
α(°)	87.798(6)	90	90
β(°)	72.497(5)	94.778(7)	101.292(9)
γ(°)	68.332(5)	90	90
Volume(Å ³)	3171.7(4)	6505.6(7)	4064.8(5)
Z	2	4	4
D _{cal} (g/cm ³)	1.480	1.527	1.415
Linear Abs. coef. (mm ⁻¹)	0.934	0.932	1.266
F(000)	1428	3016	1776
θ min. and max. (°)	1.68 to 29.51	2.08 to 26.11	2.24 to 25.96
Reflections collected/unique	43978/17509	50610/12607	14033/3946
Refinement method	Full-matrix	Full-matrix	Full-matrix
Final R indices [I>2σ(I)]	R1 = 0.0726, wR2 = 0.1813	R1 = 0.0720, wR2 = 0.2095	R1 = 0.0447, wR2 = 0.1205
R indices all data	R1 = 0.1142, wR2 = 0.2009	R1 = 0.0771, wR2 = 0.2192	R1 = 0.0556, wR2 = 0.1257
Goodness-of-fit on F ²	1.082	1.073	1.039

Table 5a

Identification code	98b	98c	100
Empirical formula	C ₃₁ H _{43.50} Br ₁₆ Fe ₄ N ₁₆ O _{0.75} {[FeBr ₄ (C ₃₁ H ₄₂ N ₄)](H ₂ O) _{0.75} }	C ₉₈ H ₁₄₈ B ₄ Br ₄ F ₁₆ Fe N ₁₂ O {[(FeBr ₄ (C ₃₁ H ₄₂ N ₄) ₃ (BF ₄) ₄] ₂ (H ₂ O) ₁₁ }	C ₆₀ H ₈₀ Cl ₂ FeN ₈ [FeCl ₂ (C ₁₅ H ₂₀ N ₂) ₄]
Crystal colour	Yellow	orange	colourless
Crystal size (mm)	0.500 x 0.283 x 0.150	0.250 x 0.167 x 0.050	0.250 x 0.200 x 0.150
Crystal system	Orthorhombic	Monoclinic	Triclinic
Space group	P n m a	C 2/c	P -1
a(Å)	9.3270(6)	20.691(3)	8.877(2)
b(Å)	20.635(2)	62.608(5)	12.628(3)
c(Å)	20.0849(15)	20.231(3)	13.810(4)
α(°)	90	90	74.68(2)
β(°)	90	118.073(11)	74.48(2)
γ(°)	90	90	83.105(18)
Volume(Å ³)	3865.6(5)	23124(5)	1436.7(6)
Z	4	8	1
D _{cal} (g/cm ³)	3.702	1.375	1.202
Linear Abs. coef. (mm ⁻¹)	18.076	1.597	0.400
F(000)	4046	9904	556
θ min. and max. (°)	1.97 to 29.49	1.16 to 22.28	1.58 to 29.21
Reflections collected/unique	49502/5500	59859/14578	21258/7748
Refinement method	Full-matrix	Full-matrix	Full-matrix
Final R indices [I>2σ(I)]	R1 = 0.0640, wR2 = 0.1434	R1 = 0.1430, wR2 = 0.3454	R1 = 0.0483, wR2 = 0.0679
R indices all data	R1 = 0.0898, wR2 = 0.1568	R1 = 0.3161, wR2 = 0.4288	R1 = 0.1396, wR2 = 0.0824
Goodness-of-fit on F ²	1.111	0.841	0.756

Table 6a.

Identification code	100b	77	56b	124
Empirical formula	C ₆₈ H ₁₀₀ Br ₂ FeN ₈ O ₂	C ₃₀ H ₃₀ Cl ₁₄ Fe ₉ O ₁₈	C ₂₅ H ₂₆ Br ₂ N ₄	C ₃₁ H ₄₀ Cl ₂ N ₄ Ni
Crystal colour	yellow	green	light yellow	red
Crystal size (mm)	0.50 x 0.50 x 0.50	0.50 x 0.30 x 0.20	0.45 x 0.45 x 0.30	0.30 x 0.30 x 0.30
Crystal system	Triclinic	Monoclinic	Monoclinic	Orthorhombic
Space group	P -1	P 21/n	P21/n	P 21 21 21
a(Å)	11.6710(8)	14.1021(11)	17.056	12.5536(6)
b(Å)	12.4758(9)	13.1512(7)	9.352	14.5647(11)
c(Å)	13.5759(10)	16.8828(14)	18.191	16.4897(9)
α(°)	64.464(5)	90	90	90
β(°)	81.515(6)	93.871(9)	108.35	90
γ(°)	88.982(6)	90	90	90
Volume(Å ³)	1761.8(2)	3123.9(4)	2754.1	3015.0(3)
Z	1	2	4	4
D _{cal} (g/cm ³)	1.204	1.783	1.308	1.318
Linear Abs. coef. (mm ⁻¹)	1.394	2.679	2.960	0.847
F(000)	676	1652	1096	1264
θ min. and max. (°)	1.68 to 29.27	2.12 to 25.95	2.36 to 25.95	1.87 to 25.13
Reflections collected/unique	23004/9443	24345/6043	21062/5346	32822/5365
Refinement method	Full-matrix	Full-matrix	Full-matrix	Full-matrix
Final R indices [<i>I</i> >2σ(<i>I</i>)]	R1 = 0.0348, wR2 = 0.0826	R1 = 0.0404, wR2 = 0.1001	R1 = 0.0674, wR2 = 0.1795	R1 = 0.0263, wR2 = 0.0607
R indices all data	R1 = 0.0444, wR2 = 0.0863	R1 = 0.0583, wR2 = 0.1055	R1 = 0.0979, wR2 = 0.1981	R1 = 0.0297, wR2 = 0.0615
Goodness-of-fit on F ²	1.018	1.045	1.050	1.028

VII. References

- [1] C. Elsechenbroich, A. Salzer, *Organometallics*, VCH, Germany **1992**.
- [2] a) L. S. Hegedus, *Transition Metals in the Synthesis of Complex Organic Molecules*, 2nd Edition, University Science Books, California **1999**. b) T. R. Younkin, E. F. Connor, J. L. Henderson, S. K. Friedrich, R. H. Grubbs, D. A. Bansleben, *Science* **2000**, 287, 460.
- [3] a) C. E. Carraher, *Giant Molecules*, Wiley-Interscience, New Jersey **2003**. b) C. Bolm, J. Legros, J. Le Pailh, L. Zani, *Chem. Rev.* **2004**, 104, 6217.
- [4] P. Wang, K. L. Tan, E. T. Kang, *J. Biomater Sci. Polym. Ed.* **2001**, 11, 169.
- [5] K. Russel, *J. Poly. Sci. Part A Poly. Chem.* **1995**, 33, 555.
- [6] S. M. Shrojal, R. P. Singh, *Adv. Polym. Sci.* **2004**, 169, 231.
- [7] E. T. Kang, K. L. Tan, K. Kato, Y. Uyama, Y. Ikada, *Macromolecules* **1996**, 29, 6872.
- [8] M. S. Shoichet, T. J. McCarty, *Macromolecules* **1991**, 24, 982.
- [9] a) N. hanunpanich, A. Ulman, A. malagon, Y. M. Strzhemechny, S. A. Schwarz, A. Janke, T. Kratzmueller, H. G. Braun, *Langmuir* **2000**, 16, 3557. b) N. hanunpanich, A. Ulman, A. malagon, Y. M. Strzhemechny, S. A. Schwarz, A. Janke, T. Kratzmueller, H. G. Braun, *Langmuir* **1999**, 15, 2089.
- [10] N. J. Hovestad, G. Van Koten, S. A. F. Bon, D. M. Haddleton, *Macromolecules* **2000**, 33, 4048.
- [11] W. Jakubowski, K. Matyjaszewski, *Macromolecules*, 38, 4139.
- [12] J. A. Hubell, M. Heuberger, J. Vörös, M. Textor, courses of biomaterial surfaces, ETHZ **2003**.
- [13] B. D. Ratner, A. S. Hoffman, *J. Appl Polym Sci.* **1994**, 18, 3183.
- [14] T. Richey, H. Iwata, H. Oowaki, E. Uchida, S. Matsuda, Y. Ikada, *Biomaterials* **2000**, 21, 1057.
- [15] J. G. Vos, R. J. Forster, T. E. Keyes, *Interfacial Supramolecular Assemblies*, Wiley-Interscience, England **2003**.
- [16] A. Alkan, D. Dolammaz, E. Uzum, E. Erden, *Swiss Med. WKLY* **2003**, 133, 465.
- [17] K. Ishihara, Y. Iwasaki, S. Ebihara, Y. Shindo, N. Nakabayashi, *Colloids Surf. B.* **2000**, 18, 325.
- [18] F. Garbassi, E. Occhiello, F. Polato, *J. Mater Sci.*, **1987**, 22, 207.
- [19] Gas Flam Treatment, Sherman Treaters SA **2000**.

- [20] K. L. Tan, L. L. Woon, H. K. Wong, E. T. Kang, K. G. Neoh, *Macromolecules* **1993**, 26, 2832. b) S. Edge, S. Walker, W. Feast, W. F. Pacynoto, *J. Appl. Polym. Sci.* **1993**, 47, 1075. c) T. Ogawa, H. Mukai, S. Osawa, *J. Appl Polym. Sci.* **1999**, 71, 243.
- [21] Y. L. Hsieh, M. Shinawarta, M. D. Castillo, *J. Appl Polym. Sci.* **1986**, 31, 509.
- [22] T. Kavc, W. Kern, M. F. Ebel, R. Svagera, P. Poelt, *Chem. Mater* **2000**, 12, 1053.
- [23] C. H. Bramford, J. C. Ward, *Polymer* **1961**, 22, 277.
- [24] W. Yang, B. Ranby, *Eur. Polym. J.* **1999**, 35, 1557.
- [25] N. Bühler, Course of photochemistry of polymers, University of Neuchâtel, **2000**.
- [26] a) K. Borgwarth, C. Ricken, D. G. Ebling, J. Heinze, *J. Anal. Chem.* **1996**, 356, 288. b) G. A. Somorjai, *J. Phys. Chem. B* **1998**, 102, 6225. c) G. Binnig, H. Recher, C. Gerber, E. Weibel, *Phys. Rev. Let.* **1982**, 49, 57.
- [27] G. Ssucs, *Biomaterials* **2003**, 24, 1713.
- [28] L. F. Boffa, B. M. Novak, *Chem. Rev.* **2000**, 100, 1479.
- [29] G. J. P. Britovsek, V. C. Gibson, D. F. Wass, *Angew. Chem. Int. Ed.* **1999**, 38, 428.
- [30] B. Cornils, W. A Herrmann, *Applied Homogeneous Catalysis with Organometallic Compounds*, VCH, Weinheim **1996**.
- [31] C. A. Tolman, *Chem. Rev.* **1977**, 77, 313.
- [32] S. D. Ittel, L. K. Johnson, M. Brookhart, *Chem Rev.* **2000**, 100, 1169.
- [33] A. K. Rappé, W. M. Skiff, C. J. Casewit, *Chem Rev.* **2000**, 100, 1435.
- [34] H. Hagihara, K. Tsuchikara, J. Sugiyama, K. Takeuchi, T. Shiono, *J. Polym. Sci. Part A : Polym. Chem.* **2004**, 42, 5600.
- [35] K. P. Arit, R. Binsack, U. Grogo, D. Neuray, US Patent 4 **1983**, 423, 196.
- [36] J. Y. Dong, Z. N. Wang, H. Hong, T. C. Chung, *Macromolecules* **2002**, 35, 9352.
- [37] T. C. Chung, D. Rhubright, *Macromolecules* **1994**, 27, 1313.
- [38] T. C. Chung, D. Rhubright, *Macromolecules* **1993**, 26, 3019.
- [39] T. C. Chung, D. Rhubright, *Macromolecules* **1991**, 24, 970.
- [40] T. C. Chung, W. Janvikul, *J. Organomet. Chem.* **1999**, 581, 176.
- [41] J. A. Ewen, *J. Am. Chem. Soc.* **1984**, 106, 6355.
- [42] H. Sinn, W. Kaminsky, H. J. Vollmer, R. Woldt, *Angew. Chem. Int. Ed. Engl.* **1980**, 19, 390.
- [43] H. Sinn, W. Kaminsky, , *Madv. Organomet. Chem.* **1980**, 18, 99.
- [44] F. R. W. P. Wild, L. Zsolnai, G. Huttner, H. H. Brintzinger, *J. Organomet. Chem.* **1982**, 232, 233.

- [45] W. Kaminsky, K. Küpler, H. H. Britzinger, F. R. W. P. Wild, *Angew. Chem. Int. Ed. Engl.* **1985**, 24, 507.
- [46] G. W. Coates, R. M. Waymouth, *Science* **1995**, 267, 217.
- [47] P. C. Möhring, N. J. Coville, *J. Organomet. Chem.* **1994**, 479, 1.
- [48] a) C. Pellecchia, A. Proto, P. Longo, A. Zambelli, *Macromolecul. Chem. Rapid Commun.* **1992**, 13, 277. b) C. Pellecchia, A. Proto, P. Longo, A. Zambelli, *Macromolecul. Chem. Rapid Commun.* **1991**, 12, 663.
- [49] R. Quyoum, Q. Wang, M. J. Tudoret, M. C. Baird, *J. Am. Chem. Soc.* **1994**, 116, 6435.
- [50] J. C. Flores, J. C. W. Chien, M. D. Rausch, *Organometallics* **1994**, 13, 4140.
- [51] J. C. Chien, B.-P. Wang, *J. Polym. Sci. Part A.* **1990**, 28, 15.
- [52] a) G. C. Bazan, G. Rodriguez, A. J. Ashe III, S. Al-Ahmad, C. Müller, *J. Am. Chem. Soc.* **1996**, 118, 2291. b) G. C. Bazan, G. Rodriguez, *Organometallics* **1997**, 16, 2492. c) J. S. Rogers, G. C. Bazan, C. K. Sperry, *J. Am. Chem. Soc.* **1997**, 119, 9305. d) R. W. Barnhart, G. C. Bazan, T. Mourey, *J. Am. Chem. Soc.* **1998**, 120, 1082.
- [53] R. Bauman, W. M. Davis, R. R. Schrock, *J. Am. Chem. Soc.* **1997**, 119, 3830.
- [54] F. Guérin, D. H. McCoville, J. J. Vittal, *Organometallics* **1996**, 15, 5586.
- [55] Y.-X. Chen, T. J. Marks, *Organometallics* **1997**, 16, 3649.
- [56] T. K. Woo, L. Fan, T. Ziegler, *Organometallics* **1994**, 13, 2252. b) T. K. Woo, P. M. Margl, T. Ziegler, P. E. Blöchl, *Organometallics* **1997**, 16, 3454.
- [57] L. Fan, D. Harrison, T. K. Woo, T. Ziegler, *Organometallics* **1995**, 14, 2018.
- [58] J. P. Hogan, *J. Polym. Sci. Part A.* **1970**, 8, 2637.
- [59] F. J. Feher, R. L. Blanski, *J. Am. Chem. Soc.* **1992**, 114, 5856. b) F. J. Feher, R. L. Blanski, *J. Chem. Soc. Chem. Commun.* **1990**, 1614.
- [60] a) K. H. Theopold, G. Bhandari, Y. Kim, J. M. McFarland, *Organometallics* **1995**, 14, 738. K. H. Theopold, P. A. White, J. Calabrese, *Organometallics* **1996**, 15, 5473. c) K. H. Theopold, B. J. Thomas, S. K. Noh, G. K. Schulte, S. C. Sendlinger, *J. Am. Chem. Soc.* **1991**, 113, 893.
- [61] a) B. L. Small, M. Brookhart, A. M. A. Bennett, *J. Am. Chem. Soc.* **1998**, 120, 4049. b) B. L. Small, M. Brookhart, *J. Am. Chem. Soc.* **1998**, 120, 7143.
- [62] G. J. P. Britovsek, V. C. Gibson, B. S. Kimberley, P. J. Maddox, S. I. McTavish, G. A. Solan, A. J. P. White, D. J. William, *Chem Commun.* **1998**, 849.
- [63] b) B. L. Small, M. Brookhart, *Macromolecul. Chem. Rapid Commun.* **1999**, 32, 2120. B. L. Small, A. J. Marcucci, *Organometallics* **2001**, 20, 5738.

- [64] a) G. J. P. Britovsek, M. Bruce, V. C. Gibson, B. S. Kimberley, S. Mastroianni, P. J. Maddox, S. I. McTavish, C. Redshaw, G. A. Solan, S. Strömberg, A. J. P. White, D. J. Williams, *J. Am. Chem. Soc.* **1999**, 121, 8728. b) G. J. P. Britovsek, V. C. Gibson, A. J. P. White, D. J. William, S. Mastroianni, G. A. Solan, S. P. D. Baugh, C. Redshaw, M. R. Elsegood, *J. Am. Chem. Soc.* **2000**, 6, 2221.
- [65] E. A. H. Griffiths, G. J. P. Britovsek, V. C. Gibson, I. R. Gould, *Chem. Commun.* **1999**, 1333.
- [66] a) L. Deng, P. Margl, T. Ziegler, *J. Am. Che. Soc.* **1999**, 121, 6479. b) D. V. Khoroshum, D. G. Musaev, T. Vreven, K. Morokuma, *Organometallics* **2001**, 20, 2007.
- [67] H. K. Luo, Z. H. Yang, B. Q. Mao, D. S. Yu, R. G. Tang, *J. Mol. Catal. A : Chem.* **2002**, 177, 195.
- [68] J. Ramos, V. Cruz, A. Munoz-Escalona, J. Martinez-Salazar, *J. Polymer* **2002**, 43, 3635.
- [69] E. P. Talsi, D. E. Babushki, N. V. Semikolenova, V. N. Zudin, V. N. Panchenko, V. A. Zakharov, *Macromol. Chem. Phys.* **2001**, 202, 2046.
- [70] a) G. J. P. Britovsek, G. K. B. Clentsmith, V. C. Gibson, D. M. L. Goodgame, S. I. McTavish, Q. Pankuhurst, *Catal. Commun.* **2002**, 3, 207.
- [71] a) D. M. Dawson, D. A. Walker, M. Thornton-Prett, M. Bochmann, *J. Chem. Soc. Dalton Trans.* **2000**, 459. b) S. Al-Benna, M. J. Thornton-Pett, D. L. Ormsby, P. J. Maddox, P. Bres, M. Bochmann, *J. Chem. Soc. Dalton Trans.* **2000**, 4247. c) R. Schmidt, M. B. Welch, S. J. Palackal, H. G. Alt, *J. Mol. Catal. A : Chem.* **2002**, 179, 155. d) C. Bianchini, G. Montovani, A. Meli, F. Migliacci, F. Zanobini, F. Laschi, A. Sommazzi, *Eur. J. Inorg. Chem.* **2003**, 1620.
- [72] a) D. Reardon, F. Conan, S. Gambarotta, G. Yap, Q. Y. Wang, *J. Am. Chem. Soc.* **1999**, 121, 9318. b) G. J. P. Britovsek. V. C. Gibson, S. K. Spitzmesser, K. P. Tellmann, A. J. P. White, D. Williams, *J. Chem. Soc. Dalton Trans.* **2002**, 1159. c) R. Schmidt, M. B. Welch, S. J. Palackal, H. G. Alt, *J. Mol. Catal. A : Chem.* **2002**, 179, 155. d) F. A. R. Kaul, G. T. Schneider, F. Bielert, D. Mihailios, W. A. Herrmann, *Organometallics* **2002**, 21, 74. e) Q. Wang, H. X. Yang, Z. Q. Fan, *Macromol. Rapid Commun.* **2002**, 23, 639. e) N. V. Semikolenova, V. A. Zakharov, E. P. Talsi, D. E. Babushkin, A. P. Sobolev, L. G. Echevskaya, M. M.. Khysniyarov, *J. Mol. Catal. A : Chem.* **2002**, 182, 283.

- [73] A. S. Abu-Sarrah, K. Lappalainen, U. Piironen, P. Lehmus, T. Repo, M. Leskela, *J. Organomet. Chem.* **2002**, 648, 55. b) I. S. Paulino, U. Schuchardt, *J. Mol. Catal. A : Chem.* **2004**, 211, 55. c) M. E. Bluhm, C. Folli, M. Döring, *J. Mol. Catal. A : Chem.* **2004**, 212, 13. d) Y. Chen, C. Qian, J. Sun, *Organometallics* **2003**, 22, 1231.
- [74] V. C. Gibson, S. K. Spitzmesser, *Chem. Rev.* **2003**, 103, 283.
- [75] F. A. R. Kaul, G. T. Puchta, H. Schneider, M. Grosche, D. Mihailios, W. A. Herrmann, *J. Organomet. Chem.* **2001**, 621, 184. b) Q. Mingxing, W. Mei, H. Ren, *J. Mol. Catal. A.* **2000**, 160, 243.
- [76] R. Quijada, R. Rojas, G. Bazan, A. J. Z. Komon, S. R. Mauler, G. B. Galland, *Macromolecules* **2001**, 34, 2411.
- [77] a) T. Yamamoto, A. Yamamoto, S. Ikeda, *Bull. Chem. Soc. Jpn* **1972**, 45, 1104. b) T. Yamamoto, A. Yamamoto, S. Ikeda, *Bull. Chem. Soc. Jpn* **1972**, 45, 1111. c) T. Yamamoto, A. Yamamoto, S. Ikeda, *Bull. Chem. Soc. Jpn* **1975**, 48, 101.
- [78] T. Ando, M. Kamigaito, M. Sawamoto, *Macromolecules* **1997**, 30, 4508.
- [79] C. Bianchini, A. Meli, *Coord. Chem. Rev.* **2002**, 225, 35. b) C. Bianchini, H. M. Lee, A. Meli, S. Moneti, V. Patinec, G. Petrucci, F. Vizza, *Macromolecules* **1999**, 32, 3859. c) C. Bianchini, H. M. Lee, A. Meli, W. Oberhauser, M. Peruzzini, F. Vizza, *Organometallics* **2002**, 21, 16.
- [80] a) E. Drent, P. H. M. Budzelaar, *Chem. Rev.* **1996**, 96, 663. b) W. P. Mul, H. Oosterbeek, G. A. Beitel, G.-J. Kramer, E. Drent, *Angew. Chem. Int. Ed.* **2000**, 39, 1848.
- [81] S. Horn, R. P. Quirk, *Transition Metal Catalyzed Polymerizations*, Hardwood, New York **1983**.
- [82] a) A. Sen, *Acc. Chem. Res.* **1993**, 26, 303. b) K. Nozaki, T. Hiyama, *J. Organomet. Chem.* **1999**, 576, 248.
- [83] S. J. Dossett, A. Gillon, A. G. Orpen, J. S. Fleming, P. G. Prigle, D. C. Wass, M. D. Jones, *Chem. Commun.* **2001**, 699.
- [84] a) P. W. N. M. Van Leeuwen, M. A. Zuideveld, B. H. G. Swennenhuis, Z. Freixa, P. C. J. Kamer, K. Goubitz, J. Fraanje, M. Lutz, A. L. Spek, *J. Am. Chem. Soc.* **2003**, 125, 5523. b) M. A. Zuideveld, P. C. J. Kamer, P. W. N. M. Van Leeuwen, P. A. A. Klusener, H. A. Stil, C. F. Roobeek, *J. Am. Chem. Soc.* **1998**, 120, 7977.
- [85] J. Liu, B. T. Heaton, J. A. Iggo, R. Whyman, *Chem. Commun.* **2004**, 1326.
- [86] M. Raemy, Dissertation Nr 1413, University of Fribourg **2003**.
- [87] T. P. Sieber, Dissertation Nr 1279, University of Fribourg **2000**.

- [88] D. Bourissou, O. Guerret, F. P. Gabbaï, G. Bertrand, *Chem. Rev.* **2000**, 100, 39
- [89] J. Huang, H.-J Schanz, E. D. Stevens, S. P. Nolan, *Organometallics* **1999**, 18, 2370.
- [90] A. C. Hiller, W. J. Sommer, B. S. Yong, J. L. Petersen, L. Cavallo, S. P. Nolan, *Organometallics* **2003**, 22, 4322.
- [91] W. Baratta, E. Herdtweck, W. A. Herrmann, P. Rigo, J. Schwarz, *Organometallics* **2002**, 21, 2101.
- [92] D. S. McGuinness, K. J. Cavell, *Organometallics* **2000**, 19, 741.
- [93] V. César, S. Bellemin-Laponnaz, L. H. Gade, *Organometallics* **2002**, 21, 5204.
- [94] N. Tsoureas, A. A. Danopoulos, A. A. D. Tulloch, M. E. Light, *Organometallics* **2003**, 22, 4750.
- [95] A. A. Tulloch, A. A. Danopoulos, G. J. Tizzard, S. J. Coles, M. B. Hursthouse, R. S. Hay-Motherwell, W. B. Motherwell, *Chem. Commun.* **2001**, 1270.
- [96] A. A. Tulloch, A. A. Danopoulos, R. P. Tooze, S. M. Cafferkey, S. Kleinhenz, M. B. Hursthouse, *Chem. Commun.* **2000**, 1247.
- [97] A. W. Waltman, R. H. Grubbs, *Organometallics* **2004**, 23, 3107.
- [98] a) G. Labat, C. Boskovic, H. U. Güdel, *Acta Cryst.* **2005**, E61, m611. b) M. B. Robin, P. Day, *Adv. Inorg. Chem. Radiochem.* **1967**, 10, 247.
- [99] H. Oshio, N. Hoshino, T. Ito, M. Nakano, F. Renz, P. Gülich, *Angew. Chem. Int. Ed.* **2003**, 42, 223.
- [100] a) R. A. Carboni, J. C. Kauer, W. R. Hatchard, R. J. Harder, *J. Am. Chem. Soc.* **1967**, 89, 2626. b) A. L. Johnson, J. C. Kauer, D. C. Sharma, R. L. Doreman, *J. Am. Chem. Soc.* **1969**, 91, 1024.
- [101] J. P. Collman, *Org. Lett.* **2000**, 2, 1233.
- [102] V. C. O. Njar, *Synthesis* **2000**, 14, 2019.
- [103] W. Fischer, *Synthesis* **2002**, 1, 29.
- [104] A. J. Arduengo III, F. P. Gentry Jr, P. K. Taverkere, H. E. Simmons III, United Patent **2001**, 6.177.575.B1.
- [105] A. A. Gridnev, I. M. Mihaltseva, *Synthetic Communications* **1994**, 24(11), 1547.
- [106] D. Davidson, M. Weiss, M. Jelling, *J. Org. Chem.* **1938**, 2, 319. b) Schulze, US Patent **1973**, 3.715.365.
- [107] W. A. Herrmann, K. Öfele, D. V. Preysing, S. K. Schneider, *J. Organomet. Chem.* **2003**, 687, 229.
- [108] A. J. Arduengo III, R. Krafczyk, R. Schmutzler, *Tetrahedron* **1999**, 55, 14534.

- [109] S. Gründemann, A. Kovacevic, M. Albrecht, J. K. Faller, R. H. Crabtree, *J. Am. Chem. Soc.* **2002**, 124, 10473.
- [110] M. V. Baker, B. W. Skelton, A. H. White, C. C. Williams, *Organometallics* **2002**, 21, 2674.
- [111] a) W. Baratta, W. A. Herrmann, P. Rigo, J. Schwarz, *J. Organomet. Chem.* **2000**, 593-594, 489. b) J. Schwarz, V. P. W. Böhm, M. G. Gardiner, M. Grosche, W. A. Herrmann, W. Hieringer, G. Raudaschl-Sieber, *Chem. Eur. J.* **2000**, 6, 1773.
- [112] a) A. A. Danopoulos, N. Tsoureas, J. A. Wright, M. E. Light, *Organometallics* **2004**, 23, 166. b) A. A. Danopoulos, J. A. Wright, W. B. Motherwell, *Chem. Commun.* **2005**, 784.
- [113] a) R. A. Andersen, K. Faegri Jr, J. C. Green, A. Haaland, M. F. Lappert, W.-P. Leung, K. Rypdal, *Inorg. Chem.* **1998**, 27, 1782.
- [114] J.-S. Sun, H. Zhao, X. Ouyang, R. Clérac, J. A. Smith, J. M. Clemente-Juan, C. Gomez-Garcia, E. Coronado, K. M. Dunbar, *Inorg. Chem.* **1999**, 38, 5841.
- [115] A. G. Orpen, L. Brammer, F. H. Allen, O. Kennard, D. G. Watson, *J. Chem. Soc. Dalton Trans.* **1989**, S1.
- [116] P. Buchgraber, L. Toupet, V. Guerchais, *Organometallics* **2003**, 22, 5144.
- [117] J. S. Haynes, J. R. Sams, R. C. Thompson, *Can. J. Chem.* **1980**, 59, 669. b) J. S. Haynes, J. R. Sams, R. C. Thompson, *Can. J. Chem.* **1986**, 64, 744.
- [118] A. L. Arduini, M. Garnett, R. C. Thompson, T. C. T. Wong, *Can. J. Chem.* **1975**, 53, 3812.
- [119] A. A. Arduengo III, H. V. R. Dias, R. L. Harlow, M. Kline, *J. Am. Chem. Soc.* **1992**, 114, 5530.
- [120] J. M. Hopkins, M. Bowdridge, J. A. C. Clyburn, K. N. Robertson, T. S. Cameron, H. A. Jenkins, *J. Org. Chem.* **2001**, 66, 5713.
- [121] a) D. M. Kurtz Jr, *Chem. Rev.*, 1990, 585., b) A. Machkour, D. Mandon, M. Lachkar, R. Welter, *Inorg. Chem.* **2004**, 43, 1545.
- [122] O. Aebischer, *Advanced work in Organometallic Chemistry*, University of Fribourg **2003**.
- [123] J. Louie, R. H. Grubbs, *Chem. Commun.* **2000**, 1479.
- [124] a) M. G. Gardiner, W. A. Herrmann, C.-P. Reisinger, J. Schwarz, M. Spiegler, *J. Organomet. Chem.* **1999**, 572, 239. b) J. M. Fraile, J. I. Garcia, M. J. Gil, V. Martinez-Merino, J. A. Mayoral, L. Salvatella, *Chem. Eur. J.* **2004**, 10, 758. c) A. A. D. Tulloch,

- S. Winston, A. A. Danopoulos, G. Eastham, M. B. Hursthouse, *Dalton Trans.* **2003**, 699.
- [125] J. D. Walker, R. Poli, *Inorg. Chem.* **1989**, 28, 1793.
- [126] V. Jorik, I. Ondrejovicová, R. B. von Dreele, H. Ehrenberg, *Cryst. Res. Technol.* **2003**, 38, 174.
- [127] Z-Z. Zhang, J-K. Zhang, W-D Zhang, H-P Xi, H. Cheng, H-G. Wang, *J. Organomet. Chem.* **1996**, 515, 1.
- [128] A. A. D. Tulloch, A. A. Danopoulos, S. Winston, S. Klinhenz, G. Eastham, *J. Chem. Soc., Dalton Trans.* **2000**, 4499.
- [129] M. J. H. Wang, I. J. B. Lin, *Organometallics* **1998**, 17, 972.
- [130] Y. A. Wanniarachchi, M. A. Khan, L. M. Slaughter, *Organometallics* **2004**, 25, 5881.
- [131] K. M. Lee, H. M. J. Wang, I. J. B. Lin, *Dalton* **2002**, 2852.
- [132] P. L. Arnold, *Heteroatom Chem.* **2002**, 6, 534. b) H. Schmidbauer, *Nature* **2001**, 413, 31.
- [133] T. Ramnial, C. D. Abernethy, M. D. Spicer, L. D. Gay, J. A. C. Clyburne, *Inorg. Chem.* **2003**, 42, 1391.
- [134] a) P. J. Barnard, M. V. Baker, S. J. Berners-Price, B. W. Skeleton, A. White, *J. Chem. Soc. Dalton Trans.* **2004**, 1038. b) D. Nemcsok, K. Wichmann, G. Frenking, *Organometallics* **2004**, 23, 3640.
- [135] a) X. Hu, I. Castro-Rodriguez, K. Olsen, K. Meyer, *Organometallics* **2004**, 23, 755. b) C. Boehme, G. Frenking, *Organometallics* **1998**, 17, 5801. c) M.-T. Lee, C.-H. Hu, *Organometallics* **2004**, 23, 976.
- [136] X. Hu, Y. Tang, P. Gantzel, K. Meyer, *Organometallics* **2003**, 22, 612.
- [137] Q.-X. Liu, F.-B. Xu, Q.-S. Li, X.-S. Zeng, X.-B. Leng, Y. L. Chou, Z.-Z. Zhang, *Organometallics* **2003**, 22, 309.
- [138] A. Melaiye, R. S. Simons, A. Milsted, P. Pingitore, C. Wesdemiotis, C. A. Tessier, W. J. Youngs, *J. Med. Chem.* **2004**, 47, 973.
- [139] M. Niehues, G. Kehr, G. Erker, B. Wibbling, R. Fröhlich, O. Blacque, H. Berke, *J. Organomet. Chem.* **2002**, 663, 192.
- [140] K. M. Lee, H. M. J. Wang, I. J. B. Lin, *J. Chem. Soc., Dalton Trans.* **2002**, 2852. b) P. L. Arnold, A. C. Scarisbrick, A. J. Blake, C. Wilson, *Chem. Commun.* **2001**, 2340. c) J. C. Garrison, R. S. Simons, J. M. Talley, C. Wesdemiotis, C. A. Tessier, W. J. Youngs, *Organometallics* **2001**, 20, 1276.

- [141] a) G. Schmid, G. Barbenheim, R. Boese, *Z. Naturforsch.* **1985**, 40b, 787. b) W. Pohl, I.-P. Lorenz, H. Nöth, M. Schmidt, *Z. Naturforsch.* **1995**, 50b, 1485. c) Cambridge crystallographic database;
- [142] S. J. Obrey, S. G. Bott, A. R. Barron, *J. Chem. Crystallogr.* **2000**, 30, 61.
- [143] G. J. Long, P. J. Clark, *Inorg. Chem.* **1978**, 17, 1394
- [144] A. Hoser, Z. Kaluski, M. Januszczyk, J. Pietrzak, T. Glowiak, *Acta Crystallogr.* **1983**, C39, 1039.
- [145] A. J. Arduengo III, F. Davidson, H. V. R. Dias, J. R. Goerlich, D. Khasnis, W. J. Marshall, T. K. Prakasha, *J. Am. Chem. Soc.* **1997**, 119, 12742.
- [146] V. H. J. Spiegel, G. Groh, H. J. Berthold, *Z. Anorg. Allg. Chem.* **1973**, 398, 225. b) T. A. Bazhenova, R. M. Lobkovskaya, R. P. Shibaeva, A. K. Shilova, M. Gruselle, G. Leny, E. Deschamp, *J. Organomet. Chem.* **1983**, 244, 375.
- [147] C. Lambert, W. Gaschler, M. Zabel, R. Matschiner, R. Wortmann, *J. Organomet. Chem.* **1999**, 592, 109.
- [148] M. Velusamy, R. S. Gopalan, G. U. Kulkarni, M. Palaniandavar, *Inor. Chem.* **2003**, 42, 8283.
- [149] a) P. S. Braterman, J.-I. Song, R. D. Peacock, *Inorg. Chem.* **1992**, 31, 555. b) J. Wang, M. S. Mashuta, Z. Sun, J. F. Richardson, D. N. Hendrickson, R. M. Buchanan, *Inor. Chem.* **1996**, 35, 6642.
- [150] I. Bernal, I. M. Jensen, K. B. Jensen, C. J. McKenzie, H. Toftlund, J.-P. Tuchagues, *J. Chem. Soc. Dalton Trans.* **1995**, 3667.
- [151] P. Mialane, A. Nivorojkine, G. Pratviel, L. Azéma, M. Slany, F. Godde, A. Simaan, F. Banse, T. Kargar-Grisel, G. Bouchoux, J. Sainton, O. Horner, J. Guilhem, L. Tchertanova, B. Meunier, J.-J. Girerd, *Inor. Chem.* **1999**, 38, 1085. b) D. Mandon, A. Machkour, S. Goetz, R. Welter, *Inor. Chem.* **2002**, 41, 5364. c) X. Wang, S. Wang, L. Li, E. B. Sundberg, G. P. Gacho, *Inor. Chem.* **2003**, 42, 7799. d) R. E. Shepherd, *J. Am. Chem. Soc.* **1976**, 98, 3329. e) C. R. Johnson, R. E. Shepherd, B. Marr, S. O'Donnell, W. Dressick, *J. Am. Chem. Soc.* **1980**, 102, 6227. f) A. Lombardi, D. Marasco, O. Maglio, L. Di Constanzo, F. Nastro, V. Pavone, *Biochemistry* **2000**, 22, 11922. g) D. R. Rosseinsky, H. Lim, X. Zhang, H. Jiang, J. W. Chai, *Chem. Commun.* **2002**, 2988. h) I. V. Korendovych, R. J. Staples, W. M. Reiff, E. V. Rybak-Akimova, *Inor. Chem.* **2004**, 43, 3930.
- [152] a) Y. Mekmouche, H. Hummel, R. Y. N. Ho, L. Que Jr, V. Schünemann, F. Thomas, A. X. Trautwein, C. Lebrun, K. Gorgy, J.-C. Leprêtre, M.-N. Collomb, A. Deronzier,

- M. Fontecave, S. Ménage, *Chem. Eur. J.* **2002**, 8, 1196. b) V. Balland, F. Banse, E. Anxolabéhère-Mallart, M. Ghiladi, T. A. Mattioli, C. Philouze, G. Blondin, J.-J. Girerd, *Inor. Chem.* **2003**, 42, 2470. c) A. Hazell, C. McKenzie, L. P. Nielsen, S. Schinler, M. Weitzer, *J. Chem. Soc. Dalton Trans.* **2002**, 310. d) F. Aguire, J. Husband, C. J. Thompson, K. L. Stringer, R. B. Metz, *J. Chem. Phys.* **2002**, 10, 4071. e) T. Paczesniak, A. Sobkowiak, *J. Mol. Cat. A : Chem.* **2003**, 194, 1. f) H. B. Dunford, *Coord. Chem. Rev.* **2002**, 233-234, 311.
- [153] J. B. Luiz, F. M. De Andrade, E. L. de Sà, G. R. Friedermann, A. S. Mangrich, J. E. Barclay, D. J. Evans, T. Hasegawa, F. S. Nunes, *J. Braz. Chem. Soc.* **2004**, 1, 1. b) C. Manzur, L. Millán, W. Figueroa, J.-R. Hamon, J. A. Mata, D. Carillo, *Bol. Soc. Chil. Quím.* **2002**, 4, 1. c) U. S. Ray, D. Danerjee, C. Sinha, *Proc. Indian Acad. Sci. (Chem. Sci.)* **2003**, 3, 169.
- [154] Kauffmann, *Angew. Chem. Int. Ed. Engl.* **1996**, 35, 386.
- [155] A. Fürstner, A. Leitner, *Angew. Chem. Int. Ed.* **2002**, 41, 609.
- [156] a) B. Scheiper, M. Bonnekessel, H. Krause, A. Fürstner, *J. Org. Chem.* **2004**, 69, 3943. b) A. Fürstner, A. Leitner, M. Mendez, H. Krause, *J. Am. Chem. Soc.* **2002**, 124, 13857. c) R. Martin, A. Fürstner, *Angew. Chem. Int. Ed.* **2004**, 43, 2.
- [157] a) R. R. Chandrick, M. Z. Zgierski, B. S. Hudson, *J. Chem. Phys.* **1991**, 95, 7204. b) P. Nallasamy, P. M. Anbarasan, S. Mohan, *Turk J. Chem.* **2002**, 26, 105. c) . Appel, T. W. Zerda, W. H. Waddell, *Applied Spectroscopy* **2000**, 54, 1559.
- [158] M. Citroni, M. Ceppatelli, R. Bini, V. Schettino, *Science* **2002**, 295, 2058. b) D. Chelazzi, M. Ceppatelli, M. Santoro, R. Bini, V. Schettino, *Nature* **2004**, advance online publication, 1.
- [159] L. Gong, R. Wool, A. D. Friend, K. Goranov, *J. Polym. Sci: Part A : Polym. Chem.* **1999**, 37, 3129. b) J. A. Frankland, H. G. M. Edwards, A. F. Johnson, I. R. Lewis, S. poshyachinda, *Spectrochim. Acta, Part A* **1991**, 47, 1511. c) J. M. Jenkins, J. G. Verkade, *Inorg. Synth.* **1968**, 11, 108. d) H. G. M. Edwards, A. F. Johnson, I. R. Lewis, S. J. Wheelwright, *Spectrochim. Acta, Part A* **1993**, 49, 457. e) S. W. Cornell, J. L. Koenig, *Macromolecules* **1969**, 2, 540.
- [160] a) R. A. Kelly, N. M. Scott, S. Diez-Gonzalez, E. D. Stevens, S. P. Nolan, *Organometallics* **2005**, 24, 3442. b) X. Wang, S. Liu, G.-X. Jin, *Organometallics* **2004**, 23, 6002. c) R. E. Douthwaite, D. Haussinger, M. L. H. Green, P. J. Silcock, P. T. Gomes, A. M. Martins, A. A. Danopoulos, *Organometallics* **1999**, 18, 4584.

VIII. Curriculum Vitae

Roger MAFUA
Chemistry Department
University of Fribourg
Route de Musée 9
1700 Fribourg
<http://www-chem.unifr.ch/tj/mafua/>

Nationality : Angolan.

Qualifications

- 2001 - 2006 : Ph.D. position in field of Homogenous Catalysis, University of Fribourg, Switzerland.
- 2004 - 2006 : Master of Business Administration (ExeMBA), ESM-BLS Management & Communication, Geneva
- October – February 2002 : Management of Project R&D, University of Neuchâtel, Switzerland.
- 1997 – 2001 : Chemistry, University of Neuchâtel, Switzerland.

Employment history:

- 2002– 2005 : Assistant for students at the University of Fribourg Switzerland.
- 2005 : Chemistry teacher for Highschool students at the Ecole des Métiers Artisanals et Professionnels, Fribourg, Switzerland.
- July – September 2000 : Practical training at Metalor (precious metals), Marin, Switzerland.
- 1998 – 2000 : Assistant at the department of Inorganic Chemistry (University of Neuchâtel), Switzerland.
- June – September 1998 : Practical training at EM – Microtechnique, Marin, Switzerland.
- From 1997 to 2001 : Employed at Papiliorama – Nocturama foundation, Neuchâtel, Switzerland.
- June – October 1995 : Practical training as assistant – nurse at the University Hospital Center (CHUV), Department of traumatology, Lausanne, Switzerland.

Languages

Portuguese (mother language), French (written & spoken), Spanish (written & spoken), Italian (written and spoken), English (scholar level), African languages (kikongo, kimbundo)